Summary

In this work the difference between steel and aluminium in sheet metal forming operations, and the influence of roughness in these operations, have been studied by making deep draw and friction experiments. The friction tests have been selected to simulate the conditions in the blankholder, because there is the main source of friction in deep draw operations (besides drawbeads).

Deep draw experiments showed that the influence of roughness is not negligible. The punch force is affected by the roughness, and related properties such as the dimensions of the product after deep drawing and the fracture limit, are affected as well. The punch force increased with increasing roughness, but the relative amount of this influence depends on the amount of lubricant, the type of product and the type of sheet metal, and can also vary with the state of the process (punch travel). For cylindrical products, the shape of the force-displacement curve differed from the classical dome-shaped curve found in textbooks. This shape was particularly sensitive to variations in the frictional conditions during deep drawing. In rectangular products the effects were less clear than in cylindrical products. Because the conditions in the blankholder are not constant over the perimeter (as for a cylindrical product), the effects are more smoothed out.

In deep drawing of aluminium the influences of process conditions are stronger than in the deep drawing of steel. When using a high speed and a substantial quantity of lubricant, the friction in the blankholder became so low that the blankholder force could be increased up to the maximum of the press without causing fracture. In these conditions the influence of material properties is modest, especially at larger blank sizes.

Friction tests showed that for steel the friction, expressed in a Stribeck curve, barely depends on the pressure. The influence of roughness on friction could be observed as a shift of the Stribeck curve as a whole, higher roughness shifts the curve to higher values of H (to the right). The value of H at the centre of the Stribeck curve (the 'position' of the curve) is proportional to the square of the roughness height. For coated steel the position of the curve is also influenced by the coating hardness, softer coatings shift the curve to smaller values of H (to the left). The friction at boundary lubrication also is affected by the coating hardness: softer coatings make friction increase. The coefficient of friction at boundary lubrications decreases with increasing pressure, notably for soft coatings; no influence of the type of roughness was found.

The friction of aluminium is much more influenced by pressure than the friction of steel. The area of mixed lubrication is very wide, making it difficult to obtain pure boundary lubrication. The coefficient of friction at boundary lubrication increases with increasing pressure. The roughness asperities were found to show extreme flattening in friction tests; when the coefficient of friction was 'corrected' for this flattening the Stribeck curves resembled those for steel. The friction of the strongly oriented roughness type MF differed from the other types (EDT and EBT); an influence of orientation of friction was observed also for MF roughness.

The mechanisms responsible for the generation of pressure in the lubricant at mixed lubrication have been examined. Several hydrodynamic mechanisms were investigated,

which all have some part in the total effect. Based on these findings a model for mixed lubrication has been developed which can describe many of the observed effects including the consequence of asperity flattening.

The phenomena encountered in deep drawing, notably the difference between steel and aluminium, could be directly related the phenomena encountered in the friction tests.

Abstract

The difference between steel and aluminium in sheet metal forming operations, and the influence of roughness in these operations, have been studied by making deep draw and friction experiments. The friction tests have been carried out with flat contacts to simulate the conditions in the blankholder.

In deep drawing the influence of roughness cannot be neglected. The punch force is affected by the roughness, and related properties such as the dimensions of the product after deep drawing and the fracture limit, are affected as well. The relative amount of this influence depends on the amount of lubricant, the type of product and the type of sheet metal, and can also vary with the state of the process. In rectangular products however the effects were less clear than in cylindrical products.

For aluminium the influences of process conditions in deep drawing are stronger than for steel, caused by strong asperity flattening. When using a high speed and much lubricant at aluminium, the friction in the blankholder became so low that the blankholder force could be increased up to the limit of the press without causing fracture.

Friction tests showed that for steel the friction as expressed in a Stribeck curve, barely depends on the pressure, while for aluminium the influence of pressure is strong. Both the position of the region of mixed lubrication, and the 'classic' friction coefficient at conditions of boundary lubrication are influenced by pressure. The influence of pressure could be linked to the phenomena encountered in the deep drawing tests successfully.

The mechanisms responsible for the generation of pressure in the lubricant at mixed lubrication have been examined. Based on these findings a model for mixed lubrication has been developed which can describe many of the observed effects including the consequence of asperity flattening.

Contents

4

List of symbols

Presented are: symbol, practical unit, description.

A	mm^2	apparent macroscopic contact area
B		general: constant, in particular in the tanhyp fit of the Stribeck curve
C		general: constant, in particular integration constant
d	μm	average depth of a roughness profile
d_0	μm	average depth of a symmetrical roughness profile before flattening, $d_0 = h_0/2$
d_r	-	relative depth of a (flattened) roughness profile, $d_r = d/d_0$
F_B	kN	blankholder force in a deep draw operation
F_L	kN	part of the normal force carried by the lubricant
F_M	kN	part of the normal force carried by the roughness peaks
F_N	kN	normal force acting on a contact, $F_N = F_L + F_M$
F_P	kN	punch force in a deep draw operation
F_T	kN	tangential force (friction force) in a contact
h	μm	height of the gap between two surfaces
h_0	μm	original height of the roughness before flattening
h_b	μm	gap height at the beginning of the flat part of the slider
h_e	μm	gap height at the end of the flat part of the slider
h_i	μm	gap height at the inlet
h_r	μm	roughness height, in particular half the peak to peak height of an artificial roughness in calculations
H	m	Hersey or Sommerfelt parameter, defined as: $H = \eta.V/P$
H_0	m	value of H at the transition from mixed to hydrodynamic lubrication
H_1	m	value of H at the transition from boundary to mixed lubrication
H_C	m	value of H at the midpoint of mixed lubrication (on a logarithmic scale), $\log H_C = (\log H_0 + \log H_1)/2$
Hd	MPa	effective hardness of the material
Hr	-	relative hardness, $Hr = Hd/P$
H*	1/m	new H type parameter defined as $H^* = H/R_{pm}{}^2$
H_0^*	1/m	value of H* at the transition from mixed to hydrodynamic lubrication
L	mm	length of the friction contact, usually the length of the jaw or slider in friction experiments
n	-	material hardening coefficient from the Ludwik/Nadai equation
N	-	height distribution of the roughness
N'	-	relative height distribution of the roughness (section 4.4.2)
p	MPa	local pressure in the lubricant
p_{av}	MPa	average pressure in the lubricant
P	MPa	average, macroscopic pressure in a friction contact
Q	-	dimensionless geometry constant
r	-	material anisotropy as determined in a tensile test
R	mm	general: radius of a toolpart

6

R_a	μm	average absolute roughness height from the centre line
R_p	μm	height of highest roughness peak measured from the centre line (equal to the average roughness depth as measured from the top)
R_{pm}	μm	average of 5 partial R_p
R_t	μm	height from lowest valley to highest peak in roughness
R_z	μm	average of 5 partial R_t
t	mm	thickness of the sheet material
t_p	-	bearing area of the roughness (notation according to DIN)
V	mm/s	velocity in the friction contact under the assumption that one contacting surface is stationary and the other one is moving with velocity V
x		unit of dimension in the direction of movement
x_i	mm	length of inlet zone in lubrication systems

α	-	fraction of the apparent area A which forms the actual microscopic contact area
ß	-	deep draw ratio for circular deep drawn parts, defined as blank diameter divided by punch diameter
		also: constant in the formula for the shear stress in the lubricant at the surface
γ	-	relative depth of penetration of a hard surface into a (softer) roughness
η	mPa.s	dynamic viscosity of the lubricant (mPa.s = 10^{-3} Pa.s)
Λ	m	length type parameter used in the mixed lubrication model
μ	-	coefficient of friction
$μ_0$	-	coefficient of friction at boundary lubrication
$μ_h$	-	coefficient of friction at hydrodynamic lubrication
σ	MPa	general: tensile stress
τ	MPa	general: shear stress
$τ_L$	MPa	the shear stress in the lubricant at the interface metal-lubricant
$τ_M$	MPa	the shear stress on the actual microcontacts in contacting asperities

Some symbols which are only used in one occasion are defined in the text.

Note: the 'old-fashioned' symbol σ is used for tensile stresses instead of the correct symbols Rp and Rm to avoid confusion with roughness parameters.

1 Introduction and background

ABSTRACT This chapter contains general background information about deep drawing, roughness, friction and tribology.

1.1 GENERAL INTRODUCTION

The last few decades have seen some important changes in the automotive world. First there has been an increasing level of automation in the press shop. The traditional man at the press, with a lifetime of experience, has disappeared gradually. This made impossible any fine tuning of the pressing conditions to (small) changes in material properties or other factors. Consequently, the tolerances imposed on the material being deformed grew more and more stringent. After the sheet metal suppliers had reduced the scatter in mechanical properties and the number of surface defects, and the press shops had installed automated lubrication devices, the surface roughness became a new parameter to be dealt with. However, contrarily to mechanical properties, little was known about the influence of roughness on pressing characteristics at that time.

Consequently, more interest in the details of the surface roughness arose. The reign of the good old Shotblast roughness came to an end. In the mid eighties, two new types of roughness were introduced: EDT and Lasertex (see section 1.3 for a definition of these terms). While EDT is similar to Shotblast in many aspects, Lasertex roughness was born out of a completely new approach: to develop a roughness where the individual parameters could be adapted separately. Although the idea behind this has never been questioned, technical problems led to a silent withdrawal from the battlefield. The niche, thus originated, has only recently been filled by EBT roughness.

Secondly, the development of techniques to simulate complex plastic deformation processes within a reasonable time, went very fast, parallel to the development of small but powerful computers. While the mechanical parameters needed for this kind of simulation became rapidly available, the coefficient of friction (let alone any implementation of friction) has been more difficult to grasp. This created a need for more detailed studies of friction in sheet metal forming and the development of models which describe the friction in these processes.

Thirdly, aluminium has been used more and more in the motor industry. In the eighties plastics have been introduced, but the euphoria silenced after some time. In the nineties, attention was again drawn to a metal to substitute the traditional steel, and aluminium has been introduced on an ever growing scale. While at first it was assumed that the experience obtained with steel could be transferred to aluminium, it became clear later on that aluminium is a material with its own properties, and experience had to be gained again the hard way.

In this light the research activities described in this work have been carried out. These activities started in 1982 with the objective to establish the relation between the roughness of steel sheet and the 'pressing behaviour' of the material. This latter is defined differently by each press shop, so a thorough understanding of the matter is needed to deal with all practical problems. The two main purposes of Hoogovens were:

- to be able to determine what type of roughness is needed for a certain product or manufacturing process, or in other words: to optimise the sheet roughness to the customer's needs;
- to be able to advise the customer to adjust its process to reach the maximum performance of a certain sheet material.

Later, a third goal was added:

- to obtain reliable friction data that can be used in computer simulations.

The roughness of the sheet influences both short-time and long-time pressing behaviour of the material. The short-time behaviour includes the friction forces that arise in the deep drawing tool and that may limit the deep drawing process. The long-time behaviour includes changes of the surface by scratches, transfer of small particles (notably with zinc-coated steel), tool wear etc. The research projects described in this work dealt only with the first aspect.

To study friction in manufacturing processes two approaches can be followed. The first is to simulate the conditions in the tools as closely as possible in the friction test. This will produce a coefficient of friction for that condition in a comparatively short time, but it will not add much to a deeper understanding of the processes involved. Therefore, at Hoogovens we decided from the beginning to study friction at lubricated flat contacts in a more fundamental way. Besides friction tests, deep drawing tests have been carried out as well. These deep drawing tests have been carried out using simply shaped products (chapter 2). Other studies have shown that a good agreement can be found between laboratory tests with simply shaped products and tests with 'realistic' products in the press shop [Langerak 1992, 1996].

1.2 DEEP DRAWING

1.2.1 General description of the process.

Deep drawing is a widely used name for a variety of processes by which a non flat product is made out of a flat sheet (called blank) in any other way then simple bending. Two groups of processes are generally distinguished: deep drawing and stretching.

In pure deep drawing, the extra surface area needed for the product is obtained by pulling some material out of a reservoir called the blankholder area. In this process there is a movement of material in the plane of the sheet (not necessarily flat), and the whole art of deep drawing is to control this movement. In deep drawing tools three parts are distinguished: the die, the punch and the blankholder. The presence of this latter part, which is used for controlling the movement of the material, distinguishes deep drawing from simple stamping. For a cylindrical product the general construction of a deep drawing tool and the outline of the deep drawing operation is presented in figure 1.1. The movement of the material out of the blankholder area is controlled by clamping the material between the die and the blankholder, the force used for this clamping is called the blankholder force. This clamping causes friction. In complex tools an extra control of the movement can be obtained by so called draw beads.
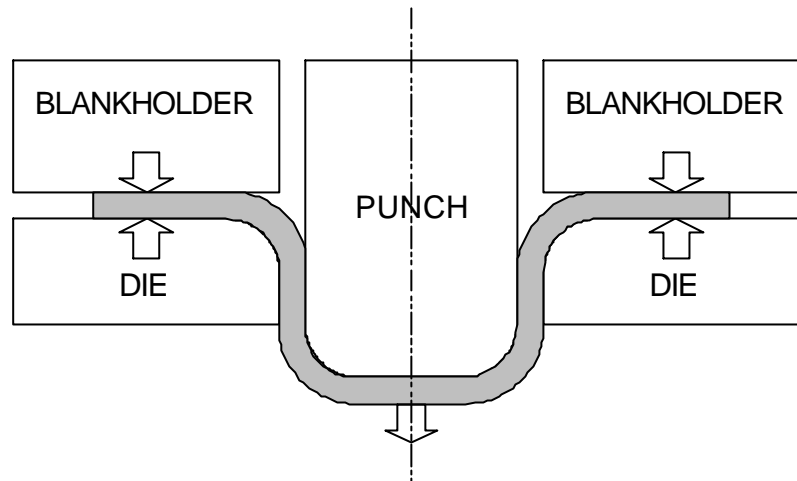
Figure 1.1. Schematic representation of the deep drawing operation, for a cylindrical tool. The area between the blankholder and the die is called the blankholder area, the material between the blankholder and the die is called the flange. The material being formed is clamped between the blankholder and the die by a clamping force (the blankholder force) and is pulled out of the blankholder area by movement of the punch (in the picture: downwards). In a stretching operation the material is completely clamped in the blankholder, the construction of the tool is otherwise similar to that of a deep drawing tool.

In pure stretching the extra surface needed for the product is obtained by stretching the material without any supply of fresh material. There are some basic differences between deep drawing and stretching. In deep drawing, the thickness of the material remains constant (in first approximation) while in stretching the material gets thinner (up to 50% in extreme cases). Furthermore, the contact in a deep drawing process is characterised by high speed of movement (equal to the punch speed) while in stretching the speed by which the material moves against the tool is low. It should be clear that in a drawing operation of a complex shape both deep drawing and stretch type deformations occur.

In the experiments described in the following chapters, both cylindrical and rectangular parts are made. Here, a basic difference occurs. In a cylindrical tool the movement of the material in the blankholder area is purely radial (neglecting second order effects), leading to a tangential symmetry in the product. During the drawing operation, the edge of the original blank gets thicker, but this thickening effect is the same on all positions on the perimeter. In a rectangular product, there is also a tangential movement of the material, in addition to the radial movement, notably around the corners. This means that the deformation state of the material differs form point to point. Consequently the thickening of the flange edge is not identical everywhere, neither are the conditions of friction.

Deep drawing and stretching are examples of sheet metal forming processes and are as such characterised by the facts that the deformation forces are oriented in the plane of the sheet, and that the surface pressures in the tool are generally (much) lower than the yield stress of the material. Other examples of sheet metal forming processes are bending, roll forming and spinning.

1.2.2 Friction conditions at deep drawing

10

In a deep drawing operation friction occurs as a result the material moving against the tool. In a traditional tool two areas of friction are distinguished: the blankholder area (simply called the blankholder) and the die radius. The third area which is sometimes mentioned, the punch radius, will not be considered in this work.
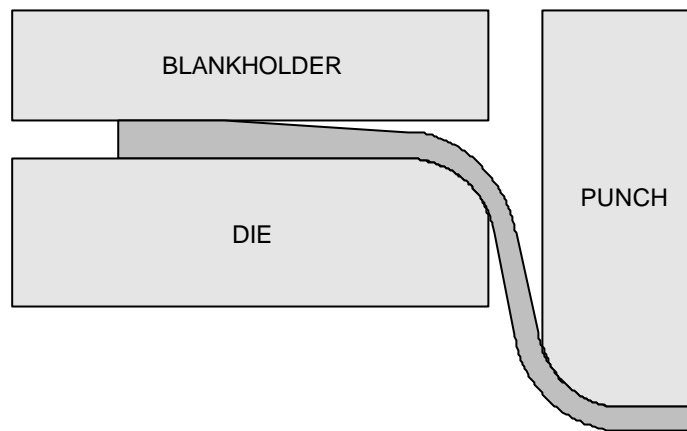
Figure 1.2 Thickening of the flange during deep drawing causes the blankholder force to concentrate on the outer part.

When the deep drawing operation starts, the blankholder closes and the blankholder force is acting on the material. Initially, the material in the blankholder (the flange) is flat, so that the blankholder force is evenly distributed over the blankholder area. As the punch moves, the material is gradually drawn out of the blankholder area. This has some consequences. Firstly the surface area of the material in the blankholder decreases, so the average surface <u>pressure</u> on the material increases (assuming that the blankholder <u>force</u> is kept constant). However, due to the plastic deformation of the material in the flange, the material thickens at the outer edge. Consequently, the blankholder force is no longer evenly distributed over the flange but concentrates on the outer part. This thickening of the outer edge may become so strong that the sheet and the blankholder get separated and the inner part of the flange loses contact with the tool. In this way, the blankholder force is concentrated further on the outer part (figure 1.2). The sum of these effects is that the surface pressure on the places in the blankholder area where the friction force is generated, increases significantly during the deep drawing operation.

Initially, the type of contact in the blankholder is flat. Inspection of deep drawn parts reveals that in most practical situations the contact area in the blankholder remains flat. Only under extreme conditions, like very low blankholder forces or extremely thick material, the flange may wrinkle to such a degree that the blankholder force acts only on the tops of the wrinkles. Under normal conditions wrinkling can occur only in the inner part of the blankholder where the material loses contact with the tool (figure 1.2). In that situation the tops of the wrinkles may touch the tool, but only in extreme situations will these contacts bear a substantial part of the load. Experience shows that this only happens for relatively thick material, and not for the situations described in chapter 2. It is therefore safe to assume that in the blankholder friction is occurring at flat contacts.
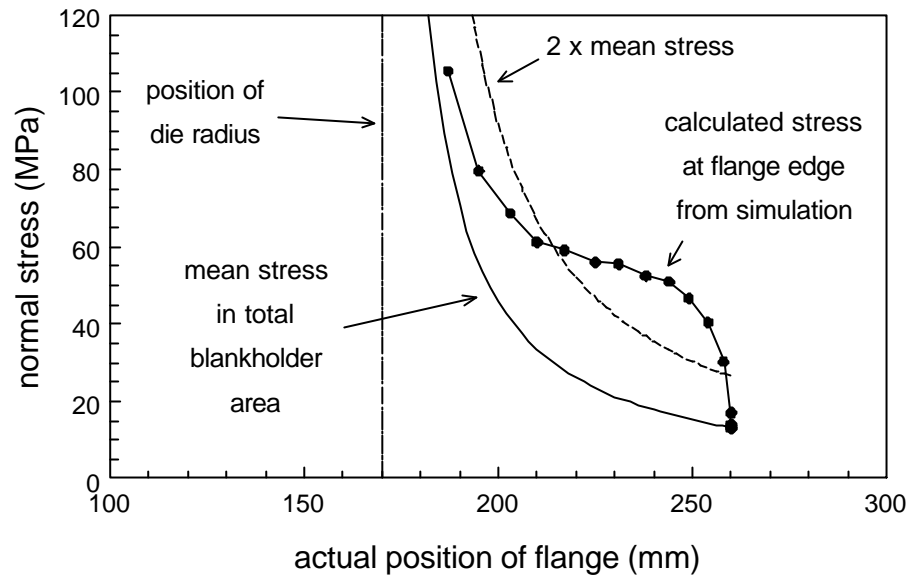
Figure 1.3. Results of a finite element simulation of the deep drawing of aluminium, showing the calculated normal pressure on the outer edge of the flange as a function of the position of the flange during the deep drawing operation. In this picture the flange edge is moving from right to left, contrary to figures 1.2, 2.29 and 5.3.

It is very difficult, if not impossible, to actually measure the pressure on the outer edge of the flange during the deep drawing operation. Therefore some results from a finite element simulation are presented in figure 1.3. The calculation simulates the drawing of aluminium equivalent to the tests described in section 2.7 [Atzema 1997]. A very high blankholder force has been used in the calculations in conjunction with a low coefficient of friction. Consequently, the calculated normal stresses (pressures) are higher than they will be in many practical situations, but the stresses (and thus also the changes in the stresses!) are proportional to the blankholder force. The calculated normal stress on the outer edge is presented together with the mean stress (pressure) defined as the blankholder force divided by the actual total area of the flange in the blankholder. At the onset of the operation the flange is still flat and the normal stress on the outer edge is equal to the mean stress. When the flange is being pulled inwards, the stress on the outer edge increases rapidly, indicating that the blankholder force concentrates on the outer part of the flange. When the stress on the edge exceeds twice the mean stress, the outer part has thickened so much that the inner part fully loses contact with the tool. When the operation continues, the blankholder force will become more uniformly distributed, due to the increasing amount of plastic deformation in the material.

For the die radius the situation is different. The material is bent over the die radius by the punch force which has to be transferred from the punch to the blankholder area. When the bending forces are neglected, the material will lie over the die radius like a membrane, and accordingly the contact is of conformal nature; the contact pressure is evenly distributed over the radius. However, in practice bending forces always occur. Recent simulations [Staeves 1996] show that the pressure gets concentrated in a few places, so that the type of contact is more like a line contact. The type of contact on the die radius can thus vary from conformal to line contact, largely depending on the ratio of material thickness to die radius.
The two main sources of friction in a deep drawing operation are the die radius and the

blankholder area, at least for simple tools as pictured in figure 1.1 and used in the tests described in this work. In practical situations, eliminating the friction at the die radius (if possible) will reduce the punch force by about 20%. Eliminating the friction in the blankholder area, however, may reduce the punch force by values of 50% or more. From this consideration, it has been concluded that the blankholder area is the major source of friction, and it has been decided to limit the experiments described hereafter to situations encountered in the blankholder, notably friction in flat contacts. The situation on the die radius may resemble more the work of Ter Haar [Ter Haar 1996], at least in situations where the ratio of material thickness to die radius is not too small.

1.2.3 Some comments on the punch force

In deep drawing operations the punch force is often measured in order to study the deep drawing process. This punch force is the force which brings about the forming operation, and is needed to deform the material in the blankholder plastically and to compensate for the friction there. Because the direction of movement of the punch is in general perpendicular to the direction of movement of the material in the blankholder, the force has to be 'bent' over 90°. This is done by drawing the material over the die radius, where an extra source of friction and deformation arises.

In the discussion of the results of the deep drawing tests the relation between the punch force and the blankholder force is studied. Therefore the exact relation between the punch force and the blankholder force, is of interest. The main sources of the punch force are the friction in the blankholder area, and the plastic deformation of the material being drawn. Neglecting bending forces and additional plastic deformation of the material over the die radius, the following expression for the punch force F_P can be written:

$$F_P = e^{\frac{\pi}{2} \cdot \mu_{die}} \cdot \left(F_B . 2 . \mu_{bl} + F_{def} \right) \cdot \frac{d_{punch}}{d_{bl,mean}} \qquad (1.1)$$

$$= \quad A \quad . \left(\quad B \quad + F_{def} \right) . \quad C$$

Here μ_{die} is the coefficient of friction on the die radius, μ_{bl} the coefficient of friction in the blankholder, d_{punch} the punch diameter, $d_{bl,mean}$ the mean diameter of the area of the flange which is actually in contact with the blankholder, and F_{def} is the force needed for plastic deformation of the material in the blankholder area.

Part A in (1.1) accounts for the effect of pulling the material over the die radius (assuming that the material lies over the die radius like a membrane), part B is the actual friction force in the blankholder (the factor 2 stems from the two surfaces of the material). There is a difference in speed between the punch (where the force is measured) and the material in the blankholder (the primary source of friction). While the total amount of work performed by the punch must be equal to the amount of work performed on the material in the blankholder, this difference in speed must be accounted for. The average thickness of the material remains more or less unchanged by the drawing operation, so the ratio of the speed can be taken equal to the ratio of diameters in part C. Assuming that the deformation force F_{def} is not affected by the blankholder force (this is true in first approximation), the derivative of the punch force F_P as a function of the blankholder force F_B can now be written as:

$$\frac{\partial F_P}{\partial F_B} = e^{\frac{\pi}{2} \cdot \mu_{die}} \cdot 2 \cdot \mu_{bl} \cdot \frac{d_{punch}}{d_{bl,mean}} \tag{1.2}$$

Assuming a value for the friction coefficient on the die radius of 0.15 (a common value), expression A in (1.1) becomes 1.26, while in practical situations expression C is 0.6-0.9. So in first (and very rough) approximation we can assume that:

$$A.C \approx 1 \tag{1.3}$$

We now introduce the term 'friction factor', defined as one half of the slope of the graph of the punch force - blankholder force relation (this terminology has been introduced originally by W. van Merkenstein of Quaker Chemical). Using the above we now find:

$$\text{friction factor} = \frac{1}{2}\frac{\partial F_P}{\partial F_B} = e^{\frac{\pi}{2} \cdot \mu_{die}} \cdot \mu_{bl} \cdot \frac{d_{punch}}{d_{bl,mean}} \approx \mu_{bl} \tag{1.4}$$

The so defined friction factor can be determined from the measured relation between punch force and blankholder force and is closely related to the coefficient of friction in the blankholder. In first, rough, approximation the friction factor is equal to that coefficient of friction.
Therefore the friction factor can be used to study the friction in the blankholder area.

1.3 ROUGHNESS

The roughness on sheet metal is normally applied by a rolling process and different types of roughness are named according to the way in which the rolls are roughened (textured). frequently used types are:

Shotblast: the rolls are roughened by blasting (bombarding) them with small hard particles; the roughness has a random nature. This way of roughening is now becoming obsolete.

EDT (Electro Discharge Texturing): the rolls are roughened by many small electric discharges similar to the process of spark erosion. This roughness also has a random nature; compared to shot-blast the peak spacing is somewhat smaller.

Lasertex (Laser Texturing): the rolls are roughened by burning small craters in the roll by means of a chopped laser beam. The roughness is not random: the craters are aligned on tangential lines on the roll (deterministic roughness). Once promising, this type of roughness is now forgotten.

EBT (Electro Beam Texturing): very similar to Lasertex, but an electron beam is used instead of a laser beam. Thus a better control of the separate crater dimensions is possible and also the lifetime of the rolls is improved (in comparison with Lasertex).
For aluminium many other types of roughness are used, we only mention:

MF (Mill Finished): the rolls are roughened by grinding them in the tangential direction.

The roughness is much finer than the types mentioned above. The use of this type of roughess for automotive applications is declining.

In practice there is a great difference in roughness on steel or aluminium, caused by the rolling process. In steel the roughness is applied in a special skin pass operation, where the reduction of thickness of the material is usually very small (0,5 - 1 %). In aluminium the roughness is applied in the last cold rolling stand, where the reduction of the thickness is larger (5 - 10 %). This larger reduction cases a certain amount of slip (relative movement) between the roll and the material, so that the roughness is somewhat smeared.

To some extent, the final roughness on the sheet also depends on the roughness of the sheet prior to the final rolling operation. For steel this roughness is quite coarse (large peak spacing) but not very high (see the graphic data in appendix A, figure A.1). For aluminium, on the contrary, this initial roughness is usually very smooth. Remnants of the initial roughness can usually be found in the final sheet roughness.

1.4 FRICTION

1.4.1 Coulomb friction

When two surfaces are pressed against each other under a normal force F_N, and these surfaces are forced to slide along each other, it will be noticed that a certain (tangential) pulling force F_T is necessary for this sliding operation. This phenomenon is called friction, and the ratio between two forces is called the friction coefficient μ:

$$\mu = F_T / F_N \qquad\qquad (1.5)$$

Friction thus described is called 'Coulomb friction'. In a first approximation the coefficient of friction μ only depends on the nature of the two surfaces and it does not depend on the normal force F_N, the size of the apparent contact area and the relative speed at which the surfaces are gliding. However, there are situations where the coefficient of friction can not be considered as a constant. These are:

- very high normal forces; the maximum shear stress at the surface is limited by the material strength, and therefore the pulling force F_T is limited as well; consequently μ decreases at very high levels of F_N;

- damaged surfaces; at high levels of friction forces the surface may get damaged by what is called scoring or galling; this increases friction;

- application of a lubricant; when the microscopic space between the two contacting surfaces is filled with lubricant, a pressure can be generated in the lubricant by hydrodynamic effects, which carries some part of the normal force F_N; this decreases the friction.

1.4.2 The Stribeck curve

The effects studied in this work focus on the last of the above phenomena. These effects

have been noticed a long time ago and some important results for journal bearings were published as early as 1902 by a German researcher named Stribeck. After that is has been discovered that these effects can be conveniently studied by plotting so called Stribeck curves, in which the coefficient of friction μ is plotted as a function of the Hersey parameter H, defined as the product of the viscosity of the lubricant η and the sliding speed V, divided by the apparent macroscopic pressure P:

$$H = \eta \cdot V / P \qquad (1.6)$$

Conventionally H is plotted on a logarithmic scale, and in the Stribeck plots so obtained three distinct regions can be observed (see figure 1.4):

- boundary lubrication, where the full load is carried by the asperities of the contacting surfaces;
- mixed lubrication, where the load is partially carried by the asperities and partially by the lubricant;
- hydrodynamic lubrication, where the full load is carried by the lubricant.
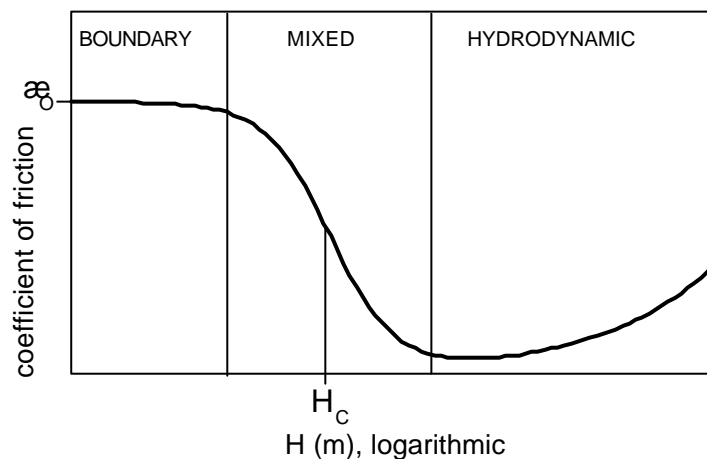
*Figure 1.4 Schematic representation of a Stribeck diagram. The coefficient of friction μ is plotted against H defined as **h**·V/P. If H is presented on a logarithmic scale, as in the drawing, three regimes of lubrication can be observed: boundary, mixed and hydrodynamic. The Stribeck curve is in first approximation characterised by two parameters: the coefficient of friction μ_0 and the midpoint of mixed lubrication H_C.*

Note that in principle there is no difference between boundary and mixed lubrication. At boundary lubrication any pressure build-up in the lubricant is neglected, but it is a matter of personal taste how to define the criteria for that. There is, however, a basic difference between mixed and hydrodynamic lubrication: at hydrodynamic lubrication the two surfaces are completely separated from each other by the lubricant, while at mixed lubrication there is physical contact between the surfaces which can be checked for example by electric measurements.

1.4.3 Analysing the Stribeck curve

In many cases it is necessary to characterise the Stribeck curve quantitatively, in order to

compare different curves. This can be done by computing the coefficient of friction at boundary lubrication μ_0, and the position of the curve expressed by H_C (figure 1.4). The latter procedure, however, is only meaningful if the shape of the curve is constant. As will be shown by the results, presented in the following chapters, this is not always the case. In practise it is therefore better to present the so called transition points, the values of H at the transition from boundary to mixed lubrication (H_1), and the transition from mixed to hydrodynamic lubrication (H_0). This can be accomplished by plotting an S-shaped curve through the measured data. Originally an arctan function has been used [Emmens 1988] but following the recommendations of Ter Haar [Ter Haar 1996] a tan-hyp function is used here. Therefore the results presented here may differ somewhat from those published previously.

The actual fit used in this work is as follows:

$$\mu = \mu_0 . F + \mu_h . (1-F)$$
$$F = F(x) = \frac{1 - \text{tanhyp}\{B(x-C')\}}{2}$$
$$x = \log H, \quad C' = \log H_C$$
$$\mu_0 = \text{constant}, \quad \mu_h = C\sqrt{H}$$

(1.7)

where μ_0 is the coefficient of friction at boundary lubrication and μ_h the coefficient of friction at hydrodynamic lubrication. The expression for μ_h will be derived in chapter 4; occasionally a constant value is for μ_h is used instead. The values of μ_0, B, H_C and C are obtained as result of the fit. Note that ^{10}log is used in all calculations.
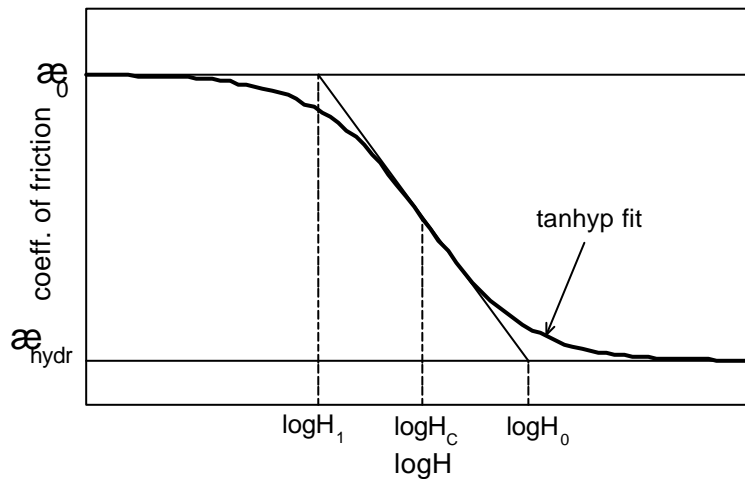
Figure 1.5 The transitions between the three regimes can be characterised by fitting the Stribeck curve with a tanhyp function, and calculating the intersection of three tangents. The values of H at the transition points are labelled H_0 and H_1.

From the tanhyp fit the transition points can be derived. These transition points are constructed by plotting the tangent of the tanhyp function in its bending point (H_C), and intersecting this line with the lines for boundary and hydrodynamic lubrication, as shown in figure 1.5. Using the formulation from (1.7) we obtain:

$$\log H_1 = \log H_C - \frac{1}{B}, \quad \log H_0 = \log H_C + \frac{1}{B} \qquad (1.8)$$

In the description of the results of the friction tests the expression 'the position of the Stribeck curve' is sometimes used as a numerical parameter. In that case any parameter establishing the position of the curve like the transition points H_0 and H_1 or the midpoint H_C can be used.

1.4.4 Hydrostatic lubrication

In the following hydrostatic lubrication is mentioned occasionally. This term refers to situations where some amount of lubricant is encapsulated in a certain area (cavity), which is totally enclosed by the roughness peaks of the two contacting surfaces. Under certain conditions such a cavity may be squeezed, resulting in a reduction of the volume available for the lubricant. Due to the limited compressibility of the lubricant, the pressure will increase. It does not matter if the squeezing of the cavity is caused by movement of one of the surfaces or not, because the pressure generated in the lubricant is determined by the compressibility of the lubricant, and not by the viscosity. These cavities are mostly micro-pockets, formed by the valleys of the roughness, although a similar mechanism has been proposed by Grahnert for macro-pockets caused by the overall geometry of the deep drawing process [Grahnert 1985].

1.5 TRIBOLOGY

Traditional tribology found its roots in problems encountered in drive systems and therefore much emphasis has been put on problems like the reduction of wear in bearings and gears. This origin still has its impact today, because many tribologists think in terms of concentrated contacts by default. Also mixed lubrication has been barely studied. If a system is lubricated, it is preferably designed in such a way that hydrodynamic lubrication occurs, thereby eliminating wear, and if a system is not lubricated it is clear that mixed lubrication can not occur at all. Recently more attention has been paid to mixed lubrication, e.g. to study phenomena which occur when in a hydrodynamically lubricated bearing the film becomes so thin that the asperities of the two surfaces touch each other. Surprisingly, only few of the studies on mixed lubrication have been carried out by performing actual friction experiments [Spikes 1996].

In general little attention is paid to flat surfaces, or more precisely: conformal surfaces. Not that these kind of tribological contacts do not occur, for example every brake surface is very conformal by nature. It has been noted that flat surfaces can generate a bearing ability in cases where classic hydrodynamic theory predicts that pressure build-up is impossible. The mechanisms for that are not fully understood yet [Lebeck 1987]. In deep drawing the main source of friction is the material being clamped in the blankholder and this type of contact is usually quite flat. Therefore the studies presented in this work will concentrate only on friction in flat contacts.

Deep drawing is an example of a manufacturing process. However, the tribology of manufacturing processes is not covered adequately by traditional tribology. There are some basic differences between the tribology of manufacturing processes such as deep

drawing and the problems dealt with by traditional tribology. These are:

- In many manufacturing processes, friction is necessary to control the process. In deep drawing, for example, friction in the blankholder is needed to control the movement in the tool and in cases where the friction in the blankholder is not sufficient, additional restraining elements like draw beads are placed in the tool! The aim of the tribology of manufacturing processes is therefore not to <u>minimise</u> friction, but to <u>control</u> friction.

- The two surfaces are only in contact once. In sheet metal forming, fresh sheet material is continuously fed into the tool, or in other words: one of the surfaces in the tribological contact has infinite length. Consequently there is almost no running in of the surfaces, the tool surface has to be in optimum condition from the very first operation.

- The material of the contacting surfaces cannot be chosen freely. Usually the nature of the material to be formed is fully prescribed by the application. In sheet metal forming the mechanical properties are prescribed and the desired surface roughness is determined by aspects like paint adherence, rather than by friction! Strictly speaking, the material of the tool can be chosen freely by the manufacturer. However, due to the demands of the process the choice is usually very limited. In sheet metal forming the tools are mainly made out of cast iron or hardenable tool steel, in some cases the tool is coated with a hard layer.

The material supplier has little control over the tribological aspect of the material being supplied. One of the possibilities is to change the surface roughness, but the roughness can be varied within a limited range only. Therefore the influence of surface roughness on friction is very important for the material supplier. An other possibility is to apply a special coating to the material. Again this possibility is very limited as in many cases the coating has to be removed from the material after forming to prevent interference with following treatments like painting.

1.6 HISTORICAL OUTLINE

The experiments described in this work span a period of fourteen years (1983-1997). It all started in 1982 when one of Hoogovens' customers complained of poor performance of a certain material during deep drawing. Inspection revealed that the mechanical properties were all within specifications, but the surface roughness differed from that of 'good' material. It has been realised then that there existed no knowledge of the influence of roughness on press performance of materials at that time. A review of literature showed that an influence of roughness in deep drawing had been noticed on several occasions, but without any consistency in the observations. Therefore it was decided to start a large research programme on the influence of friction, and the 32 variants of uncoated steel described in appendix A were produced. The actual deep drawing experiments on steel, as described in chapter 2, were performed in 1983-1985. These experiments showed that the influence of roughness revealed itself in all deep drawing experiments in the same way, so that further research could be done by performing dedicated friction tests. To that purpose a 'strip tester' has been built.

The friction tests on uncoated steel and coated steel were carried out in the years 1986 - 1988. These tests produced a consistent view of the influence of surface characteristics on friction of steel, and the friction model was developed in that period. Severe limitations of the strip tester were encountered during these tests and as a consequence a rotating tester was developed. Following this period, additional friction tests on coated steel were performed within Hoogovens R&D by other researchers [Dane 1994, Langerak 1996].

Research on aluminium started in 1994, at first with the aim of comparing the friction of MF and EDT roughness (EDT on aluminium was new at that time). Later a more detailed study of the friction of aluminium followed. In the meantime it had been noted that in deep drawing of aluminium, the punch force was sometimes totally independent of the blankholder force, indicating that the mechanism of friction of aluminium in deep drawing is fundamentally different from that of steel. Therefore more deep drawing experiments on aluminium have been carried out to study these phenomena. Some additional friction tests on steel were carried out as well to compare the results of both friction testers.

Parts of this work have been published before, mostly within the IDDRG, but often much less comprehensively as in this work. In chronological order:

- Emmens 1984: first results of deep drawing tests

- Emmens 1986a and 1986b: the results of the deep drawing tests on steel.

- Emmens 1987: results of preliminary friction tests on steel

- Emmens 1988: results of the friction tests with uncoated steel

- Emmens 1989: results of the friction tests with coated steel

- Emmens 1990b: overview of all work on steel

- Emmens 1991: presentation of limitations of strip testers, and the solution of the rotating tester

- Dane 1995: influence of jaw size on friction

- Emmens 1996: first results of the friction of aluminium

- Emmens 1997a: typical aspects of the deep drawing of aluminium

- Emmens 1997b: general overview of the behaviour of aluminium and in fact an abstract of this thesis

This work is linked to that of Vegter [Vegter 1991] in two ways.

Firstly, Vegter has used the results of the deep drawing experiments on steel to verify his deep draw simulation model. Vegter then found that the force transducer in the deep drawing tool has been poorly calibrated and the results of the deep drawing experiments in this work have been corrected according to his recommendations (the data can therefore differ from those published in 1986).

Secondly the friction model presented by Vegter is based on the friction model described in this work (section 4.3) which was originally published in 1988.

2 Deep Drawing experiments

ABSTRACT This chapter describes deep drawing experiments, both on steel and aluminium. These experiments have been carried out to see what the influence of friction is in real deep drawing. This has mostly been done by deep drawing materials with different levels and type of roughness, although other parameters have been varied as well. The results show great consistency. The friction in the tool affects the process (punch force) and the products being drawn (wrinkling, fracture, product dimensions). However there is a remarkable difference between steel and aluminium.

2.1 MATERIALS

2.1.1 Steel

For the deep drawing experiments special steel sheet with varying surface roughness has been produced. Normally, in steel for automotive applications the roughness is applied in a skin pass mill where the reduction of thickness is about 1 %. The roughness on the rolls is applied in such a way that after skin passing under normal conditions the roughness of the sheet falls within the range specified by the customer. These roughness ranges are standardised to a limited set of roughness grades which traditionally are characterised by the R_a values of the surface roughness. But this skin pass operation also influences the material properties, notably the yield stress and the hardening coefficient n. This has been taken into account by manufacturing the material in the following way.

Two slabs of continuously cast aluminium killed steel of 40 t each (one low carbon and one rephosphorised) have been produced for these experiments. The slabs have been hot rolled first, then cold rolled to a thickness of 0.80 mm and batch annealed in a conventional way (conventional in 1982!). The coils have then been cut into four parts each, and each part has been skin passed at a different roughness level with reductions varying from 0.4 % to 2.3 % (in four steps). In this way a total of 32 variants have been produced consisting of 2 material grades, 4 roughness grades and 4 different skin pass reductions. The roughness type was Shotblast. A complete list of mechanical properties has been given in appendix A; a summary of the most important properties is presented in tables 2.1 and 2.2.

Material grade	low-carbon	rephosphorised
Thickness (mm)	0.80	0.80
Yield stress (MPa)	150-200 (+)	230-260 (+)
Tensile strength (MPa)	320	390
r	1.7	1.5
n	0.19-0.24 (-)	0.18-0.23 (-)
Skin pass reduction (%)	0.44-2.34	0.32-2.11
Grain size (# ASTM)	8	10

Table 2.1. Overview of the most important mechanical properties of the materials used in the deep drawing experiments. A more detailed overview is presented in appendix A.
(+) and (-) indicate that the value increases or decreases with skin pass reduction.

Roughness grade	1	2	3	4
R_a (µm)	0.8-0.9	1.0-1.3	1.3-1.9 (+)	1.9-3.5 (+)
R_t (µm)	4.9-5.5	6.8-8.4	8.5-12 (+)	11-20 (+)
peak count (1/cm)	125-190 (+)	95-120 (+)	75-90	60-70

Table 2.2. Overview of the most important roughness data of the materials used in the deep drawing experiments. A more detailed overview is presented in appendix A. (+) indicates that the value increases with skin pass reduction.

In most tests only a selection from the 32 material variants has been used. The results described hereafter have been obtained with low carbon steel, unless otherwise stated.

Please note that for reasons of clarity the results of the experiments are presented as functions of the rated skin pass reductions. The actual skin pass reductions can be found in appendix A.

2.1.2 Aluminium

Of all the experiments described in this work, the deep drawing tests on aluminium were among the last to be carried out, almost 14 years since the first deep drawing experiments of steel had been started. In these tests aluminium with EBT roughness has been compared to aluminium with a 'normal' EDT roughness. The two materials with EBT roughness were experimental materials, with a roughness which may differ from what is normally used on steel. The experiments are included here not so much as to study the effects of EBT roughness, as to illustrate the different behaviour of aluminium in deep drawing operations compared to steel. Meanwhile however, some comments on the properties of EBT roughness can be made.

Two variants of EBT roughness have been produced in different periods, simply labelled as EBT1 and EBT2. When producing the first EBT material, part of the coil has been provided with an EDT roughness so that two materials were obtained with different roughness but exactly the same mechanical properties. The second EBT variant has been produced later, and the mechanical properties differ somewhat from the first variants, see appendix A.

2.2 EXPERIMENTAL PROCEDURES.

2.2.1 Steel

Experiments have been carried out both on a slow speed 600 kN laboratory press and on a large industrial 4100 kN hydraulic press. The punch speed on the large press was approximately 10 mm/s for the tests with a rectangular product, and 30 mm/s for the tests with cylindrical products, on the small press the punch speed was about 2 mm/s. A description of the parts and tools is given in appendix B.

A standard preservation oil (G6938) has been used as a lubricant (see appendix C for a description of the lubricants). The amount of lubricant applied has been varied to obtain two different modes of lubrication.
At first a large amount of oil has been applied to assure that the space between the work-

piece and the tool was completely filled with lubricant (full lubrication). This has been achieved by applying an overdose of oil to the tool before each pressing by means of a brush.

In the second case a small amount of oil has been applied to obtain sparse lubrication. This has been achieved by pressing without applying any (additional) oil; only the amount of oil which is normally present on cold rolled sheet for rust preventing purposes (in the order of 2 g/m²) served as a lubricant. The latter way of lubrication however has not been applied in all tests.

Hereafter, these two ways of lubrication are simply referred to as *rich* and *poor*. In the latter condition the sheet is not completely dry; pressing without any lubricant will cause severe galling after only a few parts.

The effects of material properties and process conditions are studied by examining the following themes:
- the forces acting on the product, represented by the punch force;
- the process limits, in particular as imposed by wrinkling and fracture;
- the product dimensions after drawing, in particular the flange width or diameter after drawing.

2.2.2 Aluminium

The deep drawing tests on aluminium have been carried out using the same large cylindrical tool as used for steel. In the tests two punch speeds have been used. As there is a strong interaction between the blankholder force and the speed in the press, the speeds were not constant for all products. The low speed varied between 5 mm/s and 8 mm/s, the high speed between 35 mm/s and 58 mm/s. The difference between the speed ranges however is large enough to justify a conclusion about the influence of speed.

Again two ways of lubrication have been used. While aluminium has been supplied without any oil the 'poor' lubrication had to be obtained in a way different from that for steel. N6130 has been used as a lubricant.

The richly lubricated condition has been obtained by supplying an overdose of lubricant on the sheet. The poorly lubricated condition has been obtained by distributing a limited amount of oil evenly over the sheet surface and then wiping the sheet with a dry cloth. The tool has also been wiped clean after each experiment. This way of lubrication is not very reproducible; a little too much lubricant immediately reduces the friction in the blankholder. However the influence of the amount of lubricant can be studied satisfactorily in this way.

2.3 RESULTS FOR A BENT STRIP (STEEL)

At an early stage of the research programme, drawing of strips has been performed in a conventional cylindrical deep drawing tool to simulate the movement of material in a blankholder without much plastic deformation. Unintentionally these were the first strip tests in the whole research programme, but that name was still unfamiliar at that time. These tests are not without danger for the tool, because the blankholder is not supported along the whole circumference but only at a small section, and thus it is subjected to a bending force. The strip has been drawn out of the blankholder as a flange of a normal

deep drawn product.
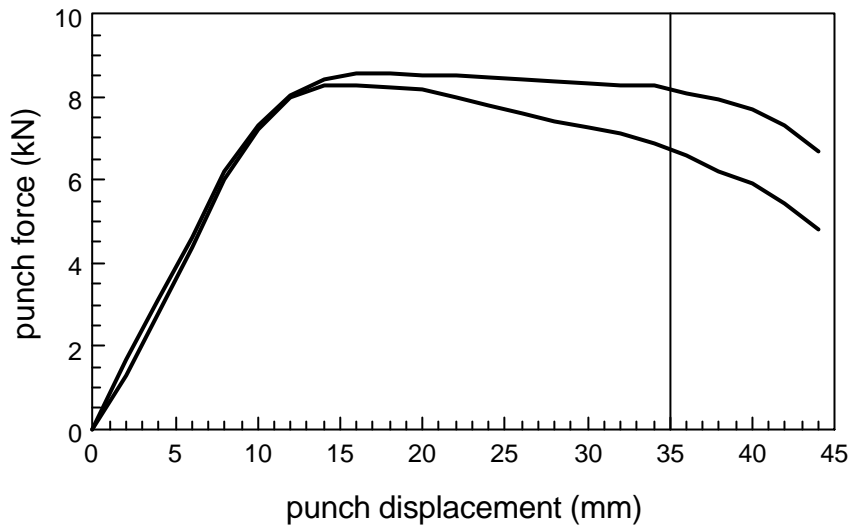
Figure 2.1. Two examples of force displacement curves obtained with the bent strip showing that the influence of roughness depends on the amount of punch displacement. Top curve: material A1L (high roughness), bottom curve material D3L (low roughness), low carbon steel.

The results showed that the force-displacement curves had been influenced by the material roughness in an unexpected way. The different roughness grades (see appendix A for roughness data) did not just give an increase or a decrease of the punch force indicating a difference in friction. It turned out that the influence of the surface roughness was not constant, but varied during the punch displacement as shown in figure 2.1.

Figure 2.2. Punch force at 35 mm punch displacement (left), and maximum punch force (right) for the bent strip, as a function of material parameters, low carbon steel. Blankholder force: 20 kN.

To analyse this phenomenon, the measured maximum punch force and the punch force at a punch displacement of 35 mm have been presented in figure 2.2. It can be seen that in general both an increasing skin pass reduction and an increasing roughness grade lead to

an increasing punch force, despite the scatter in the results. We may expect that this effect on the punch force also has an effect on the product dimensions. A higher punch force means that there is a higher load on the wall of the product being drawn, which may result in a higher strain (note that the wall is in a state of plastic deformation). This effect may thus influence the dimensions of the final product, as characterised by the product height (for fully drawn products without a remaining flange) or the flange dimensions (for not fully drawn products with a remaining flange).

This is illustrated in figure 2.3 where the remaining flange width after drawing has been presented (all strips have been drawn to the same height). The influence of the roughness grade is similar to that observed in the punch force, the influence of skin pass reduction however is the opposite of the effect found in the punch force.

To avoid the additional plastic deformation caused by rounding of the strip against the punch, the tests have also been carried out with a square punch. However, this lead to fracture of the die, so that these tests were abandoned.
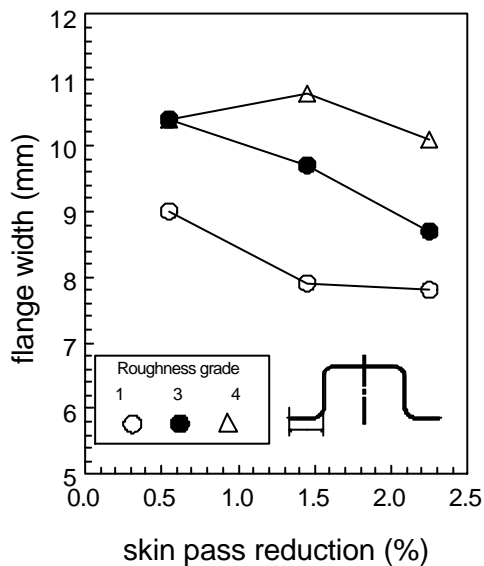
Figure 2.3. Remaining flange width after drawing of the bent strip as a function of material parameters, low carbon steel. Blankholder force: 20 kN.

Figure 2.4. Maximum punch force for the small cylindrical product as a function of material parameters, low carbon steel. Blankholder force: 40 kN.

2.4 RESULTS FOR A SMALL CYLINDRICAL PRODUCT (STEEL)

Using the same tools as used for the bent strip, cylindrical products have been drawn in a conventional way (so-called Swift cups). As can be seen in figure 2.4 the influence of the roughness grade was not clear. Probably the size/thickness ratio of this product is too small to make it sensitive to variations in friction.

2.5 RESULTS FOR A LARGE CYLINDRICAL PRODUCT (STEEL)

Further deep drawing tests have been carried out on larger products which are more sensitive to variations in friction. In these tests also the amount of lubricant has been varied

as described in section 2.2.

The results for aluminium products made with this tooling are described separately in section 2.7.

2.5.1 Tests with low carbon steel

2.5.1.1 <u>Punch</u> <u>force</u>
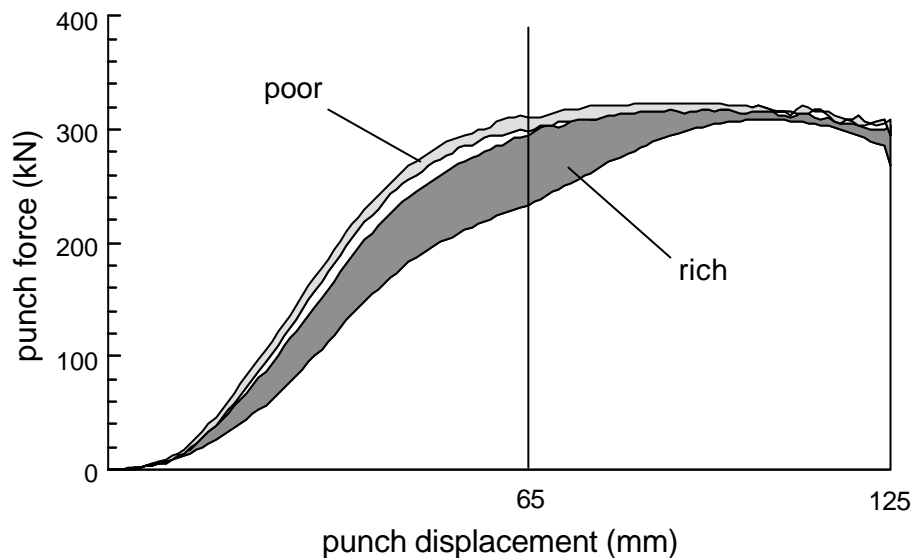
Figure 2.5. Lowest and highest force displacement curves obtained for the large cy-lindrical product for each lubrication system (poor or rich lubrication), showing the range in punch forces for all low carbon steel materials. Blankholder force: 400 kN.

The tests on the large cylindrical product showed similar results as the bent strip, to that extent that the influence of friction also depends on the punch displacement. This is il-lustrated in figure 2.5. Similar to the experiments with the bent strip, both the maximum punch force and the punch force at a punch displacement where the influence of the roughness is at a maximum have been determined and are presented in figure 2.6. The left-hand diagram shows that an influence of roughness is observed only when there is sufficient lubricant. If not, the punch force increases and the influence of roughness is reduced. When there is sufficient lubricant available, the punch force increases with in-creasing roughness grade as well as with increasing skin pass reduction. These results can also be interpreted in an other way: for materials with a high roughness there is only a small influence of lubrication, for materials with a low roughness there is a large influ-ence of lubrication. The right-hand diagram shows that the maximum punch force does not depend (much) on either roughness, lubrication condition or skin pass reduction.

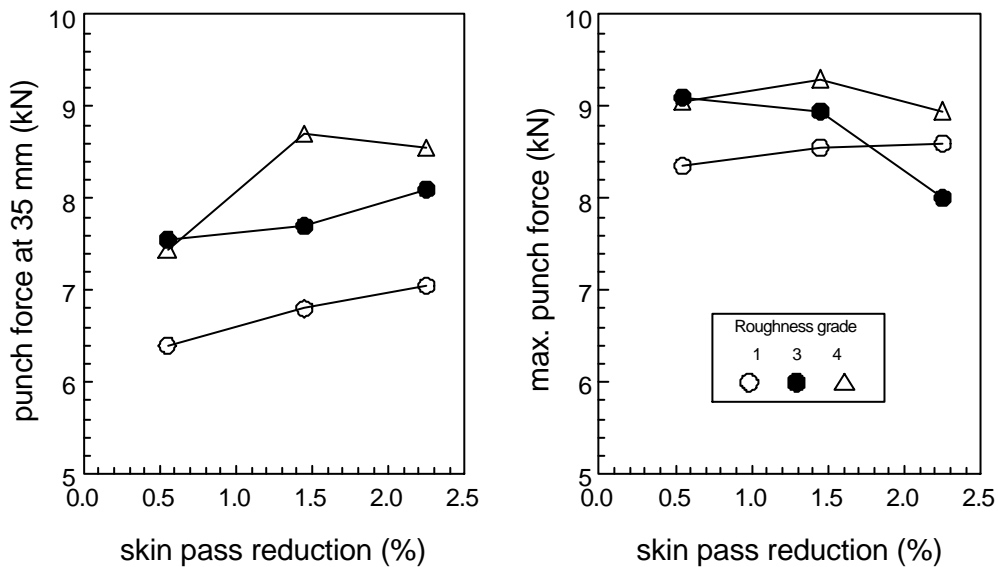2.5.1.2 <u>Working</u> <u>range</u>

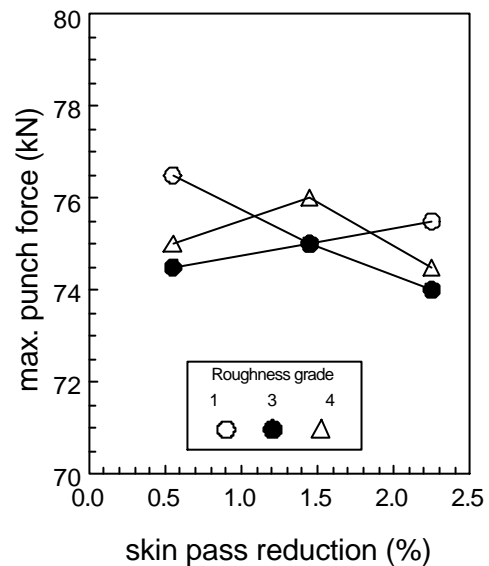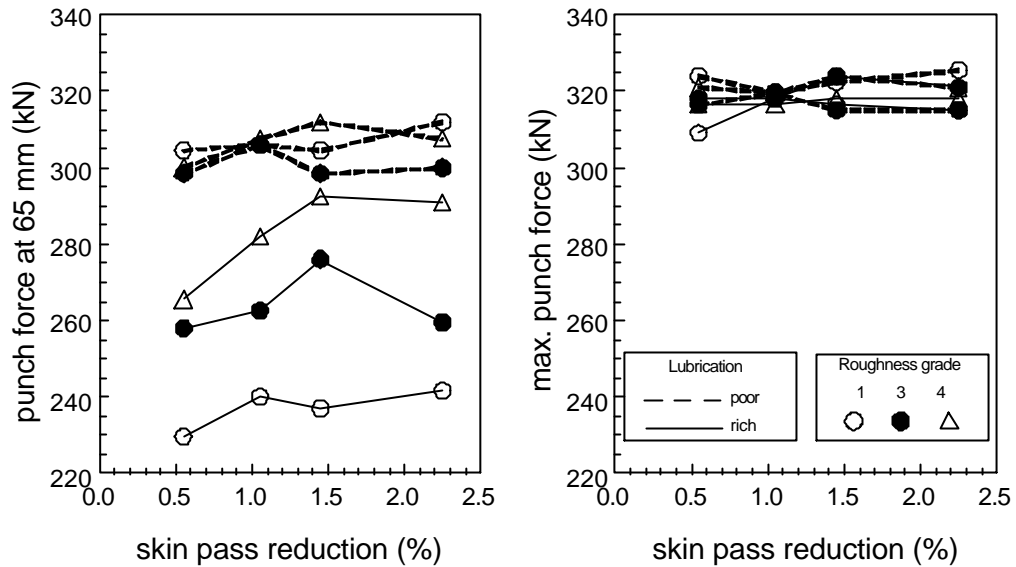*Figure 2.6. Punch force at 65 mm punch displacement (left), and maximum punch force (right) for the large cylindrical product, as a function of material parameters, low carbon steel. Blankholder force: 400 kN.*
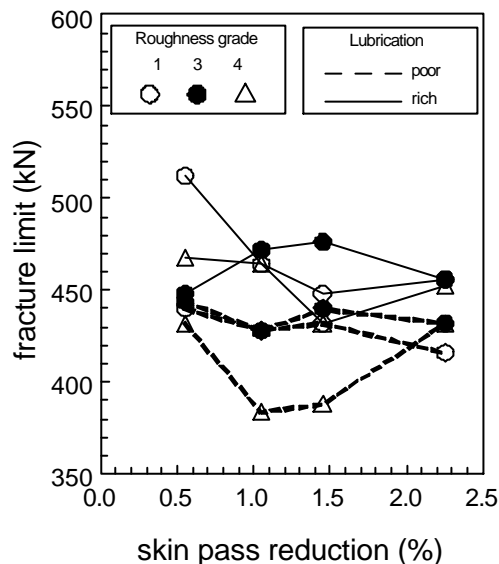
Figure 2.7. Fracture limit (the maximum allowable blankholder force for making a good product), as a function of material parameters for the large cylindrical product, low carbon steel.

A practical consequence of the effects shown in figure 2.6, left, is a possible change of the working range. This latter is defined as the range of blankholder force in which a good product can be made. This range is limited at the lower end by wrinkling of the product (wrinkling limit) and at the upper end by fracture of the product (fracture limit). It turned out to be impossible to quantify the wrinkling for this product, therefore the possible effects on the wrinkling limit could not be determined. The fracture limit, however, has been determined for all materials without much problems and is presented in figure 2.7. There is not much influence of roughness grade or skin pass reduction, only an influence of the amount of lubricant can be observed. This is not so surprising, because the fracture limit is related to the maximum punch force, and for that parameter as

well no influence of roughness grade or skin pass reduction has been observed (figure 2.6, right). An exception is the influence of lubrication: on the average the poorly lubricated condition gives lower fracture limits although there is no influence of lubrication on the maximum punch force.

2.5.1.3 Product dimensions
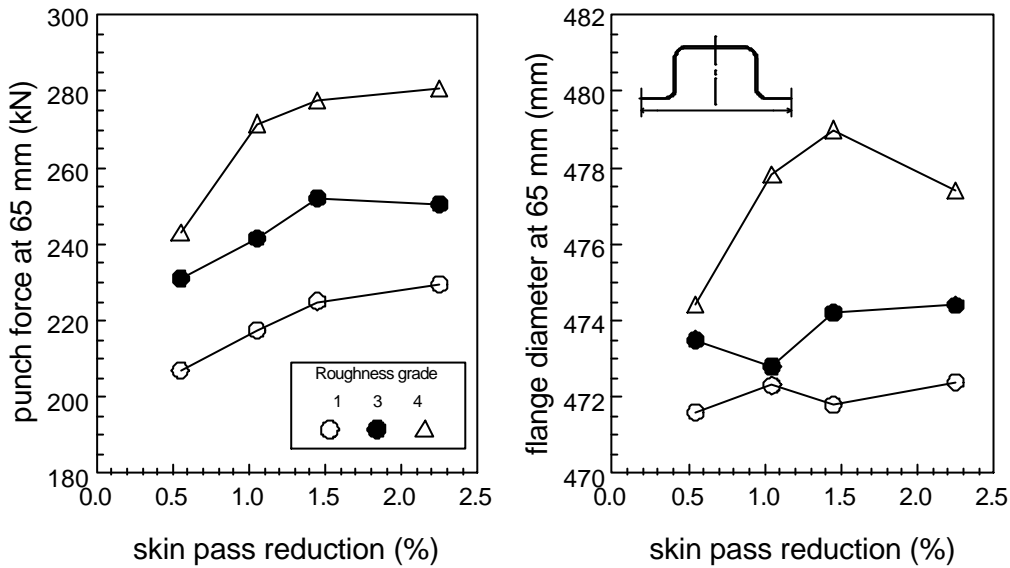
Figure 2.8. Punch force and remaining flange diameter after drawing of the large cylindrical product at 65 mm as function of material parameters, low carbon steel. Blankholder force: 400 kN.
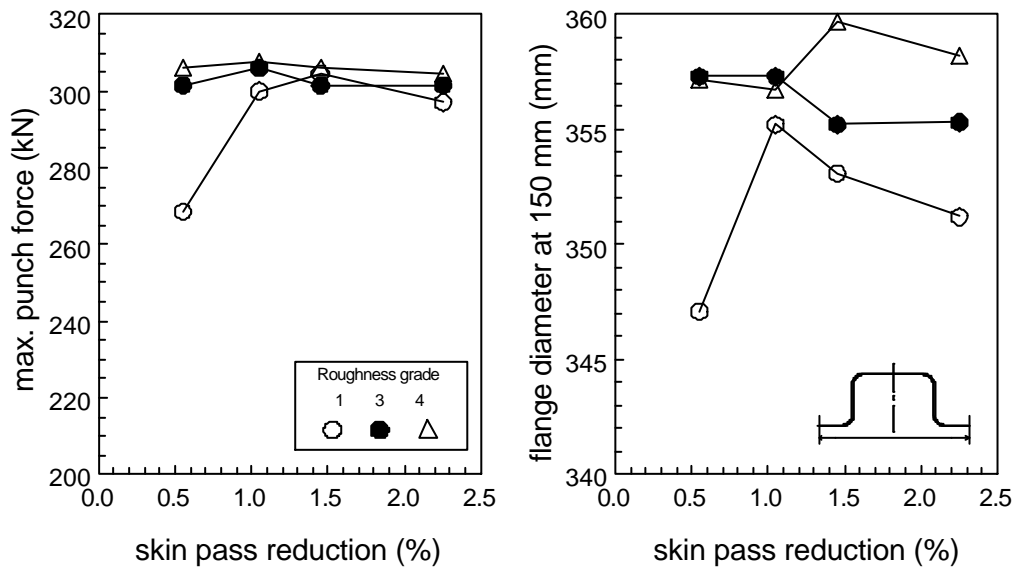
Figure 2.9. Maximum punch force and remaining flange diameter after drawing of the large cylindrical product at 150 mm as a function of material parameters, low carbon steel. Blankholder force: 400 kN.

Additional tests have been carried out to study the effects of roughness in more detail. In these tests products have been drawn in the richly lubricated condition from blanks on

which a circular grid has been applied. These blanks have been drawn to a height of 65 mm (where the influence of roughness is greatest) and to a height of 150 mm, which corresponds to an almost completely drawn product. The punch force and remaining flange diameter at a height of 65 mm are presented in figure 2.8. There is a good correlation between the flange diameter and the punch force.

The maximum punch force and the remaining flange diameter for a product height of 150 mm are presented in figure 2.9. As in figure 2.6, right, no influence of roughness is visible in the maximum punch force, while in the flange diameter the influence of roughness is still visible but with highly scattered results. The influence of skin pass reduction is no longer clear.

The products have been measured to see if the differences in flange diameter could be related to differences in strain in the product. The differences in flange diameter for a product height of 65 mm were about 1% of the original blank diameter. Since this is of the same order of magnitude as the accuracy of strain measurements by means of the circular grid method, any effect could only be seen if the difference in (total) strain is localised in some part. This however was not the case. Within the accuracy of the measurement, no significant differences between the materials could be observed. This indicates that the extra strain in the product, caused by higher friction and expressing itself in a larger flange diameter, was more or less uniform over the entire product.

2.5.1.4 Friction factor.

For a limited set of materials the friction factor, defined in section 1.2.3, has been determined. Two materials have been selected for these calculations, one with a low roughness (B1L) and one with a high roughness (A4L). These two materials have been specially chosen because friction tests have also been carried out on these materials (see next chapter). The relation between punch force and blankholder force is presented in figure 2.10, both for the maximum punch force and for the punch force at 65 mm punch displacement. The maximum punch force (bottom figure) shows the same relation for all four presented systems. For the punch force at 65 mm punch displacement (top figure), the relation at poorly lubricated condition is the same as for the maximum punch force. For richly lubricated conditions however the punch force is lower, and even more for low roughness. It is also important to notice that in all situations the relation between punch force and blankholder force is linear.

	lubrication:	rich		poor		
	punch force:	smooth	rough	smooth	rough	materials
cylindrical pr.	at 65 mm	0.058	0.092	0.126	0.122	B1L,
low carbon steel	maximum	0.134	0.130	0.135	0.138	A4L
cylindrical pr.	at 65 mm	0.050	0.048	0.094	0.100	A1R,
rephosph. steel	maximum	0.092	0.074	0.112	0.121	A4R
rectangular pr.	at 30 mm	0.068	0.088	0.132	0.138	B1L,
low carbon steel	maximum	0.094	0.082	0.136	0.143	A4L

Table 2.3. Friction factor for different systems, steel.

From the curves of figure 2.10 the friction factor has been calculated, using a simple linear regression. The results are presented in table 2.3, together with results from other

tests.
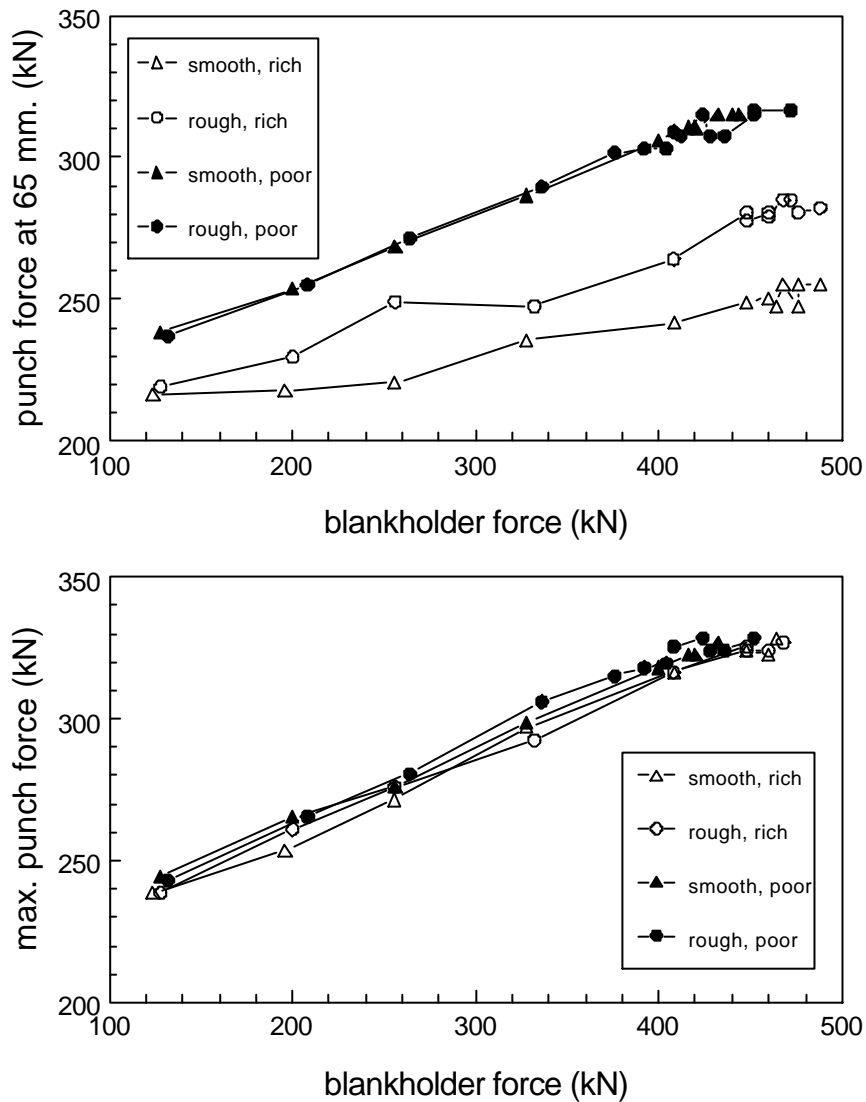
Figure 2.10. Relation between punch force and blankholder force for material with different roughness, and different lubrication conditions. Large cylindrical product, low carbon steel. Materials: B1L and A4L.

2.5.1.5 <u>Tests</u> <u>with</u> <u>thick</u> <u>material</u>

A further study of this effect has been made by drawing a thick material (3.0 mm thickness, code CR3, see appendix A) which resulted in a similar size/thickness ratio as for the small cylindrical products.
It is evident that the resulting punch forces are much larger then those found when drawing thin sheet. Thus, in figure 2.11 the punch force results are presented on arbitrary scales, chosen in such a way that the resulting curves for thin material and thick material lie in the same area of the diagram. In this figure the results for the thick material are compared to those obtained for material C1L, which has comparable roughness and mechanical properties.
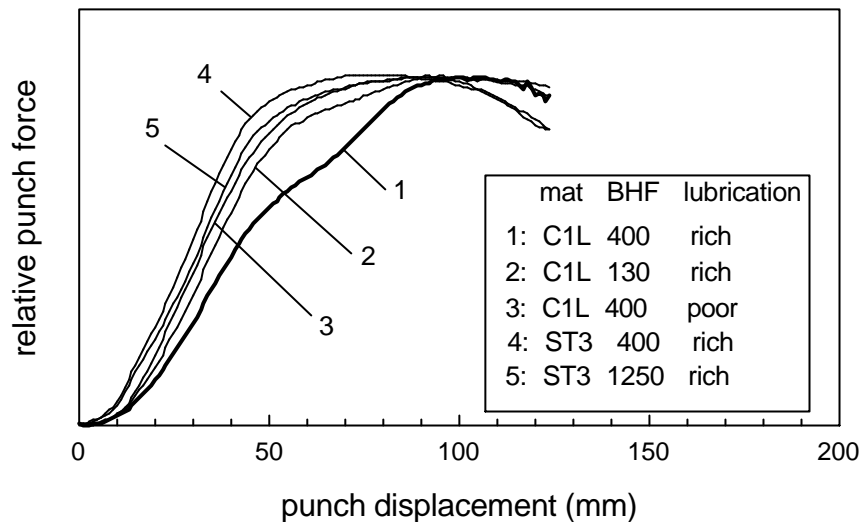
Figure 2.11. The influence of some parameters on the typical shape of the force-displacement curves, low carbon steel. The legend gives: material, blankholder force in kN (BHF), amount of lubricant.

With a (relatively) high blankholder force and much lubrication, material C1L exhibits a characteristic 'dent' in the force-displacement curve (curve 1). Lowering the blankholder force reduces but does not completely remove the dent (curve 2). Reducing the amount of lubricant results in disappearance of the dent (curve 3). Increasing the material thickness (curve 4) also reduces the dent, but increasing the blankholder force approximately proportional to the thickness, does not restore the dent in the force-displacement curves (curve 5).

The dent in the force-displacement curves is caused by phenomena which are yet unknown, but we may conclude now that these phenomena reduce or disappear when:

- the blankholder force is reduced;
- the amount of lubricant is reduced;
- the material thickness is increased.

The observed influence of blankholder force and amount of lubricant indicate that these phenomena are, at least partially, related to friction.

2.5.1.6 Tests with different blank sizes

A final analysis of the influence of roughness on the punch force has been made by drawing products of different blank diameters with an overdose of lubricant and using different blankholder forces for two materials, which represent more or less the extremes in roughness, i.e. materials B1L and A4L. The force-displacement curves obtained are presented in figure 2.12. Note that due to variations in the process, the curves for the two materials intersect at some points, while on the basis of the results presented above they are not supposed to do so. Comparing the pairs of curves provides information about the influence of roughness on the force-displacement curves. This effect is not constant for all punch displacements: there are areas where there is a large influence of roughness and there are areas of smaller influence. A striking result however is that the position of these areas seems to be independent of the blank size.

The first area of large influence occurs at a punch displacement of 40 - 80 mm. Here the

roughness effect is similar to that observed in previous tests, the results of which are shown in figure 2.6, left. For the lower blank diameter (440 mm), the influence of roughness is largest at low blankholder forces, while for the larger blank diameters the influence of roughness is greatest at high blankholder forces.

A second area of large influence of roughness occurs at punch displacements of 110 - 160 mm. This is clearly visible for the blank diameter of 600 mm, and, to some extend, also for the 520 mm diameter. The blanks of 440 mm diameter have not been drawn deeply enough to see this area. This second area results in force-displacement curves with a double maximum for low roughness materials.

A third area of large influence seems to emerge at a punch displacement of 200 mm, but this is not very clear.
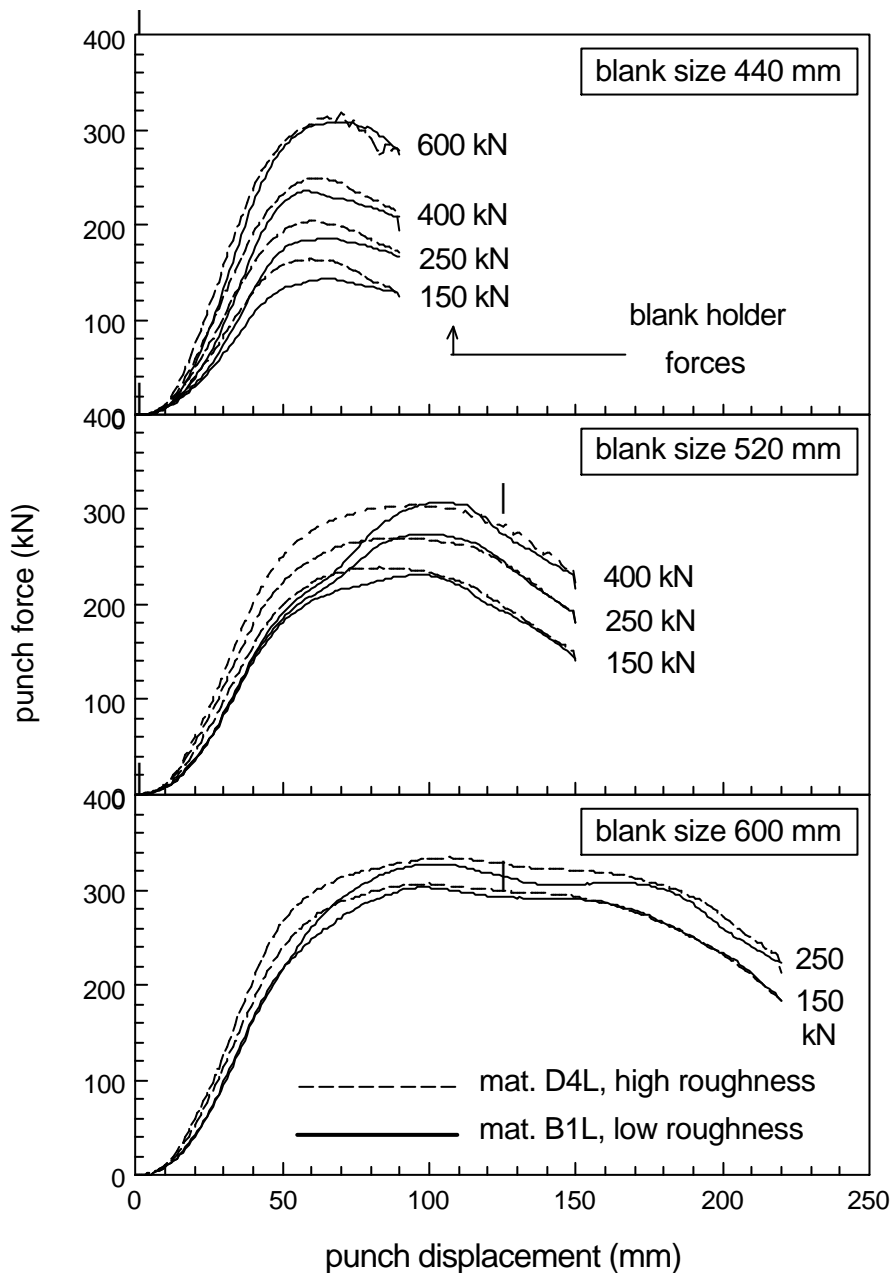
Figure 2.12. Comparison of force-displacement curves of a rough and a smooth material showing the influence of blank diameter and blankholder force on the punch force, low carbon steel.

2.5.2 Tests with rephosphorised steel

The test programme reported in section 2.5.1 for low carbon steel has been repeated with rephosphorised steel, but less extensively.

2.5.2.1 <u>Punch force</u>
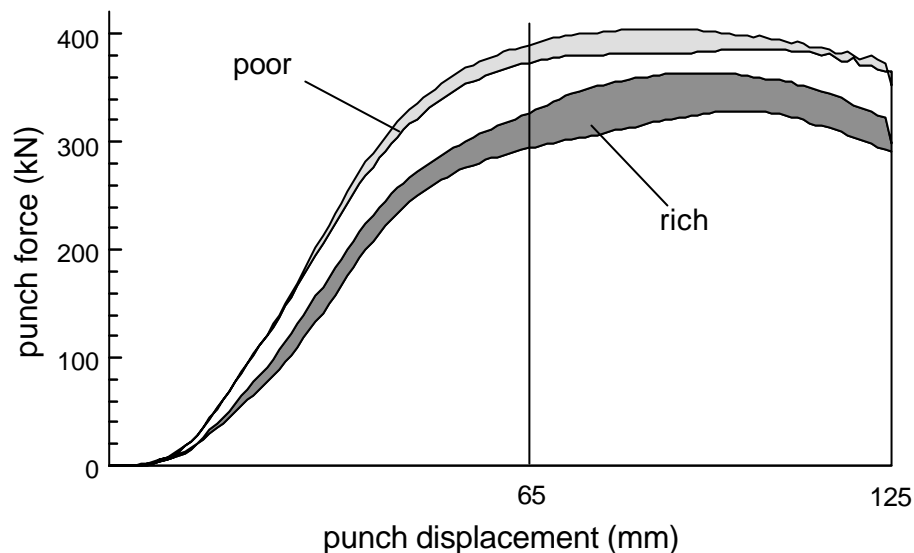
Figure 2.13. Lowest and highest force displacement curves obtained with the large cylindrical product for each lubrication system (poor or rich lubrication), showing the range in punch forces for all rephosphorised steel materials. Blankholder force: 400 kN..

The range of blankholder forces for the two lubrication systems is presented in figure 2.13 which may be compared with figure 2.5. Again we can see that with little lubricant the influence of roughness on the punch force is smaller than with much lubricant. With an overdose of lubricant the force-displacement curves also show the typical dented shape as observed for low carbon steel. However the areas of larger and smaller influence of roughness no longer exist, i.e. roughness affects the curves more uniformly. The only influence of roughness on the shape of the curve is that with insufficient lubricant supply and - thus - at high friction forces, the maximum of the curve is slightly shifted to smaller punch displacements.

The measured maximum punch forces and the punch force at 65 mm displacement are presented in figure 2.14. The punch force at 65 mm displacement has lost its significance with rephosphorised steel, but it is presented here to allow a comparison with the results for low carbon steel. Both punch forces show very much the same influence. Contrary to the results found with low carbon steel, the influence of lubrication is now clearly visible in both diagrams, i.e. less lubricant leads to a higher punch force. The influence of roughness grade is somewhat confused by the scatter in the data but in general a higher roughness results in a higher punch force. An effect of skin pass reduction cannot be clearly distinguished because of the scatter.
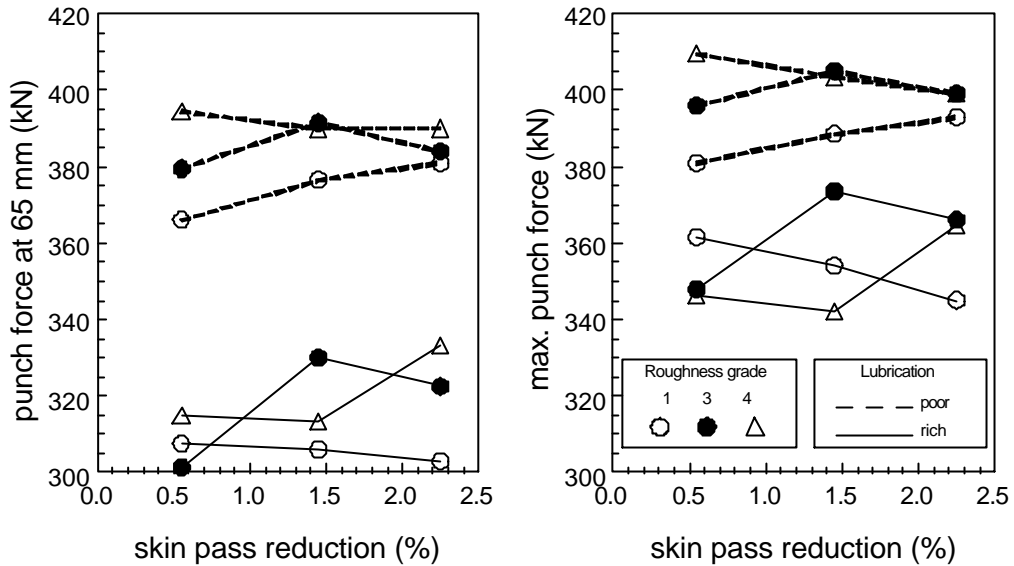
Figure 2.14. Punch force at 65 mm punch displacement (left), and maximum punch force (right) for the large cylindrical product, as a function of material parameters. Blankholder force: 400 kN. Rephosphorised steel.

2.5.2.2 Product dimensions

The flange diameter which remains after drawing is presented in figure 2.15. There is a satisfactory correlation with the measured (maximum) punch force.
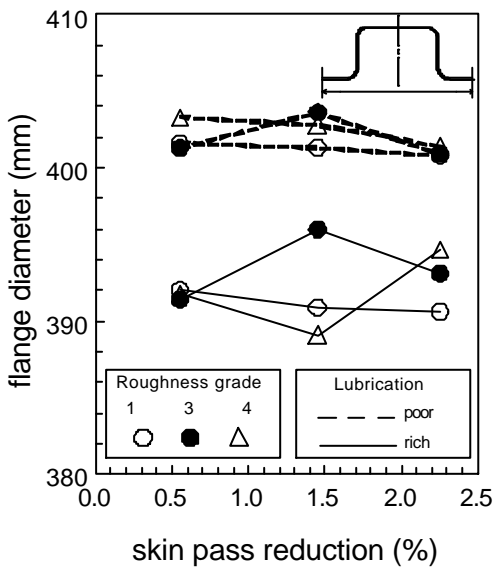
Figure 2.15. Remaining flange diameter after drawing of the large cylindrical product as function of material parameters. Blankholder force: 400 kN. Rephosphorised steel.
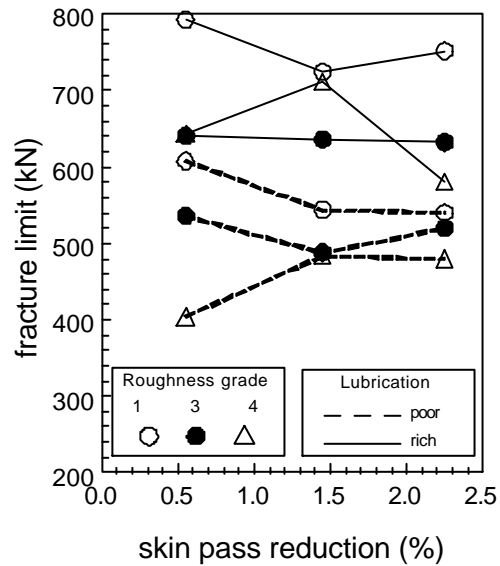
Figure 2.16. Fracture limit defined here as the largest blankholder force for making a good product of 90 mm height, for the large cylindrical product as function of material parameters. Rephosphorised steel.

2.5.2.3 Working range

The fracture limit has been determined in a way different from that for the low carbon steel. For the low carbon steel the fracture limit has been determined for each material by making many products with different blankholder forces, increasing the force by small increments. For the rephosphorised steel only two products have been drawn until fracture, with different blankholder forces, after which the relation between the blankholder force and the product height at fracture has been determined. The maximum blankholder force at which a product can be drawn to a height of 90 mm has then been calculated by linear interpolation. These results are presented in figure 2.16. The influence of lubrication and roughness grade can be correlated with the results already obtained for the punch force. There is also a clear influence of the amount of lubricant, contrary to the results for low carbon steel. In general it can be concluded that effects which lead to increasing punch force cause a reduction of the fracture limit.

2.5.2.4 Friction factor
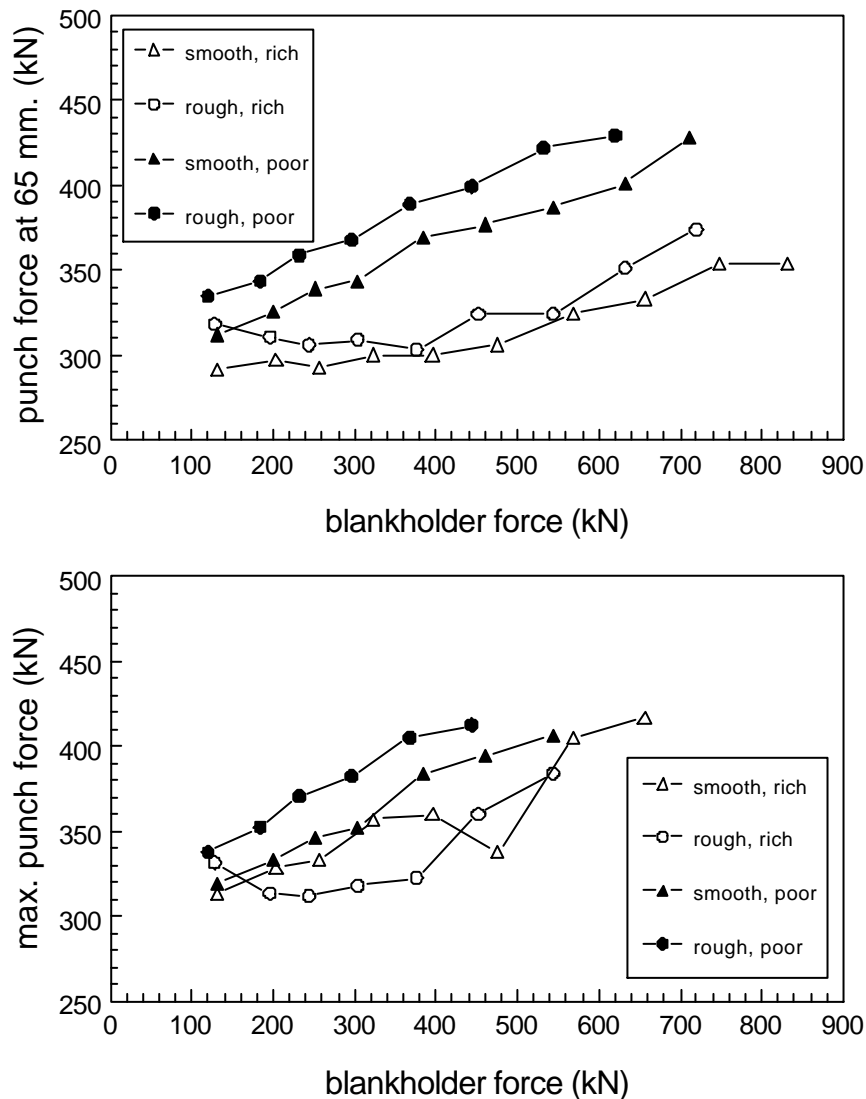
Figure 2.17. Relation between punch force and blankholder force for material with different roughness, and different lubrication conditions. Large cylindrical product, rephosphorised steel. Materials: A1R and A4R.

For a limited set of materials the friction factor has again been determined. However, the two materials for which friction data are available have not been used in the deep drawing experiments, so two similar materials have been selected (A1R and A4R). The relation between punch force and blankholder force is presented in figure 2.17, both for the maximum punch force and for the punch force at 65 mm punch displacement. Contrary to what has been found for low carbon steel, an influence of both roughness and lubrication condition is visible in the results. Note that the curves are not very straight.

From the curves the friction factor has been calculated using a simple linear regression and the results are presented again in table 2.3. The calculated data for rephosphorised steel are lower than for low carbon steel under the same conditions.

2.6 RESULTS FOR A LARGE RECTANGULAR PRODUCT (STEEL)

In addition to the cylindrical product tests have also been carried out with a large rectangular product (see appendix B for dimensions). This product has been treated very similarly to the cylindrical product. However, the tool for the cylindrical product had a force transducer built in the punch and the tool for the rectangular product had not, therefore the punch force had to be measured in a different way. For the rectangular product the force has been measured indirectly, using the oil pressure in the hydraulic system. Unfortunately this method results in higher scatter.

2.6.1 Punch force
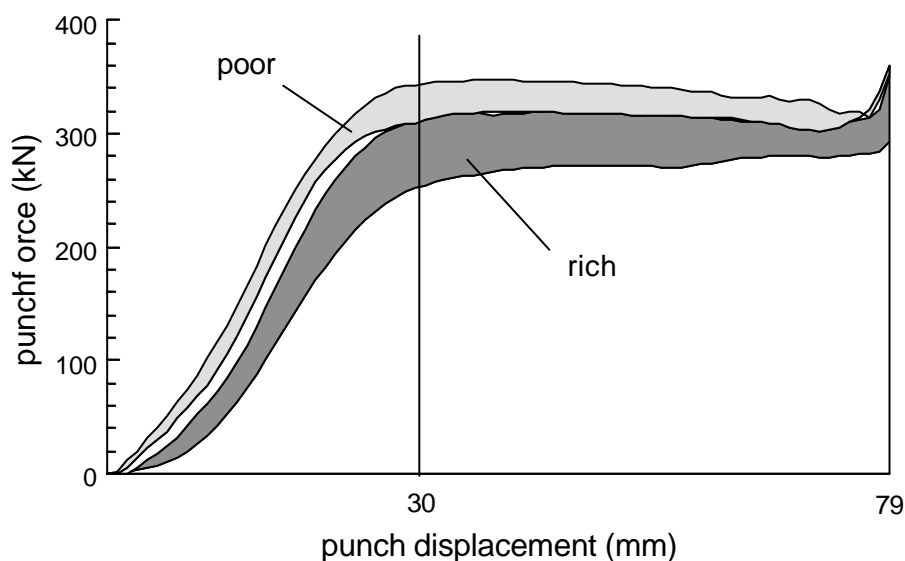
Figure 2.18. Lowest and highest force displacement curves obtained with the large rectangular product for each lubrication system (poor or rich lubrication), showing the range in punch forces for all low carbon steel materials. Blankholder force: 560 kN.

The range of punch forces is given in figure 2.18. The raise of the punch force at the end of the punch stroke is caused by the pressing of the stiffening rill (see figure B.1 in appendix B). The range in punch force is largest at a punch displacement of 30 mm. Therefore the punch force at this position, together with the maximum punch force, is presented in figure 2.19. Due to the large scatter in the data, the values in figure 2.19 have

not been obtained on a single product, but have been obtained by a regression analysis of the relation between punch force and blankholder force. The influence of roughness and lubrication is clear: the punch force increases with increasing roughness grade and decreasing amount of lubricant. The influence of skin pass reduction is less evident, there is some tendency for the punch force to increase with increasing skin pass reduction, notably with much lubricant.
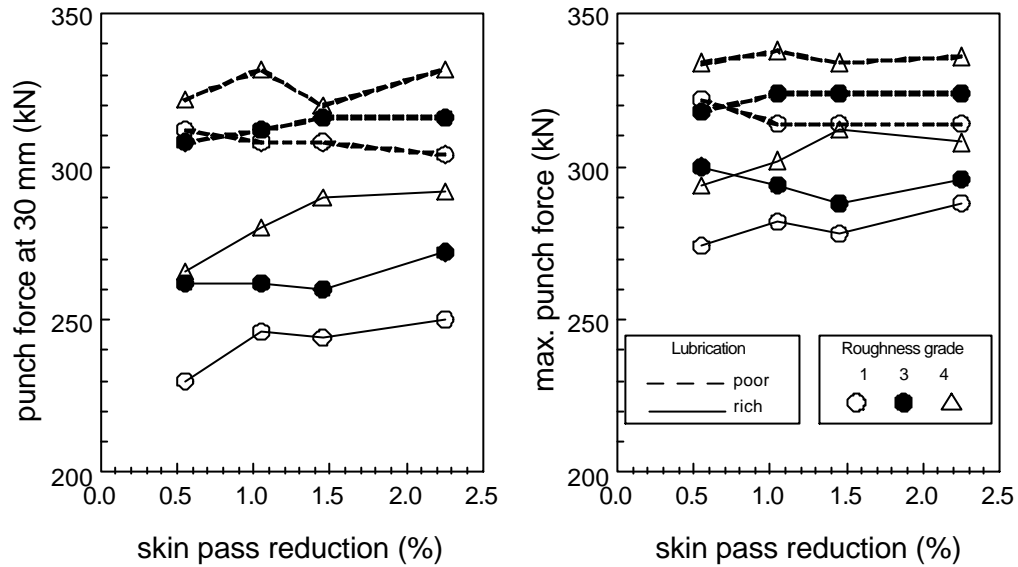
Figure 2.19. Punch force at 30 mm punch displacement (left) and maximum punch force (right) for the large rectangular product, as a function of material parameters, low carbon steel. Blankholder force: 560 kN.

2.6.2 Product dimensions
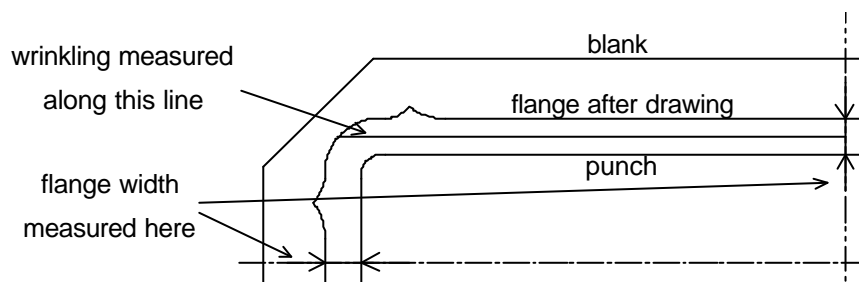
Figure 2.20. Shape of punch, blank and flange after drawing, with the positions of flange width and wrinkling measurements. Only one quarter of the product is drawn here. Drawing not to scale.

The product dimensions after drawing were more difficult to characterise because the flange width varied along the perimeter of the product as shown in figure 2.20. The flange width at the centres of the sides has been measured; the results are presented in figure 2.21. The effects on the flange width at the long side are very similar to what is found for the cylindrical product, both little lubricant and high roughness result in a larger flange width. For the flange width at the short side the situation is different. The influence of roughness is confused by the scatter, but the influence of lubrication is opposite to what has been observed on cylindrical products: little lubricant results in a smaller

flange width.
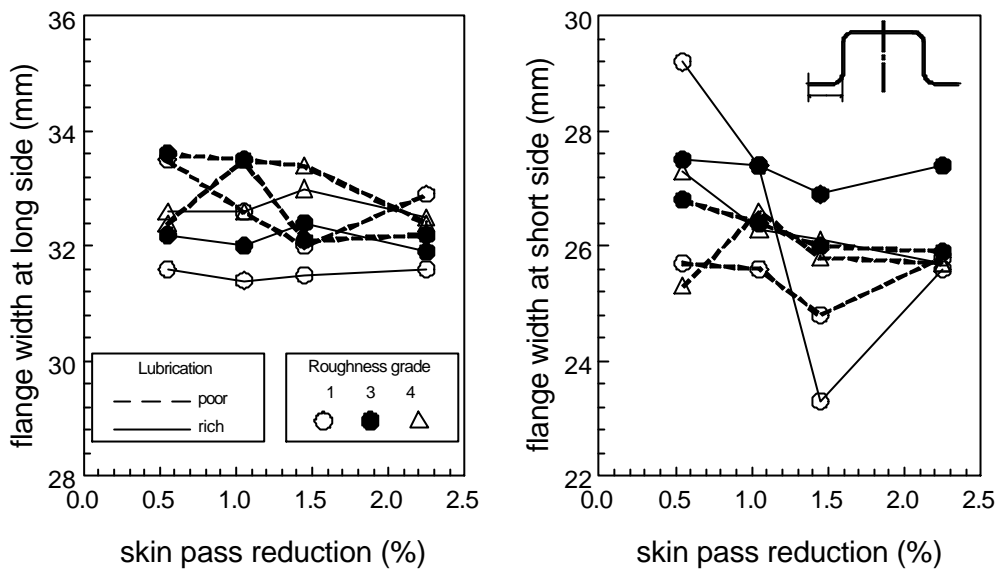
Figure 2.21. Flange width at the centre of the long side (left) and the short side (right) for the large rectangular product, as a function of material parameters, low carbon steel. Blankholder force: 560 kN.

2.6.3 Working area
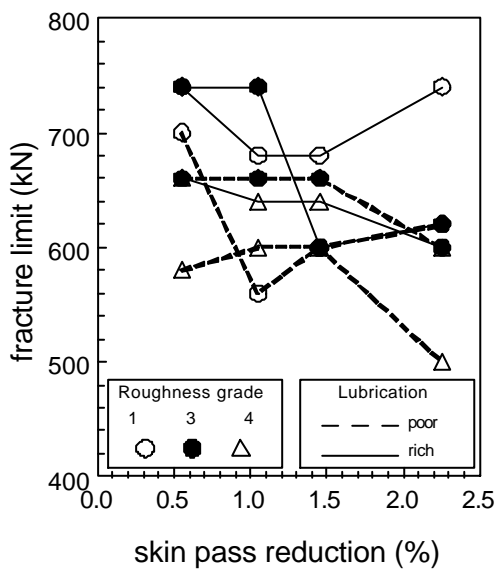
Figure 2.22. Fracture limit for the large rectangular product, as a function of material parameters, low carbon steel.
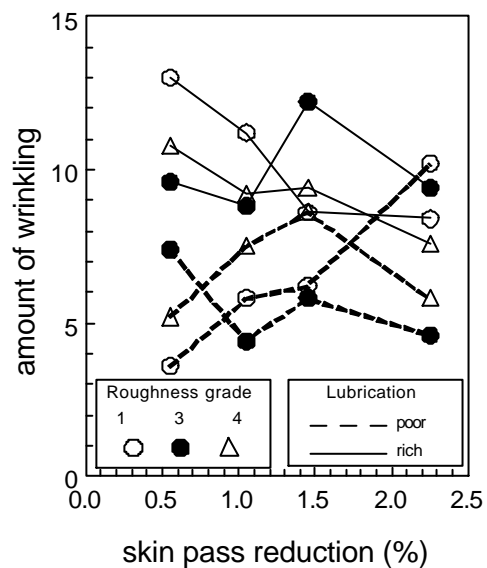
Figure 2.23. Amount of wrinkling in arbitrary units (see text) at the long side of the large rectangular product, as a function of material parameters, low carbon steel. Blankholder force: 560 kN.

Contrarily to cylindrical products, fracture occurs very gradually in rectangular products. The occurrence of fracture generally has a minor influence on the punch force and can only be observed afterwards. The fracture limit has been determined in the conventional way (by pressing numerous products); the results are presented in figure 2.22. There is

no influence of roughness or skin pass reduction, only a slight influence of lubrication: little lubrication results in a lower fracture limit.

The wrinkling behaviour of rectangular products differs fundamentally from that of cylindrical products. To study this, the degree of wrinkling has to be quantified but this is not as simple as it may seem. A suitable procedure must rate a few large wrinkles equal to a large number of small wrinkles. The following procedure was customary at Hoogovens at that time. The contour of the flange is measured and recorded on an X-T recorder, so that a 'cross-section' is obtained. The amount of wrinkling is then calculated by adding all individual top-valley heights of the flange profile. From the resulting sum the square root is taken, merely to obtain a more 'linear' result for convenience without physical meaning. The actual positions on the flange where the recordings have been made are presented in figure 2.20. The results for the long side are presented in figure 2.23. Again only lubrication has a significant influence of lubrication: much lubricant results in more wrinkling.
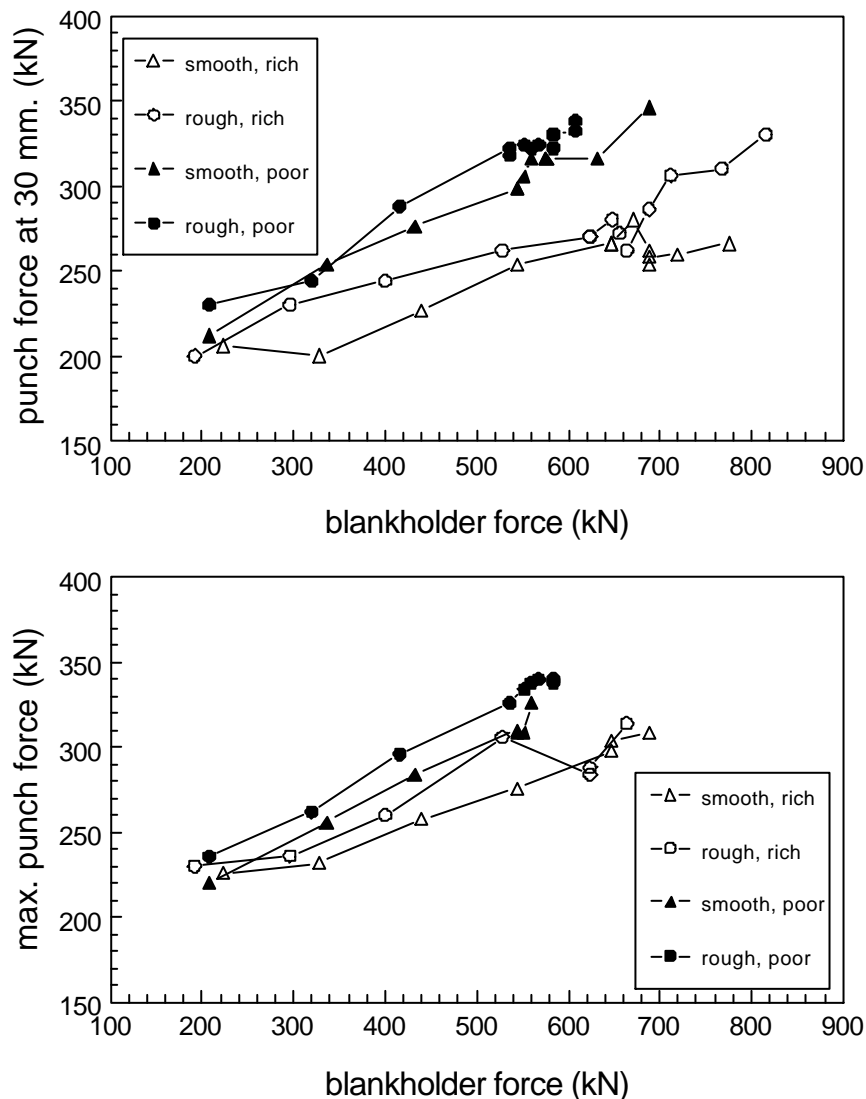
Figure 2.24. Relation between punch force and blankholder force for material with different roughness, and different lubrication conditions. Rectangular product, low carbon steel. Materials: B1L and A4L.

2.6.4 Friction factor

For the rectangular product the friction factor has also been determined for some materials. The same materials have been used as for the cylindrical product, i.e. B1L and A4L. The relation between punch force and blankholder force is presented in figure 2.24, both for the maximum punch force and for the punch force at 30 mm punch displacement. The results show more scatter than for the cylindrical product, but, to a first approximation, the relation between punch force and blankholder force can be considered linear. An influence of both roughness and lubrication condition is visible in the results, but not as clearly as in figure 2.17.

From the curves the friction factor has been calculated using a simple linear regression, the results are presented again in table 2.3. For the poor lubrication system the results show a good agreement with the data for the cylindrical product. Evidently, despite the difference in geometry of the product, the friction factor for situations of sparse lubrication is the same if the same materials (and lubricants) are being used. For the situation with much lubricant, the values differ.

2.7 RESULTS FOR A LARGE CYLINDRICAL PRODUCT (ALUMINIUM)

blankholder force (kN)	blank diameter 480 mm						blank diameter 520 mm					
	EDT		EBT1		EBT2		EDT		EBT1		EBT2	
	slow	fast	slow	fast	slow	fast	slow	fast	slow	fast	slow	fast
200	❍		❍		❍		❍		❍		❍	
300		❍		❍		❍		❍		❍		❍
400	✱		✱		❍		❍		✱		❍	
500		❍		❍		❍		❍		❍		❍
600	✱		❍		❍		❍		✱		❍	
700		❍		❍		▲①		❍		❍		❍
800	❍		✱		❍		❍		✱✝		✱	
900		❍		❍		▲①		❍		❍		▲✝
1000	✱		❍		✝		✱		✱✝		✱	
1100		❍		❍		▲①		❍		❍		❍
1200	❍		✱				✝		✱✝		✱✝	
1300		❍		❍		✱		❍		▲✝		❍
1400	❍		❍				✱✝				✝	
1500		❍		❍		❍		▲✝		▲✝		❍
1600	✝		✱									
1700		❍		✱		❍		❍				▲✝

Table 2.4. General results of deep drawing experiments on aluminium with different blankholder forces, speeds and blank diameters. Richly lubricated.
❍ *product OK, no peculiarities*   ✝ *product fractured*
✱ *small force peak*   ▲ *large force peak*
① *with these products the (large) force peak was occurring at the very end of the punch stroke; it is not known if the product would have fractured would it had been drawn any further*

2.7.1 Punch force
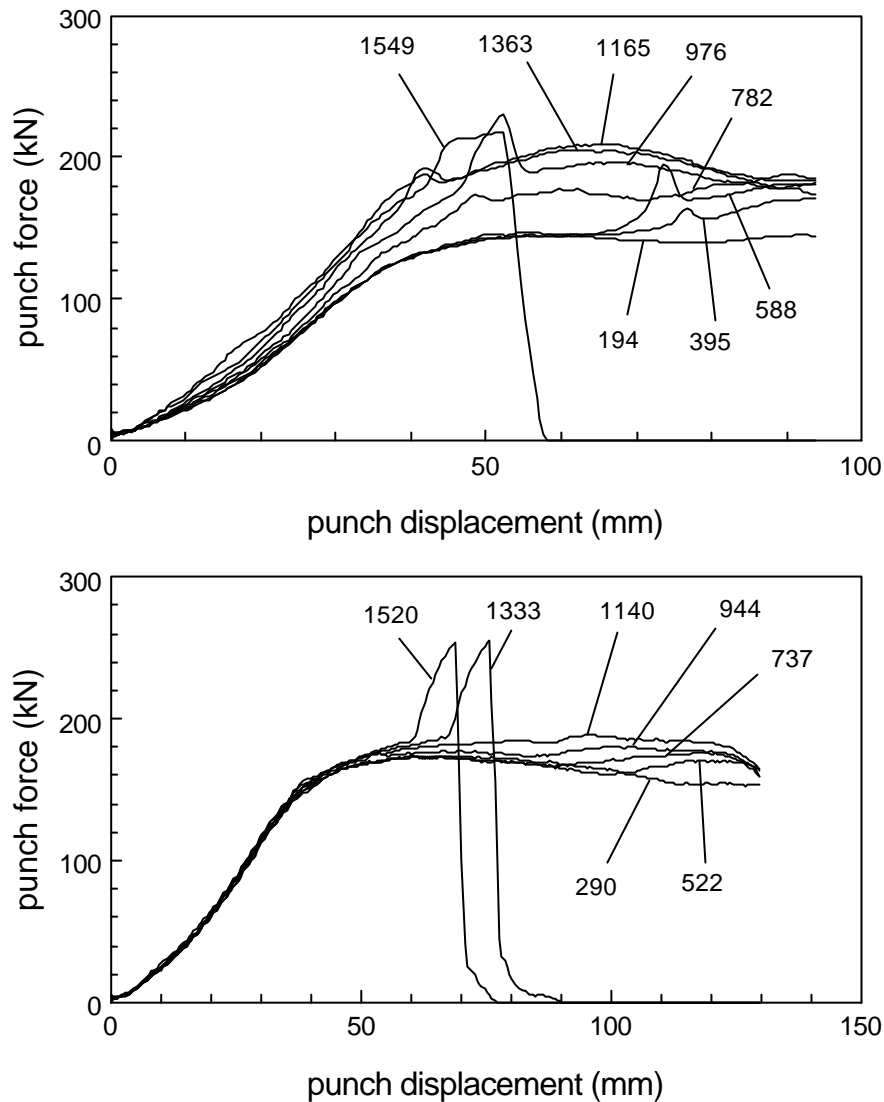
Figure 2.25. Examples of force-displacement curves for aluminium, showing the influence of blankholder force on the shape of the curves and the occurrence of force peaks. The numbers at the curves denote blankholder forces (kN).
Top: blank diameter 480 mm, slow speed, richly lubricated, material EDT.
Bottom: blank diameter 520 mm, high speed, richly lubricated, material EBT2.

Examples of force-displacement curves are presented in figure 2.25. They reveal some properties which indicate that deep drawing of aluminium is different from deep drawing of steel. The shape of the force-displacement curves changes with the blankholder force. The examples in figure 2.25 (top) show that there are areas in the force displacement curves that react differently to the variation of the blankholder force. At low blankholder forces there is a maximum in the curve at about 90 mm punch displacement. At higher blankholder forces, however, the punch force at that position no longer increases, but remains more or less constant, while a new maximum evolves at about 65 mm punch displacement.

The examples in the bottom part of figure 2.25 reveal another phenomenon: the punch force reacts hardly to changes in the blankholder force. This phenomenon has also been observed when drawing small parts from aluminium, similar to the parts used for steel described in section 2.4. This effect implies that the blankholder force can be increased

very much without causing fracture of the product. This effect also has been described in literature [Kasuga 1968], but it has never been observed with steel.
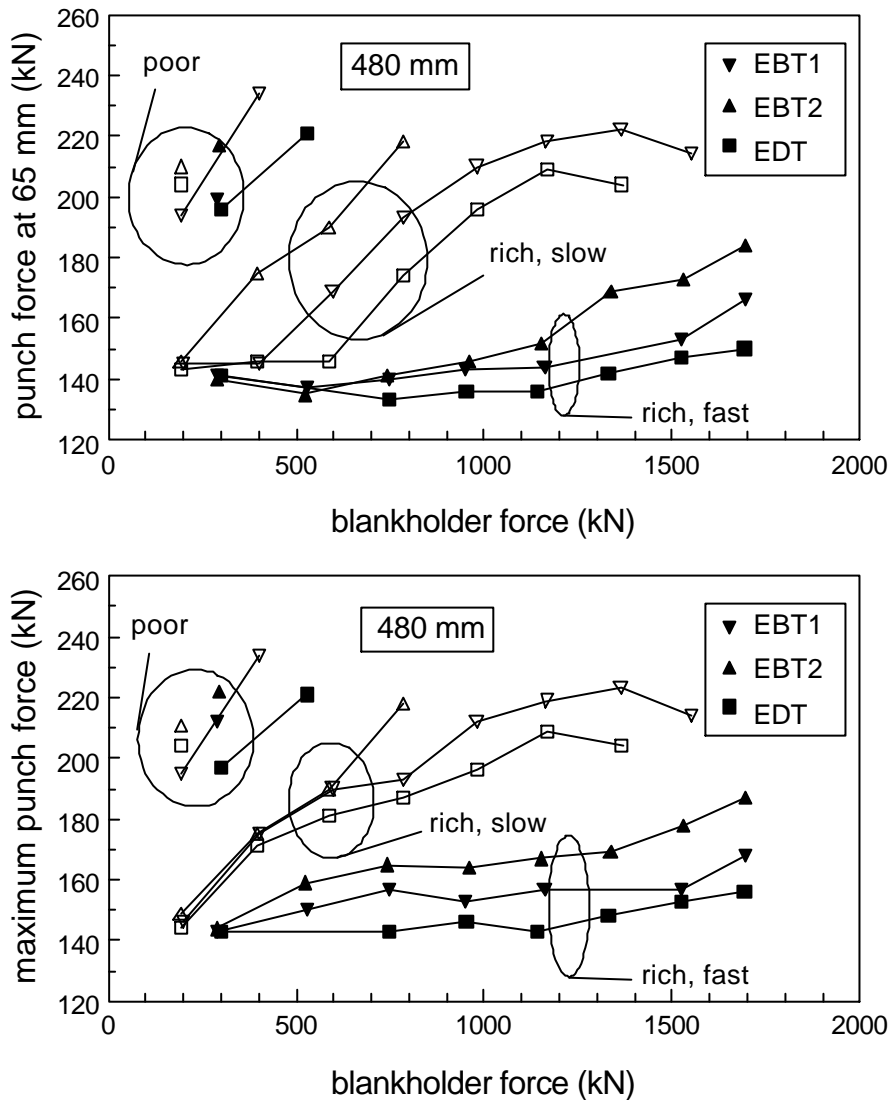
Figure 2.26. Punch force as a function of blankholder force for aluminium, for different blank diameters, speeds, lubrication conditions and materials. Punch forces with force peaks removed. Blank diameter 480 mm.

A more alarming phenomenon is the occurrence of the force peaks shown in figure 2.25. These peaks are not due to malfunctioning of the data acquisition system but are real force peaks, acting on the part. On many occasions these peaks are so high that they result in fracture of the product. Example of both large force peaks, causing fracture, and smaller force peaks are again found in figure 2.25. Although the small peaks are sometimes observed in deep drawing of steel, the large, fracture inducing force peaks have never been observed on steel.

The general results of the deep drawing experiments are presented in table 2.4 (richly lubricated condition only). This table shows that the large force peaks only occur at high punch speed, and preferably at the larger blank diameter. Moreover, the peaks occur more often with EBT roughness than with EDT roughness.
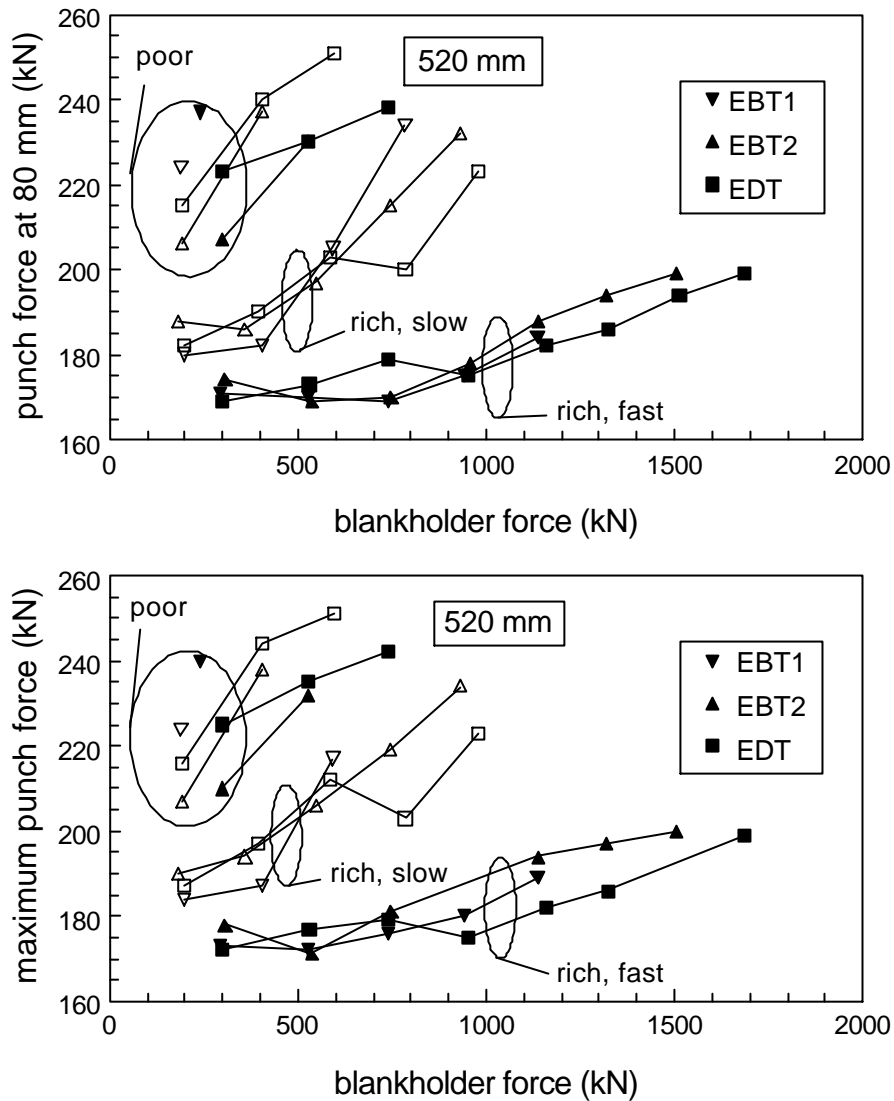
Figure 2.27. As figure 2.26, blank diameter 520 mm.

For all products the punch force has been measured. Similar to the results for steel, both the maximum punch force and the punch force at a certain punch displacement, where the punch force was very sensitive to variations in conditions, have been measured. The latter has been chosen as 65 mm for the blank diameter of 480 mm, and 80 mm for the blank diameter of 520 mm. The maximum punch force loses some importance here, because the shape of the curves strongly depends on the punch force, and consequently the punch displacement (read: forming condition) where the maximum punch force occurs, can change significantly. For the determination of the punch force the force peaks are thus considered as anomalies, so any occurring force peaks have been removed from the curves. The results are presented in figures 2.26 and 2.27. There is a clear influence of speed and lubrication. At rich lubrication a higher speed results in a lower punch force. For the poorly lubricated condition the punch force is larger than for the rich condition, and there is no influence of punch speed. The EDT material shows lower punch forces than the EBT materials, notably for the blank diameter of 480 mm.

The only probable cause of a sharp increase of the punch force as shown by the large force peaks is complete clamping of the flange in the blankholder. Due to the high surface pressure on the outer flange edge during deep drawing and the (apparent) low hard-

ness of aluminium, the conditions in the flange resemble that of forging. The material can than be 'locked' by the roughness of the tool. To verify this speculation, the tool has been extensively polished prior to additional experiments, and this eliminated these large force peaks almost completely. It can thus be concluded that the large force peaks have been caused by imperfect (but not poor!) preparation of the tool, so they should not be too concerning. Evidently, aluminium places higher demands on the tool than steel.

2.7.2 Product dimensions
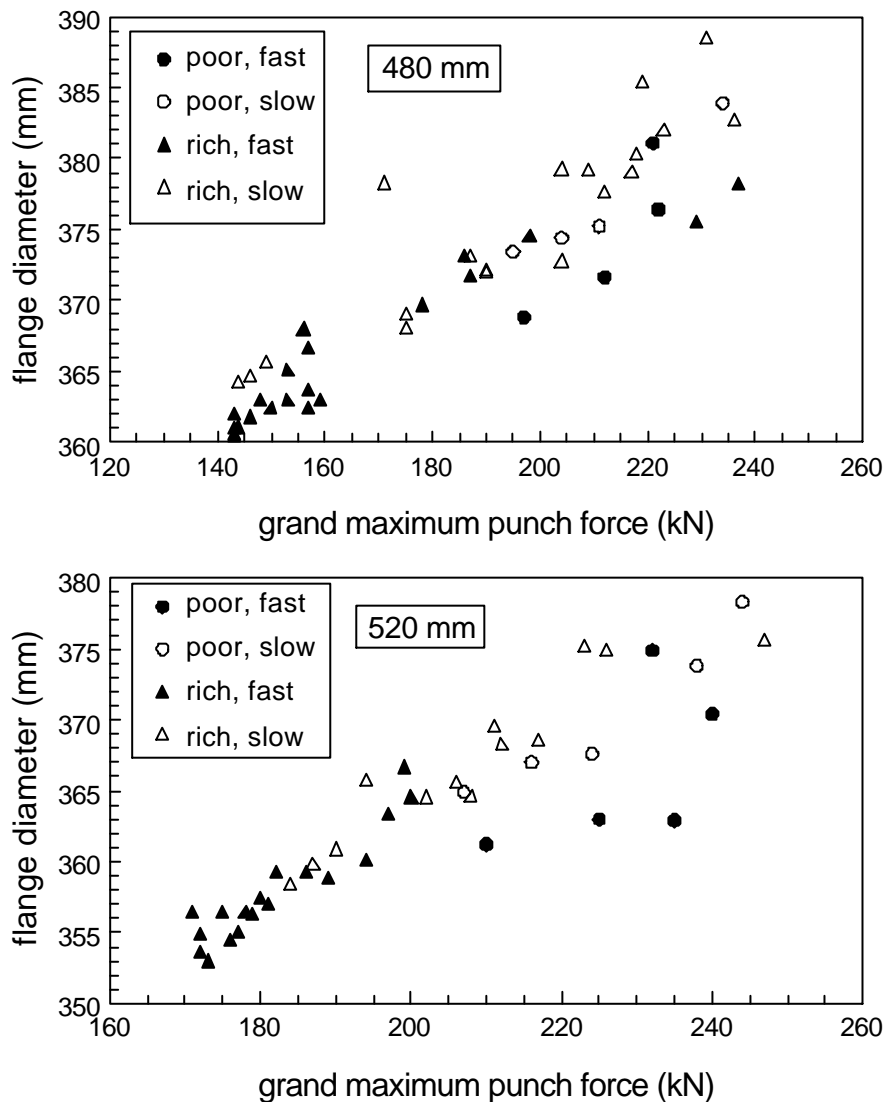
Figure 2.28. Relation between the flange diameter after drawing, and the maximum occurring punch force (including force peaks!) for aluminium.

For all products the flange diameter after drawing has been measured. These diameters have been plotted against the maximum punch force in figure 2.28. In this figure the maximum punch force is defined as including the force peaks, so presenting the actual highest force that has been acting on the wall of the part during the drawing operation. For both blank diameters a good correlation between the flange diameter and the maximum punch force was found. The data show some scatter, probably caused by measuring errors or variations in the original blank diameter. The data obtained under poorly lubricated condition and high speed show more deviation. In fact severe stick-slip occurred

and it is quite possible that this caused an error in the determination of the punch force. The good relationship between the flange diameter after drawing and the maximum punch force implies that both properties have a common origin, which evidently does not depend on the conditions during deep drawing.

2.7.3 Working area

The fracture limit, the maximum allowable blankholder force, is strongly affected by the occurrence of the large force peaks which induce fracture before the 'normal' punch force reaches is maximum (about 260 kN for these products and this material). So the fracture behaviour can be studied for the low speeds only. One expects from general experience that a larger blank size makes the process more critical, so that fracture occurs at a lower blankholder force. This is in general true for the richly lubricated condition, see table 2.4. Moreover, the fracture limit for EDT is (somewhat) higher than for the EBT materials.

For the poorly lubricated condition the situation seems opposite to what is expected (figures 2.26 and 2.27). This may be caused by the fact that the friction in poor condition turned out to be very sensitive to the actual amount of lubricant. A little too much lubricant immediately reduces the punch force. For the blank diameter of 480 mm, which has been tested last, the blanks may have been dryer than for the larger blank diameter.

2.7.4 Friction factor

blank diameter	punch force	slow			fast		
		EDT	EBT1	EBT2	EDT	EBT1	EBT2
480 mm	at 65 mm	0.033	0.032	0.059	0.004	0.008	0.017
	maximum	0.025	0.026	0.057	0.005	0.007	0.012
520 mm	at 80 mm	0.024	0.047	0.031	0.010	0.007	0.013
	maximum	0.020	0.041	0.030	0.008	0.009	0.012

Table 2.5. Friction factor for different systems, aluminium.

From the force-displacement curve in figures 2.26 and 2.27, the friction factor has been determined by fitting a straight line by means of a simple linear regression. The actual relation is not perfectly linear, notably for the blank diameter of 480 mm. So the friction factors calculated are no more than an indication of the average friction conditions. The results are presented in table 2.5. Only the values for rich lubrication are determined; for the poorly lubricated condition the amount of data available was insufficient for a reliable fit. Note that the higher values for EBT2 for 480 mm blank diameter and low speed are influenced by the fact that there are less data than for the other two materials under the same conditions. Generally the friction factor of EDT is lower than for the EBT variants, and the values for high speed are significant lower than for low speed. Important to note is, however, that the values for aluminium are much lower than for steel (table 2.3), indicating that the friction coefficient for aluminium under the applied conditions is much lower than for steel.

2.7.5 Influence of blank size

The influence of blank size is more pronounced than has been observed for steel (section 2.5.1.6). It has already been pointed out that the way the punch force reacts to different blankholder forces, is influenced by the blank diameter. Moreover, the large force peaks occur more often at the higher blank diameter, and the influence of roughness is larger for the smaller blank diameter.

It seems that in general different blank diameters cause friction conditions to differ more during deep drawing of aluminium than during deep drawing of steel, although is it not self-evident why this is the case.

2.8 DISCUSSION

2.8.1 Steel

2.8.1.1 <u>Cylindrical</u> <u>products</u> <u>and</u> <u>general</u> <u>considerations</u>

In deep drawing operations the forming force is exerted by the punch and transferred through the wall of the product to the forming zone. The forming force consists of two components: one component is the force (work) necessary to deform the material in the blankholder area, and the other component is the friction force, which in turn also consists of two components: the friction force in the blankholder, which is a direct result of the blankholder (clamping) force, and the friction on the die, which is caused by the fact that the material moves over the die radius while it is pressed against it by the tension in the wall.

The deformation force is determined by the mechanical properties of the material, more specifically: it is directly proportional to the momentary yield stress in the material. Fracture occurs when the pulling stress in the wall of the product exceeds the maximum allowable stress. In general for cylindrical products, the punch force at fracture is equal to the plane strain (!) tensile strength of the wall. It will be clear that both the forming force and the maximum allowable stress in the wall are proportional to the material strength, so the fracture limit is hardly influenced by the material strength, in particular for relatively small products.

The friction forces are determined by the coefficients of friction in the blankholder area, to be more precise the coefficients of friction on the blankholder surface, the flat die surface and the die radius. These coefficients of friction need not necessarily be equal: both the material surface and the local contact conditions may vary.

With these considerations in mind we can now analyse the results presented in the preceding sections. The influence of roughness grade (read: roughness level) is consistent: if there is an influence of roughness then a higher roughness level <u>always</u> results in a higher punch force, indicating that the friction increases with increasing roughness.

The skin pass reduction has two effects on the material properties (see figure A.1 in appendix A): the roughness increases (except for the lowest grade), and the yield stress increases (but at the same time the hardening coefficient n decreases). The effect of skin pass can also be observed in the results: a higher skin pass reduction generally results in a higher punch force.

The third major influencing factor was the amount of lubricant. Without exception a lar-

ger quantity of lubricant results in lower punch forces. This agrees with common sense experience: more lubricant gives better lubrication.

The effects of the punch force on the drawn product or the drawing process are more complex. A higher punch force results in a higher load on the wall of the partially drawn product. If this higher load is caused by changes in material properties, the effects are modest because the load on the wall and the resistance against fracture are influenced by the material properties in similar ways (at least for most practical materials). In such cases the higher punch force will but slightly affect the fracture limit or the product dimensions after drawing. If, on the other hand, the higher punch force is caused by changes in friction, this will result in a larger strain of the wall and consequently in a larger flange width (or diameter) after drawing. Also, as the strength of the wall remains the same, fracture will occur at lower blankholder forces. This is in general what has been found.

Although many observations are explained by the above, some observations require a more thorough analysis.

In many cases a low amount of lubricant results in less influence of roughness, in other words: the influence of roughness reduces when there is but little lubricant. That should not be too surprising. A low amount of lubricant means that the area enclosed by the roughness of both contacting surfaces is not completely filled with lubricant and that hydrodynamic effects, which cause mixed lubrication, can occur only partially if at all. This means that friction will be at a condition of boundary lubrication despite possible high speeds or high viscosity lubricant, and in chapter 3 it will be shown that under such conditions there is but little influence of roughness.

One of the more puzzling phenomena still is the typical shape of the force-displacement curves for the large cylindrical product, as shown in the examples of the dented curve or the curve with two peaks (see figure 2.12). These force-displacement curves have been observed in many tests, not just with steel but also with aluminium, so we must conclude that their existence is more than just a coincidence. It is important to observe here that all deep drawing simulations on cylindrical products yield simple dome shaped force-displacement curves. Although these simulations are generally quite able to describe the plastic behaviour of the material, the friction is usually implied as 'Coulomb' friction, i.e. with a constant coefficient of friction. Even simulations which include a Stribeck curve description of the friction, by which the coefficient of friction can vary with local conditions, are unable to predict the observed curves [Vegter 1991].

As explained in chapter 1 the contact in the blankholder is of a flat type and the pressure there increases significantly during the deep drawing operation. This effect of increasing pressure can be seen in the experiments with the bent strip. While there is no plastic deformation in the flange, the punch force consists almost completely out of friction force. There is a deformation force due to the bending of the material round the die radius, but this is nearly independent of the punch travel. The changes in punch force can therefore be ascribed to changes in friction force. During the 'drawing' of this product, the actual pressure in the flange increases from 15 MPa at the beginning to 80 MPa at the end of the punch travel. Figure 2.1 shows that the punch force decreases, so that it

can be concluded that the coefficient of friction decreases with increasing pressure, and this effect is stronger for low roughness heights.

A second effect is a change of the surface roughness of the flange. The plastic deformation of the material causes an increase in roughness, but the clamping action of the blankholder will smoothen the roughness. The material which is no longer in contact with the tool can deform without constraint and the amount of roughening can be related to the amount of plastic deformation and the grain size (larger grain size gives more roughening) [Sniekers 1996]. For the material which is still being clamped the situation is not that simple. The roughening under constraint has not been investigated extensively, and a good description is not available yet. Therefore it is difficult if not impossible to describe the exact contact conditions in the regions of friction (see chapter 5 for more discussion on this subject).

However some evidence can be found by comparing the results of rephosphorised steel to low-carbon steel. These materials differ in mechanical properties. The stresses in the material are higher for rephosphorised steel, indicating that the friction forces are relatively smaller. However the differences in roughness between the lowest and highest grade are also larger for rephosphorised steel (figure A.1). Therefore hardly any difference in friction during deep drawing is to be expected between these two classes of steel. There is however one major difference between the materials: the grain size. The grain size is much larger for low-carbon steel than for rephosphorised steel (average size 20 µm and 10 µm, respectively) and consequently the amount of roughening is also larger.

We can now speculate as follows. With rephosphorised steel there is little roughening of the material, the (relative) differences in roughness between the materials remain more or less the same during deep drawing. Therefore the effects of roughness and lubrication are more or less uniform during the operation. With low-carbon steel there is much roughening of the material, which is known to be independent of the original roughness. Therefore the differences in roughness between the materials disappear, all materials become very rough. Consequently the effects of roughness and lubrication are no longer constant but decrease because the material starts to behave as a very rough one.

This theory can explain some of the observed effects but not all. Firstly it does not explain the peculiar 'dented' force-displacement curves which are also found for rephosphorised steel. This peculiarity only occurs with relatively thin material, and of course the roughening has nothing to do with the thickness of the material. Secondly, at a blank diameter of 600 mm (figure 2.12) this effect seems to appear and disappear several times.

All of these observations lead to a very general conclusion that the frictional conditions change during the operation. This has been reported before, for example by Kasik [Kasik 1980] who measured the actual friction force in the blankholder using a special tool, applying different lubricants. She found that the friction force changes in a complex way and should be described by a third order polynomial function. In her tests several solid and liquid lubricants have been used, including a mineral oil similar to the oil that has been used in our tests. However Kasik found no effects with this mineral oil. This may be due to the small size of the products used by Kasik which were equal to the small cylin-

drical parts used in the experiments described in this work, for which no effect has been found as well.

Grahnert [Grahnert 1985] did similar experiments on a larger tool (punch diameter 200 mm) in which he measured the actual pressure of the lubricant in the blankholder region. He proposes that macroscopic pockets emerge during the deep drawing operation in which lubricant may be trapped so that extra hydrostatic lubrication may occur as depicted in figure 2.29, for which he found evidence in his results. This mechanism has not been accepted widely, yet recent simulations carried out by Vegter [Vegter 1996] showed effects very similar to those proposed by Grahnert. If the mechanism proposed is actually occurring, it is clear that this will lower the friction in the blankholder. Moreover, because this effect is caused by the actual geometry of the flange in the blankholder, the lowering of the friction should depend on the actual flange diameter (read: punch travel) and the ability of the material to adept its shape (read: material thickness). So there is some evidence for this mechanism in the results presented here.
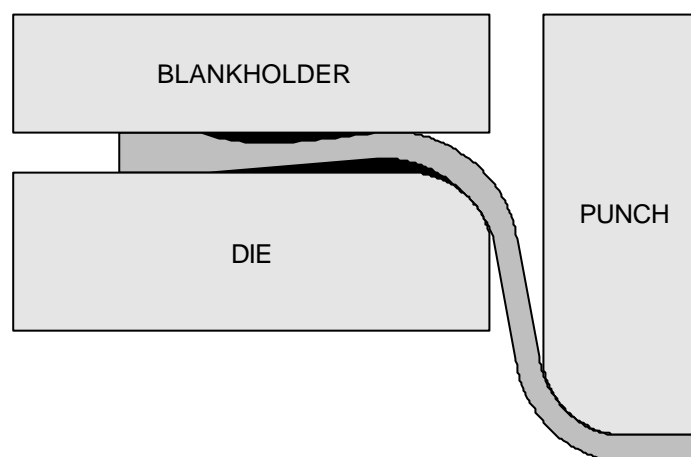
Figure 2.29. Macroscopic pockets of lubricant (black), in which extra hydrostatic lubrication can occur, can exist in the blank holder, according to Grahnert [Grahnert 1985].

2.8.1.2 Rectangular product

For the rectangular product the situation is more complex. The tangential strains are not uniform over the flange perimeter. They are largest in the corners and smallest on the straight sides. When a product is very long compared to its height and corner radius (as is the product used here), the tangential strains in the middle of the long side are zero and the material is drawn out of the blankholder without any deformation in the flange.
The thickening of the material in the flange is not uniform either. At the very corners the flange is thickest at the inside of the flange, not at the outside as found in cylindrical products [Grahnert 1985]. In the regions adjacent to the corners the thickest part is at the outside, but the thickening will decrease at places farther away from the corners. The blankholder force is therefore concentrated in a limited region around the corners (assuming infinitely stiff tools), so macroscopic lubricant pockets as found in cylindrical products can not exist in rectangular products. The measured punch force is an integral of all deformation states present in the flange, and local changes in the state of deformation are not reflected in the punch force. This actually happened at the product used here,

where it could not be seen from the force-displacement curve if a product was broken or not, in contrast to cylindrical products where failure of the product immediately results in a drop of the punch force. Therefore there is little correlation between the punch force and the fracture limit.

The flange width after drawing needs to be considered as well. At the long side the material is drawn out of the blankholder without plastic deformation. There is only some plastic deformation when the material is bent and unbent at the die radius. The wall is subjected to a friction force arising at the die radius, this friction being related to the material properties and the lubrication in the familiar way. The same holds for the flange width after drawing, due to stretching of the wall by this friction force. At the short side the situation is different. There is no significant influence of the material properties but the influence of lubrication is opposite to what has been found elsewhere: much lubricant (lower friction) leads to a larger flange width after drawing. This at first sight puzzling phenomenon can be explained when we consider the observed effect of lubrication on wrinkling: much lubrication leads to more wrinkling. The material at the short side is still subjected to tangential compressive strain from the corners. This gradient of compressive strain causes a transport of material from places of high strain (the corners) to places of low strain (the centres of the sides). Therefore the width of the flange after drawing will be larger then when this compressive strain was not present. When there is much lubrication there will also be more wrinkling and the compressive stress can ease by forming wrinkles in the flange so that the flange width will be smaller.

2.8.2 Aluminium

In general the considerations presented above are also valid for aluminium. There is, however, a major difference with respect to steel, i.e. the level of the coefficient of friction. From the observation that the punch force increases only very little with increasing blankholder forces, and the calculated friction factors, it can be concluded that the coefficient of friction in the blankholder is much lower than for steel. Furthermore there are some unpredictable aspects with aluminium which are possibly related to this condition.

The influence of blank size is not as straightforward as is generally expected and as is observed for steel. Normally, at a larger blank size more material has to be deformed in the blankholder area and, consequently, the punch force is higher. This in turn gives a lower fracture limit and in general a more critical process. This effect of lower fracture limit is not reflected very well in the results (table 2.4), although the tendency is correct. Another effect of blank size is that at larger blank sizes the influence of material roughness seems to decrease. This effect has been observed in other experiments as well. The only points in the Stribeck curve where there is no (or little) influence of material roughness, is at boundary lubrication or hydrodynamic lubrication. The very low friction factors obtained during these tests (in particular at high speed) indicate that the friction on the flange is at a condition not far from pure hydrodynamic lubrication (an explanation for that will be given in section 5.1). However, this still does not explain why there is an influence of the blank size. Apparently different (tribological) conditions on the flange are different for different blank sizes. Unfortunately, computer simulations did not reveal any differences; they predicted that the conditions are determined by the actual flange diameter and not by the original blank diameter [Atzema 1997].

3 Measurement of friction on flat contacts

ABSTRACT In this chapter the friction testers used at Hoogovens are presented and the limitations of strip testers in general are discussed. Comparison of the testers revealed an influence of the size of the slider on friction at mixed lubrication. The friction results obtained with these testers on steel and aluminium are presented. In particular the influence of roughness and pressure has been investigated. The influence of pressure is significantly different for steel and aluminium.

3.1 INTRODUCTION

The frictional aspects of sheet metal forming can be studied in two ways, i.e. by doing actual forming tests as described in the previous chapter, or by doing application-oriented friction experiments on small material samples. Most of the friction tests which apply to studies of sheet metal forming can be categorised into one of the following three groups:

- friction tests on flat samples (flat strip tests);
- friction tests on strips which are bend around a tool (bend strip tests);
- draw bead simulator tests.

A survey of frequently used tests can be found in [Sniekers 1996].

In deep drawing operations the major part of the friction arises in the blankholder, where the contacting surfaces are conformal, and predominantly flat (see section 1.2.2). Therefore at Hoogovens the friction tests have been restricted to tests with flat contacts, notably with flat strips. This method has the advantage that all process parameters can be adjusted independently. However, without special measures, simultaneous plastic deformation of the specimen does not take place.

In practice, however, large restraining forces are generated by so called draw beads as well. The friction conditions in draw beads differ from those which occur in the tests described in this work.

3.2 TRIBOLOGY OF FLAT CONTACTS

In tribology most experiments are carried out on concentrated contacts (line or point contacts), either because this geometry is relevant for practice or because under those conditions the contact geometry is well defined. In fact, many useful results have been obtained [Schipper 1988, Ter Haar 1996]. However, there are fundamental differences between friction tests on concentrated contacts and tests on flat contacts, which makes it dangerous to transfer results, obtained with one type of test to the other type. This will be explained below.

In concentrated contacts the geometry of the contact zone is determined primarily by (macroscopic) elastic deformation of the contacting surfaces. In those situations the pressure in the contact zone is described by a Hertzian distribution, and is not proportional to the load. Moreover the length of the contact zone depends on the process conditions. This has some important implications. Schipper has found that Stribeck curves obtained at different pressures do not coincide. More precisely: the curve shifts to the left as the pressure increases (if $\eta V/P$ is used). This has been shown to be typical

left as the pressure increases (if $\eta V/P$ is used). This has been shown to be typical for line and point contacts and for conditions under which Schipper has performed his experiments. Later, Ter Haar showed that under other conditions and for line contacts the curves can also shift to the right, when the pressure increases, assuming Hertzian pressure distribution.

For flat contacts the contact zone is (to a fair approximation) independent of the process conditions. The length of the contact zone is determined by the length of the tool (the slider) and the pressure is proportional to the external load. Later it will be shown that the position of the Stribeck curve hardly depends on pressure.

The above highlights the basic differences between flat contacts and concentrated contacts, and therefore it should be emphasised that one cannot use results obtained with one type of contacts in situations where the other type of contact occurs.

NOTE: in all situations described in this chapter and the next one it is assumed that the area between the two contacting surfaces is completely filled with lubricant, i.e. that lubricant starvation does not take place. This condition applies to all friction tests.

3.3 MEASUREMENT OF FRICTION

3.3.1 Hoogovens strip tester

A special friction tester was built at Hoogovens Research Laboratory in 1986 to test friction on flat strips. In principle, with flat contacts, special care must be taken that the contacting surfaces are aligned perfectly, to ensure an even pressure distribution. However, the construction should also be able to adjust itself to small differences in sheet thickness when the strip is pulled through. This is only possible by applying self adjusting jaws, but with self adjusting jaws the jaws may tilt causing a squeezing effect, as will be explained later. The specifications for the new strip tester are listed in table 3.1, the construction is shown schematically in figure 3.1.

max. speed	determined by the testing machine
max. clamping force	50 kN
max. strip width	50 mm
max. jaw length	50 mm
max. travel	150 mm

Table 3.1. Specifications for the Hoogovens strip tester.

The force is applied by means of a hydraulic actuator. Because only a force range of 1:6 could be obtained with one actuator, two different actuators with different forces ranges are present, making the overall clamping force range 1.5 - 30 kN. In the construction special care is taken to ensure proper aligning. The jaws can self adjust in the vertical direction by means of the pivots shown in figure 3.1, and in the horizontal direction by the elasticity of the thin wings near the hinge. The clamping force is aligned by putting the actuator, the load transducer and the pivots of the jaws all in one line, and the pulling force is aligned by making the hinge of the wings as small as possible. However, the con-

struction of the hinge limits the maximum travel of the specimen to approximately 150 mm.
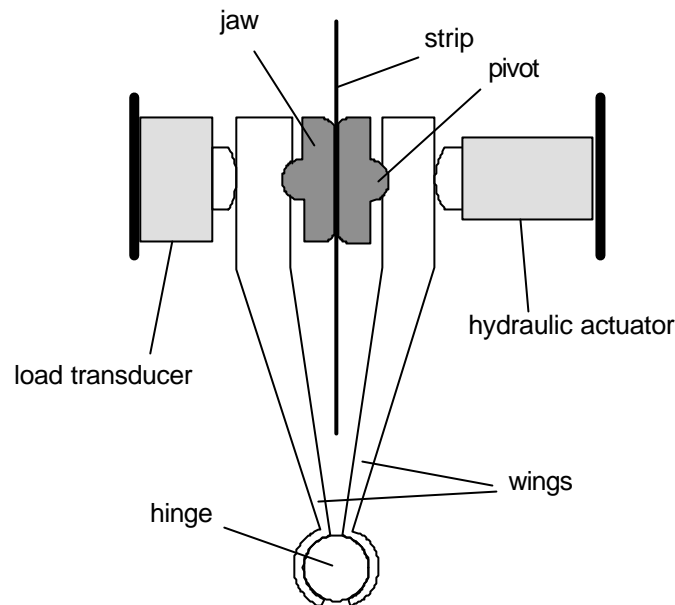
Figure 3.1. Schematic representation of the Hoogovens strip tester. The strip is pulled out of the jaws in vertical direction for which the device is placed in e.g. a tensile testing machine.

Initially the construction had been placed in a mechanical tensile testing machine, but soon the maximum speed of the machine (500 mm/min) turned out to be far too small. Therefore the construction has been placed in the large hydraulic press, allowing speeds of 80 mm/s, while in one occasion speeds exceeding 300 mm/s have been obtained by using the fast closing action of the press. In later experiments the construction has also been placed in a fast hydraulic testing machine.

After completion of the tests described in this work the construction has been placed in a hydraulic device purposely constructed for the strip tester, allowing speeds of 5 - 100 mm/s.

3.3.2 Limitations of strip testers

Due to errors that can occur during testing, strip testers show a number of limitations. These errors are presented schematically in figure 3.2 and will be discussed now.

1 Misalignment of the jaws.

Any misalignment of the jaws will cause an uneven force distribution and therefore wrong results [Monfort 1990, 1991]. To be more precise: the misalignment should be small compared to the roughness depth of the strip material, which can be as low as 1 μm for aluminium with mill finished roughness, even when the construction is deformed elastically by the pulling force. Misalignment can only be prevented by making the jaws self-adjusting.

misalignment of jaws

squeezing effect of jaws

$$\frac{^3P}{P} = 6æ\frac{D}{L}$$

elastic deformation of jaws

yield of strip

$$P_{max} = \frac{å_{max}}{2æ} \cdot \frac{t}{L}$$
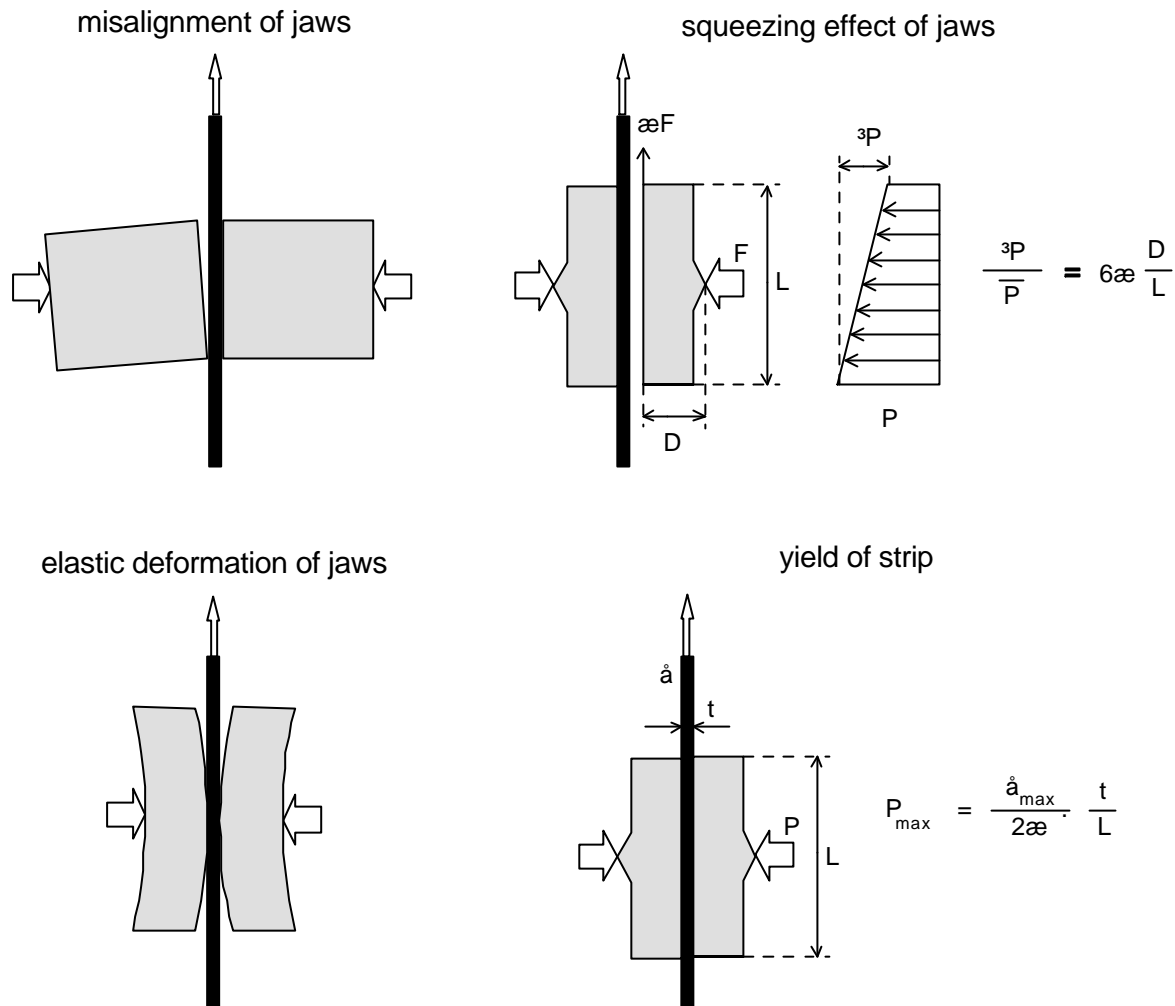
Figure 3.2 Limitations of flat strip testers, see text for explanation.

2 Elastic deformation of the jaws

Normally some elastic deformation of the jaws will always occur under influence of the clamping force. This will lead to an uneven pressure distribution or in extreme cases to only partial contact with the strip. The cure is to use thick jaws with sufficient stiffness.

3 Squeezing effect of the jaws

When the strip is being pulled out of the jaws, a tangential (friction) force is acting on the jaws. This causes a momentum which tends to tilt the jaws, resulting in an uneven pressure distribution. The relative variation in the pressure over the jaws is:

$$\frac{\Delta P}{P} = 6.\boldsymbol{m}\frac{D}{L} \tag{3.1}$$

where D is the distance from the pivot to the jaw surface. This leads to a construction with jaws as thin as possible. The tilting momentum can be compensated by placing the pivot point off centre (in the direction of movement of the strip), but this is only correct for one specific value of the coefficient of friction μ.

4 Plastic yield of the strip

The pulling force exerted on the strip is limited by the yield stress of the material. This leads to a limited pressure on the surface of the strip. The maximum obtainable pressure P_{max} is limited by the maximum allowable stress in the material σ_{max}:

$$P_{max} = \frac{\sigma_{max}}{2\mu} \cdot \frac{t}{L}$$

(3.2)

For example, when t = 0.8 mm, L = 50 mm, σ_{max} = 160 MPa and μ = 0,16 (all typical values), the pressure is limited to merely 8 MPa. A pulling stress exceeding the yield stress of the material can cause plastic deformation of the strip, notably into a 'banana' shape. The limited pressure can be increased twofold by clamping and pulling two strips simultaneously; sometimes this trick has been used in the experiments.

Other points of concern for the construction of a strip tester are:
- the elastic deformation of the device under load (pulling and clamping) should not limit the self adjusting capabilities of the jaws;
- stick-slip can occur when the stiffness of the device is low;
- it should be easy to inspect the jaws for damage like scratches and transfer of metal, and it should be easy to exchange them, if necessary.

Unfortunately, the choice of the size of the jaws is problematic: to increase the maximum allowable pressure small jaws are necessary, but to avoid an uneven pressure distribution large jaws are required. Moreover, for a uniform pressure distribution thin jaws are required, but these will be subject to considerable large elastic deformation. Some of these limitations can be overcome by clever constructions, but the maximum allowable pressure will always be limited.
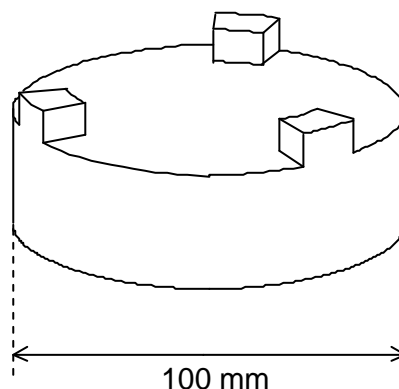
3.3.3 Hoogovens rotation tester

Figure 3.3. Punch with three notches as used in the rotating tester.

After some years of successful use, the limitations of the strip tester were felt more and more. Therefor a new friction tester was constructed in 1990 with the main specifications as in table 3.2.

| speed | 1 - 1000 mm/s |

pressure	1 - 50 MPa

Table 3.2. Main specifications for the new Hoogovens friction tester.

The requirement for high pressure can only be met by a solution which enables the use of very small jaws, without reducing the stability of the system. This has been achieved by a construction inspired by a catamaran boat hull, where the stability is given by the overall width but the water resistance by the individual hulls. A solution has been found by constructing a rotating tester using a punch with three notches as presented in figure 3.3, which is pressed against a flat specimen and then rotates. High pressures can be obtained by making the individual notches very small. This principle has the following additional advantages:

- the punch can be made self adjusting by using a central pivot which also ensures that the load is equally distributed over the three notches;
- elastic deformation can be minimised by making he punch relatively thick, so also minimising stick-slip;
- the net tangential force on the punch is zero, therefore tilting or squeezing does not occur;
- only one side of the specimen is tested, making it possible to test material with different surfaces (like one-sided galvanised steel);

However, also this system has some drawbacks:

- due to the rotating movement, no information on the influence of the direction of movement (related to the rolling direction) on friction can be obtained;
- the track length is limited to 120° revolution, after that the notches pass material which has already been in contact with the previous notch and shows some amount of roughness flattening.

The total construction has been depicted in figure 3.4. In the actual apparatus the punch is stationary and the specimen rotates in a special holder. Simple square specimens of 120x120 mm² can be used without any further preparation such as deburring. Operating the device is very simple and the notches can easily be inspected for damage.

A computer controlled, brushless servo drive with low inertia reduction gear drives the specimen holder, which makes it possible to apply the full range of speed without any alterations to the device. The range of pressure can be obtained by applying punches with notches of different size. After some years of testing a punch with very small notches has been constructed enabling pressures of up to 200 MPa, but this has only been used in one special test series.

This tester is now being used as the standard friction tester, but the strip tester is still available for special purposes. The rotating tester may show some similarity with the more familiar pin-on-disc machine. However the latter is used for wear testing, the pin moves repeatedly over the same track. In fact the rotating tester can be used for such wear testing by altering the motor control program, as has been done in some cases.
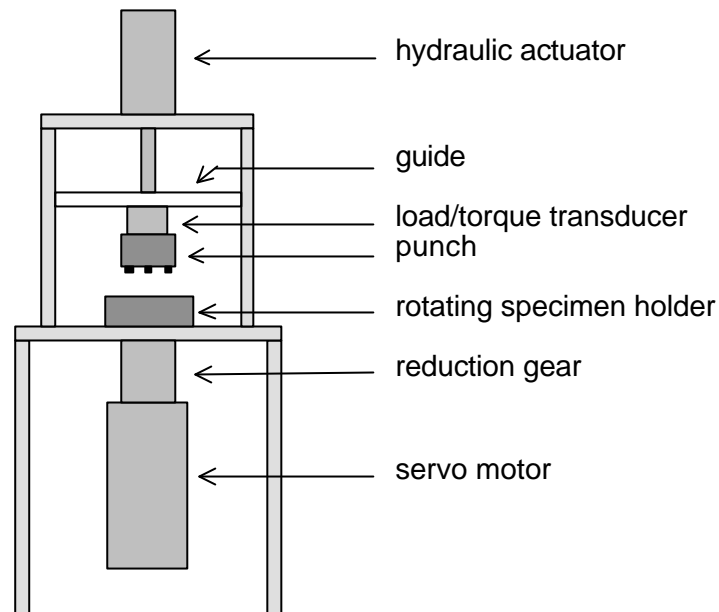
Figure 3.4. Overall construction of the Hoogovens rotating friction tester.

Typical for the rotating tester is that the surface of the three notches must be all in one plane. The allowable deviation is small compared to the roughness height of the material, so the surface should be machined to an absolute accuracy of 0.1 µm or better. This is almost impossible. In many cases the notches had to be corrected by hand with fine polishing paper, until the traces left on the specimen (noticeable by the flattening of the asperities) are completely even. In the early stages of testing this aspect has not been fully recognised.

This problem also applies to the flat strip tester, but in general it is easier to polish a larger surface without disturbing the shape (curvature).
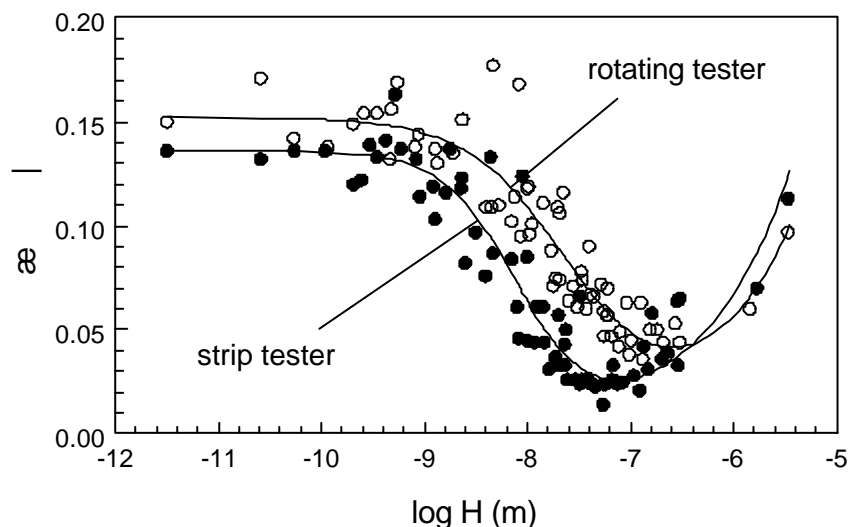
Figure 3.5. Comparison between the strip tester and the rotating tester, with friction tests on steel.

3.3.4 Comparing the testers, influence of jaw size.

After completion of the rotating tester, an extensive test programme has been run to see

if both testers produce the same coefficient of friction. Even after careful checking, a systematic difference remained between the two testers. Compared to the strip tester, Stribeck curves measured on the rotating tester, are shifted to higher values of H. An example is given in figure 3.5. The results have been obtained on steel specimens with R_{pm} of 5.0 μm and a wide range of pressures (which was the same for both testers and thus limited by the strip tester). These tests will be not discussed here in detail, the results are presented just as an example of the differences observed.

One of the major differences between the two testers is the jaw size. In the strip tester the jaw size is 50x50 mm², while the largest jaws (notches) for the rotating tester measure only 11x11 mm². A special series of tests has been carried out to check the influence of jaw size. The conditions for the tests are listed in table 3.3. Five to ten tests have been carried out for each combination of material and jaw size. Due to a limited amount of material being available, jaw labels B and E have not been tested with material ST18.

material	ST17, ST18
lubricant	SG0029, 11-16 g/m²
tester	both strip tester and rotating tester
jaw size	all possible sizes, see appendix A
speed	100 mm/s
pressure	5 MPa
number of tests	5 - 10

Table 3.3. Conditions for the friction tests to study the influence of jaw size.

The results are presented in table 3.4. In some cases the friction decreased during the tests, for those cases the friction range has been given instead of the average friction.

jaw label	jaw length	jaw width	friction ST17	friction ST18
A	50	50	0.020-0.035	0.045-0.055
B	50	20	0.025-0.035	(not tested)
C	20	50	0.045	0.075
D	12	12	0.070	0.095
E	20	20	0.045	(not tested)
1	11	11	0.040-0.055	0.080
2	7	7	0.125	0.135

Table 3.4. Results from the friction tests to study the influence of jaw size.

The results indicate that jaws with the same length but different widths also have the same friction (compare A with B, and C with E), or, in other words, there is no influence of jaw width. The jaw length, however, has a strong influence, a larger jaw length gives lower friction. In fact, the friction seems to be approximately proportional to the inverse jaw length, at least for the strip tester (see figure 3.6).
The results for the rotating tester do not fully blend with the results for the strip tester. This may be caused by poor calibration procedures of the rotating tester, which have been applied at that time, and some amount of non-flatness of the very small notches. The two materials show the same effects, for the rougher material ST18 the friction is

somewhat higher that for material ST17.
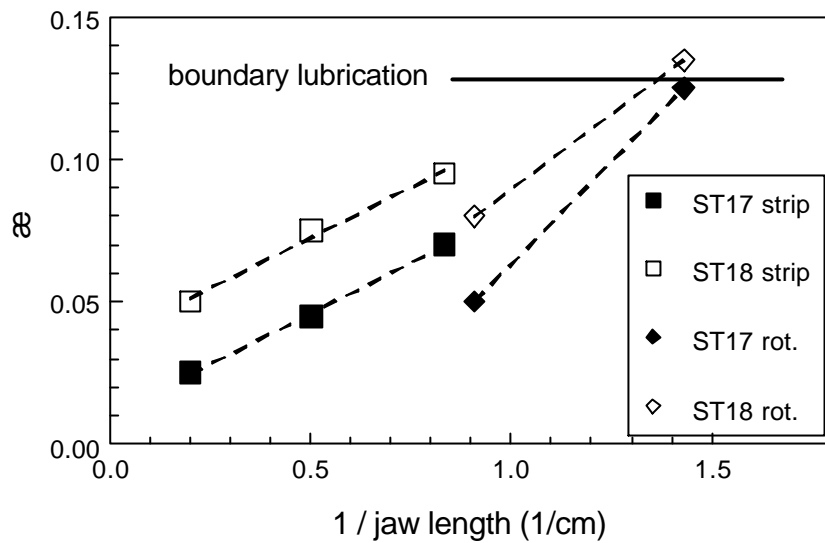
Figure 3.6. Coefficient of friction obtained with different jaws plotted against the inverse jaw length. Data with equal jaw lengths have been combined. The approximate level of the boundary lubrication for both metals as obtained with other tests is presented as well.

3.3.5 Fitting friction results

In the following, results from friction tests are fitted by means of a tanhyp function as explained in section 1.4.3. However, fitting Stribeck curves does have some limitations. Firstly both tanhyp and arctan fitting functions assume a purely flat boundary part, meaning that the coefficient of friction at boundary lubrication is constant. However, in many cases it can be noticed that recorded Stribeck curves do not have a flat boundary part, but that at boundary lubrication the friction still increases slightly with decreasing H (a striking example can be found in figure 3.21). Consequently, at boundary lubrication the fit will often be imperfect.

Secondly, when there are only few measuring points at boundary lubrication, the prediction of H_1 becomes uncertain. The slope of the curve is usually fitted quite well, but the level of boundary lubrication and the value of H_1 may be subject to a large scatter, and be influenced by the accidental position of some points.

Similarly, the friction at hydrodynamic lubrication μ_h may be uncertain when there are but a few measuring points in that area. In such cases it may be wise to use a constant friction at hydrodynamic lubrication and skip all points with a value of H exceeding, say, 10^{-7} m. By experience a constant friction, set to 0.01 for hydrodynamic lubrication, gives acceptable fits in the lower region in most cases and produces good values of H_0. This adaptation has been used in many cases.
As with all fits, one has to become sure that the fit result does not depend strongly on a very limited amount of measuring points. Visual inspection of the result and the actual data will give a good impression. In particular a limited amount of data in the mixed regime can give unreliable results.

3.4 FRICTION TESTS ON STEEL

3.4.1 First series on uncoated steel

3.4.1.1 <u>Experimental</u> <u>procedures</u>

The first series of friction tests have been carried out using the strip tester. After preliminary tests with the tester installed in a mechanical testing machine, had revealed that the speed in the tests should be much higher, the tester has been installed in an industrial hydraulic press. This allowed more realistic operating speeds of the tester. A view of operating conditions can be found in table 3.5 and more extensively in appendix B; lubricant has been applied generously on the samples using a brush. The materials tested were all uncoated steel with different types of roughness (materials ST01- ST09 from appendix A), the two variants of deterministic Lasertex have been tested in two orientations to see if there is an influence of direction of movement. The materials can be divided into three groups: low roughness (1,3), medium roughness (5,6,7) and high roughness (2,4,9).

Tester	strip tester, jaws 50x50 mm²
Speed	2-80 mm/s
Pressure	0.6 - 6 MPa
Lubricants	N100, N500, B.S., cylinder oil

Table 3.5. Main conditions for the first series of friction tests.

For all tests the force-displacements curves have been recorded and the average coefficient of friction has been determined from the data. It has been observed that in many cases the friction varied significantly during one test. In those cases a calculated mean coefficient of friction is unreliable. Later this has been found to be caused by an overdose of lubricant on the specimens as explained in the next section. Therefore it has been decided to exclude all tests where the friction varied more than a certain value over the length of the strip (different variation limits have been tested). Unfortunately this applied to nearly all observations with the lowest pressure (0.6 MPa), so that only the observations for 2.7 and 6 MPa will be analysed further. Moreover, the measurements under mixed conditions have been affected more heavily than measurements under boundary or hydrodynamic lubrication conditions.

For further analysis of the results tanhyp functions have been fitted through the measured data. By applying different variation limits to the results (0.02, 0.03 and 0.04 have been used as limits for the maximum allowable variation of the friction coefficient over the strip length) it could be shown that the centre of the region of mixed lubrication was only slightly affected by the choice of the variation limit and therefore this parameter could be determined reliable. The position of the transition points however was strongly affected by the choice of the variation limit, and consequently these parameters could not be determined reliable.

3.4.1.2 <u>Influence</u> <u>of</u> <u>pressure</u>

It has been observed by Schipper that the position of the Stribeck curve (or more pre-

cisely the position of the transition points) depends on the pressure. This has been checked for our experiments by plotting the values of H at the midpoint of mixed lubrication (H_C) against pressure as done in figure 3.7. This figure shows that the Stribeck curve shifts slightly to the left (lower values of H) with increasing pressure. The friction at boundary lubrication (μ_0 from the fit) is plotted against pressure in figure 3.8. For most material the friction at boundary lubrication decreases with increasing pressure.
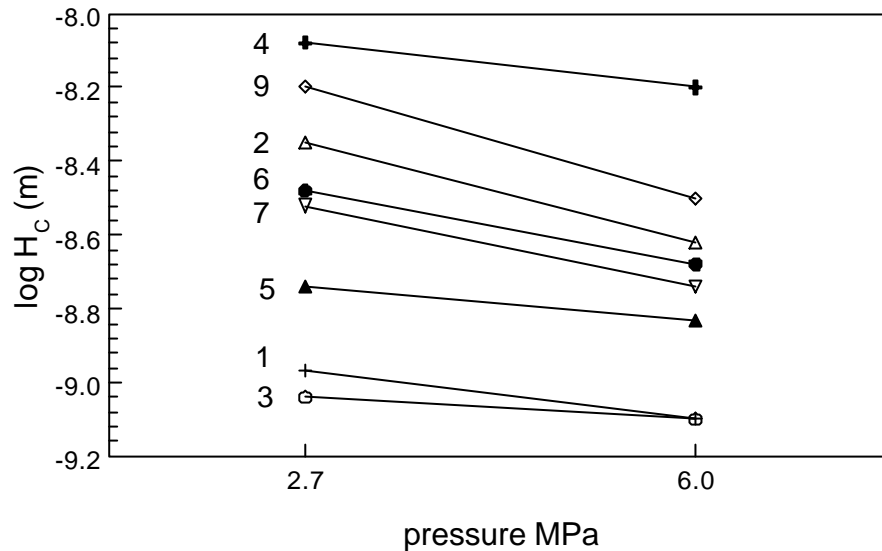
Figure 3.7 Position of the Stribeck curve as a function of pressure (uncoated steel). Labels 1 - 9 denote different materials.
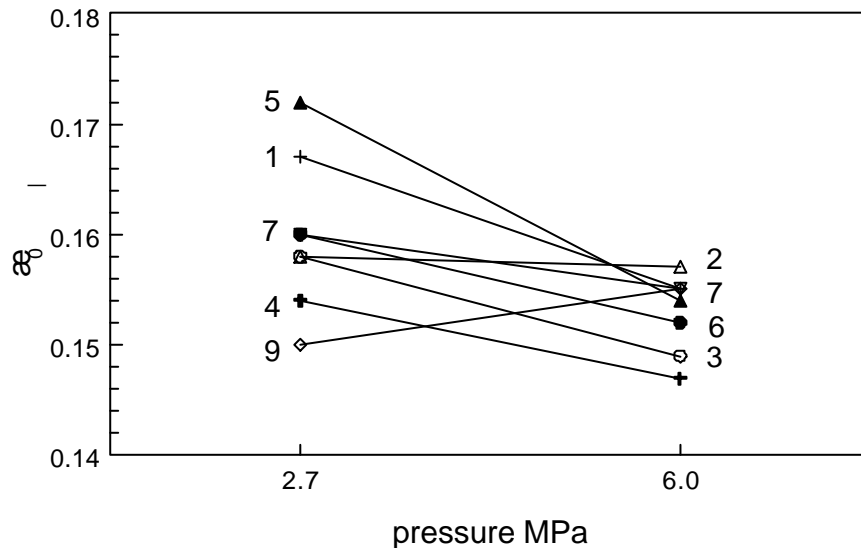
Figure 3.8 Coefficient of friction at boundary lubrication as a function of pressure (uncoated steel). Labels 1 - 9 denote different materials.

As the effect of pressure is not very large, in the following the readings for 2.7 and 6.0 MPa have subsequently been combined to obtain more reliable fits, and a value of 0.02 for the variation limit has been applied.

3.4.1.3 Influence of roughness.
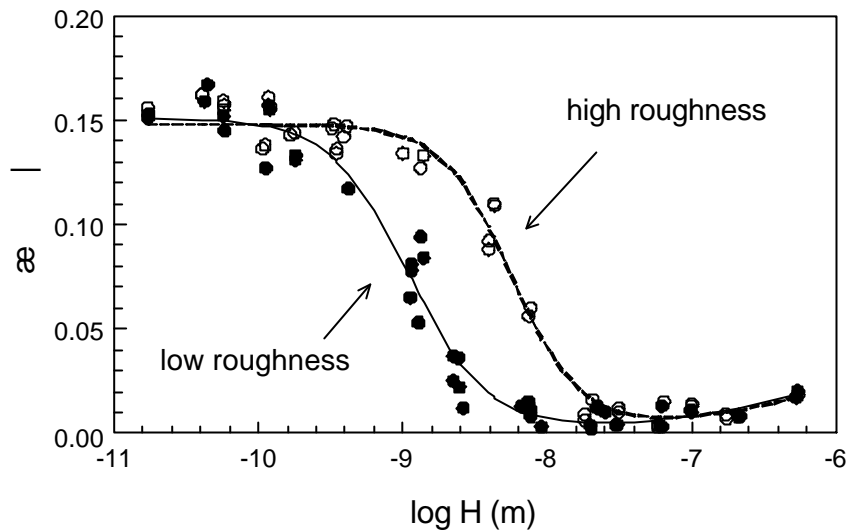
Figure 3.9 Example of the effect of roughness on the Stribeck curve for two sets of materials with extreme roughness (uncoated steel).
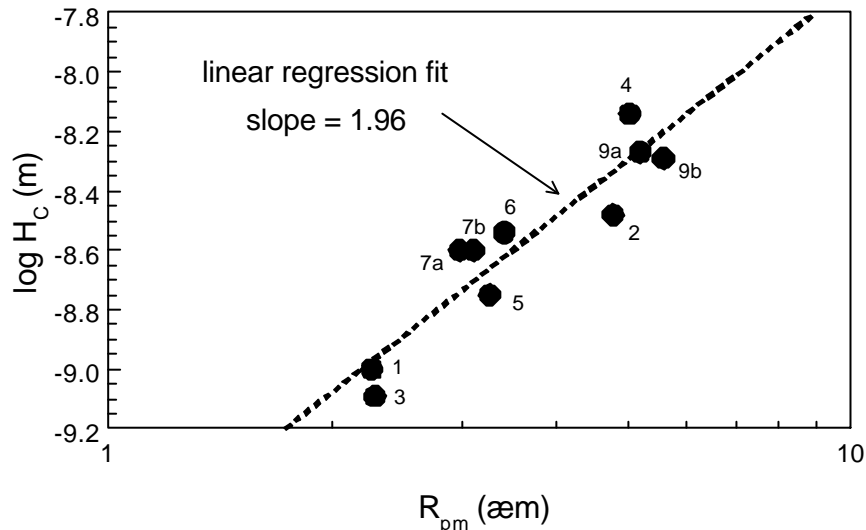
Figure 3.10 Position of the Stribeck curve as a function of material roughness (uncoated steel). Labels 1-9 denote different materials.

The influence of surface roughness on friction is illustrated in figure 3.9, where Stribeck curves for two material sets with extreme differences in roughness (ST01 and ST03 combined, versus ST09a and ST09b combined) are compared. Clearly, an increase in roughness causes the Stribeck curve to shift to the right without changing the shape or the height of the curve very much. This effect has been quantified in figure 3.10 where the position of the Stribeck curve as defined by the midpoint H_C has been plotted as a function of the average roughness depth R_{pm} (logarithmically). The Lasertex variants 7 and 9 are each represented by two points, one for each orientation. The linear regression fit gives a slope of 1.96 from which it can be concluded that the position of the Stribeck curve is proportional to the square of the roughness height. In accordance with this result a 'new' parameter H^* is defined as

$$H^* = \frac{H}{R_{pm}{}^2}$$

A theoretical basis for this parameter is given in the next chapter. The data from the friction tests have been plotted as a function of this parameter in figure 3.11. The data now form a single curve, there is no (large) difference between the types of roughness (Shotblast, EDT, Lasertex).
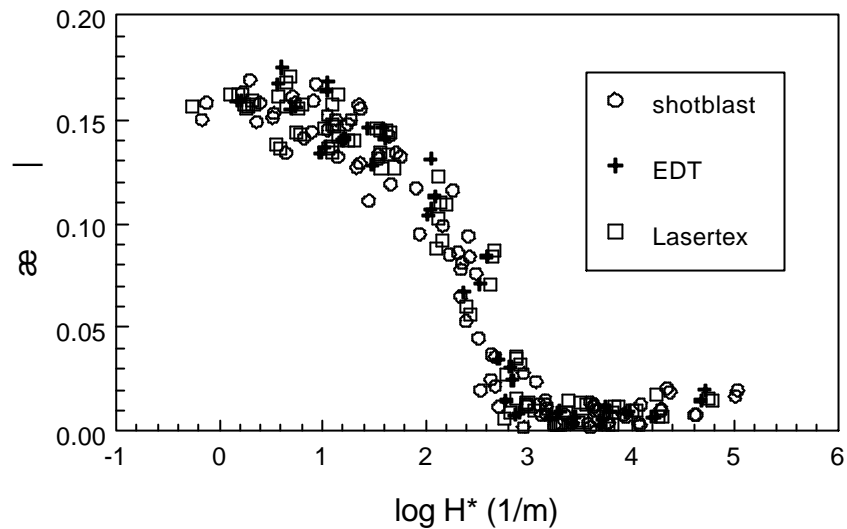
Figure 3.11 Stribeck curve with influence of roughness 'corrected' by plotting the coefficient of friction against the new parameter H* (described in the text), uncoated steel.
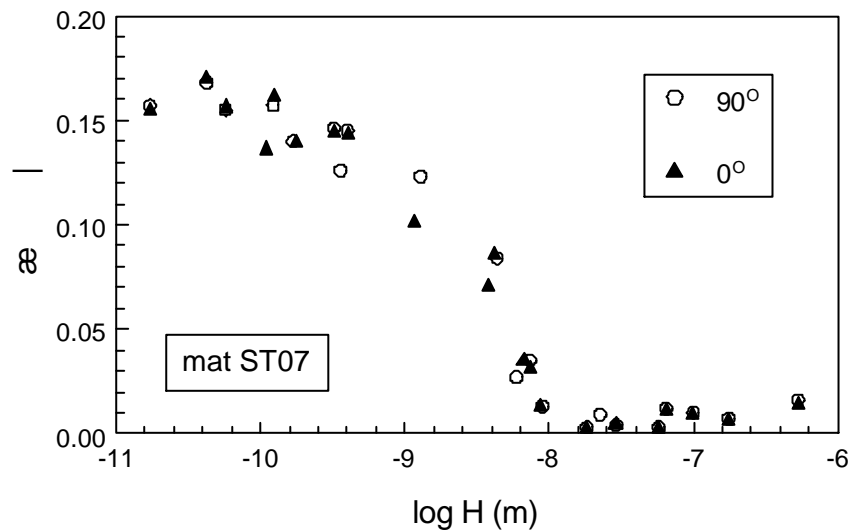
Figure 3.12 Influence of orientation of movement relative to rolling direction for Lasertex material ST07 (uncoated steel).
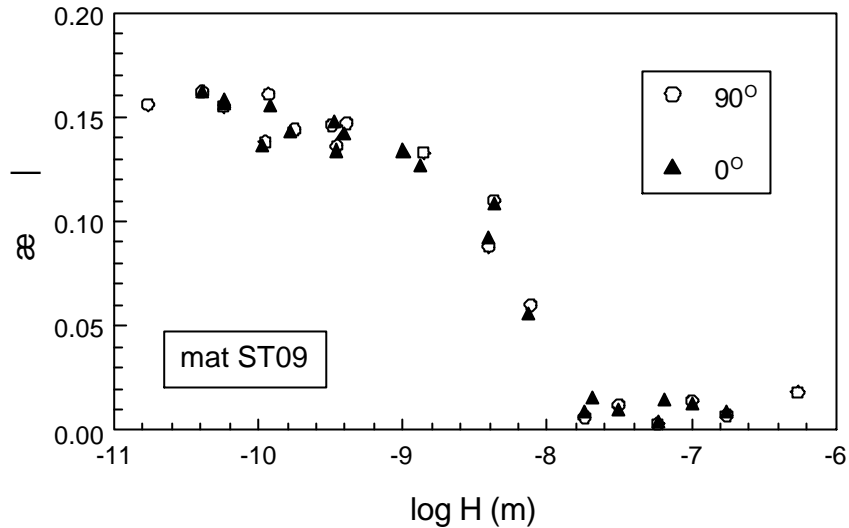
Figure 3.13 Influence of orientation of movement relative to rolling direction for La-sertex material ST09 (uncoated steel).

3.4.1.4 Influence of orientation.

The influence of orientation on the friction of the two Lasertex materials has been de-termined by plotting the data for the two orientations in one plot, see figure 3.12 for ma-terial ST07 and figure 3.13 for material ST09. No significant influence of orientation can be observed. It must be emphasised however that these 'prototype' Lasertex materi-als are much less deterministic than the aluminium EBT materials tested later on.

3.4.1.5 Flattening of roughness.
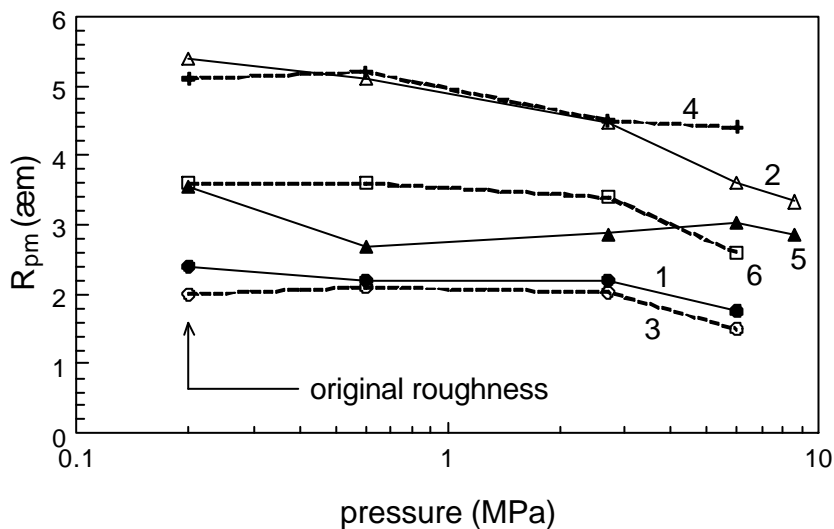
Figure 3.14 Reduction of roughness by friction testing for uncoated steel. Labels 1-6 denote different materials. (2 mm/s, lubricant N100).
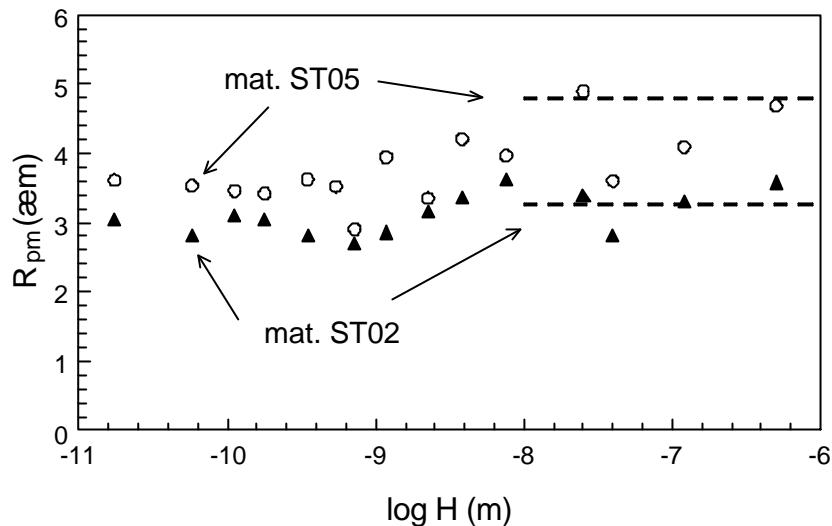
Figure 3.15 Reduction of roughness for materials ST02 and ST05 at 6 MPa (uncoated steel). The level of the original roughness is indicated by the dashed lines.

For a limited number of samples the roughness of the strips after the friction tests has been measured. The results are presented in figure 3.14, all data in this figure have been obtained with a speed of 2 mm/s and lubricant N100 (please note that roughness measurements are subject to large scatter, 10% is quite normal). It shows that the roughness is flattened by the friction tests. The rougher materials (2 and 4) are affected stronger than the other materials, which only show some flattening at higher pressures. The effects for materials 2 and 5 are presented in more detail in figure 3.15, the data in this figure have been obtained for 6 MPa pressure. For material 5 only a minor reduction of roughness is noticed while for material 2 the reduction of roughness is stronger. The flattening of roughness occurs for values of logH < -8 and seems to be completed for values of logH < -9.

3.4.2 Coated steel

3.4.2.1 Experimental procedures

Friction tests on coated steel have been carried out as a part of a round robin test organised by the GDDRG (German Deep Drawing Research Group). The materials have been supplied by the German steel industry, an uncoated steel has been included as a reference. Several variants have been produced with equal bulk properties and roughness heights as far as possible. The materials are described in appendix A under the designations ST11 - ST16. The friction of the materials has been tested under more or less the same conditions as have been applied for the uncoated steels of section 3.4. The way of lubrication, however, has been changed. For these tests the materials have been covered with an overdose of lubricant using a brush or cloth and the surplus of lubricant has been removed from the surface by carefully scraping with a plastic scraper over the asperities of the roughness (clear plastic drawing triangles were found to be particularly suitable). This method reduces the scatter in the roughness measurements significantly, yet enabling full hydrodynamic lubrication. This method has been selected to be the standard method of lubrication and has been used in all further experiments. The main conditions are summarised (again) in table 3.5 and further described in appendix B.
The results of the measurements have been treated in a similar way as those described in

section 3.4.1. The variation in the friction was much smaller, no results had to be excluded from further processing. When drawing the Stribeck curves, we discovered that there are two major differences between these measurements and the measurements on uncoated steel (section 3.4.1). For the coated materials the region of mixed lubrication was larger (the slope of the Stribeck curve was smaller), and at hydrodynamic lubrication the measured friction was about three times as high as for the tests on uncoated steel. This also applied to the uncoated material which has been used as a reference, so these phenomena have not been caused by the coating. Evidently the conditions under which the friction has been measured were not the same as for the first series on uncoated steel, but the precise nature of this difference has never been found.

3.4.2.2 Influence of pressure
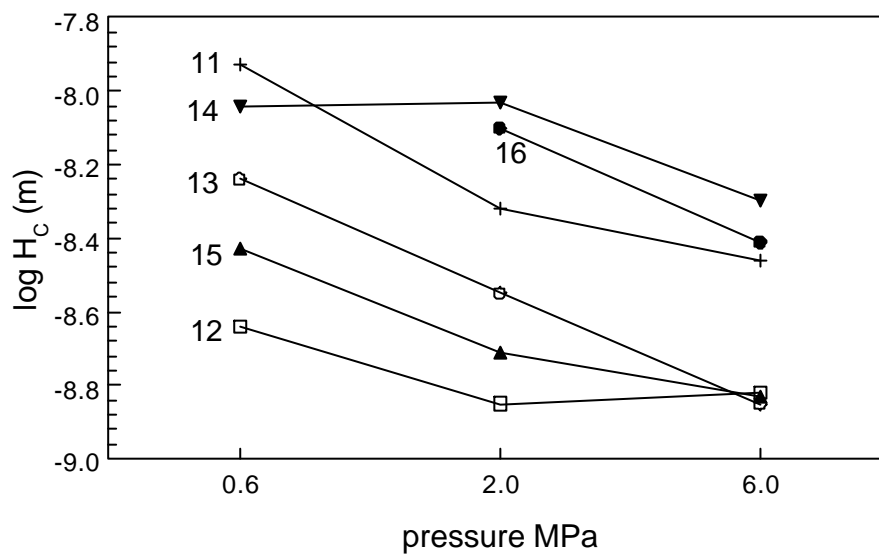
Figure 3.16 Position of the Stribeck curve as a function of pressure (coated steel). Labels 11 - 16 denote different materials.

The influence of pressure on the position of the Stribeck curve has been determined in the same way as for the tests on uncoated steel, the results are presented in figure 3.16. For the tests at a pressure of 0.6 MPa, however, there were only few points in the boundary regime so that the fit is not very reliable, for material 16 a reliable fit could not be made at all. For the test at a pressure of 11 MPa a Stribeck fit was impossible for lack of sufficient data. Notwithstanding these limitations, the observed influence of pressure is found to be similar to that for the uncoated materials.

The influence of pressure on the friction at boundary conditions μ_0 is presented in figure 3.17, where the data for the highest pressure have been obtained by manual fitting. The effects are evident: the friction at boundary lubrication reduces with increasing pressure. The extent of this effect, however, depends very much on the material used, material 12 (soft!) shows very large effects, while material 14 (hard!) is only little effected.
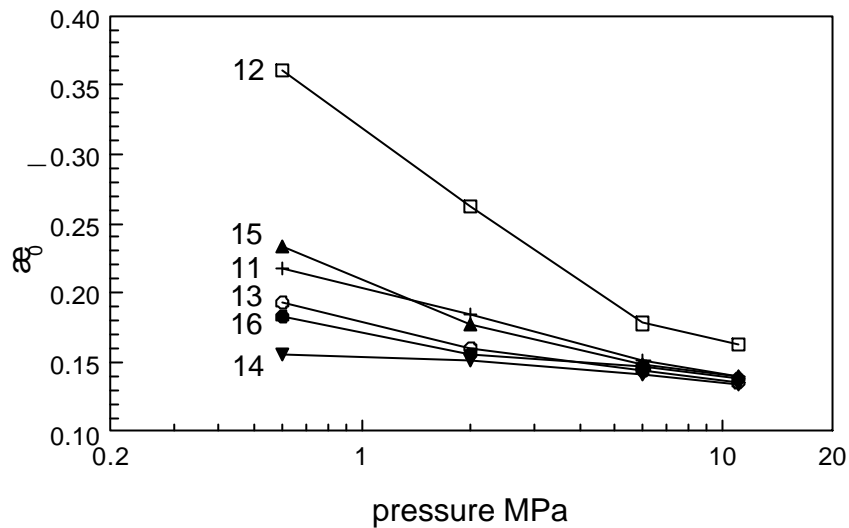
Figure 3.17 Coefficient of friction at boundary lubrication as a function of pressure (coated steel). Labels 11 - 16 denote different materials.

3.4.2.3 Influence of roughness and hardness

For a detailed study of the influence of material properties the data obtained at different pressures cannot simply be combined as for the uncoated steel. Therefore a relative coefficient of friction μ_r is introduced:

$$\mu_r = \frac{\mu}{\mu_0} \tag{3.4}$$

By using this relative coefficient of friction the effects of pressure on the 'height' of the curves are eliminated and the 'relative' curves for different pressures can be combined without much problems. In this way the position of combined Stribeck curves has been determined for all materials.
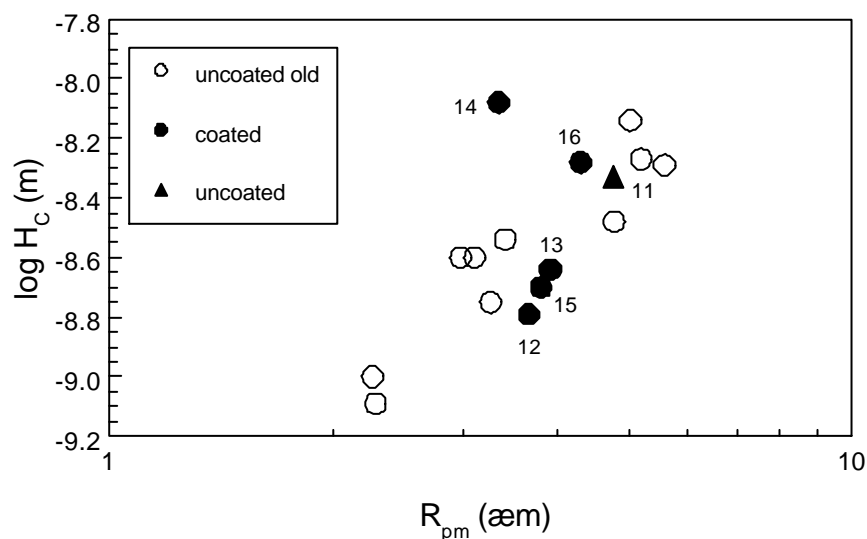
Figure 3.18 Position of the Stribeck curve as a function of material roughness (coated and uncoated steel). Labels 11-16 denote different materials.
The effect of roughness on the position of the curves does not obey the relationship

found for the uncoated materials (section 3.4.1.3). This can be seen in figure 3.18 where the data of both test series have been combined; note, however, that the result for the uncoated reference material ST11 fits nicely. It has been noticed that the materials with a hard surface (11,14,16) all give Stribeck curves which are shifted more to the right, compared to the curves for material with soft coatings (12,13,15). In an effort to deal with this effect, the position of the curves has been plotted against a combination of roughness and (micro) hardness as in figure 3.19. Now the results for all materials do fit together. The parameter defined in this way ($R_{pm}^2.H_V$) has no physical meaning, it only illustrates the influence of the surface hardness on the position of the Stribeck curve. For this action the hardness of the phosphate coated material ST13, which could not be measured, has been assumed to be equal to that of the related material ST12.
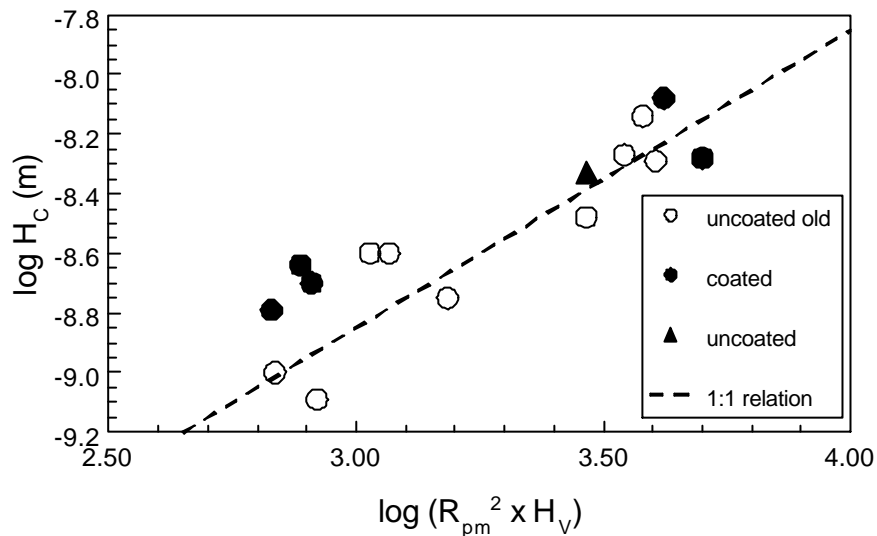
Figure 3.19 Position of the Stribeck curve as a function of material roughness and hardness (coated and uncoated steel).

The effect of the coating hardness on the Stribeck curves is illustrated further in figure 3.20 by examples of three materials. Comparing a soft coating (material ST12) with a hard coating (ST14), one sees that the softer coating has a higher friction at boundary condition (which also depends more on pressure, see figure 3.17), and the Stribeck curve is shifted to higher values of H_C. The effect of hardness can probably be ascribed to the fact that for coated materials flattening of the asperities by plastic deformation plays a relatively important role. The behaviour of material ST13 is particularly interesting. This material is equivalent to material ST12 (galvanised), except for a very thin layer of phosphate. This thin layer does not affect the position of the curve, but it reduces the friction at boundary lubrication to the level for hard coatings.
The Stribeck curve for the uncoated variant was similar to the one for material ST14.

These observations are in general agreement with those of Dane although the difference in lubricant caused some difference in the influence of pressure on the friction at boundary lubrication [Dane 1994].
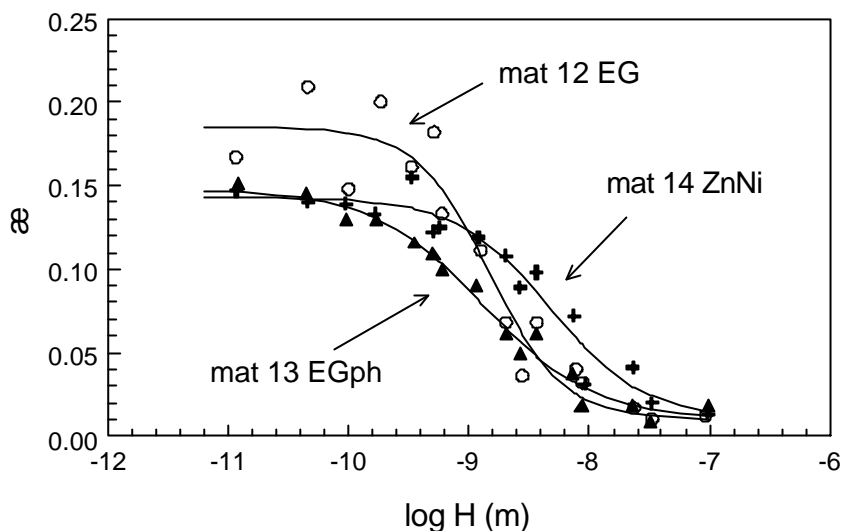
Figure 3.20 Effect of coating type on the Stribeck curve illustrated for three materials (coated steel). Pressure 6 MPa.

3.4.3 Second series on uncoated steel

So far, all friction tests on steel have been carried out using the strip tester, while most of the friction tests on aluminium described hereafter, have been carried out on the rotating tester. Consequently, a direct comparison is not possible, because both testers can give different results (section 3.3.4). Therefore some additional tests with steel have been carried out on the rotating tester, using as much as possible the same conditions that have been used in the friction tests with aluminium. These tests on steel in fact have been carried out after the tests on aluminium described in section 3.5.

3.4.3.1 Experimental procedures.

Four materials have been selected for these tests. To reduce plastic deformation of the roughness peaks as much as possible, some harder materials than usual have been chosen, as well as materials with different roughness levels. Three of the four materials have been drawn from the original set of 32 steel variants (section 2.1.1), the fourth had not been tested before. The materials have been labelled ST19, ST20, ST21 and ST22. The properties of the materials can be found in appendix A.

The conditions for the tests were very similar to those used for the last tests on aluminium and can be found in table 3.6 and, more extensively, in appendix B.

Tester	rotating tester, notches 11x11 mm²
Speed	1-1000 mm/s
Pressure	2 - 20 MPa
Lubricants	N6130, N500, N100

Table 3.6. Conditions for the second series of friction tests on uncoated steel.

3.4.3.2 Influence of lubricant.

During the tests a peculiar phenomenon showed up, i.e. the results obtained for the three lubricants did not blend into a single curve. A striking (and extreme) example is given in figure 3.21. The lubricants N100 and N500 give results which form a single curve, but the results obtained with N6130 are different. The difference in behaviour of these lubricants is the friction at boundary lubrication. For N6130 the friction at boundary lubrication is constant, but for the other two materials the friction at boundary lubrication still increases when the speed is decreased. The friction at mixed lubrication is not affected, all three lubricants give identical results. This makes it different to fit the data by means of a tanhyp function, because this fit assumes that at boundary lubrication the friction is constant. Therefore a subset of data has been formed, consisting of the results obtained with N6130, and the results obtained with N500 for speeds of 100 mm/s and higher. As the friction at mixed lubrication is not affected, the transition points can still be determined reliably from this subset of results.

The above difference between the lubricants has not been observed in the tests with aluminium in which the same lubricants (N6130 and N500) have been used. These results are described below but they have been obtained before these tests on steel. Two possible reasons can be found for this. Firstly the region of mixed lubrication is much wider for aluminium, and little data have been obtained under true boundary conditions, so this phenomenon may not have been noticed. Secondly the lubricants may just behave differently in combination with aluminium.
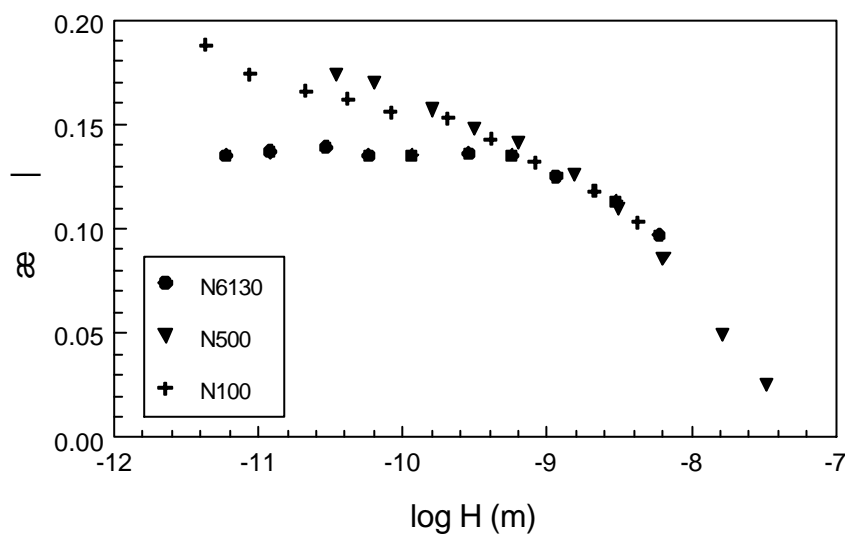
3.21 Influence of lubricant on the coefficient of friction at boundary conditions (uncoated steel). Material ST19, 10 MPa.

3.4.3.3 Influence of pressure.

The results from the above subset of data are presented in figure 3.22, together with the tanhyp fits. The Stribeck curves do not form nice 'parallel' lines as in figure 3.9, at least not as well as frequently observed for aluminium (see following sections). The slope of the region of mixed lubrication differs so that the Stribeck curves intersect occasionally. Notably material ST21 exhibits overall a lower slope that the other materials. In general, the height of the curves is not much influenced by the material type.
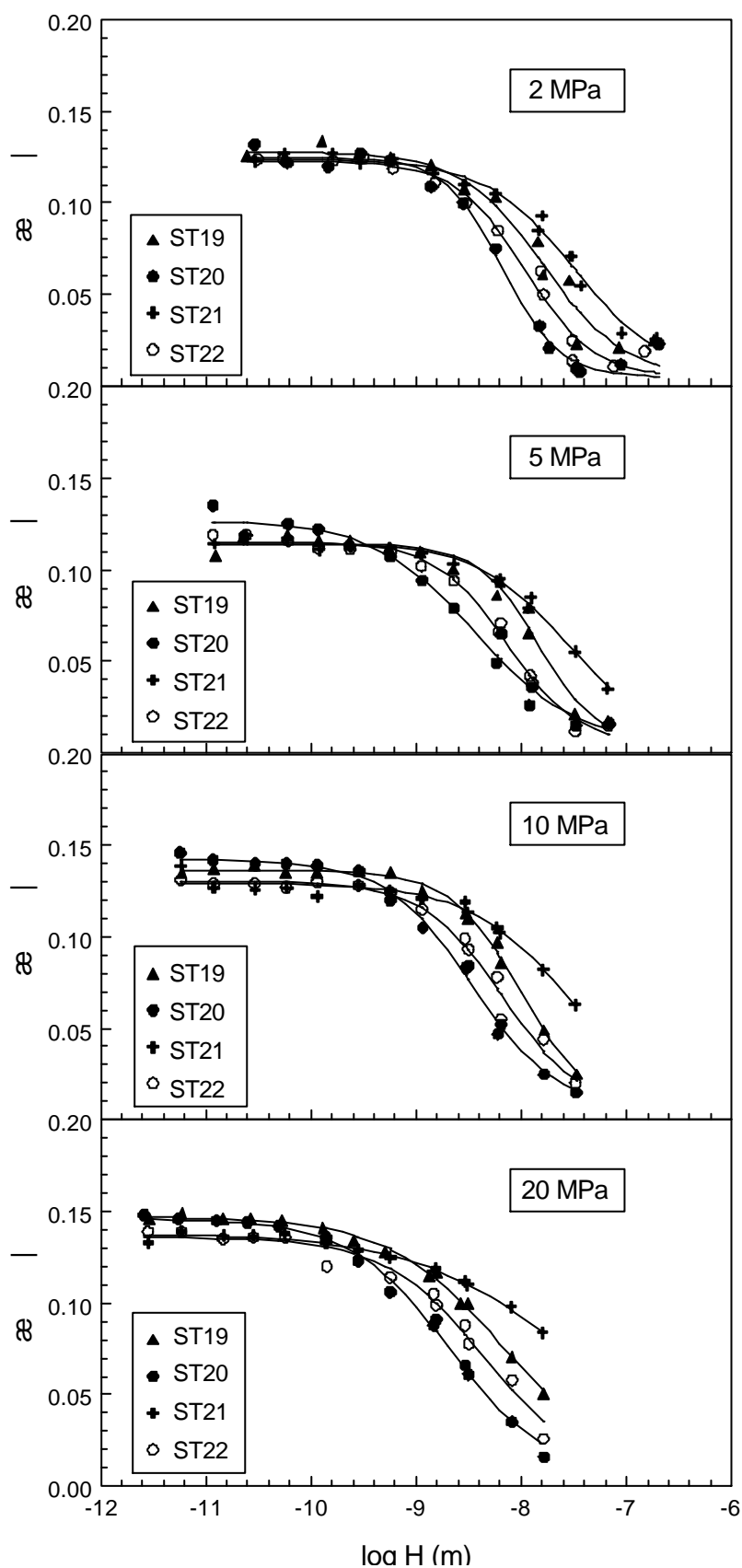
Figure 3.22 Influence of pressure on friction coefficient for uncoated steel.

Unfortunately, compared to earlier results for steel obtained using the strip tester, or the results obtained with aluminium using the rotating tester (described in the following), the curves are shifted more to the right. Consequently no much data have been gathered in

the 'lower' mixed region.

The transition points obtained from the tanhyp fits are presented in figure 3.23 (left hand side). Owing to the varying width of the mixed region the values of the transition points also show large scatter. The right hand side of figure 3.23 presents the position of the Stribeck curves as characterised by the midpoint H_C. This parameter shows but little scatter. Except for material ST21, the curves shift slightly to the left with increasing pressure. Evidently, when there are only a limited number of data points in the mixed region, the width of the mixed region seems to be more sensitive to scatter in the results than the midpoint. This has also been found in the results obtained using the strip tester. Material ST21, which showed a wider mixed region that the other three materials, notably at higher pressures, has also been tested in the first series on the strip tester where this material also showed a wider range than the other materials. Surprisingly the midpoint for this material matched the results for the other materials quite nicely.
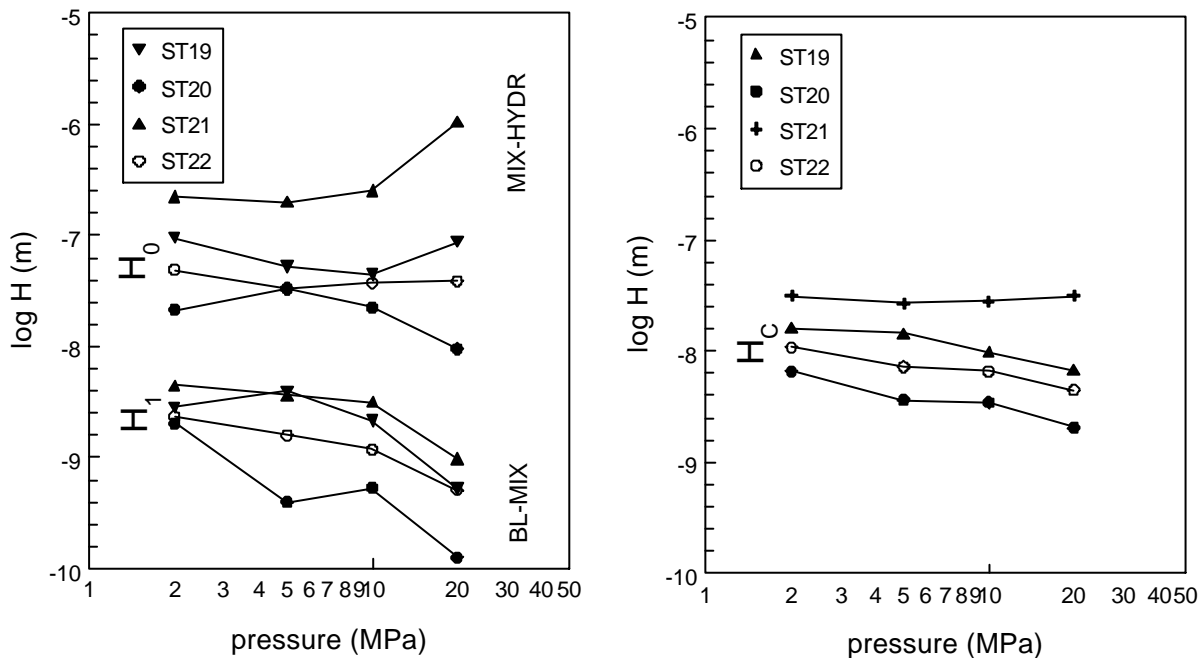
Figure 3.23 Transition points (left) and midpoints (right) as calculated from tanhyp fits for uncoated steel. BL = boundary lubrication, MIX = mixed lubrication, HYDR = hydrodynamic lubrication.

The friction at boundary lubrication has also been calculated from the fits, but obviously this value is only valid for lubricant N6130. The results are presented in figure 3.24. Apparently the friction at boundary lubrication tends to increase with increasing pressure. This is inconsistent with the results obtained on the strip tester, which in general showed that the friction at boundary lubrication decreases with increasing pressure (figures 3.8 and 3.17). The influence of pressure however is much smaller than has been found for aluminium (see following sections).

The value of the friction at boundary lubrication is lower than has been found previously with the strip tester but this may well be an effect of the lubricant.
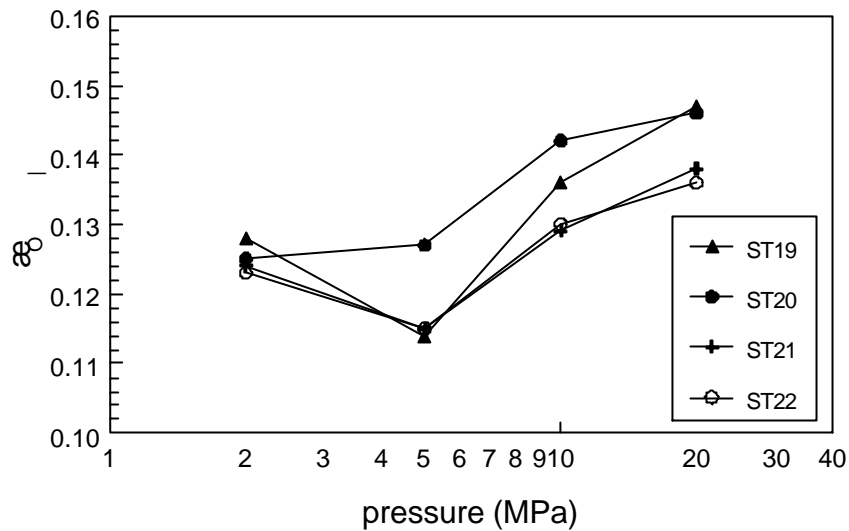
Figure 3.24 Coefficient of friction at boundary conditions as calculated from tanhyp fits, for uncoated steel.

3.4.3.4 Influence of roughness.

The differences between the materials, shown in figure 3.23, can be largely eliminated by plotting the results as a function of the new parameter H^* (see section 3.4.1.3), or, to be more specific, by calculating the corrected position of the Stribeck curve $H_C^* = H_C/R_{pm}^2$. The results are presented in figure 3.25, which has been plotted to the same scale as figure 3.23 for easy comparison. The differences between the materials are now greatly eliminated, with an exception for material ST21 at higher pressures. The results of figure 3.22 reveal, however, that for this material and higher pressures, no results have been obtained in the 'lower' mixed region, therefore the fit of the tanhyp function may be incorrect.
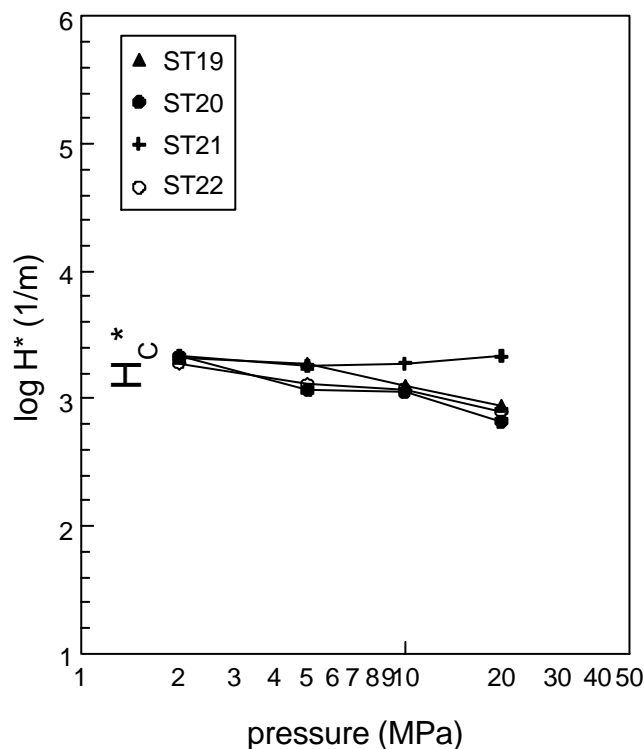
Figure 3.25 Midpoints corrected for the influence of roughness, for uncoated steel.

The fact that the difference between the materials can be fully ascribed to the difference in roughness implies that the difference in hardness of the materials has little or no influence. Probably, plastic deformation of the asperities is not very large compared to the elastic deformation which does not depend on hardness. This seems to contradict with the results for coated steel where an influence of hardness has been found (section 3.4.2.3). However, the results here have been obtained with materials harder than normal, while for coated steels large effects have only been found for soft coatings.

Figure 3.24 further reveals that for the two rephosphorised materials (ST20 and ST21) the rougher material has a slightly lower friction coefficient at boundary lubrication than the smoother material. This effect can also be seen in figure 3.9, but it is almost negligible there.

3.5 FRICTION TESTS ON ALUMINIUM

In many cases the friction tests on aluminium have been performed with material which was still under development. Therefore in many cases fresh (up to date) material has been supplied for each test. The friction tests started well after completion of the rotating tester, so that, with only a few exceptions, all friction tests have been carried out on that tester.

3.5.1 First series of friction tests on aluminium (MF and EDT).

3.5.1.1 Experimental procedures

The first series of friction tests on aluminium have been performed with an aim to study the difference between MF and EDT roughness. Two materials have been used, AL01 and AL02 (see appendix A). A summary of the testing conditions can be found in table 3.7 and, more comprehensively, in appendix B). Examples of MF and EDT roughness on aluminium can be found in figure A.7 in appendix A.

Tester	rotating tester, notches 11x11 mm²
Speed	1-1000 mm/s
Pressure	2 - 20 MPa
Lubricants	N100, N200, N500

Table 3.7. Conditions for the first series of friction tests on aluminium.

After completion of the tests a defect in the measuring system has been discovered; consequently many observations had to be discarded. This affected notably readings with low friction forces (low pressure, low friction or low roughness). It also has been noticed that full boundary lubrication has not been achieved in the tests. As a result it was not possible to construct full Stribeck curves and to fit them by a tanhyp function.

3.5.1.2 Influence of pressure

The effect of pressure on friction is presented in figure 3.26 for both types of roughness. The influence of pressure is clear, higher pressure shifts the Stribeck curves to the left, and this effect is stronger for EDT roughness than for MF roughness (this pressure

effect will be dealt with in more detail when discussing the next series of tests).
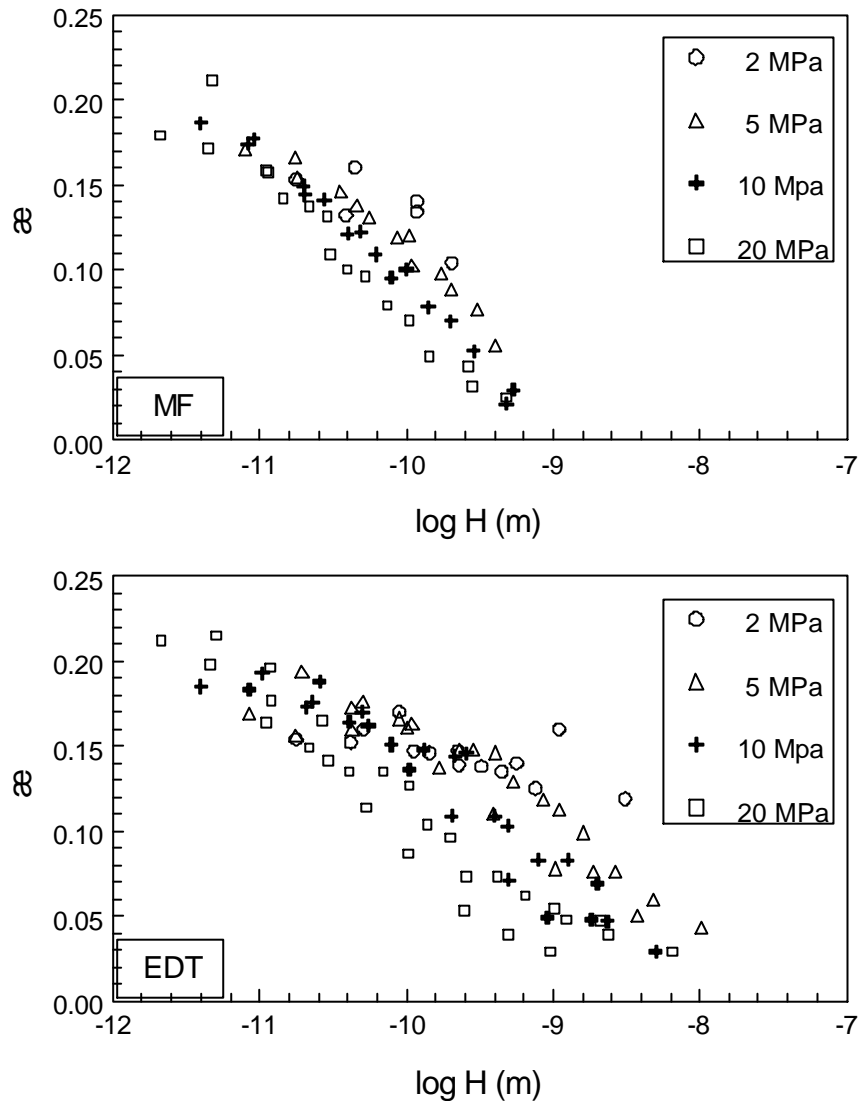
Figure 3.26 Influence of pressure on coefficient of friction for aluminium (mat. AL01, AL02).

3.5.1.3 Influence of roughness

The difference between MF and EDT roughness for each value of the pressure can be seen in figure 3.27. In general EDT gives higher friction than MF. This is not surprising, because it is in agreement with the general observation for steel that under mixed conditions higher roughness gives higher friction. Also it can be noticed that the friction under boundary conditions is higher for higher pressure, compare for example the values for H $= 10^{-11}$ m. This effect can also be noticed by careful examination of the results in figure 3.26. It contradicts with the observations for steel, where higher pressure give lower friction (see figure 3.17).
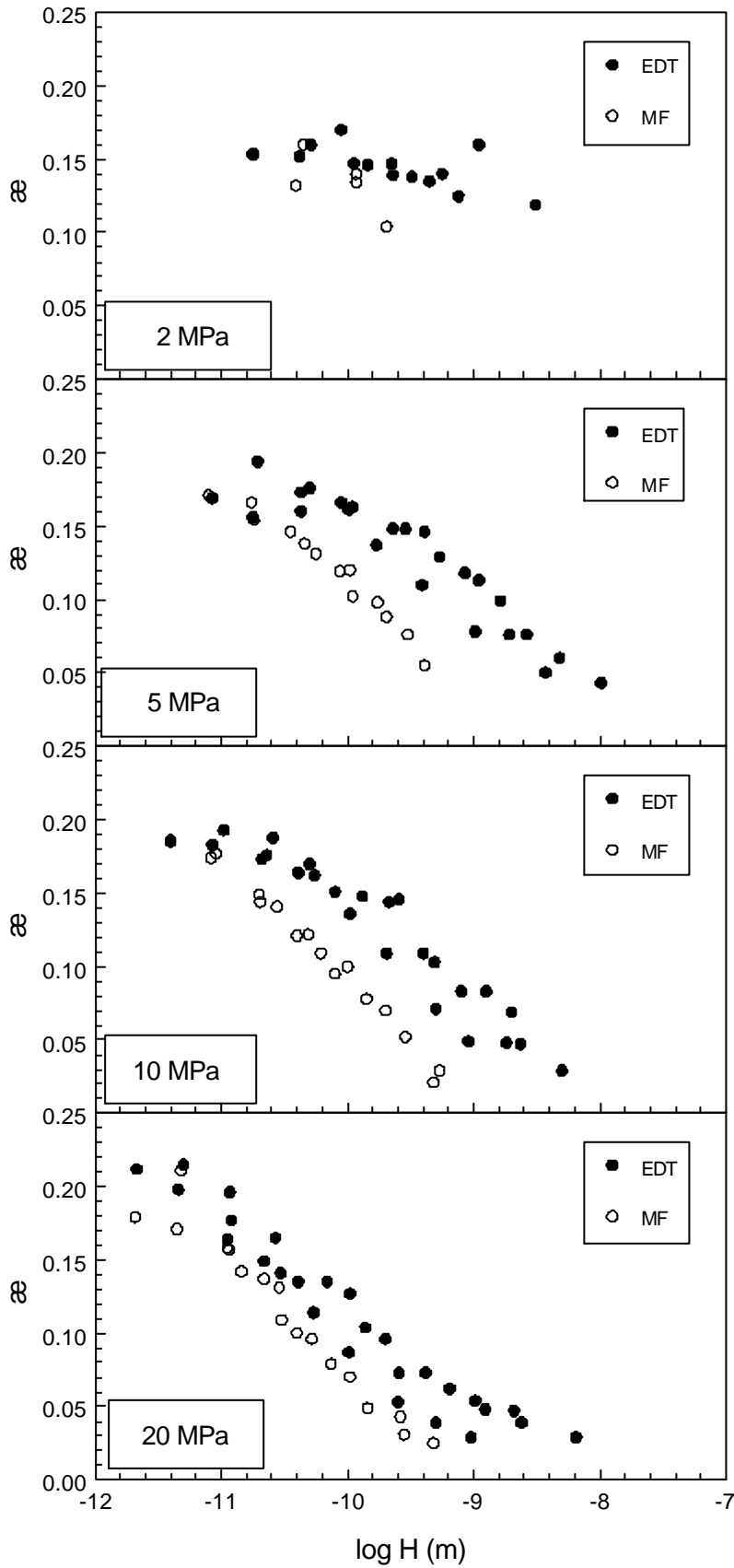
Figure 3.27. Difference between MF and EDT roughness at different pressures, aluminium (mat. AL01, AL02).

3.5.1.4 <u>Influence</u> <u>of</u> <u>orientation</u>

MF type roughness has a very strong directional texture. In fact, this type of roughness can be described as a system of parallel grooves, all oriented in the rolling direction. It may therefore be expected that the friction also depends on the orientation of movement. This effect cannot be studied using the rotating tester, therefore some additional experiments have been carried out using the strip tester. The conditions can be found in appendix B and the results in figure 3.28. In this figure results from the rotation tester are presented as well for comparison, although both testers may give different results (see section 3.3.4). Please note also that the results for the rotating tester have been obtained at 2.0 MPa in stead of 2.4 MPa. Obviously an orientation of 90°, where the movement is perpendicular to the 'grooves' of the roughness, gives higher friction than at an orientation of 0°. This indicates that the generation of pressure in the lubricant is stronger in the 90° direction. The results are in agreement with those published by Saha [Saha 1996]
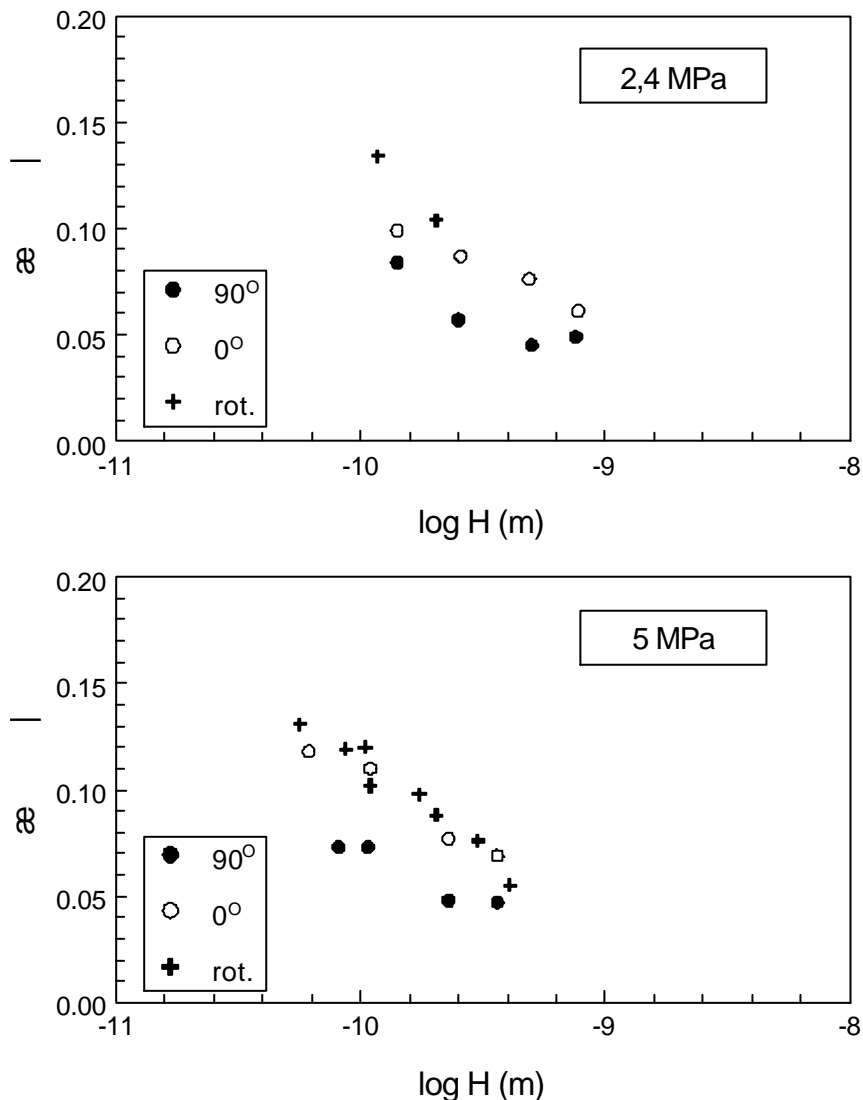
Figure 3.28. Influence of orientation of movement (relative to rolling direction) for aluminium with MF roughness, compared with results from the rotating tester (mat. AL01).
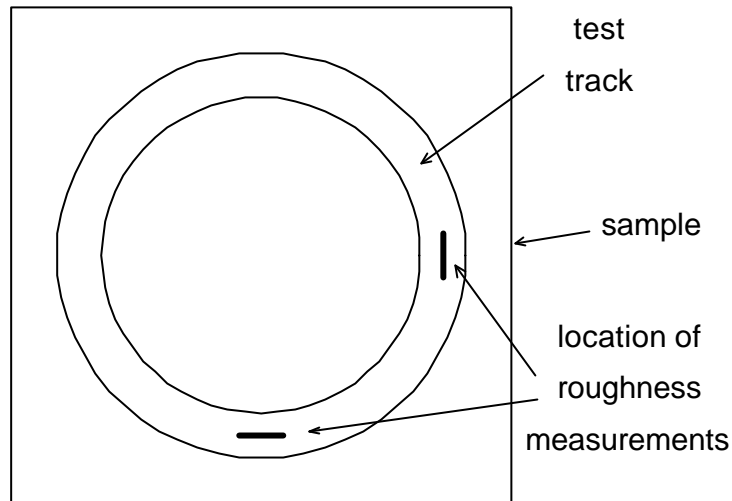
Figure 3.29 Locations on the specimen where the roughness has been measured after friction testing.
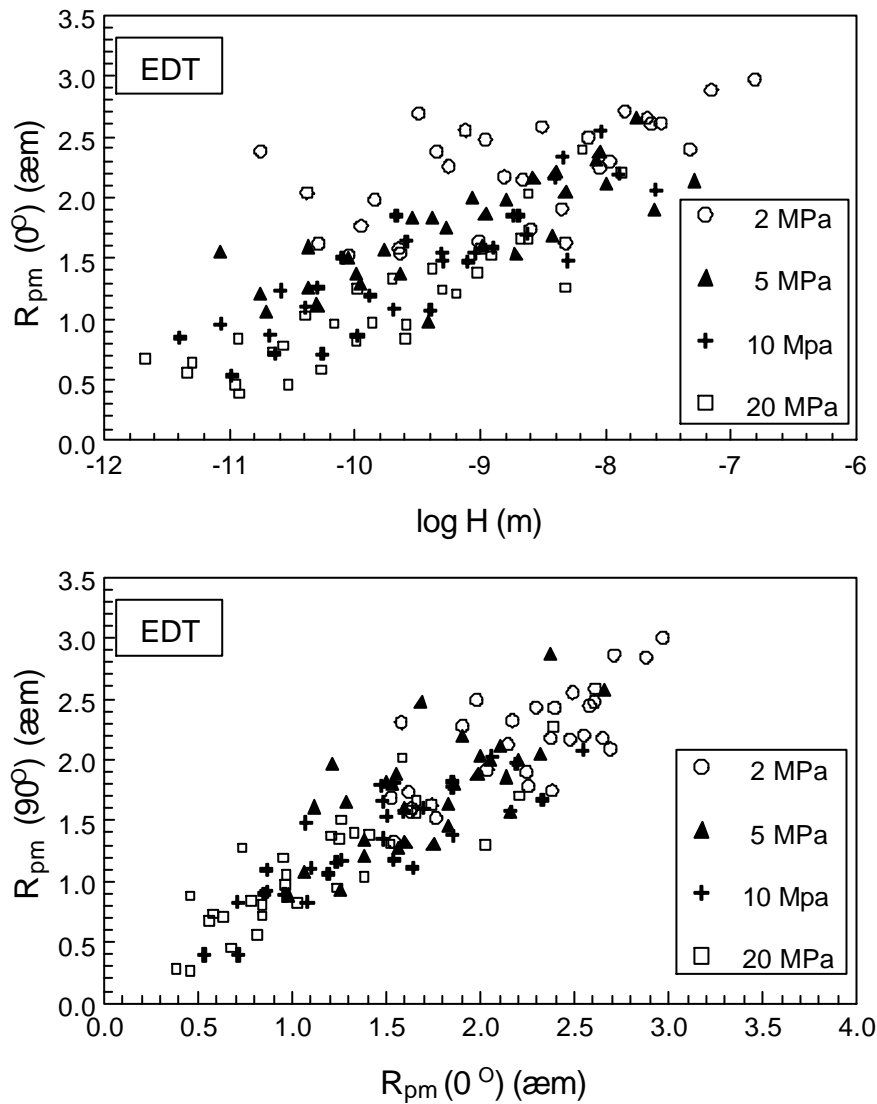
Figure 3.30 Flattening of the roughness by friction testing for EDT roughness, aluminium (mat. AL02).

3.5.1.5 Flattening of roughness

During these experiments, which formed the first larger friction study on aluminium, it has been noticed that the roughness of the material was much more flattened than had been observed for steel. To study this effect in more detail, the roughness of the samples after friction testing has been measured. The roughness has been measured parallel to the direction of movement in two orientations on the samples as shown in figure 3.29, and for all samples. To limit the amount of work, only one roughness measurement has been carried out on each position, which consequently increases the scatter in the results. Results for EDT roughness are presented in figure 3.30. The top figure shows the reduction in roughness for the 0° orientation. The roughness reduces significantly with decreasing value of H, and this effect is stronger for higher pressures. A comparison between the results in both orientations is made in the bottom figure from which we can conclude that there is no systematic difference between the observations in both orientations.
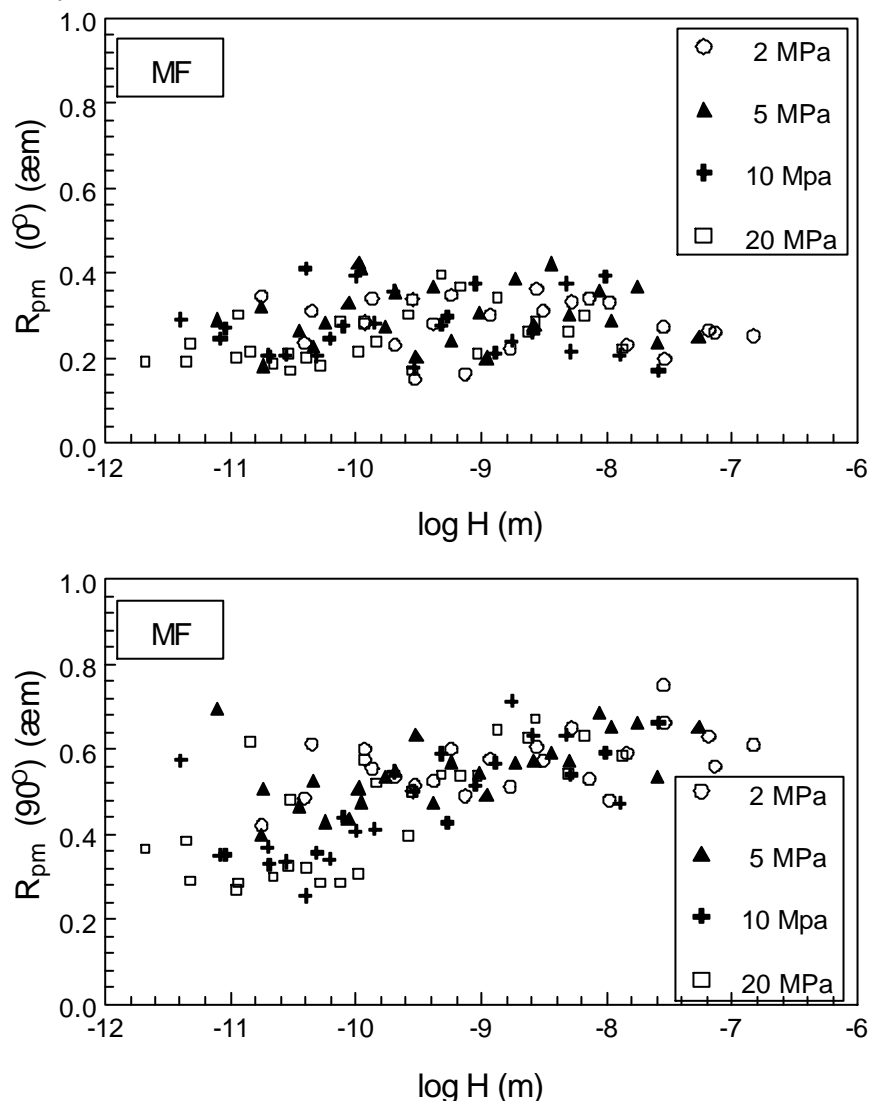
Figure 3.31 Flattening of the roughness by friction testing for MF roughness, aluminium (mat. AL01).

The results for MF roughness are presented in figure 3.31 for both orientations. The roughness parallel to the 'grooves' is hardly affected by the friction tests, as can be seen in the top figure. The roughness perpendicular to the 'grooves' is reduced by the tests in

a similar way as with the EDT roughness but on a smaller scale. The amount of reduction is not as high as for EDT roughness and the influence of pressure on the amount of flattening is also smaller.

This severe flattening of aluminium has also been observed by Dinkel [Dinkel 1997]

As roughness has a strong effect on friction (see section 3.4.1), we may expect that flattening of the material has affected the friction of these materials. So it is tempting to try to include the influence of roughness by plotting the friction data as a function of the parameter H* defined in (3.3), just as has been done for steel. This approach calls for a decision which value of R_{pm} is to be applied. For EDT roughness this is not difficult, as the values in both measuring directions are the same, so the average value of these two can be used.
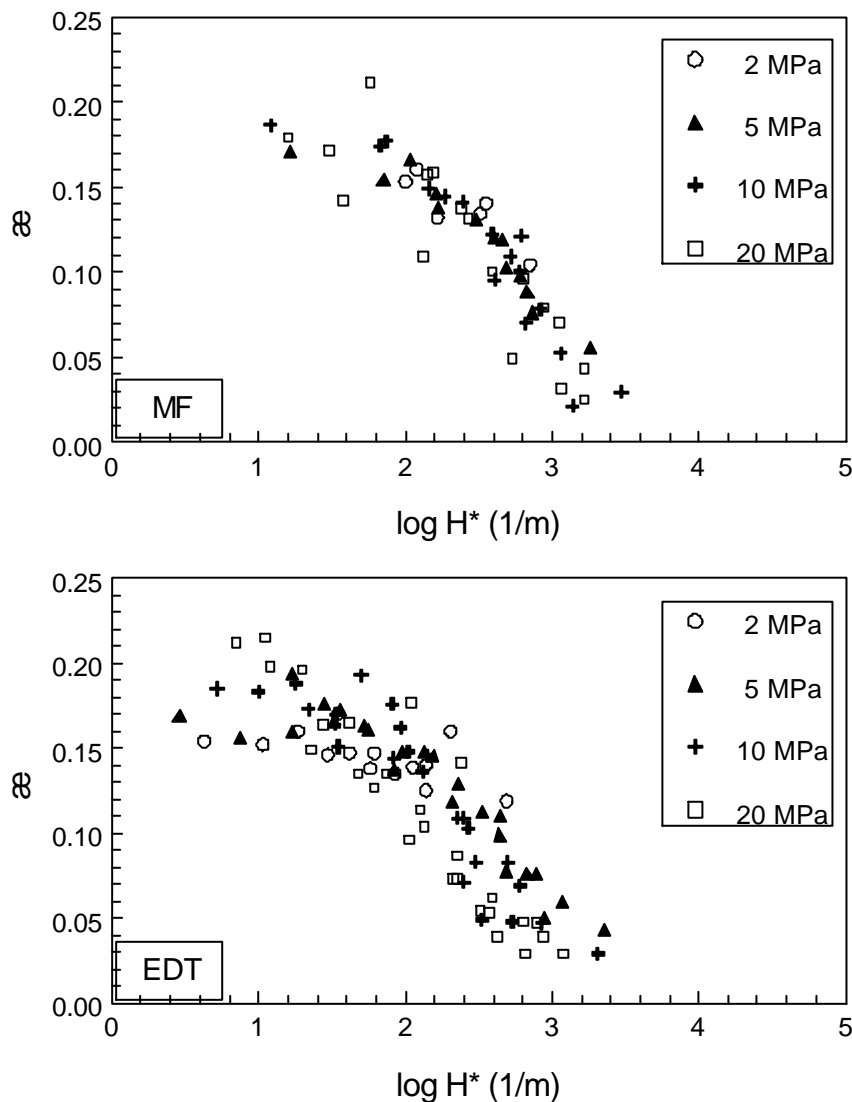
Figure 3.32 Results of the friction tests after 'correction for roughness' as described in the text, aluminium.

For MF roughness the situation is more complex. The generation of pressure in the lubricant at mixed lubrication is governed by two roughness parameters: the (total) height of the roughness and the texture of the roughness (although it is unclear how to quantify the latter). In principle the general texture of the roughness (a series of parallel grooves)

is not altered by flattening of the highest parts. It is therefore assumed here that the overall height (or: depth) determines the friction and as this is given by the measurement in the 90° direction, the R_{pm} values in that direction are used here. The results are presented in figure 3.32. Due to the (additional) scattering of the roughness measurements, the scatter in the data is larger than for the 'uncorrected' data (figure 3.26). For MF roughness the influence of pressure vanishes almost completely, with only a few exceptions at 20 MPa (for these points the measured roughness deviated from the values for other points). For EDT there is still an influence of pressure present, but this influence is smaller than for the 'uncorrected' data. Moreover, the Stribeck curves are steeper than with the original data.

A further analysis of the flattening of the roughness has been made out by performing 3D roughness measurements. Only a very limited amount of samples could be measured, therefore a selection had to be made. After careful examination samples have been selected which all have been tested at the same pressure and with the same lubricant, and with which different values of H have been obtained by changing the speed (table 3.8). By doing so various levels of flattening were included, which provided a representative set. Measurements on as-received material have been used as well. For each surface two recordings have been made at different magnifications.

Materials	aluminium EDT and MF (AL01 and AL02)
Speed	1-1000 mm/s (10 values)
Pressure	10 MPa
Lubricants	N100

Table 3.8. Selection of samples for 3D roughness measurements.
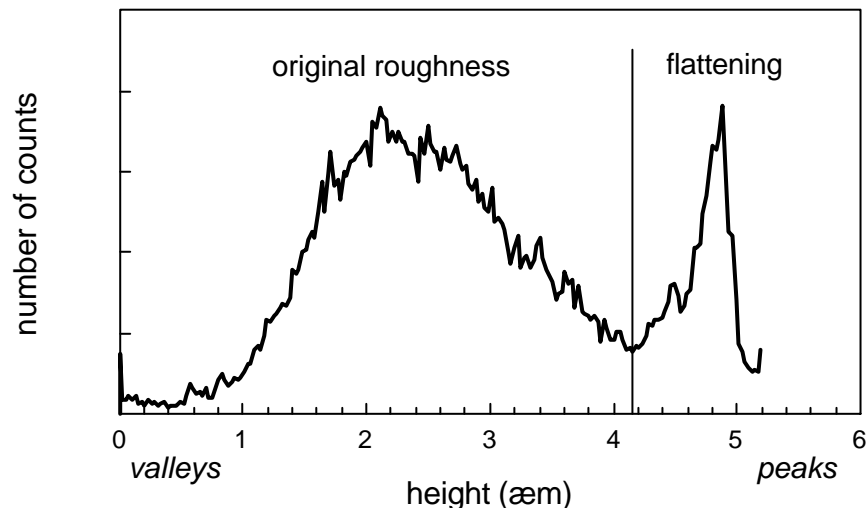
Figure 3.33 Example of height distribution of flattened roughness, showing both remnants of the original roughness and the flattened part. The height is measured upwards from the bottom. The bearing area at the transition height (4.15 µm in this example) is taken as the amount of flattened area.

From each series of 11 measurements for each material (10 samples after friction testing + 1 original surface) four samples have been selected, which gave a good overall impression of the flattening. From each of these four samples a coloured contour plot and a

photographic plot are presented in appendix A (figures A3 - A6). Examination of the pictures reveals some interesting details about the flattening of the roughness. With EDT material severe flattening creates isolated pockets arising from valleys of the original roughness. If these pockets are still filled with lubricant and the material is flattened further, hydrostatic pressure will be generated in these pockets which reduces the friction and reduces the sensitivity to galling [Lange 1988, Schedin 1990]. With MF type roughness these isolated pockets do not exist. The surface is severely scratched by the slider and the flattened roughness forms long channels, which are inter-connected by these scratches, with the result that hydrostatic pressure cannot be generated.
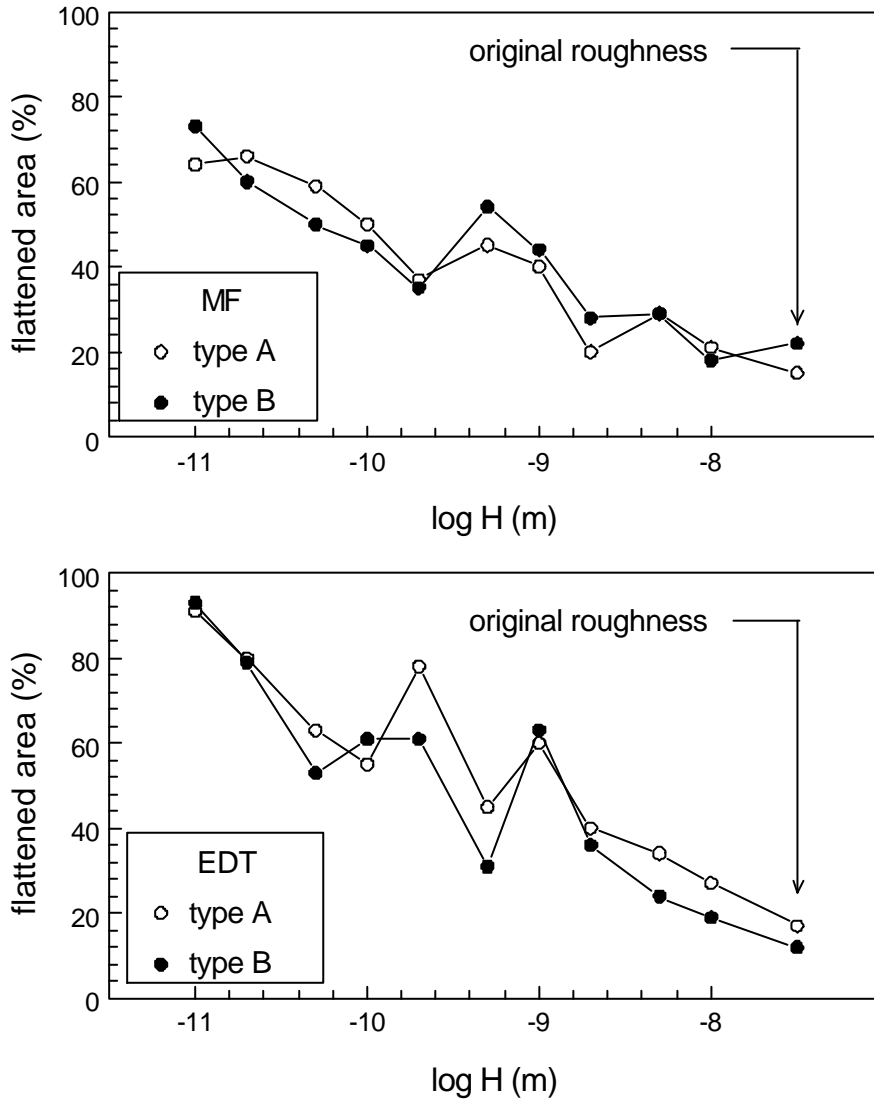
Figure 3.34 Amount of flattened area as calculated from the 3D roughness measurements for two magnifications. A: measured area = 1.75x1.35 mm², B: measured area = 0.44x0.34 mm², aluminium.

From the 3D measurements the amount of flattened area has been estimated by splitting up the roughness height distribution into two parts, one for the flattened surface and the other for the remaining parts of the original roughness. These two parts can clearly be distinguished in the height distribution as the example of figure 3.33 shows. The bearing area (the relative amount of 'metal' found in a cross section through the roughness at a certain height) at the transition between these two parts as indicated in figure 3.33, is

then taken as the flattened area. The results are presented in figure 3.34 for both types of roughness. Note that the as-received roughness also has some flattened part. These flat asperities are in fact remains of the sheet roughness, present before final cold rolling, which is much smoother than the final roughness. These results show a considerable flattening, for EDT roughness even more that for MF roughness. This flattened area should not be confused with the actual contact area. This actual contact area is much smaller that the flattened area which is the combined result of all micro flattening, caused by the colliding asperities in the contact zone.

3.5.2 Second series of friction tests on aluminium (MF and EDT).

The second series of friction tests has been performed to compare two levels of EDT roughness, a normal level with $R_a \approx 1 \mu m$ and a low level with $R_a \approx 0.5 \mu m$. MF roughness has also been tested as a reference. The EDT materials are denoted 'EDT high' and 'EDT low', respectively.

3.5.2.1 Experimental procedures

In the first series of friction tests on aluminium it has been noted that true boundary lubrication is very hard to obtain for aluminium (e.g. figure 3.27). Therefore we tried to obtain lower values of H by applying a very low viscosity lubricant 241 (see appendix C for a list of lubricants). Preliminary tests showed that this lubricant offered inadequate protection at high pressures, causing metal transfer (adhesion). After consulting the supplier, a mixture has been made of this lubricant and the more or less standard lubricant N6130. This mixture offered satisfactory protection, combined with reduced viscosity. The conditions are presented in table 3.9 and, more comprehensively, in appendix B. The three materials that have been used are labelled AL03, AL04 and AL05 (appendix A).

Tester	rotating tester, notches 11x11 mm²
Speed	1-1000 mm/s
Pressure	2 - 20 MPa
Lubricants	Qmix, N6130, N500

Table 3.9. Conditions for the second and third series of friction tests on aluminium.

3.5.2.2 Influence of pressure.

Complete Stribeck curves have been constructed for each pressure value and these are presented in figure 3.35. The results show a remarkable difference between MF and EDT roughness. The curves for EDT roughness are more or less parallel in each diagram (for each pressure). This means that the low and high EDT roughness behave similarly. The difference in roughness height causes a shift of the Stribeck curve as already noted for steel and an effect on the friction at boundary lubrication.
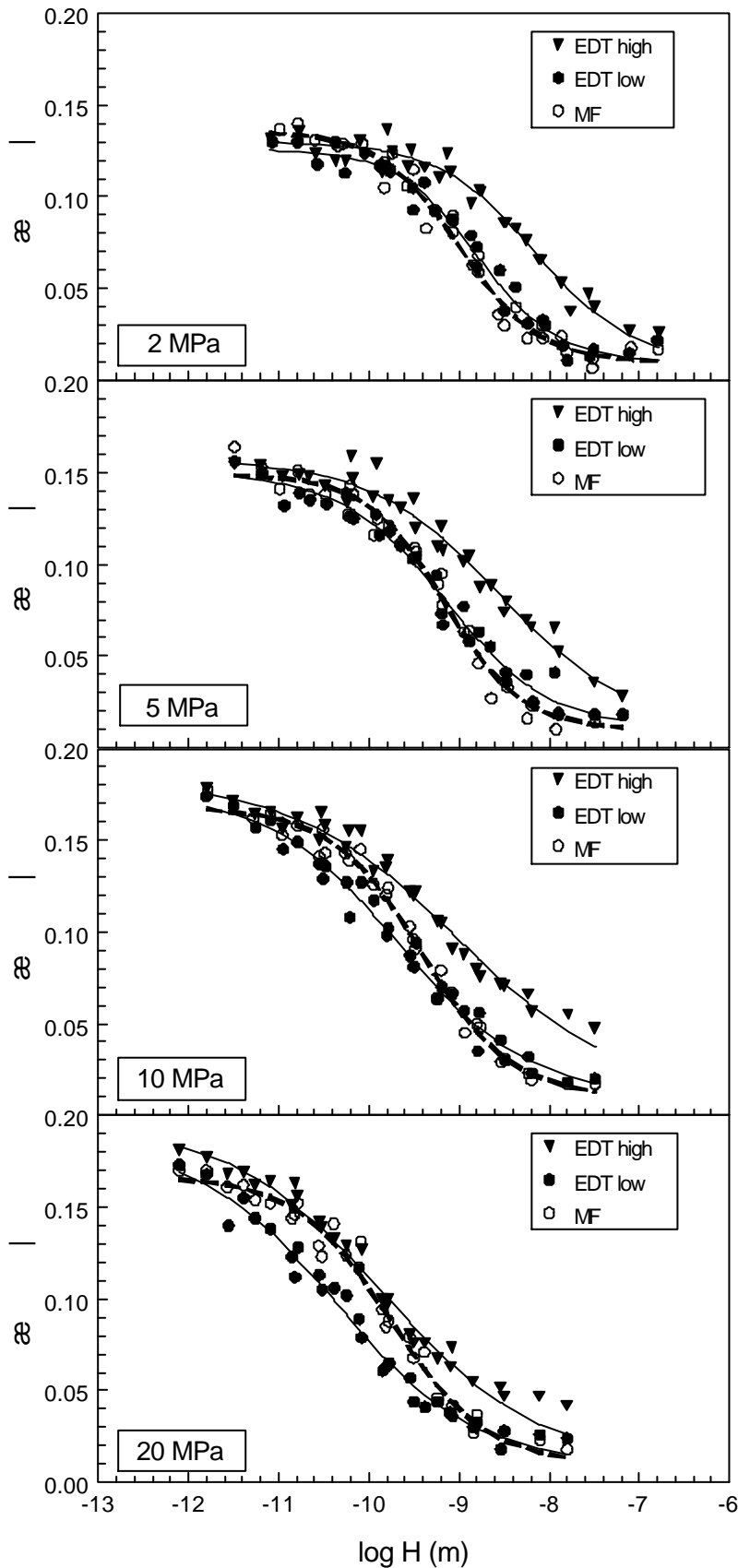
Figure 3.35 Influence of height of EDT roughness on aluminium, compared with MF roughness (mat. AL03, AL04, AL05).

The MF roughness, however, causes a different behaviour. At low pressures the friction

of MF roughness is similar to that of the low EDT roughness. At high pressures the friction resembles more that of the high EDT roughness, but because the Stribeck curve is steeper for MF roughness than for EDT roughness, a direct comparison does not lead to useful results.

Figure 3.36 Coefficient of friction at boundary lubrication for aluminium, as determined with a tanhyp fit of the Stribeck curve, as a function of pressure. (mat. AL03, AL04, AL05).

Figure 3.37 Transition points as a function of pressure for aluminium. BL = boundary lubrication, MIX = mixed lubrication, HYDR = hydrodynamic lubrication. (mat. AL03, AL04, AL05).

The friction at boundary lubrication has been derived from the tanhyp fits shown in figure 3.35; the results are presented in figure 3.36. Contrary to what has been observed for steel (figures 3.7 and 3.17), for aluminium friction at boundary lubrication increases with increasing roughness. The boundary friction depends less on pressure for the MF

roughness than for EDT roughness.

From the tanhyp fits the transition points H_0 and H_1 have been calculated as described in section 1.4.3. The results are presented in figure 3.37; in this figure the midpoints H_C are also presented for comparison with steel. Both EDT materials show a similar behaviour, the influence of pressure is more or less equal. MF roughness shows a different behaviour, i.e. the influence of pressure is smaller than for EDT roughness, notably for the transition boundary-mixed. Note that for EDT roughness the influence of pressure on the transition boundary-mixed is <u>very</u> large.

3.5.2.3 <u>Influence</u> <u>of</u> <u>roughness.</u>

Comparing the results for both EDT types of roughness gives an impression of the influence of roughness height. The friction at boundary lubrication is higher for the higher roughness, as can be seen in figure 3.36, contrary to what has been found for steel (section 3.4.3.4). Moreover for the higher roughness the Stribeck curves are shifted to the right, resulting in higher transition points. The average (logarithmic!) difference in the transition points is 0.35 for the transition boundary-mixed and 0.86 for the transition mixed-hydrodynamic. As the difference in roughness height is about a factor of 2.3 for the R_{pm} value (0.36 logarithmic) we can conclude that the transition boundary-mixed varies with, roughly, the 1st power of the roughness height and the transition mixed-hydrodynamic varies with the roughness height to the power of 2-3. This also implies that the width of the region of mixed lubrication is smaller for lower roughness. Furthermore the friction at boundary lubrication is somewhat higher for the high level EDT roughness than for the low level EDT roughness, contrary to the observations for steel (section 3.4.3.4).

3.5.3 Third series of friction tests on aluminium (EDT and EBT).

The third series of friction tests on aluminium has been performed to compare the friction of EBT roughness with the more conventional EDT roughness. This EBT roughness has been produced experimentally in co-operation with Sidmar. Two prototypes of EBT roughness have been produced. The types are labelled EBT1 and EBT2. The two types of EBT roughness have been produced in different batches and have been tested separately. For comparison, an EDT roughness has also been applied on exactly the same material as one of the EBT variants (EBT1).

3.5.3.1 <u>Experimental</u> <u>procedures</u>

The experimental procedures for these tests were the same as for the tests with 'low' EDT roughness, described in section 3.5.2. The conditions are presented in table 3.9 and more comprehensively in appendix B. The three materials used are labelled AL06, AL07 and AL08 (appendix A).

3.5.3.2 <u>Influence</u> <u>of</u> <u>pressure.</u>

Complete Stribeck curves have been constructed from the results; they are presented in figure 3.38 for the EBT1 (AL06 vs. AL07) and in figure 3.39 for EBT2 (AL06 vs. AL08). From figure 3.38 it can be concluded that the differences between EDT and EBT1 are surely not very large, as the differences are of the same magnitude as the scatter in the

data.
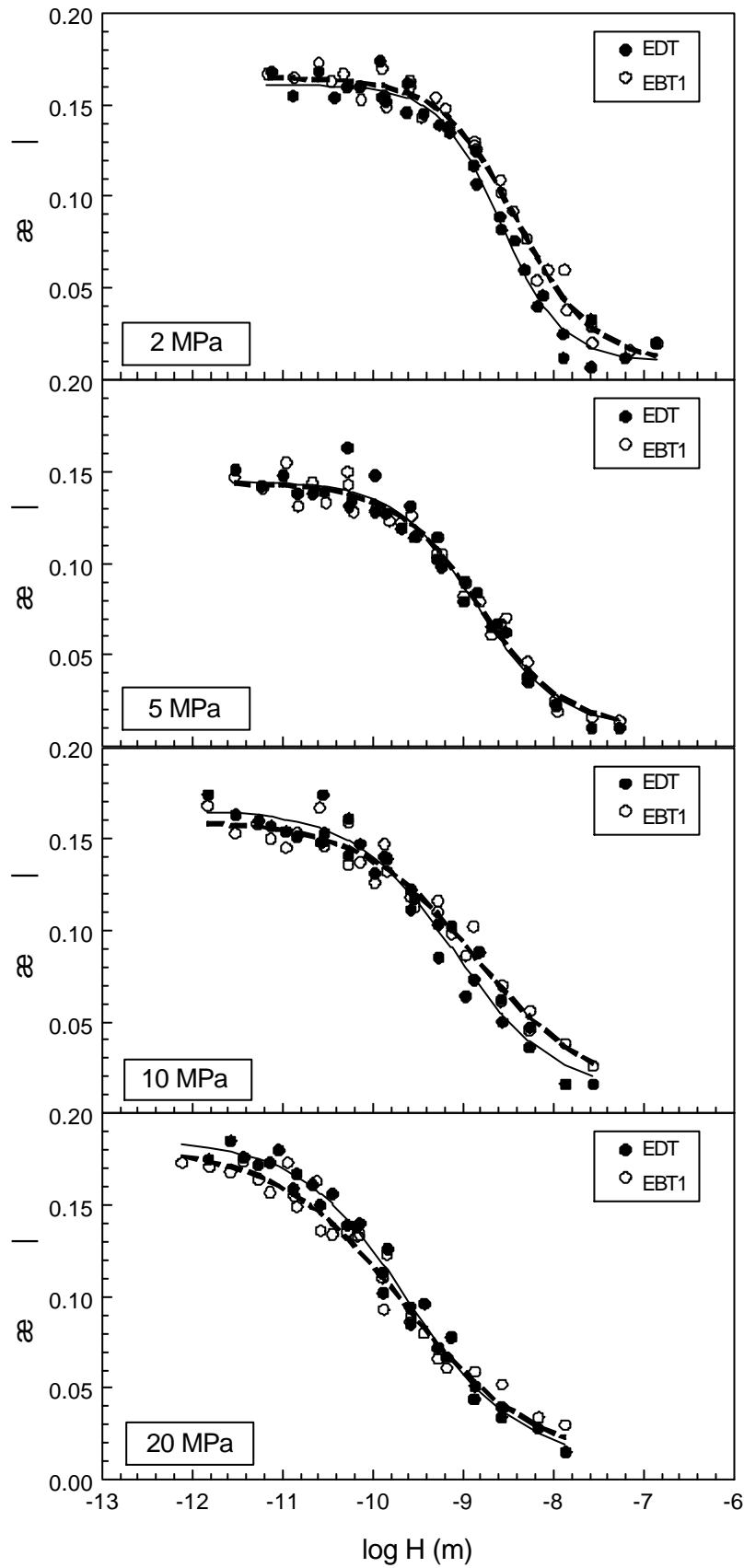
Figure 3.38 Difference between EBT and EDT roughness, first series, aluminium. (mat. AL06, AL07).
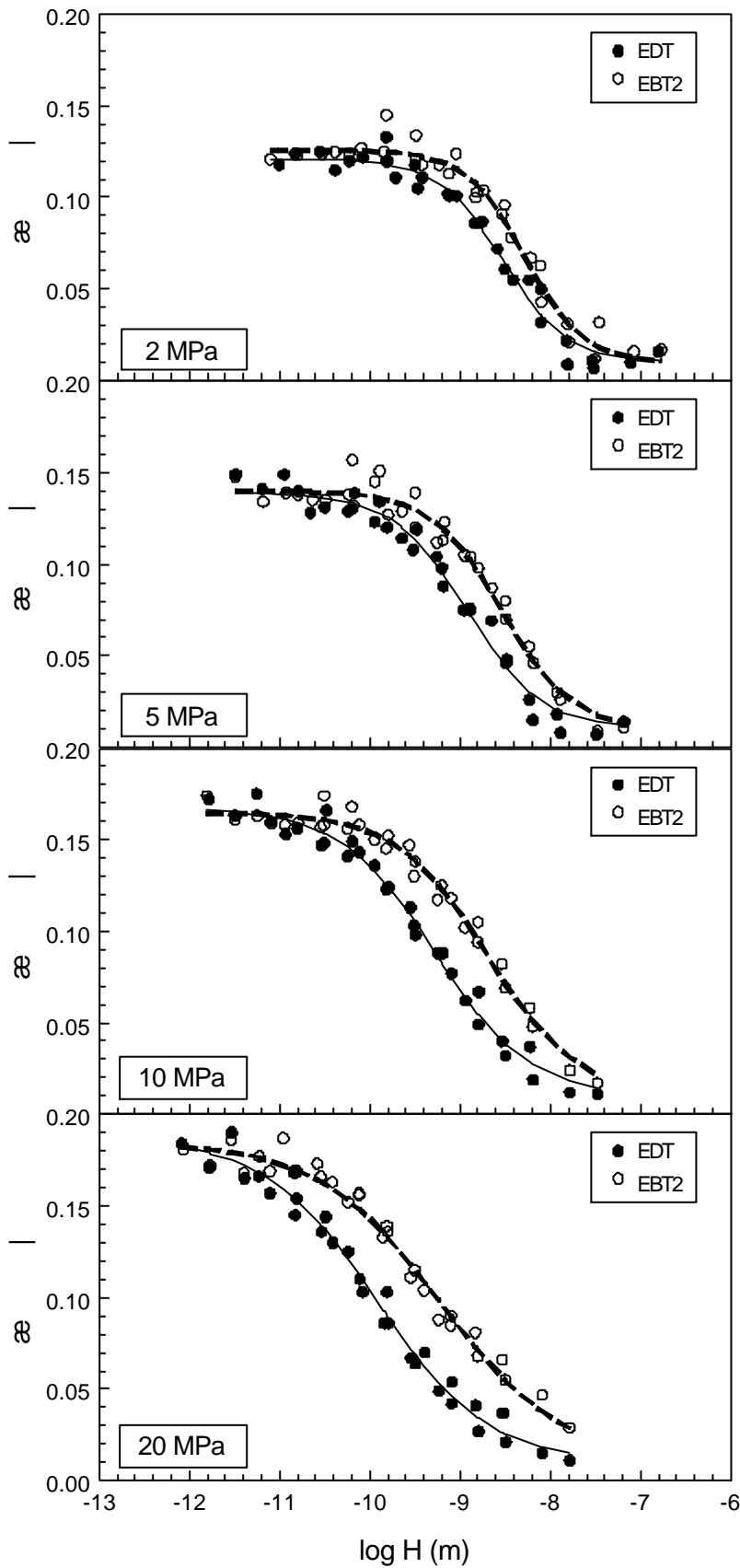
Figure 3.39 Difference between EBT and EDT roughness, second series, aluminium. (mat. AL06, AL08).

The EBT2 roughness, however, gives Stribeck curves which are clearly shifted to the right, compared to the EDT roughness (the EDT roughness in both figures concerns the

same material). Under conditions of mixed lubrication this causes higher friction for the EBT2 roughness.
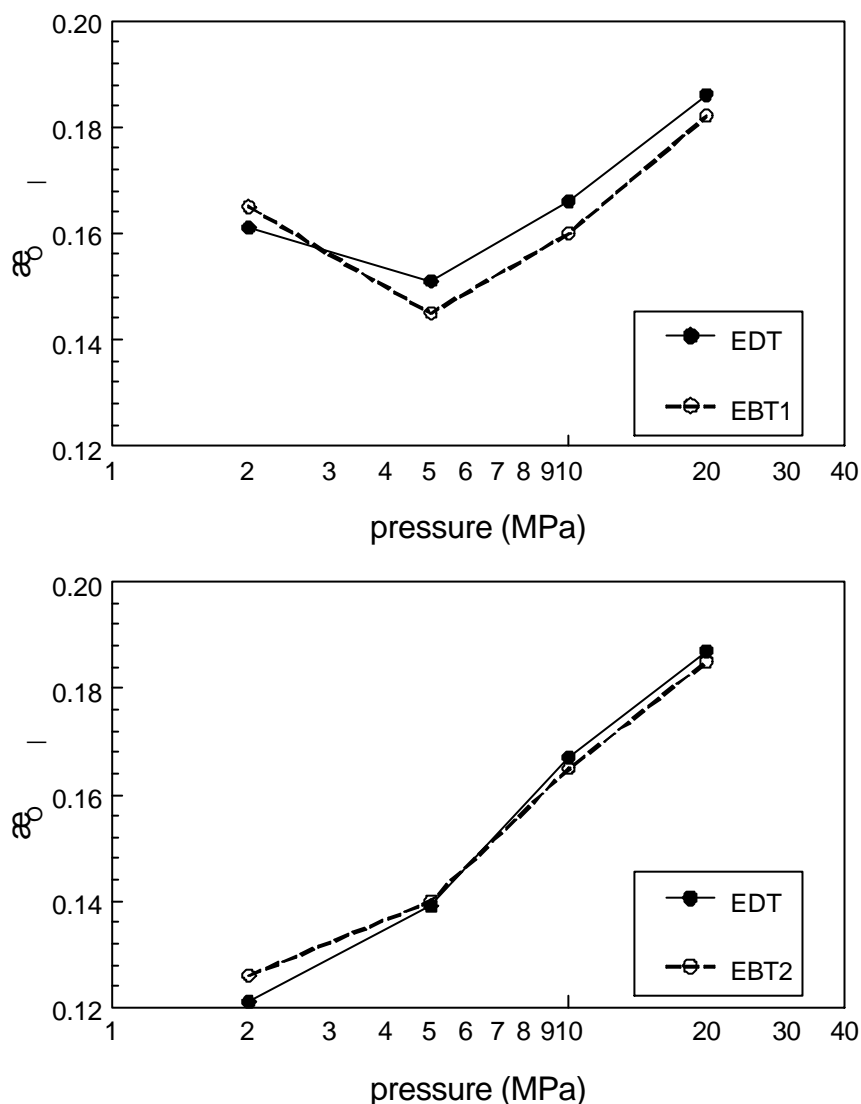
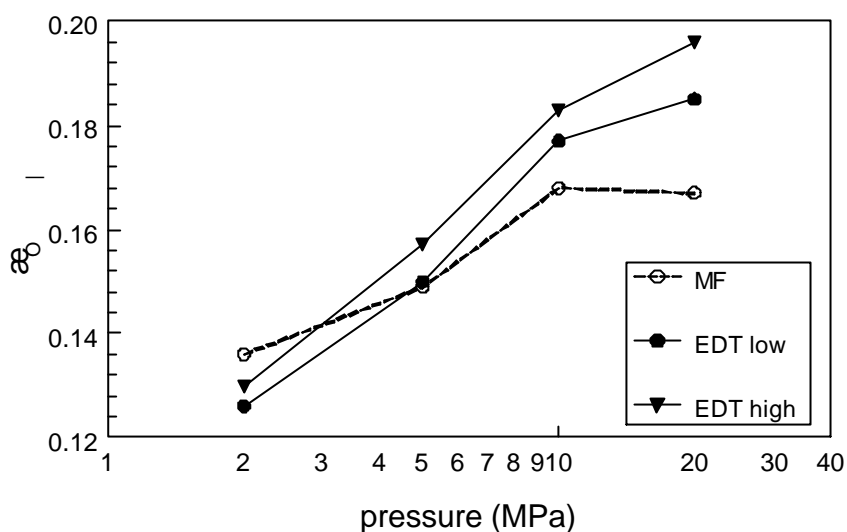*Figure 3.40 Coefficient of friction at boundary lubrication as determined with a tan-hyp fit of the Stribeck curve, as a function of pressure, aluminium. (top: mat. AL06 and AL07, bottom: mat. AL06 and AL08).*
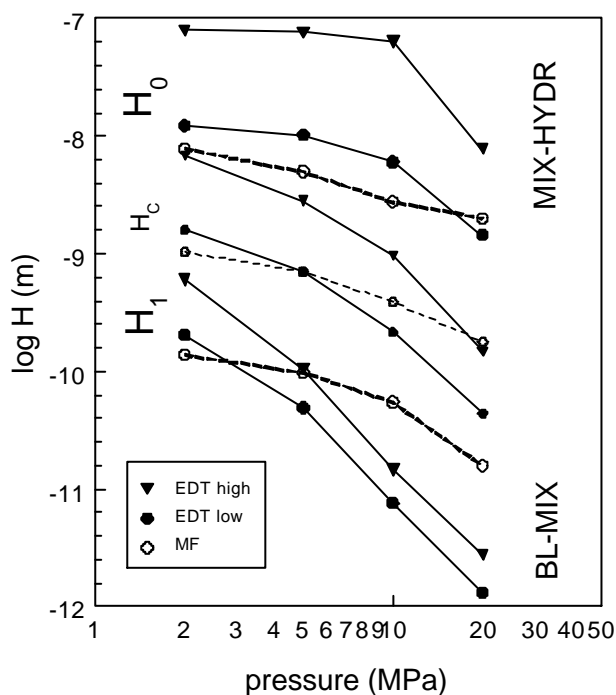
The friction at boundary lubrication has been determined from the Stribeck curve by applying a tanhyp fit, the results are presented in figure 3.40. This figure shows a striking difference in behaviour of the EDT material in both series. Although the material in both test series has been taken from the same stock, the influence of pressure on the friction at boundary lubrication is different. In the second series (bottom part of the figure) the friction at boundary lubrication simply increases with increasing pressure, similarly to the results obtained for EDT in other tests (compare with figures 3.32 and 3.36). In the first series, however, the friction initially decreases with increasing pressure and then increases again. The cause of this difference is unknown. Probably slight differences in the geometry of the notches have a stronger effect than has been expected.

The friction at boundary lubrication for the second type of EBT roughness is very similar to that for EDT roughness. For the first type of EBT roughness, the friction at boundary

lubrication is somewhat lower than for EDT roughness, except at the lowest pressure. From the Stribeck curves the transition points H_0 and H_1 have been determined by applying a tanhyp fit, the results are presented in figure 3.41 together with the midpoints H_C. The results for the EDT roughness are almost the same in both test series. The first type of EBT roughness shows little difference with respect to the EDT roughness, except for some scatter. The second type of EBT roughness shows transition points with a higher level of H, in agreement with the conclusions drawn from figure 3.33.
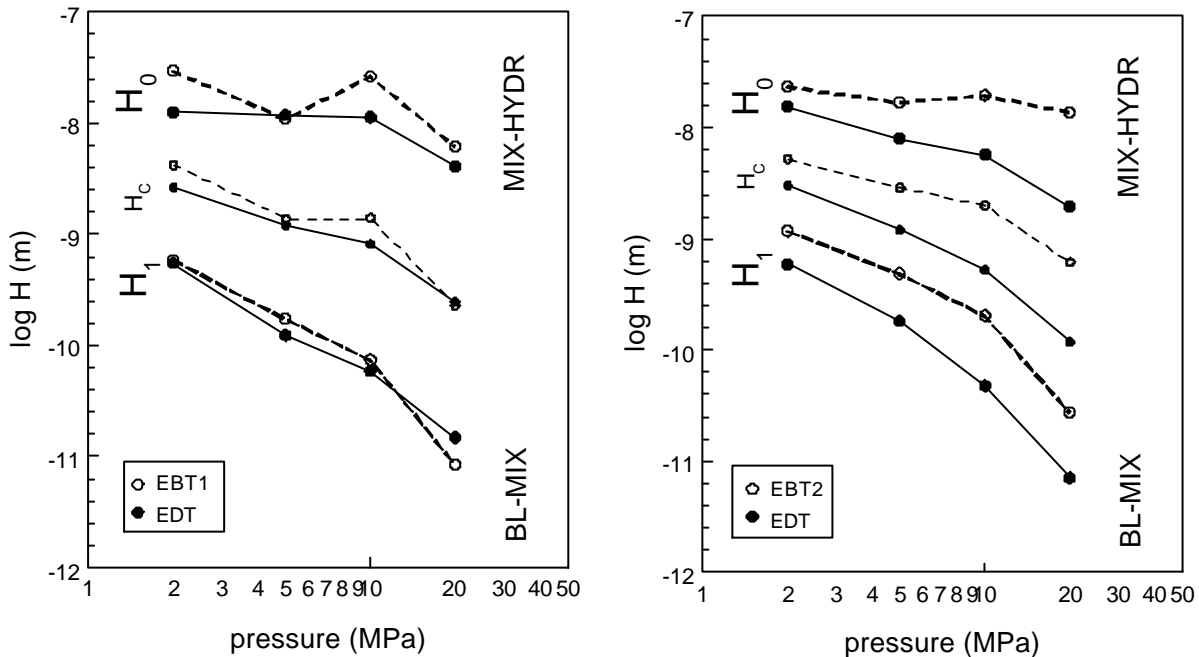
Figure 3.41 Transition points as a function of pressure, aluminium. BL = boundary lubrication, MIX = mixed lubrication, HYDR = hydrodynamic lubrication. (left: mat. AL06 and AL07, right: mat. AL06 and AL08).

3.5.3.3 <u>Influence of roughness.</u>

The EBT types of roughness are higher than the EDT roughness (see appendix A for roughness data). Based on the experience with aluminium EDT and steel, described above, it is to be expected that the Stribeck curves for the EBT roughness are shifted to higher values of H. This is indeed the case for the second type of EBT roughness (figure 3.39); the Stribeck curves are shifted to higher values of H while the shape of the Stribeck curves is very similar to that of the Stribeck curves for EDT roughness.

The first type of EBT roughness, however, does not exhibit much difference compared to EDT roughness despite the larger roughness height (figure 3.38). In other words: under conditions of mixed lubrication the friction is lower than might be expected from the roughness height alone. A possible explanation is that the first type of EBT roughness has isolated valleys around the peaks, which may act as a source of extra hydrostatic lubrication when lubricant is trapped in these valleys (see the micro-pictures in figure A.8 in appendix A). For the second type of EBT roughness the valleys have more interconnections, making it harder for lubricant to be trapped in isolated pockets.

3.5.4 Friction tests on aluminium at high pressure.

Friction tests at (very) high pressure have been carried out to test the hypothesis that for

aluminium the friction at high pressures and under boundary conditions is not constant, but reduces with pressure, resembling Von Mises friction. This hypothesis has been based on observations from deep drawing experiments, where the punch force became almost totally independent of the blankholder force (see section 2.7).

3.5.4.1 Experimental procedures.

For these tests three materials have been selected for which deep drawing results were available (not presented in this work), labelled as AL09, AL10 and AL11 (see appendix A). This selection implies both EDT and MF roughness, and 5000 as well as 6000 alloy type aluminium. To obtain high pressures a punch with very small notches has been made. A punch with larger notches has also been used for obtaining results at intermediate pressures. The conditions are summarised in table 3.10 and appendix B.

Tester	rotating tester, notches 7x7 mm² and 4x4 mm²
Speed	5-100 mm/s
Pressure	5 - 180 MPa
Lubricants	N6130

Table 3.10. Conditions for the friction tests on aluminium with high pressure.

In the tests the pressure has been increased in small steps until excessive wear occurred (for the small notches only). Examination of the samples with excessive wear revealed that this wear has been caused by bulk plastic deformation under the notches. We also noticed that at all other pressures no wear occurred, not even on a small scale.

3.5.4.2 Results

The results are presented in figure 3.42. A number of interesting conclusions can be drawn from this figure. Firstly, the effects are the same for all three materials, there is no influence of roughness or material type. Secondly, higher speed gives lower friction in all cases. Thirdly, the friction initially increases with increasing pressure and later decreases with increasing pressure; the pressure where the friction reaches a maximum value decreases with increasing speed. Finally, large notches give higher friction than small notches, which seems to contradict earlier results (section 3.3.4).

The influence of speed seems to indicate that friction has been occurring under mixed lubrication conditions, although the pressure was (extremely) high. Although the friction reduces with increasing pressure, notably for EDT roughness, the friction is not purely of the Von Mises type. At pure Von Mises friction the tangential stress at the surface is constant (and also the friction force) so that the effective coefficient of friction is inversely proportional to the pressure, which is clearly not the case in these experiments. The effect of notch type is puzzling. This effect (larger notches give higher friction) can only be noticed in the initial part, where the friction increases with increasing pressure. In the second part the 'curves' for both types of notches seem to blend (to some degree).
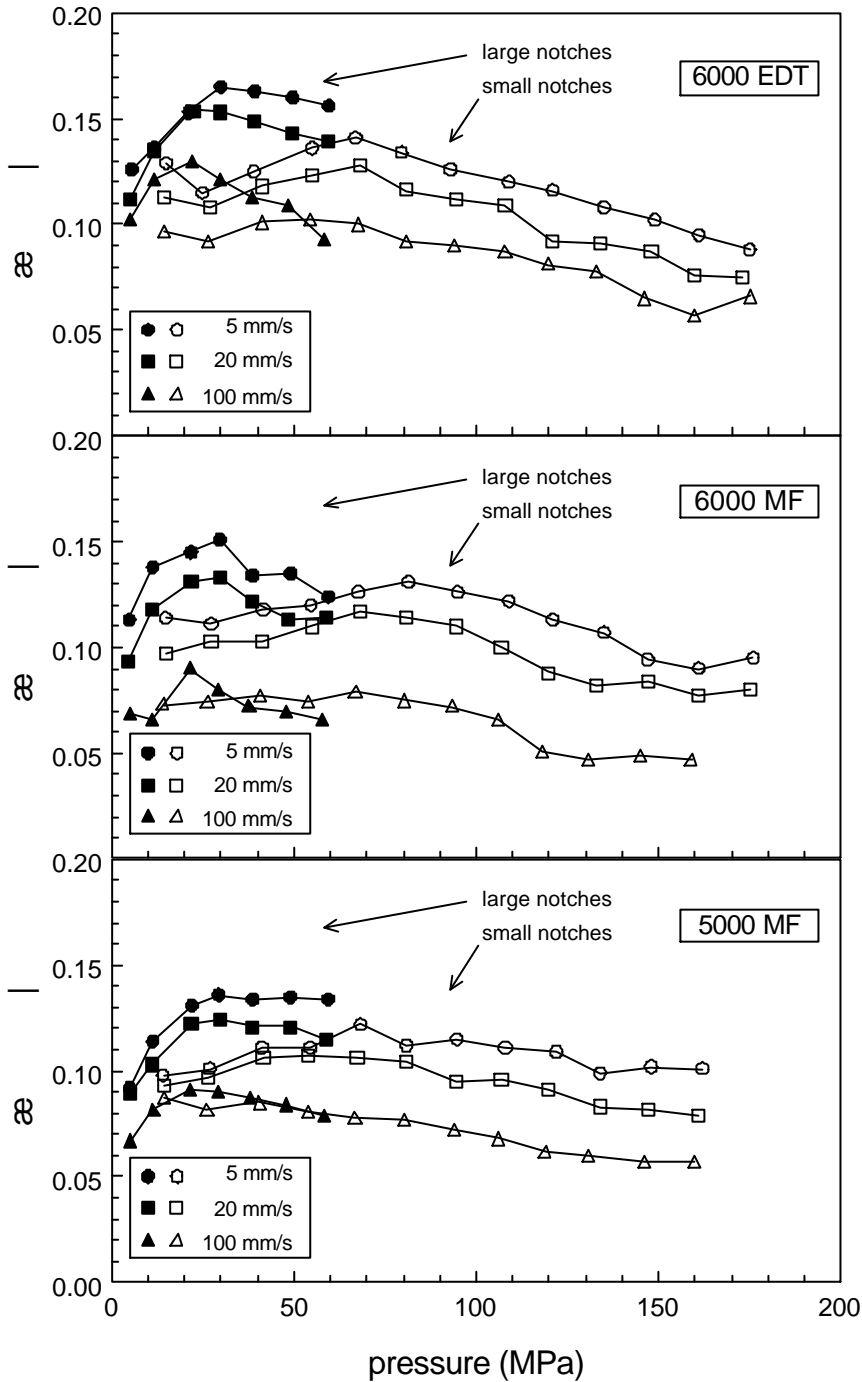
Figure 3.42 Results of friction tests at high pressures for aluminium. (mat. AL09, AL10, AL11).

3.6 DISCUSSION

This chapter deals with the measurement of friction with flat contacts. It has been shown (and painfully experienced) that this is not as simple as one might expect beforehand. The demands on the testing equipment are severe, notably in regard to the flatness of the slider. In this respect friction experiments with a concentrated contact are much simpler.

3.6.1 Influence of way of testing

An ideal experiment should give results which do not depend on the way of testing. Unfortunately this is not the case here. A most remarkable fact is that the friction depends on the size of the slider. This has been noticed by other researchers [Staeves 1996, Wagner 1995], but the nature of the effects is not always the same. In general there is a consistency in so far that larger sliders give lower friction, but the precise influence of length and width of the slider may be different. The consequences are clear: a whole series of friction tests must be performed using one and the same slider, it is not allowed to perform for instance part of the series with a smaller slider to obtain higher pressures. Furthermore, comparison of friction tests carried out at different institutes should be done with extreme care. It is not quite clear how this effect originates. A possible cause may be the existence of edge effects, i.e. that the conditions near the edges are different from those in the centre of the slider. Examples of these effects may be that the pressure near the edges is higher than in the centre owing to elastic deformation of slider or workpiece, or that the pressure in the lubricant under conditions of mixed lubrication is lower at the edges than in the centre (at the very edges the pressure is always equal to the atmospheric pressure). Edge effects have in common that their relative contribution is smaller with larger sliders. Lower lubricant pressure near the edges at mixed lubrication will increase the overall friction, but the effect of higher pressure near the edges depends on the way the friction reacts to changes in pressure.

In the tests at (very) high pressure, described in section 3.5.4, the opposite influence of the slider size has been found. The very small notches gave lower friction than the medium sized notches, at least at medium pressures. The conditions under these very small notches are much more severe than with the larger notches, used in standard tests. To understand the phenomena in detail the exact conditions must be known and these cannot be derived from simple considerations.

An other effect that has been encountered is that the friction at boundary condition may react strongly to minor changes in the slider geometry, as has been observed for aluminium (see figure 3.40). This indicates that friction experiments should be carried out in a comparative way, meaning that the tribological properties of a material can only be measured by comparing it with a 'standard' material in the same test. Furthermore, experiments should be carried in such a way that global changes in conditions (like room temperature) do not influence the principal results. In particular, in friction tests it should be avoided to refurbish the sliders halfway the test series because of damage, but this is not always possible by nature of the experiments.

As a consequence one should be careful to draw conclusions from the absolute value of the friction coefficient at boundary lubrication.

3.6.2 Influence of lubricant

The lubricant affects friction at boundary lubrication as well as friction at mixed lubrication, but in a different way.

At mixed lubrication pressure is generated in the lubricant by hydrodynamic effects and this pressure strongly affects friction. This generation of pressure is related to the viscosity of the lubricant, and this is taken into account in the definition of the Hersey pa-

rameter H. Without exception it has been found that different lubricants always give results which merge into a single Stribeck curve within the 'normal' scatter (all lubricants used in the experiments show Newtonian behaviour).

The friction force at boundary lubrication is product of the total contact area and the mean shear stress on those contacts. The latter is strongly affected by the lubricant properties, and an influence of lubricant has been found for steel (figure 3.21 shows a striking example, see also [Monfort 1990, 1991] and [Schey 1994]). For aluminium this effect has not been noticed in our experiments, where the same lubricants have been used as for steel. This may be caused by different (chemical) reactions between the lubricants and the metal surface. On the other hand, for aluminium, true boundary lubrication has hardly been encountered in the experiments, so that a lubricant effect may have occurred, but remained unnoticed.

The difference between the lubricants as such are clear. N100 and N500 are pure paraffinic base oils without any additives, while N6130 has advanced lubricating properties by applying (mostly) EP additives. At the onset of mixed lubrication, both types of lubricant give equal friction. For the base oils reducing the speed causes an increase in friction, but for N6130 the friction remains constant. A mechanism for the first effect has been proposed by Felder [Felder 1994] who states that at the very contact spots microhydrodynamic effects may occur, which induce a reduced form of mixed lubrication and hence an influence of speed. The effect of an additive in this proposed mechanism is not clear.

The first series of friction tests on uncoated steel (section 3.4.1) have completely been carried out using lubricants N100, N500 and related types, so the effect of influence of speed on friction at boundary lubrication must also appear there. This is confirmed by careful examination of the results, e.g. those presented in figure 3.12 and 3.13. Because less data at boundary lubrication became available in the first series of tests compared with the later tests for uncoated steel, this effect was not very pronounced in the first series. Finally, a similar speed effect has also been noticed by Ter Haar [Ter Haar 1996].

3.6.3 Influence of pressure

The influence of pressure is very strong, and there is a profound difference between steel and aluminium.

3.6.3.1 Boundary lubrication

For steel the coefficient of friction at boundary lubrication generally decreases with increasing friction [Monfort 1990, 1991, Schedin 1988, 1991]. This effect is very strong with soft coatings, with hard coatings there is little effect. These findings agree with the idea that at boundary lubrication the friction force is the product of the actual contact area and the shear stress in the contact spots. The shear stress is supposed to be largely determined by the lubricant or plastic properties of the metal, so that variations in friction must be caused by variation in the actual contact area. This effect of constant shear stress has been observed by Kasuga for aluminium [Kasuga 1968], and can also been found for steel in the extensive work of Schedin [Schedin 1988, 1991]. For softer mate-

rials the actual contact area will be larger, because a larger actual area is needed for bearing the load (this is a complex way of saying: the hardness is lower). This larger contact area causes an increase in friction. The actual contact area also increases with pressure. If the relation between pressure and actual contact area would be perfectly proportional as is frequently assumed, the coefficient of friction would become independent of pressure. However, due to work hardening of the asperities, the actual contact area increases less then proportional with pressure [Monfort 1988, Schedin 1991], resulting in a decrease of friction with pressure. This can be shown as follows.

The normal and tangential forces in a contact can be described as:

$$F_N = P.A, \quad F_T = \tau_M.\alpha A, \quad \alpha << 1 \tag{3.5}$$

with P the apparent pressure, A the apparent contact surface (l.b) and τ_m the shear stress in the contact spots. The coefficient of friction μ then becomes:

$$\mu = \frac{F_T}{F_N} = \frac{\tau_M.\alpha}{P} \tag{3.6}$$

We now assume that α is a function of pressure which in a limited region can be approximated by a linear relation [Monfort 1991]:

$$\alpha = a + b.P, \quad a, b > 0 \tag{3.7}$$

The positive value of a makes the relation between α and P less than proportional. This gives:

$$\mu = \frac{\tau_M.(a+b.P)}{P} = \tau_M.(b+\frac{a}{P}) \tag{3.8}$$

This very simple model predicts that the coefficient of friction decreases with increasing apparent pressure, and that the effect can only be noticed at low pressures. These conclusions agree with the observations for coated steel (figure 3.17), and with observations by Monfort [Monfort 1990, 1991].

Again, however, there is an influence of the size of the slider: tests with the rotating tester showed a decrease of the coefficient of friction with increasing pressure at boundary lubrication. This finding may well have the same cause as the overall influence of size of the slider on the level of the friction at boundary lubrication.

For aluminium this model is not valid, the friction at boundary lubrication increases significantly with increasing pressure (figures 3.36 and 3.40). However, in this case the asperities have also been found to show a large amount of flattening with aluminium, much larger than with steel. It may therefore be assumed that the actual contact area increases also more than proportionally with pressure, so that in agreement with the mechanism described above also the coefficient of friction at boundary lubrication increases.

The influence of high pressures, as described in section 3.5.4, is a completely different story. The influence of speed which is still found at high pressures indicates that mixed lubrication still occurs. At low pressures the coefficient of friction increases with increasing pressure in agreement with the results of figures 3.36 and 3.40. At higher pres-

sures the coefficient of friction reduces again with increasing pressure, as if mixed lubrication starts all over again.

3.6.3.2 Mixed lubrication.

The influence of pressure in mixed lubrication manifests itself in the position of the Stribeck curve, or, more precisely, the position of the transition points H_0 and H_1. The apparent pressure P forms the denominator of the Hersey parameter H. As will be shown in chapter 4, for the flat-on-flat contact geometry used in the present tests, the values of H_0 and H_1 should be independent of P. Indeed, for steel only little influence of pressure is found, the Stribeck curves shift slightly to the left when the pressure increases (figures 3.7, 3.16 and 3.22). In a first approximation this influence of pressure may be neglected.

Aluminium shows a large influence of pressure. The Stribeck curve again shifts to the left (lower values of H) as a result of increasing pressure, but much more than for steel (figures 3.37 and 3.41). The results show that this effect is even stronger for higher pressures.

It has been shown that this phenomena can be related to the flattening of asperities, which is much stronger for aluminium than for steel. When the results are corrected for the actual, flattened roughness, the influence of pressure is reduced considerably; for MF roughness it vanishes almost completely. Steel shows only little flattening of the asperities and consequently the influence of pressure on the position of the Stribeck curve is very small, in accordance with theory.

3.6 4 Influence of roughness

3.6.4.1 Height of roughness

The influence of roughness has already been mentioned above. For steel it has been shown that the 'position' the Stribeck curve (the midpoint H_C) is proportional to the square of the roughness height (or better: the mean depth of the roughness). The shape of the curve itself is hardly affected by the roughness, the curve shifts as a whole (figures 3.9 and 3.22), and the type of roughness (Shotblast, EDT or Lasertex) does not have any noticeable influence. The friction at boundary lubrication is hardly influenced by the roughness of the sheet, in agreement with observations by Monfort [Monfort 1988, 1990, 1991].

For aluminium the situation is more complicated because different textures have been tested. For variants of roughness of the same type, but with different heights, the situation is much the same as with steel (see materials EDT low and EDT high in figure 3.35). The influence of roughness on the position of the transition point is not equal for both points, the transition boundary-mixed seems to be affected stronger than the transition mixed-hydrodynamic (figure 3.37). There is also a minor effect on the roughness at boundary lubrication, the higher roughness leads to a slightly higher friction. It is not known if this is generally true for EDT roughness on aluminium.

3.6.4.2 Type of roughness

An influence of the type of roughness has only been found for aluminium MF. The Stribeck curves are steeper for MF roughness than for EDT roughness, and the influence of pressure is different also. For all other combinations of roughness, the influence of the type of roughness is negligible, although for EBT1 some minor differences with respect to EDT can be found.

The conclusion is that the type of roughness must deviate tremendously from the classic stochastic types of roughness before any influence can be noticed. The deterministic types of roughness Lasertex and EBT do not deviate sufficiently from the classic Shotblast and EDT roughness to produce an effect (at least for the variants tested in these experiments). The only possible effect of type of the roughness is associated with the generation of hydrostatic pressure in isolated lubricant pockets. It has already been explained in section 3.5.3.3 that this might be occurring in material EBT1.

3.6.5 Influence of hardness

The influence of surface hardness is seen most clearly in the tests with different coatings (section 3.4.2). The friction at boundary conditions is considerably affected by the coating hardness, softer coatings give higher friction then harder coatings. This is in agreement with the general experience that softer materials exhibit more friction. The reason for this is that with soft materials, the actual contact area is larger and this will lead to higher friction as explained above. Later experiments, however, have shown that this effect depends on the lubricant; in particular with zinc coated steel the lubricant may react with the surface, so that the friction at boundary condition differs from what has been shown here.

The hardness also influences the position of he curve. Soft coatings make the Stribeck curve shift to the left (lower values of H). This may be caused by flattening of the asperities similarly to aluminium, resulting in a lower effective roughness in the contact. This of course can only happen when the coating is sufficiently thick. For the materials tested here, the thickness of the coating is almost equal to the height of the roughness, except for the ZnNi coating (see appendix A). Interesting is the behaviour of the phosphated electro-galvanised material ST13. The phosphate forms a very thin (in the order of 0.1 µm) layer with an extremely high hardness (estimated as something like 600 Vickers). The position of the Stribeck curve is the same for the normal electro-galvanised material, indication that the flattening of the asperities is hardly reduced by the phosphate layer. The friction at boundary lubrication however is more like that of the hard coatings. Apparently the actual areas of contact are much reduced by the phosphate layer in comparison with the normal electro-galvanised material.

The bulk hardness of steel did not show much influence. However, only variants with a higher hardness have been tested, and the hard coatings did not differ much from the uncoated steel variants as well.

For aluminium no effect of the hardness has been found either, despite some large differences in the measured values (appendix A). For aluminium the flattening of the asperities is much larger than for steel, and this effect may rather be determined by the bulk hardness. Furthermore the individual micro hardness measurements for aluminium showed a large scatter, probably due to differences in the oxide layer.

3.6.6 Flattening of asperities.

The question still remains why for aluminium the asperities flatten so much more than for steel. A contact model like that of Greenwood and Williamson cannot be used here because it is only valid for situations with (mainly) elastic deformation of asperities [Greenwood 1966]. Though aluminium is softer than steel, see for example the hardness readings presented in appendix A, the difference in hardness is not so spectacular that it can explain the large difference in amount of flattening that has been observed in the friction tests. Furthermore, the Young's modulus of aluminium is also smaller than that of steel, indicating that plastic deformation if asperities is more difficult to achieve.

It has been observed during the tests that flattening of asperities only occur when sliding occurs. A static load does not flatten the asperities very much, not even when applying high pressures. Only when the slider really moves over the surface the asperities flatten. This means that a shear stress on the micro contacts seems to be needed for flattening.

It is known that the (apparent) hardness of the asperities decreases when the material is subjected to bulk plastic strain [Saha 1994]. Softening of the asperities leads to a larger microscopic contact, or, in other words: flattening of the roughness peaks. Tabor pointed out that the same effect arises when the peaks are subjected to a shear stress on the top, which also induces a situation of multi-axial stress state [Tabor 1959]. This effect will cause an almost complete flattening of the asperities, unless there is an (intermediate) contact layer present between the contacting asperities which limits the actual shear stress on the summits. Examples of these contact layers are oxide layers and a lubricant boundary layer. It is well known that the oxide layers of steel and aluminium are different, aluminium oxide is very hard, much harder than iron oxide. The lubricant boundary layers generally have low shear strengths (if one can define such a parameter for these kinds of layers), and because the tests on aluminium and steel have been carried out using the same lubricant (partly), a great difference between steel and aluminium is not expected. The exact microscopic phenomena on the summits of the asperities are not well known, but there are indications that under certain conditions the lubricant is squeezed out [Melsen 1997]. In that case the difference between the oxide layers of steel and aluminium might cause the observed effects, but this is still speculative.

4 Modelling of friction on flat contacts

ABSTRACT This chapter describes the mechanisms which generate pressure in the lubricant, and so mixed lubrication. A simple model for mixed lubrication is developed, in which the consequences of severe asperity flattening are described in particular. The model is validated by comparing the shape of the predicted Stribeck curve, the influence of roughness height, and the influence of pressure on the position of the Stribeck curve, with results from experiments.

4.1 INTRODUCTION

The previous chapter describes many results from friction tests. The results show a difference in behaviour between steel and aluminium, which is most clear in the region of mixed lubrication. Notably the influence of pressure on the position of the transition points was different for steel and aluminium. To better understand these phenomena, it is necessary to acquire a better understanding of the mechanisms involved, in particular the mechanisms which create a pressure in the lubricant, and so cause mixed lubrication. In the following, some models are presented. In all models it is assumed that the pressure in the lubricant is generated by hydrodynamic phenomena that can be described by the Reynolds equation. In the first part (section 4.2) the pressure in the lubricant is calculated on the basis of the geometry of the gap between slider and workpiece. In the second part (sections 4.3 and 4.4) a more general model is developed, partly based on the results from section 4.2.

4.2 ANALYSIS OF MIXED LUBRICATION

4.2.1 Solving the Reynolds equation

In the situation of mixed lubrication a pressure exists in the lubricant between the two contacting surfaces, which carries part of the load. The friction in such a system depends on the fraction of the load which is carried by the lubricant, and so by the level of the pressure generated in the lubricant. If we assume that this pressure is generated by hydrodynamic effects, then the pressure can be calculated by applying the Reynolds equation. When the highest roughness peaks are just touching each other, the space between the two surfaces, created by the small spaces between the roughnesses of both surfaces, is generally described as a gap between two flat surfaces with a height equal to the depth of the combined roughness. For the roughness of a single surface the average depth is described by the parameter R_p or R_{pm}

If the gap is shallow and relatively wide, the Reynolds equation can be written as:

$$\frac{\partial}{\partial x}\left(h^3 \frac{\partial p}{\partial x} \right) = 6\eta V \frac{\partial h}{\partial x} \tag{4.1}$$

This equation can be integrated to:

$$h^3 \frac{\partial p}{\partial x} = 6\eta Vh + C \qquad (4.2)$$

This can be rewritten as:

$$\frac{\partial p}{\partial x} = 6\eta V \frac{(h - h_0)}{h^3} \qquad (4.3)$$

The constant h_0, thus defined, has a physical meaning. From (4.3) it follows that if $h = h_0$ then also $\partial p/\partial x = 0$, or in other words: when the gap height is equal to h_0, the pressure reaches a maximum (or minimum). Consequently, the flow of lubricant is of purely Couette type then, so the net mass flow per unit width is equal to $\frac{1}{2}h_0.V$.

The Reynolds equation can be solved by applying the boundary condition $p = 0$ at the inlet and at the outlet. Strictly p should be taken equal to the atmospheric pressure, but this is mostly low compared to the pressure in the lubricant, or better: the mean macroscopic pressure on the contact. If the geometry of the gap remains constant (which means that the height and length are scaling proportionally to changes in the dimensions), a general solution of the Reynolds equation is:

$$p_{av} = 6\eta V \frac{L}{h^2} Q \qquad (4.4)$$

where Q is a dimensionless constant, determined by the actual geometry of the gap.

In the following examples equation (4.3) is integrated numerically by taking $p = 0$ at the inlet, determining the gap height $h(x)$ for x increasing by small increments of x, calculating $\partial p/\partial x$ and so finding the next value of $p(x)$. The constant h_0 is determined by iteration from the condition that $p = 0$ at the outlet. In this way the pressure distribution can be calculated and in particular the average pressure in the lubricant is determined. Note: in the computer program used for the calculation, local negative pressures are allowed, because instructions like 'IF P<0 THEN P = 0' rendered iterations impossible.

In the following calculations, a situation has been selected for which friction data have been measured with sufficient accuracy, in particular the conditions used in the tests to assess the influence of slider length described in section 3.3 are applied. From these tests one condition has been selected as stated in table 4.1. Under this condition a coefficient of friction ranging from 0.020 to 0.035 has been measured (the friction was not constant during a single test, but varied with slider travel). Under boundary lubrication conditions the coefficient of friction is about 0.13. This means that under conditions of mixed lubrication, the coefficient of friction is about 20% of the value at boundary lubrication condition. This implies that the pressure in he lubricant is about 80% of the external pressure, or approximately 4 MPa. In other words: calculations of the pressure at conditions given in table 4.1 should yield a pressure in the lubricant of about 4 MPa. In addition to the situations of table 4.1, different values of slider radius and slider length have been applied to study the influence of these parameters.
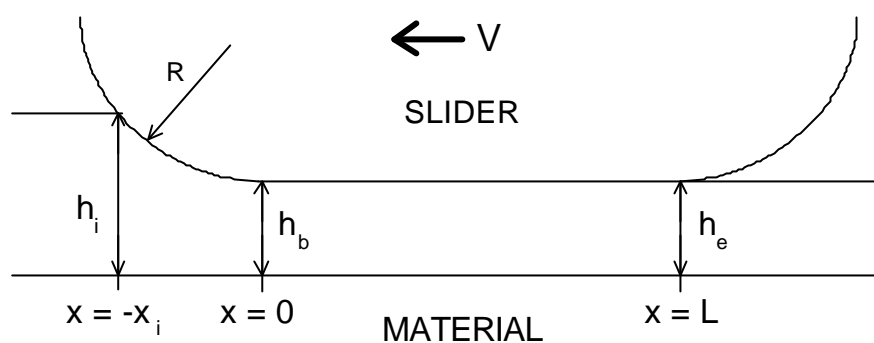
Figure 4.1. Schematic representation of a flat and smooth gap.

In the calculations the thickness of the layer of lubricant (film thickness) h_i has been varied as well (see figure 4.1). If h_i is smaller than the height of the gap at the beginning of the flat part h_b, the calculation has not been carried out, but the pressure is put equal to 0. Due to the movement of the slider, some amount of lubricant will be pushed forward, so that the actual film thickness at the inlet will not be known beforehand in many situations.

The gap height at the end of the flat part of the slider h_e is taken equal to the (combined) roughness depth R_{pm}, while the gap height at the beginning of the flat part of the slider h_b is related to this according to the shape of the gap. The gap height at the inlet h_i is taken equal to the thickness of the lubricant film on the sheet prior to the friction test, and the position of the inlet x_i (see figure 4.1 for definitions of these terms) can be calculated from these values.

The outlet is considered to be at the end of the flat part of the slider (x=L, see figure 4.1).

Lubricant viscosity	η	600 mPa.s
Sliding speed	V	100 mm/s
Slider radius	R	2 mm
Slider length	L	50 mm
Gap height	h_e	3 μm

Table 4.1. Conditions used in the pressure calculations. The gap height is equal to the average depth of the roughness R_{pm} for material ST17.

4.2.2 Results - global effects

Note: in the following analysis roughness is introduced in two different ways. Firstly, at mixed lubrication the smallest gap height h_e is assumed to be determined by the roughness of the material, or in other words: h_e is a measure for the actual sheet roughness. Secondly, a sinusoidal roughness with height h_r is mentioned. This roughness is a hypothetical roughness which is used in the simulations and has no direct relation to the actual sheet roughness.

4.2.2.1 Smooth and flat gap

The geometry of a smooth and flat gap is presented schematically in figure 4.1. In this case h_b is equal to h_e. In figure 4.2 the average pressure generated under the slider under the conditions of table 4.1 is presented as a function of the inlet gap height h_i. In addition to the conditions of table 4.1, a radius of 1 mm of the slider has also been used in the calculations. The results show a strong effect of both the gap height h_e and the film thickness h_i. An influence of the slider radius R is noticed as well: a smaller radius produces a lower pressure.
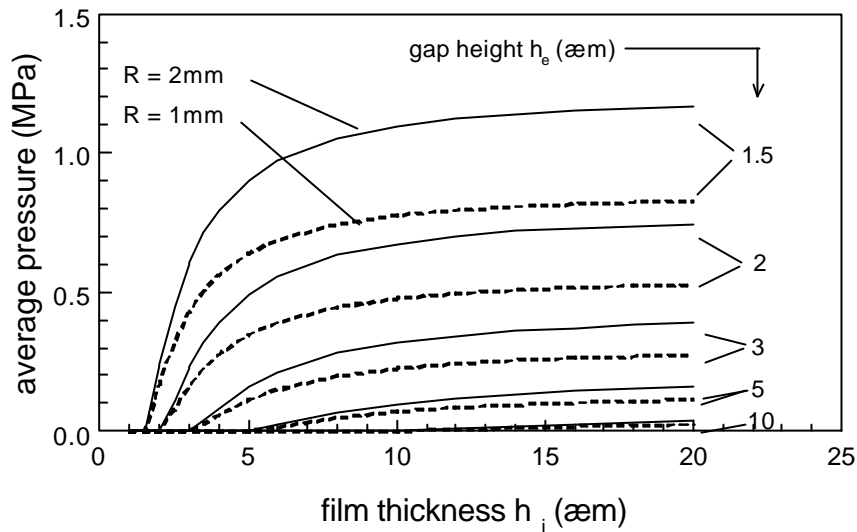
Figure 4.2. Pressure calculated in a flat and smooth gap, with additional the influence of radius.
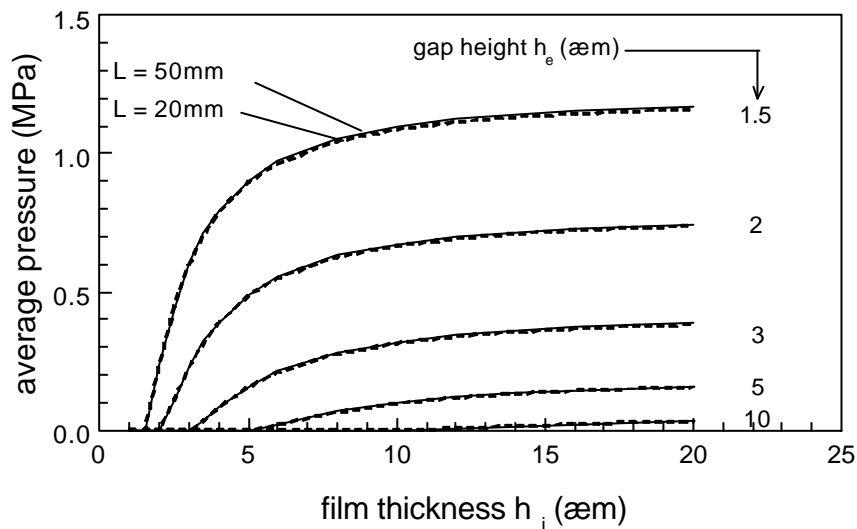
Figure 4.3. Pressure calculated in a flat and smooth gap, with additional the influence of slider length.

Figure 4.3 shows similar results, but now with a second value of the slider length L (20 mm). The results show no significant influence of the slider length, the results for L = 20 mm and L = 50 mm can hardly be discriminated. An analysis of the pressure distribution reveals that the pressure is fully generated in the inlet zone (under the radius) and

then decreases linearly to zero under the flat part of the slider; the length of the slider has hardly any influence (at least if the length of the straight part L is much larger then the length of the inlet zone x_i).

The pressure in the lubricant at conditions of table 4.1 has been calculated as about 0.3 MPa, which is much lower than the 'target' pressure of 4 MPa mentioned above.

4.2.2.2 Non flat gap (macro wedge)

The calculations presented in section 4.2.2.1 have been carried out under the assumption that the surfaces of slider and material were perfectly parallel. In practice this will not be the case. Firstly, because a perfectly flat surface cannot be produced, and secondly, because of the self adjusting mechanism and the fact that the pressure distribution is not uniform (at the inlet there is a higher pressure then at the outlet), a deviation from the parallel position may and probably will occur. Figure 4.4 presents the results for the case of the inlet side of the gap being 1 µm higher than the outlet side ($h_b = h_e + 1$ µm). Comparison with figures 4.2 and 4.3 shows that the effects are dramatic: the pressure increases by orders of magnitude, notably at low gap heights.
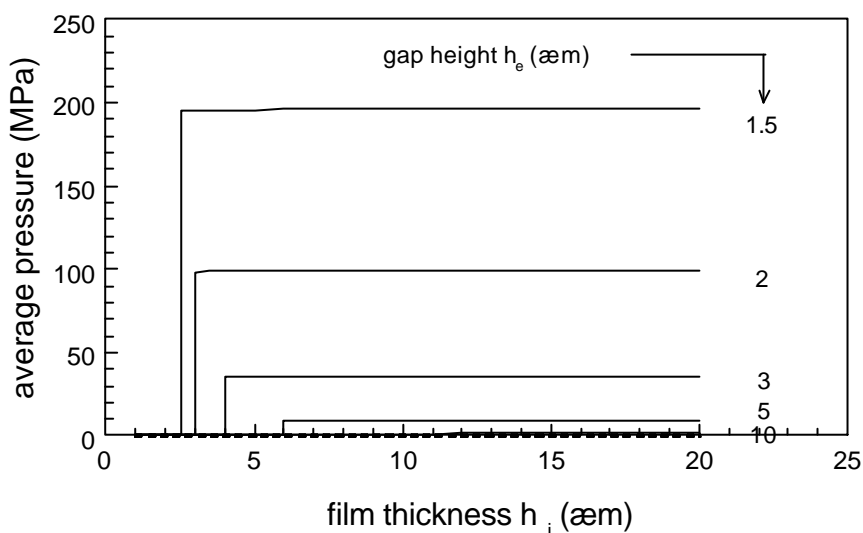
Figure 4.4 Pressure calculated in a non flat gap where the front edge is 1 µm higher than the end.
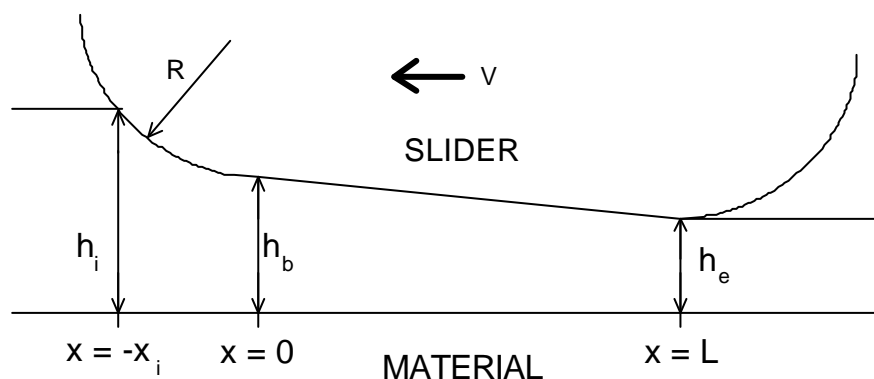
Figure 4.5 Schematic representation of a non-flat gap acting as a Michell bearing.

The gap geometry obtained in this way is similar to that of a Michell bearing (see figure 4.5), the theory of which is well known. For such a geometry the average pressure is given by expression 4.4, the constant Q being given by:

$$Q = \frac{1}{(m-1)^2}\left[\ln m - \frac{2(m-1)}{m+1}\right], \quad m = \frac{h_b}{h_e} \tag{4.5}$$

The geometry constant Q reaches a maximum value of 0.0267 for m = 2.2.
Because now the pressure is generated under the straight part of the slider instead of in the inlet zone (under the radius), the pressure no longer depends on the radius R or the film thickness h_i, but it does depend on the slider length L. The maximum pressure which can be generated (for m = 2.2, so $h_b = h_e$ x 2.2) is presented in figure 4.6 for two slider lengths. The pressure is indeed independent of film thickness, is proportional to the jaw length and inversely proportional to the square of the gap height.
The pressure in the lubricant at conditions of table 4.1 has been calculated as 20 - 30 MPa, this is much higher than the target pressure of 4 MPa.
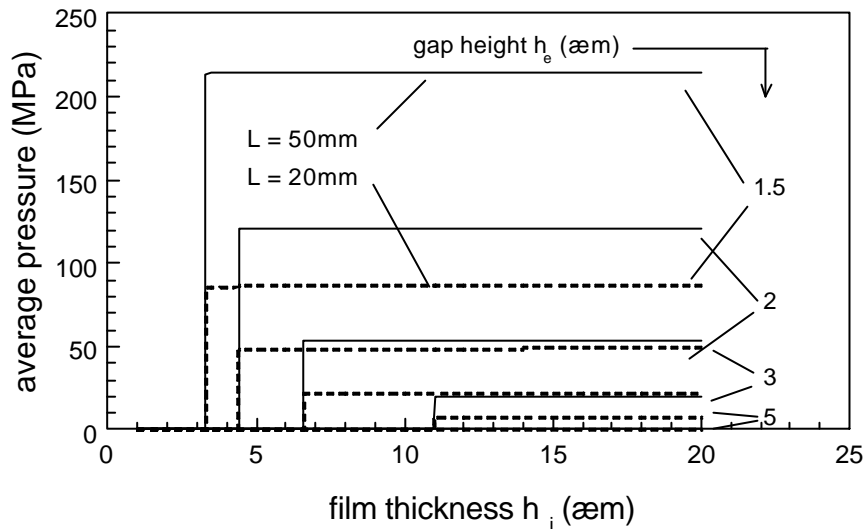
Figure 4.6 Pressure calculated in a non-flat gap where the front edge is 2.2 times as high as the end.
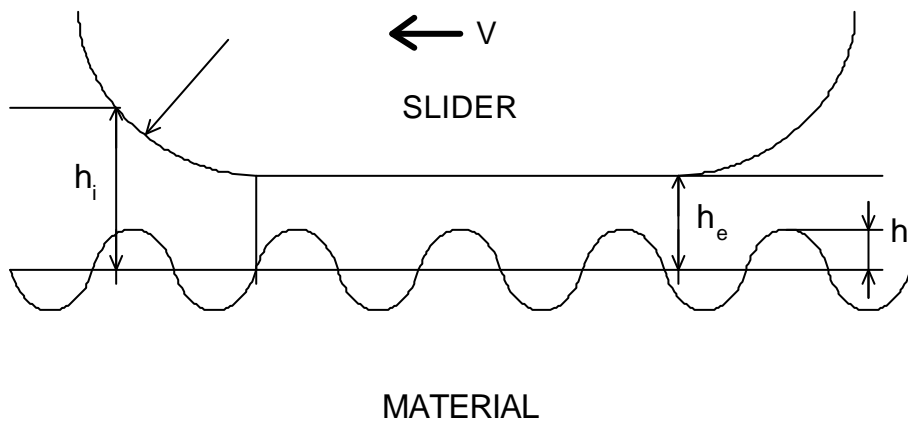
Figure 4.7 Schematic representation of a flat gap, which has a roughness on one side. The level of roughness is defined as h_r/h_e x 100%.

4.2.2.3 Rough gap

In reality the surfaces are not smooth but have a certain amount of roughness. Conse-quently there are places where the gap is smaller, and places where the gap is larger than the average gap height. As the pressure is a non-linear function of the gap height, this will change the average pressure in the gap. To study this, an artificial roughness has been applied to the material in the form of a sinusoidal wave with a wave length of 0.1 mm (a typical value for actual surface roughness) and a variable height as shown in figure 4.7. Of course, in reality the roughness is not sinusoidal, but these calculations have only been carried out in order to get an idea if actual roughness has an effect on the hydrody-namic pressure. The length of the inlet zone x_i covers only a limited amount of wave lengths, so the calculation can be strongly affected by the actual phase of the sine wave. Therefore several calculations have been made with different phases and the results have been averaged. A preliminary test showed that in most cases averaging over six phase angles (0°, 60° etc.) produces reliable results.
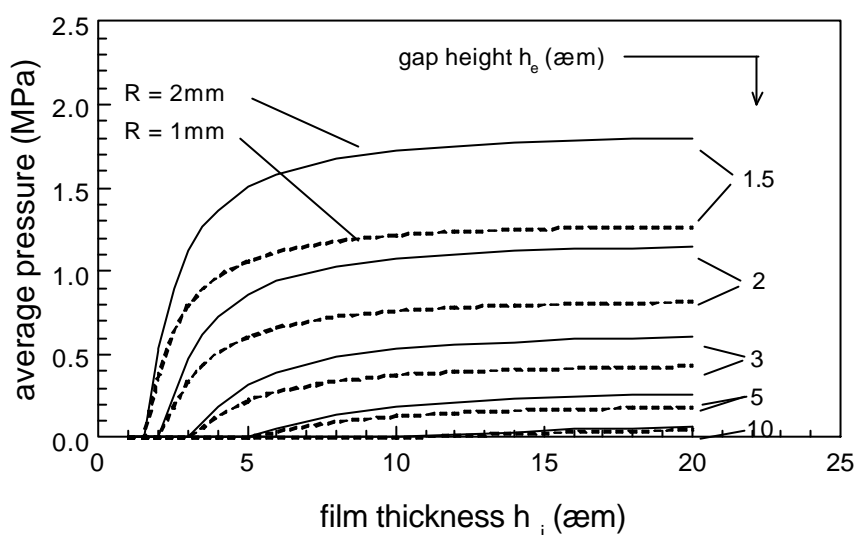
Figure 4.8 Pressure calculated in a flat gap with 50% roughness.
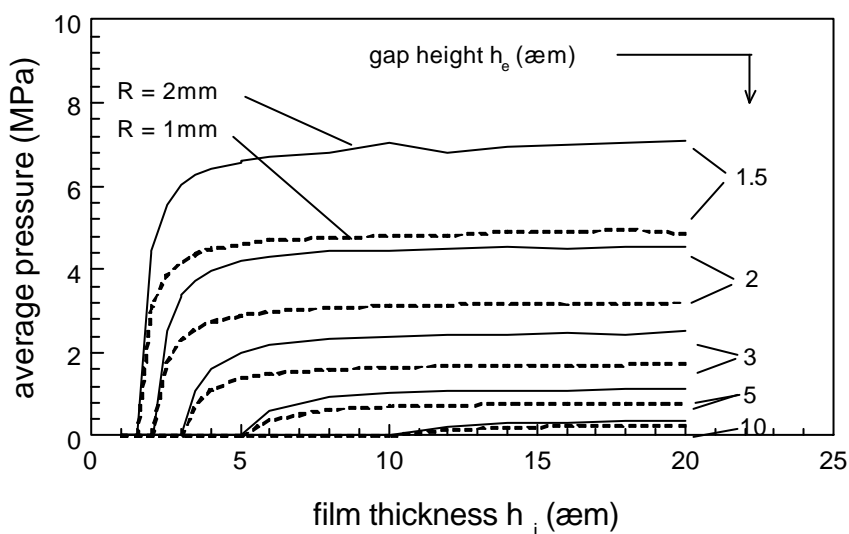
Figure 4.9. Pressure calculated in a flat gap with 90% roughness.

Calculations have been carried out with a maximum roughness height equal to 50% or

90% of the gap height ($h_r = 0.5h_e$ and $h_r = 0.9h_e$), while on the average the gap is assumed to be flat ($h_b = h_e$). The results are presented in figures 4.8 and 4.9. At mixed lubrication the roughness height by definition is equal to the gap height ($h_r=h_e$), but this situation cannot be represented by the simple model used here (the gap height becomes zero locally); for that situations a full 3D calculation is necessary. The results show that, due to the roughness, the average pressure in the lubricant is higher than without roughness and this effect is stronger as the amount of roughness approaches 100%. A related effect is that the value of h_o decreases, so that also the net mass flow decreases.

Figure 4.9 shows that the influence of film thickness reduces if there is a roughness. The effect of the roughness height can thus be studied more quantitatively by plotting the pressure at a film thickness h_i of 20 µm as a function of the mean gap height h_e (indicating the actual sheet roughness), as presented in figure 4.10. From this analysis we can conclude that the pressure is inversely proportional to the gap height to the power 1.5, and proportional to the square root of the radius.

The pressure in the lubricant at conditions given in table 4.1 has been calculated to be approximately 0.5 MPa for 50% roughness, and 2.5 MPa for 90% roughness. This means that a roughness on the surface causes the calculated pressure to increase to values of the order of the target pressure.
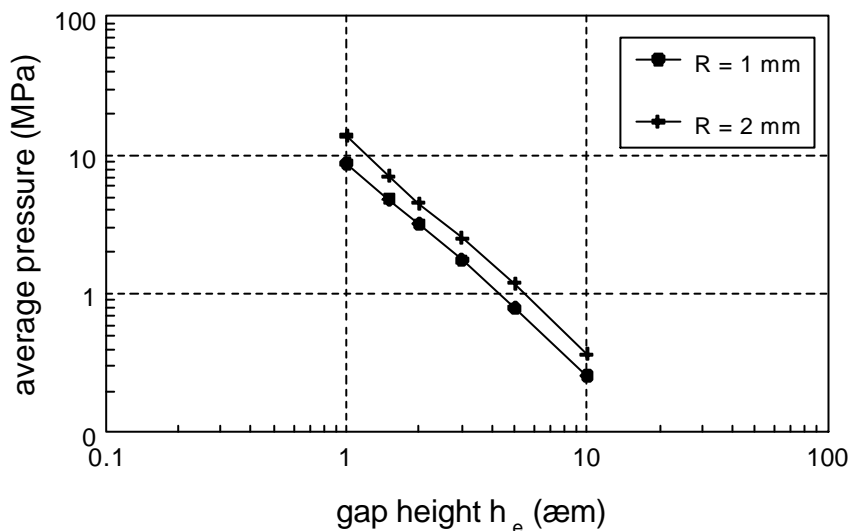
Figure 4.10 Mean pressure in a gap with 90% roughness an a film thickness h_i of 20 µm.

4.2.2.4 Rough, non flat gap.

A combination of both effects (roughness and non-flatness) leads to even higher pressures. Not only does the pressure increase even more, the value of m, where the mean pressure has its highest value, shifts to lower values, as can be seen in figure 4.11. In other words: the effect of a small deviation from perfect flatness is larger when there is a roughness. Additionally, the location where the pressure reaches its maximum value shifts towards the inlet. The value of h_o also decreases as a result of the roughness.
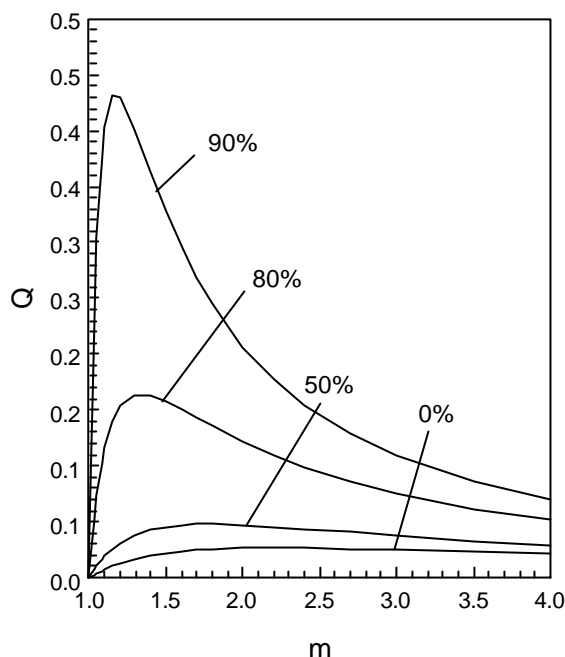
Figure 4.11. Pressure generated in a non flat-gap with roughness. The geometry constant Q from formula 4.4 is presented as a function of the ratio between begin and end gap height m (m = h_b/h_e) for different roughness levels. The values for 0% roughness correspond with formula 4.5.

4.2.2.5 Other global effects

There are some other effects which may affect hydrodynamic pressure.

- The viscosity of the lubricant increases with increasing pressure. This means that the generation of pressure is stronger when the lubricant is already under some pressure. As a rule of thumb: at 5 MPa the viscosity has increased by 10%. Effect: the actual hydrodynamic pressure will be higher than estimated when neglecting this effect.

- The actual roughness is a combination of roughness of slider and sheet material, and consequently larger than just the sheet roughness. Moreover, it is not clear how the roughness has to be measured to obtain a correct value (R or P profile, cut off 0.8 or 2.5 mm etc.). Effect: the actual hydrodynamic pressure will probably be lower than estimated when only considering the measured sheet roughness.

- Under the slider the actual roughness will be reduced by (elastic) deformation of the asperities. Effect: the actual hydrodynamic pressure will be higher than estimated when neglecting this effect.

4.2.3 Results - local effects

4.2.3.1 Micro wedge

Some years ago the author presented a mechanism by which pressure is generated on local slopes in the roughness profile, which serve as a kind of miniature Michell bearings [Emmens 1988, Dane 1995].

The pressure is given by formula 4.4. Because we are only interested in an estimation of the maximum effect, we use a value of 0.0267 for Q. For h we must use the smallest height of the micro wedge and not the end height h_e of the total gap. By using a value of 1 µm for h (very arbitrarily!) the mean pressure becomes:

$$p_{av} = 9.6 \text{ MPa/mm} \cdot L \tag{4.6}$$

This means that for a typical length of 0.1 mm the extra local pressure becomes about 1 MPa. This is below than the target pressure ($\approx$ 4 MPa) but of the same order of magnitude. Although this effect certainly cannot be the sole source of the pressure in the lubricant, the additional effects should not be neglected completely. On the contrary, Kimura carried out calculations on parallel sliders with a two-dimensional sinusoidal roughness, and found that the bearing capacity of the leading flanks of the peaks was in agreement with experiments [Kimura 1985].

4.2.3.2 Micro channel

From the theory of spiral groove bearings it is known that a pressure can be generated in a medium between two parallel surfaces sliding along each other. This happens if in one of the surfaces grooves have been cut, but under the condition that these grooves are neither perfectly parallel with or perpendicular to the direction of movement. In practical situations one of the surfaces may be provided with a system of parallel grooves of rectangular cross section at an angle of 45° to the direction of motion. We can now look at the roughness as a random network of interconnected grooves, and it is interesting to see if a practical pressure level can be generated therein.
Wildman [Wildman 1968] derives an expression as a limiting case for the average pressure in relatively long channels with sinusoidal cross section (not to be confused with the sinusoidal roughness of figure 4.7), which can be rewritten to:

$$p_{av} = \varepsilon^2 \frac{3}{8} \frac{6\eta V}{h^2} \cdot a \cdot \sin 2\theta \tag{4.7}$$

where ε is a geometry factor for the relative height of the roughness, comparable to the roughness level defined in figure 4.7, h the average profile depth (equal to h_e), a the length of the channels projected perpendicular to the moving direction, and θ the complement of the angle between moving direction and direction of the channel. This again equals formula 4.4 with:

$$\frac{L}{Q} = \varepsilon^2 \frac{3}{8} \cdot a \cdot \sin 2\theta \tag{4.8}$$

When we average over all directions and introduce the actual channel length L we get:

$$p_{av} = \varepsilon^2 \frac{3}{8} \frac{6\eta V}{h_e^2} \cdot 0.42 \cdot L \tag{4.9}$$

For closed channels (100% roughness) ε becomes 1 and the pressure becomes:

$$p_{av} = 6.3 \text{ MPa/mm . L} \tag{4.10}$$

This value is of the same order of magnitude as that calculated for the micro wedges, so the comments made there apply here also.

4.2.3.3 Entrapped lubricant

One of the strongest effects in hydrodynamics is the pressure generated in a gap closed at one side (no outlet), a Raleigh bearing with a closed outlet. The generated pressure is given by equation 4.4 with Q equal to 0.5. The average pressure therefore is almost 20 times as high as for a Michell bearing. Applying the same values for the parameters as for the micro wedge (section 4.2.3.1) the average pressure becomes:

$$p_{av} = 180 \text{ MPa/mm . L} \tag{4.11}$$

This is a considerable effect, and even much larger than found for the macro wedge. It is, however, very unlikely that by pure chance the combination of roughness on the tool and the material forms a closed micro gap. A more likely situation is that liquid will be trapped in a pocket, formed as a result of the deformation of the roughness. This, however, will only occur in situations where the roughness is severely flattened, and even then it may be rare. Besides, in situations where the lubricant is actually trapped hydrostatic pressure is more likely to occur.

4.2.4 Additional friction tests with ring shaped slider

To see if an inlet is necessary for generating lubricant pressure and mixed lubrication, a special slider has been made for the rotating tester. This slider has the form of a ring (punch 5 in appendix B). The friction tests have been carried out in the same way as the tests described in section 3.3.4; the conditions are presented in table 4.2. Due to the large surface of the slider, compared with normal sliders with three notches, only relatively low pressures could be obtained.

material	ST17
lubricant	SG0029, 11-16 g/m²
tester	rotating tester, ring shaped slider
speed	variable
pressure	3 MPa, 0.3 MPa

Table 4.2. Conditions for the friction tests with ring shaped punch

Stribeck type results are presented in figure 4.12. For comparison the results for the strip tester with jaws A and a pressure of 5 MPa (see section 3.3.4) are presented as well. The coefficient of friction with a pressure of 0.3 MPa was far from constant, so the values for that pressure are not very reliable. The results show a Stribeck type of relation, from which it can be concluded that mixed lubrication occurs, and, thus, hydrodynamic pressure is generated in the lubricant under the slider without an inlet. The data do not fit with results for 'normal' sliders, for which generally full hydrodynamic lubrication is

obtained for values of $H > 10^{-7}$ m, as can be seen in many results already presented in chapter 3.
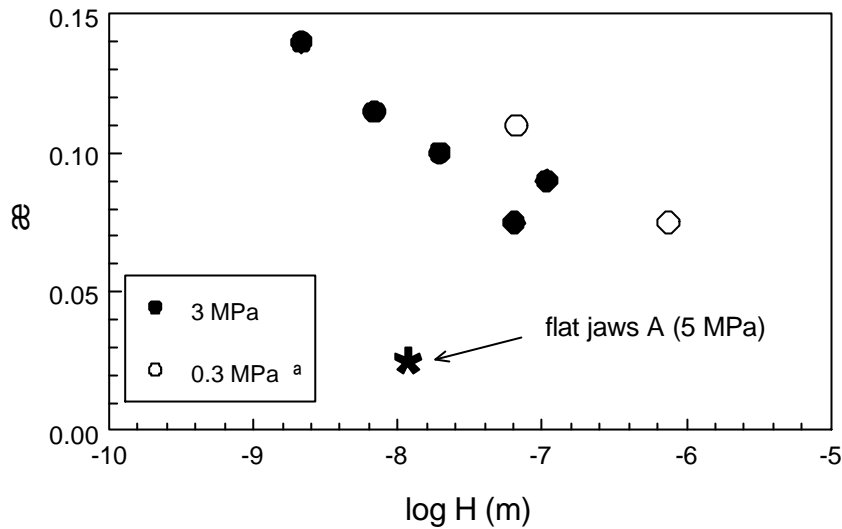
Figure 4.12 Results of friction tests with a special ring shaped slider without inlet.

4.3 FRICTION MODEL

We can now derive a simple model for mixed and hydrodynamic lubrication. The following assumptions are made:

1) The roughness of the material is hardly flattened by friction.
2) The pressure in the lubricant is generated by hydrodynamic phenomena described by the Reynolds equation.
3) The deformation of the slider is negligible.
4) The coefficient of friction under conditions of boundary lubrication (μ_0) is constant, this also applies to asperity contacts which occur in the regime of mixed lubrication.
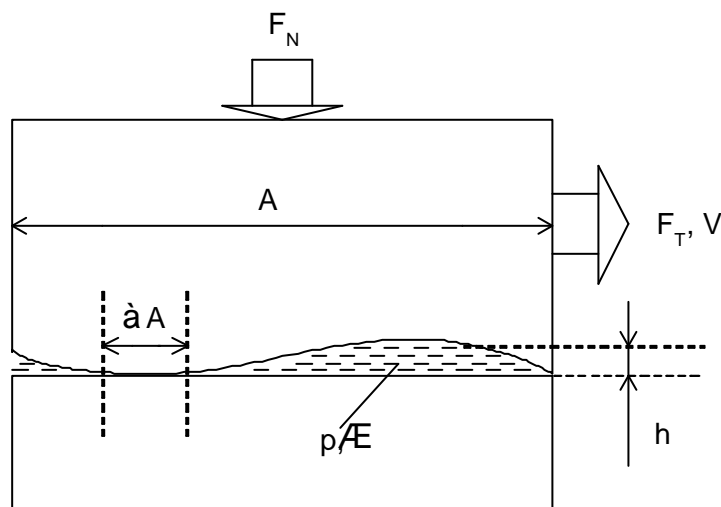
Figure 4.13 Definition of symbols used in derivation of a friction model.

Assume a situation where two surfaces with area A are in contact, a normal force F_N is

acting on the contact, and one of the surfaces moves with velocity V under the influence of a tangential force F_T; see figure 4.13. Assume further that only a fraction α of the area is in actual contact through the asperities. In the following the index M is used for the 'metal' part of the contact (the roughness asperities) and L for the 'liquid' part of the contact.

The normal force is divided into two parts (a 'metal' and a 'liquid' part):

$$F_N = F_M + F_L \tag{4.12}$$

Further:

$$F_L = p_{av}.A_L = p_{av}.(1-\alpha).A \tag{4.13}$$

So:

$$F_M = F_N - p_{av}.(1-\alpha).A \tag{4.14}$$

Also:

$$F_T = F_M.\mu_0 + \tau_L.A_L \tag{4.15}$$

Here τ_L is the shear stress in the lubricant at the jaw surface:

$$\tau_L = \eta \left(\frac{dv}{dz}\right)_{surface} = \beta\eta\frac{V}{h}, \quad \beta \leq 4 \tag{4.16}$$

The limiting value of ß follows from the assumption that the average speed of the lubricant cannot be larger than the speed of the moving surface, or, more popular: if one of the surfaces is held stationary and the other moves, the net mass flow will not be opposite to the moving surface [Vegter 1991, our parameter β equals Vegter's parameter θ + 1]. For pure Couette flow ß=1. So:

$$F_T = F_M\mu_0 + ß.\eta.\frac{V}{h}.A_L = F_M\mu_0 + ß.\eta.\frac{V}{h}(1-\alpha)A =$$
$$= F_N\mu_0 - p_{av}(1-\alpha)A.\mu_0 + ß.\eta.\frac{V}{h}(1-\alpha)A \tag{4.17}$$

and consequently:

$$\mu = \frac{F_T}{F_N} = \frac{F_T}{P.A} = \mu_0 - \frac{p_{av}}{P}(1-\alpha)\mu_0 + \frac{ß.\eta.V}{h}.\frac{1-\alpha}{P} \tag{4.18}$$

We still have to find an expression for the pressure p in the lubricant. Based on assumption 2 we assume that, independently of the precise nature of the pressure generating mechanism, the pressure is given by an expression like (4.4):

$$p_{av} = 6\eta V \frac{L}{h^2} Q \qquad (4.4)$$

For h we can take the average depth of the roughness, expressed by R_{pm}, but the values of L and Q are still unknown. We define a new parameter Λ as:

$$\Lambda = 6.L.Q \qquad (4.19)$$

This parameter has unit length but a yet unknown physical meaning. We also define a new parameter, related to the well known parameter H:

$$H^* = \frac{H}{h^2} = \frac{\eta.V}{h^2.P} = \frac{\eta.V}{R_{pm}^2.P} \qquad (4.20)$$

This parameter has already been introduced in chapter 3 on the basis of the observation that the position of the Stribeck curve is proportional to the square of the roughness height (section 3.4.1.3). Equation 4.18 can then be rewritten to:

$$\mu = \mu_0(1-(1-\alpha).\Lambda.H^*) + (1-\alpha).\beta.h.H^* \qquad (4.21)$$

In sheet metal forming the normal pressure P will generally be low compared with the yield stress of the material. In that case $\alpha \ll 1$, so:

$$\mu = \mu_0(1-\Lambda.H^*) + \beta.h.H^* \qquad (4.22)$$

We can now conclude that for $\alpha \ll 1$ the coefficient of friction is a linear function of H^* (and of course also of H). As in reality the hydrodynamic pressure p in the lubricant cannot exceed the external pressure P, the product $\Lambda.H^* = p_{av}/P$ cannot be larger than 1. This limiting value is reached for $H^*=H_0^*$. Thus we find:

$$\Lambda = \frac{1}{H_0^*} \qquad (4.23)$$

From the results of the friction tests on both aluminium and steel, we may conclude that the value of H_0^* is approximately 1000 m^{-1} (figures 3.11 and 3.32, on a logarithmic scale!), resulting in a value of Λ of the order of 1 mm.
Neglecting the shear stress in the lubricant, and assuming the linear relation between μ and H as given in (4.22), the coefficient of friction can be approximated by:

$$\boxed{\mu = \mu_0(1-\frac{H}{H_0}) = \mu_0(1-\frac{H^*}{H_0^*}) = \mu_0(1-\frac{p_{av}}{P})} \qquad (4.24)$$

Under conditions of hydrodynamic lubrication the situation becomes very simple. Necessarily, the pressure in the lubricant is equal to the external (macroscopic) pressure. This gives (see equation 4.18 and 4.19):

$$p_{av} = P = \Lambda \frac{\eta . V}{h^2} \tag{4.25}$$

So:

$$h^2 = \Lambda \frac{\eta . V}{P} = \Lambda . H \tag{4.26}$$

or rewritten:

$$h = \sqrt{\Lambda . H} \tag{4.27}$$

For the coefficient of friction we get:

$$\mu = \frac{\tau_L}{P} = \beta \frac{\eta . V}{h} . \frac{1}{P} = \beta \frac{H}{h} \tag{4.28}$$

Combining (4.27) and (4.28):

$$\mu = \beta . \sqrt{\frac{H}{\Lambda}} \tag{4.29}$$

Using (4.23), and R_{pm} as a measure for the depth of the roughness, this can also be expressed as:

$$\boxed{\mu = \beta \frac{\sqrt{H.H_0}}{R_{pm}} = \beta\sqrt{H.H_0^*} = \beta\sqrt{H^*.H_0} = \beta . R_{pm.}\sqrt{H^*.H_0^*}} \tag{4.30}$$

The major conclusions from the above are:
- at mixed lubrication the coefficient of friction is a linear function of H, and so a function of the square of the roughness height
- at hydrodynamic lubrication the coefficient of friction is proportional to the square root of H

4.4 FRICTION MODEL INCLUDING FLATTENING

The friction model derived in section 4.3 assumes that the asperities are rigid and do not deform under load. In practice however, the asperities will always show some amount of elastic deformation and in many cases also plastic deformation. For aluminium it has been shown that the amount of flattening by plastic deformation is considerable, so in that case the above model is not valid. In this section we will expand the model to include the effect of the flattening of the asperities.

In this model we start with a roughness with a certain height h_0, which is presented as a triangular shape in figure 4.14. We take the plane of reference at the tops of the peaks, the height is measured downwards. As a consequence of the contact with the punch or slider, which is considered as infinitely smooth and hard, a certain flattening of the as-

perities will occur, as shown in figure 4.15. We now assume that the punch has penetrated the roughness over a certain height h. We further define the relative penetration γ as:

$$\gamma = \frac{h}{h_0}, \quad 0 < \gamma \le 1 \tag{4.31}$$

To calculate the friction for this situation, three questions have to be answered:
- how large is the penetration γ;
- what is the actual contact area α;
- what is the average depth d of the remaining roughness.
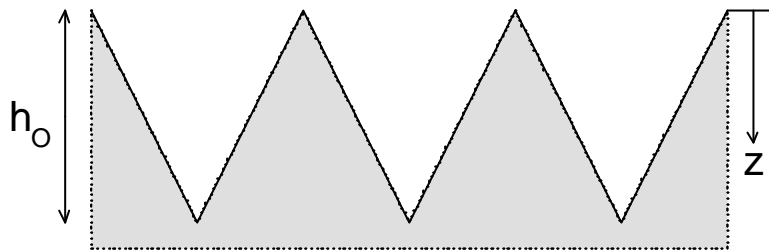
Figure 4.14 Schematic representation of the roughness
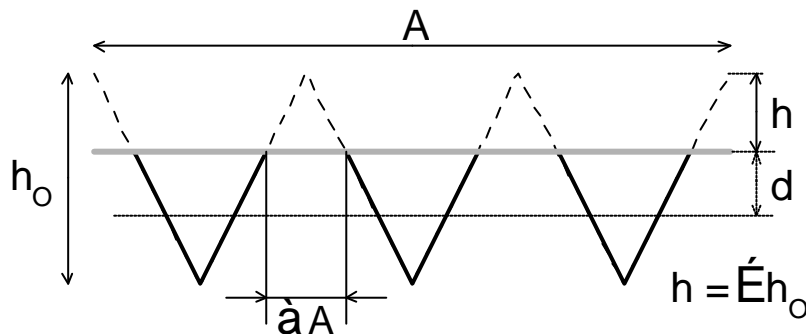
Figure 4.15 Definition of some terms used in the friction model with flattening.

4.4.1 Depth of penetration

To determine the depth of penetration we suppose that the roughness is flattened to such a degree that the actual contact area is (just) large enough to carry the load. This load on the asperities is not equal to the total load, because a certain part of the total load will be carried by the pressure in the lubricant. Further we suppose that on the actual places of contact a certain normal pressure exists which is equal to the hardness Hd of the material. This hardness is not necessarily equal to the hardness as measured with a hardness tester. Due to several effects (like plastic deformation of the bulk), the effective hardness which manifests itself in a friction test can be much lower than the hardness measured with a hardness tester [Saha 1994, Tabor 1959]. If we assume further a constant coefficient of friction on the asperities, this assumption of constant hardness leads to a situation where the shear stress on the contacting spots is constant. The latter has been observed in experiments [Kasuga 1968].

We now split the total normal force F_N into a part F_M, carried by the roughness, and a part F_L, carried by the lubricant, similar to what has been done in section 4.3:

$$
\begin{aligned}
F_N &= F_M + F_L = P.A \\
F_M &= Hd.\alpha A \\
F_L &= p_{av}.(1-\alpha)A
\end{aligned}
\tag{4.32}
$$

We now define the relative hardness Hr as:

$$
Hr = \frac{Hd}{P} > 1
\tag{4.33}
$$

In the hypothetical situation Hr < 1, the normal load exceeds the bearing capacity of the material, and this will lead to a total collapse of the surface in some way. This situation is considered unrealistic.
Combining (4.32) and (4.33) results in:

$$
\boxed{1 = Hr.\alpha + \frac{p_{av}}{P}(1-\alpha)}
\tag{4.34}
$$

This equation is the basis for the model derived here, because it describes the equilibrium of forces on the surface. Both p and α are functions of the depth of penetration γ and when these relations are known, equation 4.34 can be solved.

Please note that, when neglecting the lubricant pressure, (4.34) can be rewritten to: $\alpha = 1/Hr$. In other words: the effective hardness Hr can be derived from the observed amount of flattening of the roughness peaks under conditions of boundary lubrication. For the extreme amount of flattening observed for aluminium (section 3.5.1.5) the relative hardness would be as low as 1.25.

4.4.2 Actual contact area

The actual contact area in figure 4.15 is nothing but the bearing area t_p (DIN notation) of the roughness. This area can be derived from the height distribution of the roughness N (or the relative height distribution N') by definition:

$$
N(h) = N'(\gamma), \quad \int_0^1 N'(\gamma)d\gamma = 1
\tag{4.35}
$$

$$
\alpha = \alpha(\gamma) = t_p(\gamma) = \int_0^\gamma N'(z)dz
\tag{4.36}
$$

4.4.3 Mean roughness depth

The mean depth d of the roughness profile under the plane of contact can also be derived from the height distribution:

$$d = d(h) = \int_{h}^{h_0} (z-h)N(z)dz \tag{4.37}$$

For the calculations we define the relative roughness depth d_r as:

$$d_r = \frac{d}{\frac{h_0}{2}} \tag{4.38}$$

The division by $h_0/2$ stems from the fact that for a non-flattened, symmetric roughness profile, the mean depth is equal to $h_0/2$.

We now get:

$$d_r = \frac{1}{2}.\int_{\gamma}^{1} (z-\gamma).N'(z)dz \tag{4.39}$$

4.4.4 Friction

To calculate the friction we define the mean depth of the original, non-flattened roughness as d_0:

$$d_0 = \frac{1}{2}h_0 \tag{4.40}$$

 so that (4.38) can be written as

$$d_r = \frac{d}{d_0} \tag{4.41}$$

The friction which occurs in the contact with flattening will be compared to the friction in the original, non-flattened roughness. We assume that for this latter case the values of μ_0 and H_0 are known. Furthermore we assume that μ_0 is not changed by the flattening, and that the characteristics of the roughness do not change significantly by flattening (the geometry of the micro parts which are not in contact does not change much) so that the value of Q can be taken equal to that of the original roughness.

Bearing in mind that the mean roughness depth is now represented by d, (4.4) can be written as:

$$p_{av} = 6\eta V \frac{L}{d^2}Q \tag{4.42}$$

Using (4.19). the definition of H, (4.23) and (4.41), successively, we get:

$$p_{av} = \eta V \frac{\Lambda}{d^2} = P.H\frac{\Lambda}{d^2} = P\frac{H}{H_0^*}.\frac{1}{d^2} = P\frac{H}{H_0^*}.\frac{1}{d_0^2.d_r^2} \qquad (4.43)$$

While d_0 is the mean roughness depth of the original roughness, and so equal to h in (4.20), we get:

$$H_0^*.d_0^2 = H_0 \qquad (4.44)$$

So, combining (4.43) and (4.44):

$$\frac{p_{av}}{P} = \frac{H}{H_0}.\frac{1}{d_r^2} \qquad (4.45)$$

Equation (4.34) can now be solved using (4.36), (4.39) and (4.45), and the friction can be calculated using (4.24).

Based on the formulas arrived above, a computer program has been written which calculates Stribeck curves based on arbitrarily height distributions and a given value of Hr. The height distribution is integrated numerically.

4.5 DISCUSSION AND VALIDATION

4.5.1 Calculation of pressure in the lubricant

The calculation of pressures in the lubricant revealed a strong influence of non-flatness of the slider. A small deviation from perfect flatness can induce a giant effect. To establish the effect upon H_0, we now derive another expression for the position of the Stribeck curve as characterised by the parameter H_0. Using equations (4.4), (4.19) and (4.20):

$$p_{av} = \Lambda \frac{\eta V}{h^2} = \Lambda.H^*.P \qquad (4.46)$$

Using (4.23):

$$H_0^* = \frac{1}{\Lambda} = \frac{H^*P}{p_{av}} \qquad (4.47)$$

This means that when at a certain set of material and process conditions, as expressed by H* and P, the pressure in the lubricant p increases as a result of non-flatness, the position of the Stribeck curve expressed by H_0* changes inversely proportionally with that pressure. The calculations in section 4.2 showed that minute changes in flatness may increase the pressure in the lubricant by orders of magnitude. A practical consequence of this might be for instance that if the sliders have been ground and polished again after some damage, the measured Stribeck curves might well be shifted considerably. This, however, is not the case, as can be concluded from the results presented in the previous chapter. The position of the curves seems to be quite reproducible, and in many cases

hydrodynamic lubrication starts at H $\approx 10^{-7}$ m. Moreover the pressure in the lubricant, generated by a macro wedge, has been calculated to be very much higher then observed in the tests. This again indicates that generation of pressure by a macro wedge does not occur.

Several mechanisms for generating pressure in the lubricant have been mentioned in section 4.2. From this we can conclude:

A. If the pressure is generated in the inlet zone and thus depends on the inlet radius, the pressure does not depend on the slider length and is related to the roughness height to the power of 1.5
B. If the pressure is generated by global shape effects, the pressure is proportional to the slider length and is related to the square of the roughness height
C. If the pressure is generated by local roughness effects, the pressure does not depend on the slider length and is related to the square of the roughness height

From the experiments with the ring shaped slider it can be concluded that only part of the pressure is generated by mechanism A. The above considerations lead to the conclusion that mechanism B is not occurring, and it has already been shown that mechanism C can only have a minor effect. This conclusion bears a rather unsatisfying resemblance to the work of Lebeck, who also analysed many possible mechanism for generation of pressure in the lubricant at flat surfaces [Lebeck 1987]. Lebeck concluded that none of the proposed mechanisms could be (totally) responsible for the observed effects, but probably a combination of several effects occurs. Assuming that pressure is generated by hydrodynamic effects, which can be described by the Reynolds equation, Lebeck developed a mixed lubrication model, very similar to that presented in section 4.3. He also discovered that the shape of the Stribeck curves predicted by his model (or our model) agreed well with the Stribeck curves which had been published in literature.

Some imaginable effects have not been discussed yet.

Firstly, long wavelength components are present in the roughness profile (wavelengths > 1 mm). These long parts are barely visible in the roughness profile but sometimes show up after painting, becoming a car maker's nightmare. It is not known to what extend these long wavelength components contribute to the generation of pressure in the lubricant.

Secondly, there may be hydrostatic effects, caused by entrapping lubricant in microscopic pockets formed by deformation of the roughness profile. These pockets should not be confused with the macroscopic pockets proposed by Grahnert (section 2.7). These microscopic pockets can only arise in case of considerable flattening of the roughness. Some evidence has been presented that this might occur with aluminium.

The calculations presented here show some similarity to studies on the effect of roughness in hydrodynamically operated bearings with shallow gaps. These studies also indicate that the existence of a roughness increases the pressure generated in the lubricant, thereby enhancing the load bearing capability. These studies also predict a dependency on orientation similar to what has been observed in the friction tests with MF aluminium in section 3.5.1.4 [Spikes 1996].

4.5.2 Discussion of the friction model

In section 4.3 a friction model for mixed and hydrodynamic lubrication has been developed from which some conclusions have been drawn. We can now consider the validity of this model by testing the assumptions on which this model has been based. These are:

1) The roughness of the material is not much flattened by friction.
This matter has been dealt with in the extension of the model (section 4.4).

2) The pressure in the lubricant is generated by hydrodynamic phenomena described by the Reynolds equation.
This will certainly be true in situations of hydrodynamic lubrication, but at mixed lubrication other effects can also exist (such as hydrostatic effects). Moreover, not all hydrodynamic effects do produce the same relations. The influence of roughness height, for example, is different for pressure generated under the inlet radius and for pressure generated under the flat part of the slider.
In the Reynolds equation, the temperature dependency of lubricant density and viscosity is neglected. However, due to dissipation of friction heat the temperature in the gap will rise. Studies of Rodkiewicz [Rodkiewicz 1993] have shown that these temperature effects should not be neglected. He showed that in true parallel sliders a bearing force will be generated by this effect which has been mentioned in literature as the 'thermal wedge' [Lebeck 1987, Rodkiewicz 1993]. This indicates that a thorough analysis of the situation is needed to understand all phenomena in narrow gaps and that a simple approach as used here may overlook certain aspects.

3) The deformation of the slider is negligible.
Some elastic deformation will always occur, but it is not easy to estimate its magnitude. In general this leads to a non-uniform pressure distribution, but the mean macroscopic pressure is as expected. If the observed phenomenon is more or less a linear function of the pressure, the effects will level out and the error will be zero. In many practical situations the effects of a non-uniform pressure will not be larger than the normal scatter in the measured data.
Things get worse if the deformation of the slider is so large that some parts of the slider are no longer in contact with the material, like bending of the plates as depicted in figure 3.2. In that case the average pressure is higher then expected. We will now try to establish if this effect could have been occurring in the friction tests with the strip tester. In the experiments described in section 3.3.4 an influence of jaw size on the friction has been noticed. The flat jaws used in these experiments, labelled 1 - 4, all have the same external dimensions. The effective contact area is determined by the elevated parts of the jaw, not by the overall dimensions, as can be seen in the picture B.2 in appendix B. The bending of the jaws by the clamping force should thus be comparable for all jaw sizes. That means that the observed influence of the jaw length cannot be caused by macroscopic deformation of the jaws. In other words: should there be any bending of the jaws, causing a line contact with Hertzian pressure distribution, than the length of the contact area is large, at least comparable to the length of the longest jaw (50 mm).

4) Friction at boundary lubrication is constant (on the tops of the asperities as well).

The coefficient of friction under conditions of macroscopic boundary lubrication is definitely not constant. It certainly depends on pressure, and probably also on the roughness of the material. However some theories have been developed [Kasuga 1968] indicating that, for a certain material combination, the shear stress on the asperities is constant and that the macroscopic friction at boundary lubrication is determined by the total actual contact area; this has been confirmed by the results of Schedin [Schedin 1991]. This explains the dependence on the (macroscopic) pressure (section 3.6.3.1).

4.5.3 Validating the friction model.

The best way to validate the model is by comparing predictions of the model with experimental results. The model describes two aspects: the influence of roughness and the shape of the curve. The influence of roughness is described as H_0 being proportional to the square of the height of the roughness. This has been validated already in the friction tests on uncoated steel, see sections 3.4.1.3 and 3.4.3.4.

The model predicts Stribeck curves of the form:

at mixed lubrication:
$$\mu = \mu_0(1 - \frac{H}{H_0})$$
(4.48)

at hydrodynamic lubrication:
$$\mu = C.\sqrt{H}$$
(4.49)

These expressions can be used for fitting curves of this shape through the measured data, the parameters μ_0, H_0 and C are then obtained as a result.
At first sight it would seem possible to link the parameters C and H_0 according to (4.29). However, under conditions of hydrodynamic lubrication with very thin films, the pressure in the film is influenced by the roughness on the sheet very similarly to the effects calculated in section 4.2.2.3, if the two surface are separated by a very small gap only [Spikes 1996]. Thus the actual gap height for a certain set of conditions will usually be larger than expected from equation (4.27).

Fitting is only meaningful if the data are in agreement with the assumptions underlying the model, in particular that the asperities show negligible flattening. This means that only results obtained on uncoated steel can be used. Also, the model assumes that the coefficient of friction under conditions of boundary lubrication is constant, and this is not always the case in practice. A further limitation of the model is that all asperities are assumed to have the same height (or: only one asperity is present). This produces a very sharp transition from mixed to hydrodynamic lubrication. In practice the height of the asperities follows a statistical distribution, so that the transition from mixed to hydrodynamic lubrication is more subtle.
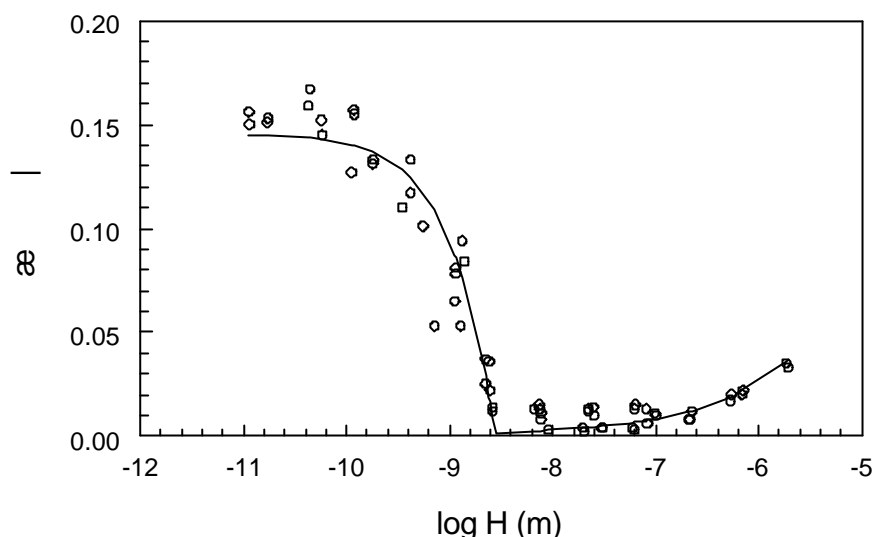
Figure 4.16 Example of Stribeck fit using a linear function for mixed lubrication, and square root function for hydrodynamic lubrication. The friction data have been obtained on uncoated steel (materials ST01 and ST03 combined).
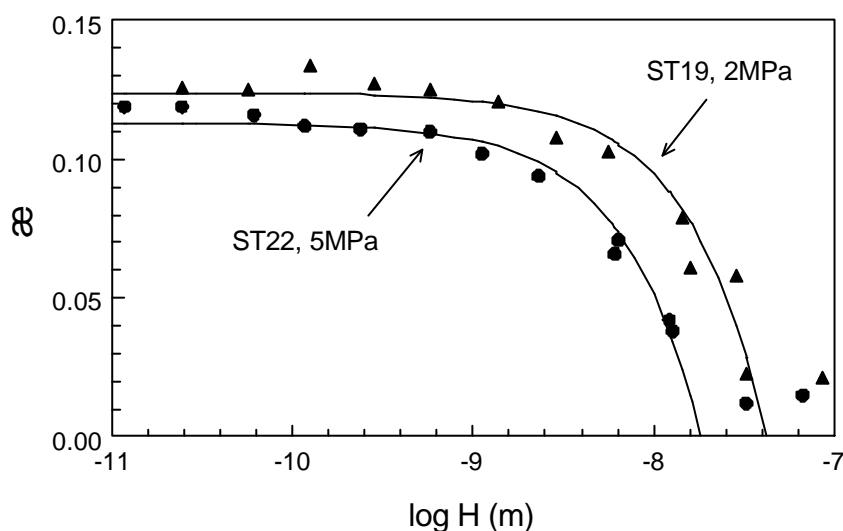
Figure 4.17 Examples of Stribeck fit using a linear function for mixed lubrication. The friction data have been obtained on uncoated steel.

Figure 4.16 shows the result of a fit according to formulas 4.48 and 4.49 using data obtained from the friction experiments described in section 3.4.1 (materials ST01 and ST03 combined to obtain sufficient data). The fit is satisfactory. Another example is presented in figure 4.17, using data from the experiments described in 3.4.3, again showing a satisfactory fit.

A more severe test is plotting the Stribeck curve to a linear scale for H instead of the usual logarithmic scale, and checking if the curves form a straight line according to (4.47). The data and fits from figure 4.17 have therefore been plotted to a linear scale in figure 4.18. The agreement is again satisfactory, although the difference in sharpness of the transition from mixed to hydrodynamic lubrication between fit and data is now more pronounced.
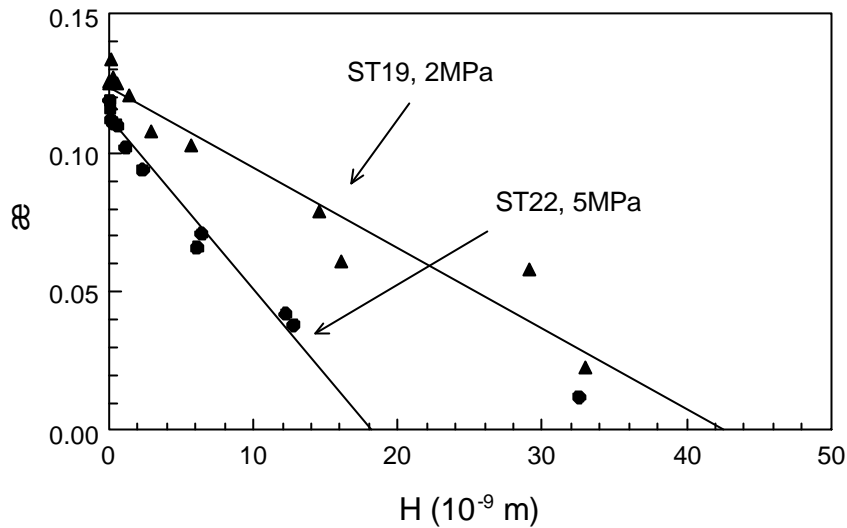
Figure 4.18 The data and fits from figure 4.17 plotted to a linear scale.
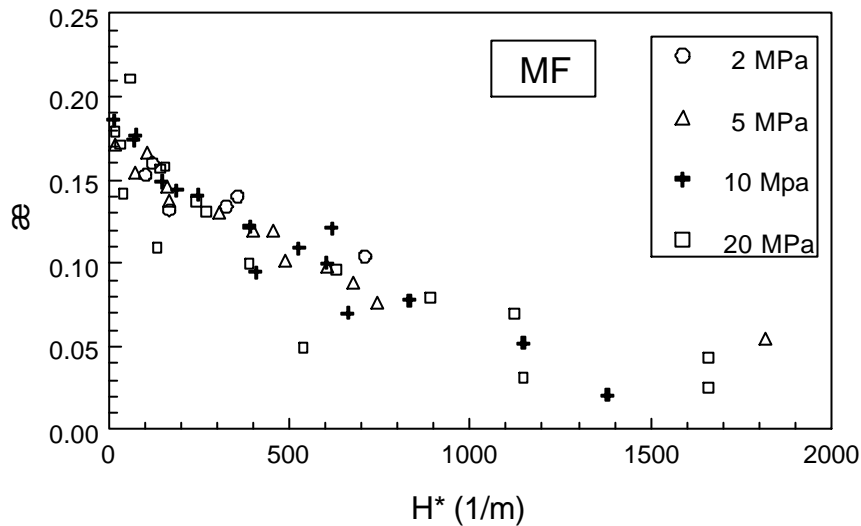
Figure 4.19. Results from friction tests on aluminium, with influence of flattening corrected, plotted to a linear scale (compare with figure 3.32).

A more elaborate check can be carried out using the results on aluminium, where the roughness has been measured after the friction tests. It has already been shown that the influence of pressure could be compensated by correcting the friction data for the actual roughness (section 3.5.1.5), at least for MF roughness. The 'corrected' data from figure 3.32 have been plotted to a linear scale in figure 4.19, and indeed a linear relation is now obtained. These observations show that both the predicted influence of roughness height and the shape of the Stribeck curve are validated satisfactorily by the results.

It is noteworthy to mention that the friction model developed here, has been extended by Monfort, who has been able to link the parameter Λ with actual length parameters of the measured roughness [Monfort 1990, 1991]. He found an excellent agreement between model and experiment.

4.5.4 Influence of flattening.
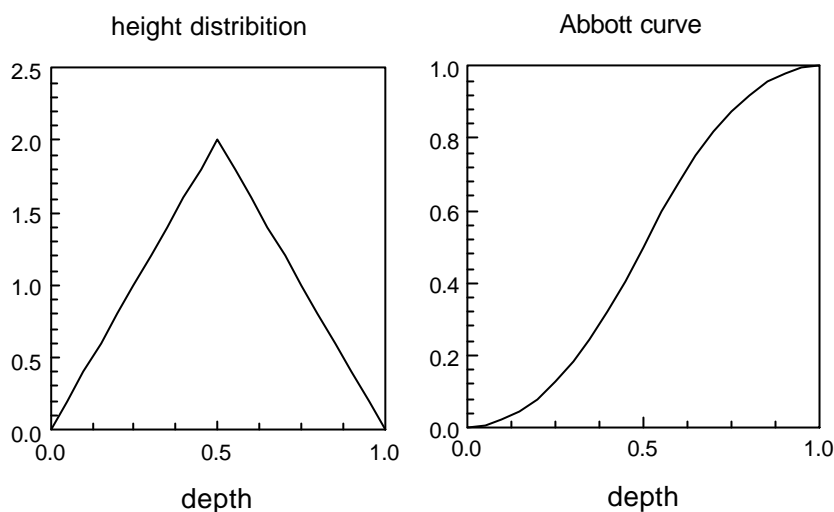
Figure 4.20 Height distribution and Abbott curve (= cumulative height distribution) of a simple roughness used in calculations applying the friction model with flattening.

For validating the extension of the friction model with flattening, calculations have been carried out using a height distribution and Abbott curve as shown in figure 4.20. This roughness can be considered as a system of peaks and valleys, equally shaped as pyramids, making the roughness symmetric. Calculations have been carried out with a relative hardness of only 30 MPa to suit the observations on aluminium. Results are shown in figure 4.21, in which the situation without flattening (or: at a pressure =0) has been presented as well. Actually recorded Stribeck curves for aluminium are presented in figure 4.22, or rather the tanhyp fits through the data (the results of EDT roughness from figure 3.39 have been used). Because the friction model does not describe any effects on the friction at boundary lubrication, the relative friction $\mu_r = \mu/\mu_0$ has been plotted. Despite the simple model of roughness used in the calculations, the agreement is satisfactory. Some consequences of severe flattening of the asperities, which are predicted correctly, are:

- the Stribeck curves are less steep;
- the Stribeck curves shift to the left;
- the transition boundary - mixed is more strongly affected by pressure than the transition mixed - hydrodynamic.

These conclusions confirm what has been already noticed during the friction tests, i.e. that the region of mixed lubrication is much wider for aluminium than for steel. It is therefore very difficult to obtain true boundary lubrication, which has also been noticed by Saha [Saha 1996]. The predictions made by this model are in agreement with those by Christensen, who derived a similar model, but based on a different approach [Christensen 1972].

From this it can be concluded that the mechanisms determining the influence of pressure on the position of the Stribeck curve, are described sufficiently well by the friction

model. For a more detailed study of the influence of flattening, a more elaborate contact model is needed which describes the flattening of the asperities more accurately. Possible, a 3D description of the surface is then needed as well.
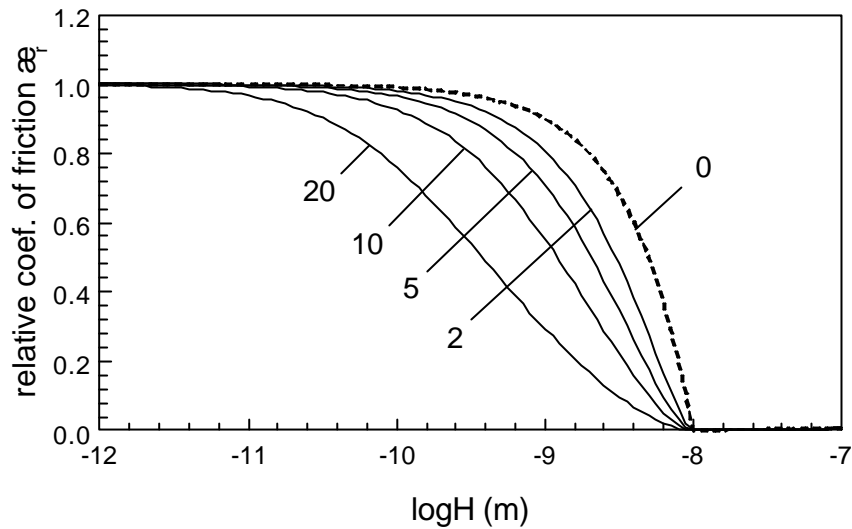
Figure 4.21 Results of calculations with the friction model with flattening, applying a roughness as shown in figure 4.20 and an effective hardness of 30 MPa. The numbers at the lines denote pressures (MPa). The line for 0 MPa corresponds to a situation without flattening.
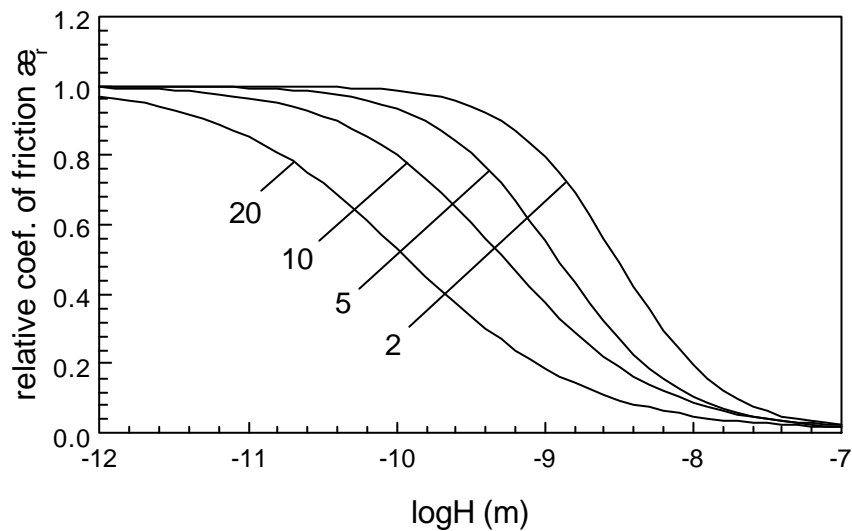
Figure 4.22 Tanhyp fits of actually recorded Stribeck curves for aluminium. The data for the EDT roughness of figure 3.39 (material AL06) have been used. The numbers denote pressures (MPa).

5 Putting the pieces together

ABSTRACT In this chapter the results of the deep drawing tests and the friction tests are compared. The effects of asperity flattening agree in both types of tests. The roughness of actual deep drawn parts is examined and some additional subjects are discussed. An extensive summary of this work is presented.

5.1 COMPARING DEEP DRAWING AND FRICTION EXPERIMENTS

blank diameter (mm)	440	480	520	560	600
mean pressure in the blankholder at 100 kN blankholder force at the beginning of the deep drawing operation (MPa)	1.62	1.11	0.82	0.64	0.52
logH at 40 mm/s, 400 kN blankholder force and 39 mPa.s (lubricant N100)	-9.20	-9.36	-9.49	-9.60	-9.69

Table 5.1. Friction conditions in the deep drawing tool.

We shall now compare the results of the deep drawing experiments with the results of the friction tests. In particular, this will be done for the results obtained with the large cylindrical product (with a punch diameter of 293 mm), for which results of both steel (section 2.5) and aluminium have been obtained (section 2.7).

To compare the results the frictional conditions in the blankholder must be known. These are summarised in table 5.1. In this table the conditions at the beginning of the deep drawing process, when the blank is still perfectly flat, are summarised. For a practical blankholder force of 400 kN, the mean pressure in the blankholder area at the beginning of the process is 2 - 6 MPa, depending on blank diameter. The values of logH at those conditions range from -10 to -9. Comparing these settings with the results of actual friction experiments reveals that under those conditions boundary lubrication occurs or the region of mixed lubrication is just attained, depending on material roughness. Under those conditions, little influence of material roughness or operating conditions is expected, which is not in agreement with the results of the deep drawing tests described in chapter 2.

To better understand the phenomena, we should recall some observations made before. Firstly, the friction conditions in the blankholder area are characterised by the fact that during the deep drawing process the effective pressure in the blankholder area increases significantly; this has already been explained in chapter 1. Secondly, the position of the Stribeck curve depends on pressure, to a small degree for steel, but to a large degree for aluminium. The consequences of the latter will be explained now.

Figure 5.1 shows a schematic transition diagram, in the same way as used in chapter 3. The labels B, M and H denote the three lubrication regimes: boundary, mixed and hydrodynamic lubrication. The position of the transition points as a function of pressure is represented by a line, and some possible H-P relations are shown in the figure. The lines 1 and 3 represent the situation for materials which show only a small influence of pressure on the transition points, as has been found for steel. Line 1 represents the transition mixed-hydrodynamic, and line 3 represents the transition boundary-mixed. The lines 2

and 4 represent the situation for aluminium in a similar way. Actual transition diagrams for aluminium can be found in the figures 3.37 and 3.41.
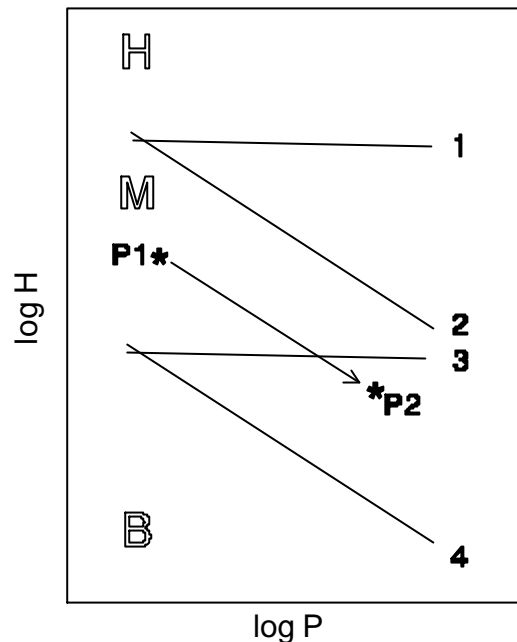
Figure 5.1 Schematic representation of a transition diagram. See text for explanation.

In the diagram a tribological condition, defined by viscosity, speed and pressure, is represented by a certain position. Suppose now that the conditions in the blankholder at the onset of the drawing operation are represented by point P1. As has been shown, during the drawing operation the (effective) pressure in the flange will increase, the representation of the condition shifts to position P2. The line connecting these two points has a slope of -1 (the value of H is inversely proportional to the pressure). In the situation depicted in figure 5.1, the trajectory P1-P2 intersects line 3. This means that in situations where there is only a minor influence of the pressure on the transition points, increase of the pressure will eventually cause the friction to operate under conditions of boundary lubrication. This is happening with steel.

For aluminium the situation is as represented by the lines 2 and 4. The trajectory P1- P2 does not intersect these lines. This means that a situation of boundary condition will not occur. If the transition mixed-hydrodynamic also shows a strong influence of pressure it might be that, eventually, near-hydrodynamic lubrication will occur. Some evidence for that can be found in the results for EDT and EBT at pressures of 20 MPa.
All this implies that:

with aluminium it is not possible to go from mixed lubrication to boundary lubrication just by increasing the pressure

This can also be observed in the results from the tests at very high pressures (figure 3.42), where even at the highest pressures a strong influence of speed is seen.

This has the following consequences for the friction in deep drawing:

- In deep drawing of steel, the friction in the blankholder area will eventually operate under conditions of boundary lubrication.
- In deep drawing of aluminium, the friction in the blankholder area will eventually operate under conditions of mixed lubrication, which may even be close to hydrodynamic lubrication.

This explains why in the deep drawing experiments of aluminium very low friction factors have been found (table 2.5), as well as the observed strong influence of speed and amount of lubricant (figure 2.26).

For steel the situation is more complicated. In general one expects that the friction at boundary lubrication is constant, which means: independent of process conditions or roughness. However this is not observed in the experiments: the friction during deep drawing was not constant at all, although the friction factors found for low carbon steel at poor lubrication (table 2.3) are comparable with the measured friction coefficients at boundary lubrication (figure 3.8).

Firstly, there is an influence of pressure. The friction tests revealed that the friction at boundary lubrication decreases with pressure. This has also been found in the deep drawing experiments. Although in actual deep drawing tests the influence of pressure is difficult to separate from other factors, in the experiments with the bent strip the friction clearly decreased with increasing pressure (section 2.3). The effect, however, is much stronger than anticipated from the friction experiments with the strip tester. The conditions in both ways of testing are different: in the bent strip tests much higher pressures (80 MPa) have been obtained than in the friction strip tests (11 MPa). Furthermore, the bent strip tests have been carried out in a standard deep drawing tool not designed for these tests, so that the tool has been stressed in an unforeseen way. It is quite possible that, due to elastic deformation of the tool, the pressure has been concentrated on the very outer edge of the strips. Despite these differences, the trend in both tests is the same.

Secondly, there is still an influence of roughness. Although in the friction tests no influence of roughness has been found at conditions of boundary lubrication (at least for steel), in the deep drawing tests an influence of roughness on the punch force has been found in all cases, including the bent strip. The influence of roughness was such that a lower roughness gives a lower punch force. This shows a similarity with mixed lubrication, where also a lower roughness causes lower friction.

Thirdly, there is a very clear influence of the amount of lubricant in the deep drawing experiments. The influence of amount of lubricant has not been examined in the friction tests (see comments hereafter), but it can be expected that under conditions of boundary lubrication little influence of the amount of lubricant will be observed as long as there is enough lubricant available to maintain the actual boundary layer.

Fourthly, there is still an influence of speed. In the friction tests evidence has been found that under conditions of boundary lubrication the friction still increases with decreasing speed, at least in some cases.

Summarising, despite the above conclusion that in deep drawing of steel the friction in the blankholder will eventually act under conditions of boundary lubrication, phenomena have been found which indicate mixed lubrication. Some possible explanations will be discussed now.

Some of the phenomena may well be caused by the lubricant. An example has been presented in figure 3.21, where the friction at boundary lubrication is different for different lubricants. Moreover, the observed influence of speed at conditions of boundary lubrication seems to be caused by the lubricant. An other example is presented in figure 5.2. From the same friction experiments on steel, the difference in friction for different lubricants has been obtained for the lowest value of H for which results for lubricant N500 could be obtained. This figure not only highlights the effect of the lubricant, it also shows an influence of pressure, notably for the difference in friction between N6130 and N100. At 2 MPa there is little difference in the friction of N6130 and N100; at 5 and 10 MPa the difference is larger, the difference in the coefficient of friction is about 0.02. At 20 MPa the difference in friction is somewhere in between. This effect is similar for all materials. The difference between lubricants N500 and N6130 depends less on pressure, and also shows more scatter.
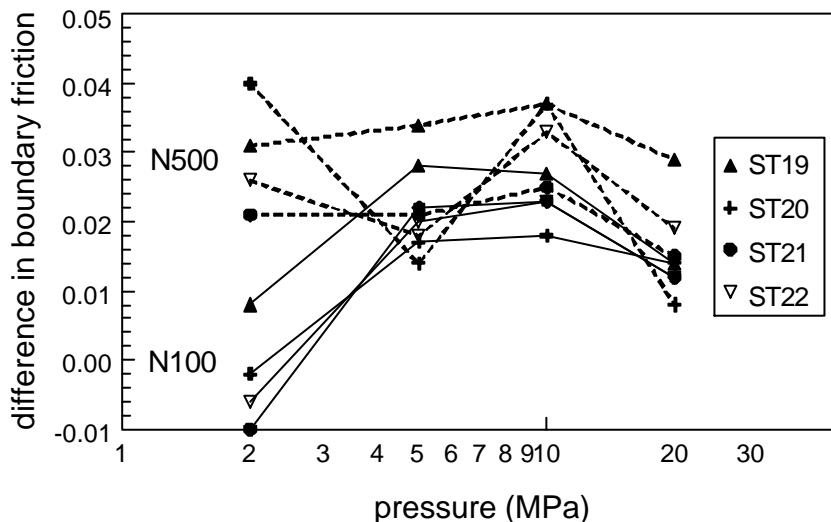
Figure 5.2 Combined effect of pressure and lubricant on friction at boundary lubrication. Presented is the coefficient of friction at boundary lubrication for lubricant N100 or N500, minus the coefficient of friction at boundary lubrication for lubricant N6130, as defined in the text. Results for steel.

Felder analysed different mechanisms which affect friction, partly based on results from experiments described in this work [Felder 1994]. He suggests that on the (flattened) tops of asperities micro-hydrodynamic phenomena may occur. This is an interesting statement, because it can explain a lot of 'mixed' phenomena under conditions where boundary lubrication is expected to occur. Indeed, the actual tops of the asperities are not perfectly flat, but still show some relief. The actual film thickness on these tops is much smaller than the average roughness depth. The strongly flattened aluminium specimens from section 3.5.1 still show on the flattened roughness parts a roughness profile with a height of approximately 0.1 µm. It is therefore save to assume the actual rough-

ness on the tops of the asperities to be of this order of magnitude. The lubricants used in the experiments do exhibit Newtonian behaviour in films with a thickness of this size, and even in more shallow gaps (up to 10 to 20 nm) [Melsen 1997]. Therefore the mechanism proposed by Felder may occur, but it is difficult to check the existence of such effects by direct measurement, so it still remains uncertain if the observed phenomena are caused by this effect. On the other hand, due to the very small gap height any hydrodynamic effects will be strong.

Another possible effect is the occurrence of hydrostatic lubrication. Hydrostatic lubrication arises when lubricant is trapped into a pocket formed by a valley of the original roughness. When the roughness is flattened, this valley may become isolated from its neighbours, so that the lubricant cannot escape when the volume of the pockets decreases due to further flattening. In that case hydrostatic pressure will be generated in the lubricant. This effect will only occur with materials which show a fair amount of flattening, such as aluminium. Evidence for this phenomenon has been found in the friction tests on aluminium described in section 3.5.1; also evidence has been described in literature [Kasuga 1968]. Recently Azushima published results of friction tests on commercially pure annealed aluminium where he concluded that at 'medium average pressure' the friction regime is characterised by hydrostatic pressure generated in closed lubricant pools [Azushima 1997].
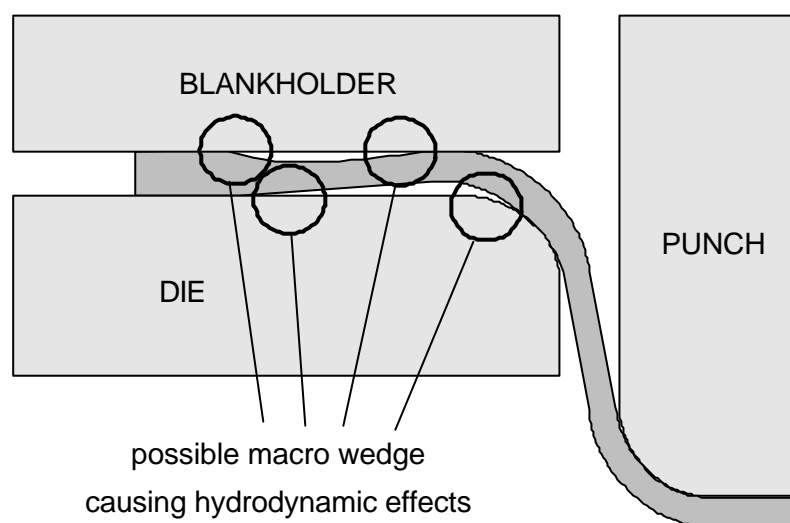
Figure 5.3 Location in a deep drawing tool where macro wedges may exist which can cause extra hydrodynamic lubrication.

An effect more difficult to grasp lies in the geometry of the deep drawing process. In a typical deep drawing tool, the material moves over the die radius. Due to a combination of effects (thickening of the edge, bending resistance of the material) the material does not touch the die and blankholder at all places. This will create macroscopic holes which may be filled with lubricant (if sufficient lubricant is available). This effect has led Grahnert to propose the concept of macro pockets, where hydrostatic pressure can be generated, see figure 2.25 [Grahnert 1985]. However, pure hydrodynamic effects can also occur, e.g. at the macro wedge between working material and die, as shown in figure 5.3. These effects will reduce the friction on the die radius, and possibly also in the die. Under practical conditions, the end of this gap, where the working material touches the die,

is not fully closed, but a small gap exists caused by the (actual) roughness of the material. This will cause the generation of hydrodynamic pressure to depend on the roughness of the material (or what is left of it), according to the observations from the deep drawing experiments on steel described in chapter two. This effect will also depend on the properties of the tool (in particular the stiffness), the amount of lubricant and the geometry of the product (the actual shape of the flange). Disappointing as it is, by its nature this effect cannot be simulated by simple friction tests.

5.2 A FURTHER LOOK AT ASPERITY FLATTENING

5.2.1 The roughness of actual deep drawn parts

punch	diameter 293 mm, radius 20 mm
die	gap 3.5 mm. radius 20 mm
product height	100 mm
press speed	12 mm/s
lubricant	N6130, limited amount

Table 5.2. Conditions of deep drawing tests.

In the previous chapter we have demonstrated that the strong flattening of asperities on aluminium in friction tests causes several important phenomena. Furthermore it has been demonstrated above that many features which have been established in friction tests, can also be observed in deep drawing experiments. However, in deep drawing operations the material is plastically deformed as well, which causes an increase in roughness [Saha 1996]. It is therefore not known beforehand if the phenomena at deep drawing of aluminium are indeed caused by flattening of the asperities. For this reason the roughness on actual deep drawn parts has been measured, namely on large cylindrical products. The experiments which produced these products are not discussed in this work, but they were similar to the tests described in chapter 2. The press conditions are presented in table 5.2. The roughness has been measured by means of special equipment, allowing roughness measurements on curved surfaces and in any orientation. However, only a limited amount of parameters could be measured using that equipment, and the values may differ from those, obtained by using other kinds of equipment.
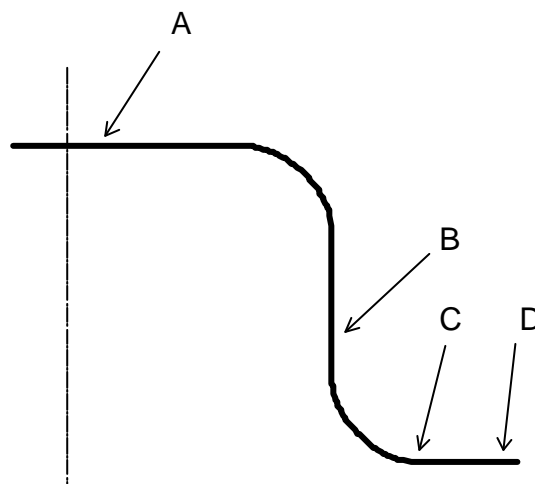
Figure 5.4 Locations on deep drawn parts where the roughness has been measured.

The locations at which the roughness has been measured have been indicated in figure 5.4. These are:

A. in the centre of the flat bottom;
B. on the wall, at approximately 2/3 of the height measured from the bottom;
C. on the flange, just at the beginning of the die radius;
D. on the flange, at the very outer edge.

Results for aluminium are presented in figures 5.5 and 5.6; the results for R_a and R_z are very similar and will be discussed simultaneously.

Figure 5.5 Actual roughness height on aluminium deep drawn products with MF roughness. The approximate level of the original roughness is indicated by the dashed lines. The roughness has been measured at 90° to rolling direction. A-D: location of measurement as in figure 5.4. Material AL09.

At position A the roughness is hardly changed, the difference between MF and EDT is still present. There is a slight influence of the blankholder force. At higher blankholder forces the material on top of the punch is stretched; this plastic deformation increases the roughness.

At position B the material is deformed in the flange and then drawn over the die radius, and there is some deformation by the bending/unbending operations. The roughness has

increased, there is little influence of the blankholder force. For EDT the roughness of the material is not much higher than the original roughness (compare with position A), but the visual aspect has become quite different due to roughening by plastic deformation and successive flattening over the die radius.

At position C the material is considerably deformed, to some degree without contact with the tool. The roughness has increased significantly. At positions B and C there is a slight tendency for the roughness to decrease with increasing blankholder force.

At position D the material is even more deformed that at position C, but at the same time flattened by the blankholder force, which is acting on the outer part of the flange. There is a strong influence of the blankholder force. At higher blankholder forces the material is severely flattened and the roughness is smaller than the original sheet roughness.
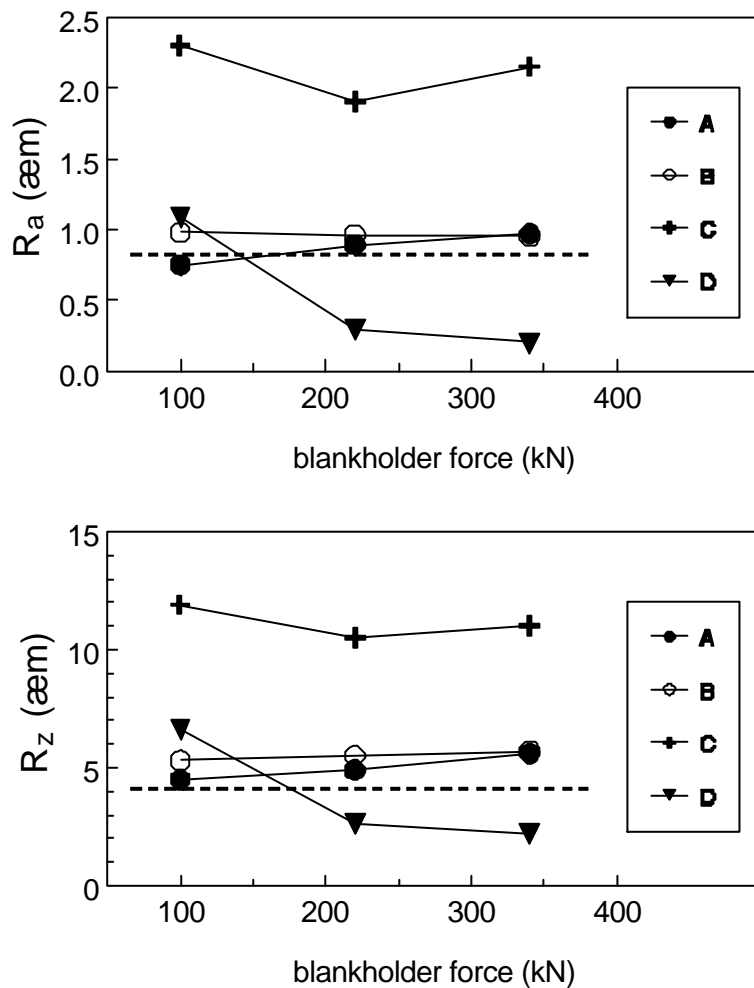
Figure 5.6 Actual roughness height on aluminium deep drawn products with EDT roughness. The approximate level of the original roughness is indicated by the dashed lines. A-D: location of measurement as in figure 5.4. Material AL10.

Results for steel are presented in figure 5.7. The steel products have been drawn using the same tooling as in drawing the aluminium products, under as much as possible identical conditions. The results show the same effects as discussed for aluminium. Comparing the results with those for aluminium with EDT roughness, one can see that the abso-

lute roughness level is almost the same for both materials. The difference is in the roughness at the outer edge of the flange, position D. One should bear in mind that the roughness of the flange will not become less than the roughness of the tool, so a complete flattening cannot occur.
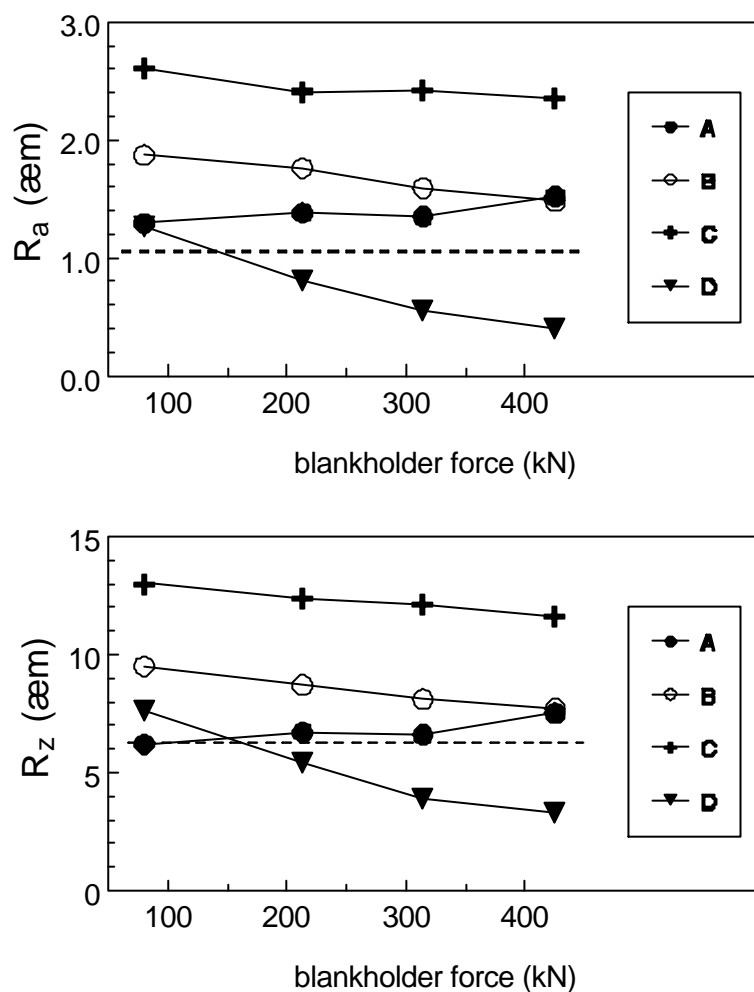
Figure 5.7 Actual roughness height on steel deep drawn products with EDT roughness. The approximate level of the original roughness is indicated by the dashed lines. The roughness has been measured at positions on a line approximately 45° to rolling direction. A-D: location of measurement as in figure 5.4. Material ST19.
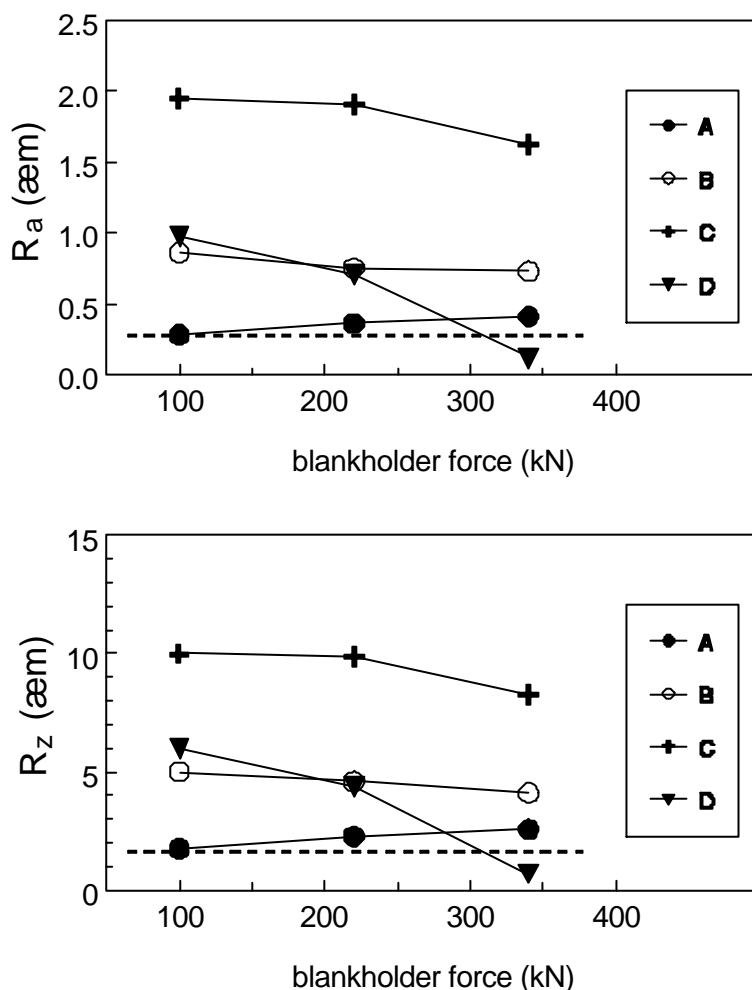
For aluminium with EDT roughness, the roughness is already substantially flattened at 200 kN blankholder force, increasing the blankholder force to 350 kN will not reduce the roughness height much further. For aluminium with MF roughness the blankholder force has to be at least 300 kN to obtain a substantial amount of flattening. This is in agreement with the results of friction tests presented in section 3.5.1.5, where it has also been shown that MF roughness exhibits less flattening than EDT roughness. For steel the amount of flattening is not as high as for aluminium. At a blankholder force of 400 kN the roughness height is reduced by approximately 50% compared with the situation at low blankholder forces. A much larger blankholder force is needed to obtain an amount of flattening comparable to that of aluminium, again in agreement with the results of friction tests.

Concluding: the flattening of the roughness, which has been observed in friction tests, also occurs in deep drawing operations at those locations where the major part of the

136

friction arises: at the flange edge. The influence of the material (steel or aluminium) observed here is the same as observed in the friction tests. This again confirms that the phenomena encountered in friction tests, will also occur in deep drawing operations.

5.2.2 The influence of the oxide layer on aluminium
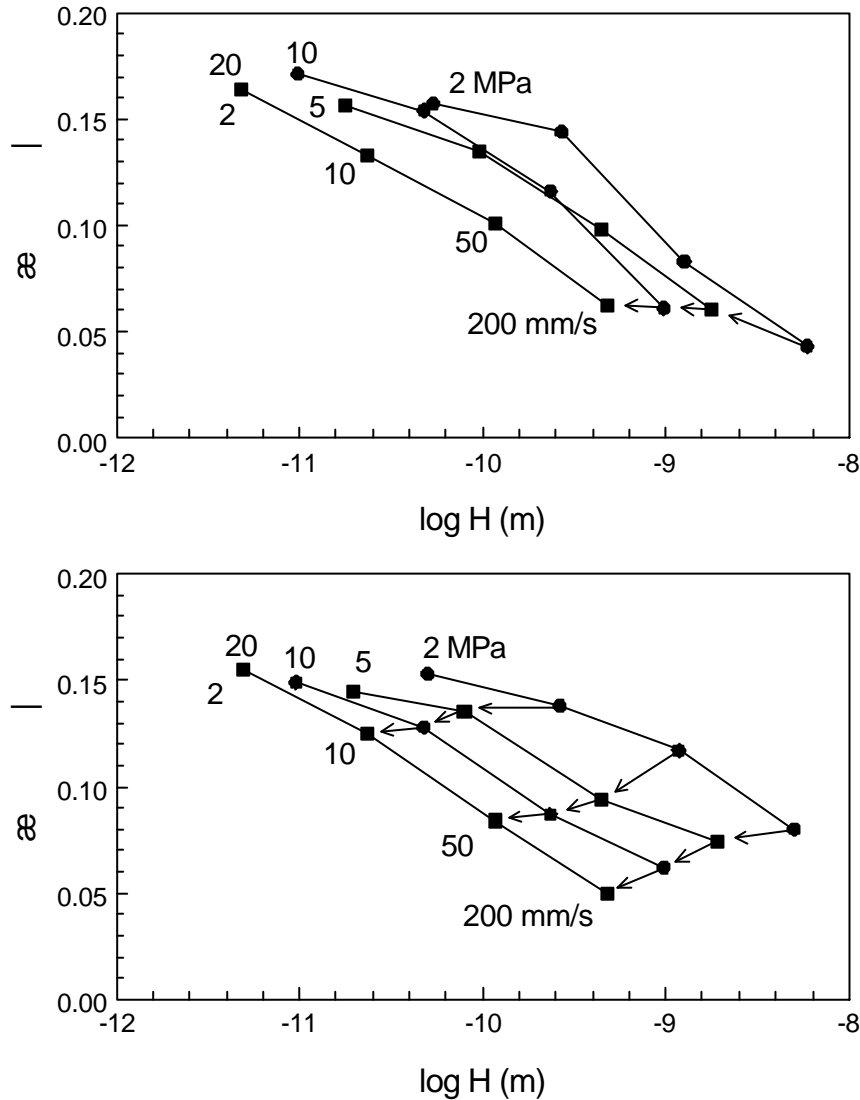
Figure 5.8 Results of friction tests on anodised aluminium. Top: results for 5000 type aluminium with MF roughness in the as-received condition. Bottom: results for the same material coated with an oxide layer of approximately 0.1 μm thickness (anodised).

In section 3.6.6 it has been speculated that the severe flattening of aluminium compared with steel can be caused by the hardness of the oxide layer at aluminium, according to the theory of Tabor. Evidence for this can be found in the results presented in figure 5.8. These results have been taken from a series of tests which are not discussed in detail here, but which were very similar to those described in chapter 3. The results, shown in the top part of figure 5.8 have been obtained on a 5000 type aluminium alloy with MF roughness in the as-received condition, the results shown in the bottom part have been obtained on the same material, coated with an oxide layer of about 0.1 μm thickness

(anodised). The results show that different pressures yield different Stribeck curves as noticed before, although for the as-received condition this effect is somewhat diffused by the scatter in the results. The main difference between these two sets of data lies in the influence of pressure on the friction at a constant speed. For example, examining the results at a speed of 200 mm/s (follow the arrows), one can see that for the as-received material the coefficient of friction increases with increasing pressure. For the anodised material, however, the coefficient of friction decreases with increasing pressure. For the latter material the position of the Stribeck curves is so strongly affected by the pressure that the friction approaches a situation of hydrodynamic lubrication. This effect can also be seen for the other speeds, but the results for the as-received material are obscured by the scatter in the results. These results indicate that indeed the oxide layer has an important effect, and it also illustrates the shifting of the Stribeck curve by pressure as explained in section 5.1.

5.3 PROBLEMS NOT DEALT WITH SO FAR

As this chapter would become unpleasantly long, it is not the intention to list all the problems, which have not been dealt with so far in this work. Three exceptions, however, will be made for problems which have been encountered along the way. Other influencing factors have been examined by Monfort [Monfort 1990, 1991]

5.3.1 Amount of lubricant

In all friction tests, and in most of the deep drawing experiments, enough lubricant has been applied to the material to eliminate sparse lubrication. This, however, is not in agreement with everyday's practice, where in many cases the amount of lubricant will be as small as possible. In the deep drawing tests, an effect of the amount of lubricant has been encountered: a small amount of lubricant will give a somewhat higher friction than a large amount. CRM has carried out some studies on this effect [Monfort 1990], and results are presented in figure 5.9. When there is only a very low amount of lubricant available, hydrodynamic effects will not occur, neither can mixed lubrication. When there is a little more lubricant, hydrodynamic effects can occur in the shallower parts of the roughness (or at places where the local amount of lubricant is larger due to non-uniform distribution of the lubricant), and mixed lubrication can occur to some extent. Only if there is enough lubricant available to fill the roughness valleys completely, mixed lubrication will occur everywhere. A further increase of lubricant will not reduce the friction any more. By own experience, an overdose of lubricant in friction tests will increase scatter in the results at situations of near hydrodynamic lubrication, but in deep drawing tests no detrimental effects of an overdose of lubricant have been found.

An additional effect can arise with materials which do show a fair flattening of the roughness. By flattening the effective height of the roughness profile decreases, so that after some flattening the actual roughness may become completely filled with lubricant allowing mixed lubrication. Some tests indicate that, under such conditions, materials which exhibit more flattening than other materials will have lower friction, though under conditions of pure boundary lubrication these materials might all have the same friction.

5.3.2 Technical lubricants

The experiments described in this work where carried out using lubricants with little or no additives. This approach has deliberately been chosen to reduce the number of possible influencing factors. In practice, however, these lubricants are rarely used, the chemical industry develops new lubricants with improved performance on a daily basis. Some effects have been described in section 3.4.3.2, and also in this chapter. It is known that, in particular with coated steel, the coefficient of friction can be strongly influenced by additives in the lubricant, or more generally: by the lubricant chemistry [Monfort 1990, Schey 1994]. This indicates that the results presented in this work may differ from those published elsewhere.

5.3.3 The choice of roughness parameter

This and other work on the influence of roughness on friction all showed a relationship with the height of the roughness. The question is now which roughness parameter should be taken for quantifying the influence of roughness

Traditionally the roughness height is characterised by the parameter R_a. This parameter is widely accepted and nearly all material supplied by the sheet metal producers is specified by its R_a value. There are two reasons to chose this parameter: tradition and the fact that this parameter is hardly affected by sheet imperfections like scratches and therefore can be measured with relatively high accuracy. However R_a has little physical meaning. From all the existing parameters used to measure the height of the roughness, only R_p (or R_{pm}) has a physical meaning. This parameter describes the average depth of the roughness profile from the top, or in other words: the amount of free space in the roughness, the amount of lubricant that the roughness can contain, or the mean height of the gap between two contacting surfaces. For this reason this parameter has been chosen in this work for correlation with the friction; it also showed the best correlation among all parameters used. R_p is also one of few height parameters which is sensitive to lack of symmetry in the roughness. It is known from experience that materials with equal R_a and R_z values, but different R_p values can exhibit significant different characteristics in press forming operations.

One of the aims of a material supplier is to equip its material with a roughness that suits the customer's demands best. This does not necessarily mean that the friction should be as low as possible. If the roughness is not altered very much (as for steel), the sheet roughness as provided determines the working characteristics. However, if the roughness is significantly altered by the forming process, the sheet roughness should be chosen such that the altered roughness has optimum properties. In practise this is almost impossible, but it does emphasise that a type of roughness which is ideal for steel, is not necessarily ideal for aluminium. Examples of this have been encountered in the tests. In these cases, correlation of the working properties with the original, undeformed sheet roughness will always be limited and it is of little importance to debate over the question which roughness parameter is the best.

The reader should not be too much concerned with the accuracy of roughness measurements. Studies by the BDDRG showed that, under ideal conditions, the best possible absolute accuracy of roughness measurement is about 10% [Emmens 1990a]. Fortunately,

however, roughness measurements, carried out using the same equipment and under the same conditions, can show a better repeatability, so that more accurate comparison of measurements is possible.

5.4 IMPLEMENTATION IN FEM CODES

One of the goals of friction research is to develop friction models which can be implanted in FEM codes. Vegter has used a description based on the model developed here: a linear μ-H relation in the mixed regime, and a constant value for μ for the hydrodynamic regime (a value of 0.01 is suitable in many cases). Unfortunately, as the deep drawing experiments verified by Vegter's model operated mostly under boundary conditions, not much effect has been found [Vegter 1991].

Ter Haar proposes a description based on the tanhyp function which has successfully been used to fit the experiments [Ter Haar 1996]. The positions of the transition points can be used as input parameters. This description has been used by Carleer in FEM calculations [Carleer 1997].
The description by Ter Haar uses the L number, defined as $L = H/R_a$, to describe the influence of roughness. This parameter has been derived from the work of Schipper who established the number on the basis of models for boundary and full-film lubrication and verified this number in experiments with concentrated contacts [Schipper 1988]. This L number has been used by both Ter Haar and Carleer in relation to deep drawing operations, but as yet the validity of this parameter has only been proven for concentrated contacts.
It has been emphasised in this work that at least in the blankholder of deep drawing tools the type of contact is flat. Based on the results presented in this work, which predict a relation with the square of the roughness height in flat contacts, it is questionable if the L number should be used in deep draw simulations.

In general one should be careful to apply data from friction experiments in FEM simulations, because many friction properties depend on the (local) conditions. Two approaches can be useful: to study these dependencies and make physical models which describe them as accurately as possible, or to carry out friction experiments under conditions as closely as possible equal to those acting in the process being simulated. This latter approach has been followed by Sniekers with some success, but for each part of the process being simulated, a separate friction test is needed [Sniekers 1996]. Also Langerak has used this approach successfully [Langerak 1996].

For application in FEM codes, boundary friction and mixed friction should be treated separately. The friction at boundary lubrication is not constant, examples have been presented in this work. Influences of lubricant, pressure and speed have been observed, while there is also an influence of the way of testing (in particular the dimensions of the slider in friction tests). At this moment a good friction model for boundary lubrication, which describes all these effects, is lacking, and much work in this area is still needed.
At mixed lubrication, the coefficient of friction can be estimated from the coefficient of friction at boundary lubrication (presuming this is known) by considering the pressure that is generated in the lubricant. When this pressure is assumed to obey the Reynolds equation, the model for mixed lubrication presented in this work can be applied.

In cases where the friction does not depend much on pressure, as found for steel, the friction can be described by the parameters μ_0 and H_0 which both can be derived from friction tests, while the influence of roughness can be described by H^*. Then, the description proposed by Vegter can be used.

In cases where the friction depends on pressure, as observed for aluminium, the flattening of the asperities should be taken into account. As soon as a good model for the flattening of the asperities becomes available, it will be possible to relate to the actual roughness in the contact using the mixed lubrication model developed in this work and the description proposed by Vegter. Until then, the simple friction model with flattening, developed in this work, can be applied when the effective hardness of the material can be estimated. However, also in this field much work still has to be done.

A true numerical simulation should also take into account all the macroscopic geometry effects, like macroscopic lubricant pockets and macro wedges. At this moment, few if any codes are available which include these effects.

5.5 EXTENSIVE SUMMARY OF THIS WORK

In chapter 2 many results of deep drawing experiments have been presented for different product shapes. The influence of roughness on the punch force, if present, is always such that a larger material roughness results in a larger punch force. The effect of skin pass reduction is less evident; the skin pass reduction affects both the mechanical properties and the roughness. The amount of lubricant also showed a clear influence: a small amount of lubricant (sparse lubrication) leads to a higher punch force. This also affected the relative influence of roughness: with much lubricant the influence of material roughness was larger than with little lubricant. A peculiar phenomena encountered in the tests was that the friction in the tool is not constant over the whole punch travel. This caused a force-displacement curve which deviates from the normal dome shaped curve. The curves were 'dented' and in several cases have more than one maximum (in Dutch the indications 'camel type' and 'dromedary type' are used). These particular shape effects (and the related frictional phenomena) seem to disappear as the blankholder force is decreased, the amount of lubricant is reduced or the material thickness is increased. The first two factors point to a friction effect, the latter to a geometry effect. Also an effect of material properties has been observed: material with fine grain (producing less roughening by plastic deformation) showed less effect than material with coarse grain (producing much roughening by plastic deformation).

The effects on the punch force are also reflected in related effects: the product dimensions after drawing and the fracture limit. The product dimensions are influenced by the punch force, or more properly: the force load on the wall of the product during the deep drawing process. A higher punch force induces more plastic strain in the wall, and consequently the remaining flange after drawing is larger. This effect is relatively small, mostly a few percent of the overall product dimensions. However, in critical situations this may be important. The fracture limit, defined as the maximum allowable blankholder force before failure of the product, has been affected stronger: a variation by a factor of two has been observed for one product.

For the rectangular product the effects are somewhat diffuse. Rectangular, or more cor-

rectly: non-cylindrical products, lack the rotational symmetry of a pure cylindrical product. Consequently the condition in the blankholder varies from point to point. As an exception: the influence of the amount of lubricant has always been found, but the product dimensions are less clearly affected by the differences in punch force resulting from this. However, looking at the degree of wrinkling, the product dimensions could be related to the amount of lubricant.

Deep drawing of aluminium differs from deep drawing of steel in several respects. The influence of the amount of lubricant on the punch force is much larger than for steel. Moreover, a strong influence of punch speed has been observed (this has not been found in the tests with steel). These observations indicate that the friction in deep drawing of aluminium is affected stronger by the operating conditions than for steel. It has also been observed that with high speed and much lubricant, the friction in the blankholder was so small that the blankholder force could be increased to the limit of the press without causing failure. This effect has repeatedly been observed for aluminium, but never for steel. Furthermore a peculiar effect of blank size has been encountered: the influence of material roughness (or more generally: material properties) is smaller when using a larger blank size.

In chapter 3 the ins and outs of friction testers using flat sliders have been discussed. Several limitations of these kinds of testers have been presented, and the two testers used in the experiments have been examined. An alarming influence of slider size has been observed: smaller sliders resulted in higher friction. In one of the tests on aluminium an influence of slider preparation has been found as well, although the sliders were supposed to have been prepared in identical ways. Additionally, the influence of pressure on the friction at boundary lubrication also seems to be different for both testers used in the tests. This makes it difficult to compare results obtained in different laboratories, or to determine absolute values of friction coefficients.

The results obtained with uncoated steel showed that both the coefficient of friction at boundary lubrication and the position of the Stribeck curve hardly depend on pressure. A change in roughness shifts the Stribeck curve as a whole and the position of the curve is proportional to the square of the roughness height. The position of the Stribeck curve did not depend on the type of roughness: relating the position of the curve to the height of the roughness eliminated the influence of the type of roughness (Shotblast, EDT or Lasertex). Also, no influence of orientation could be observed for the deterministic Lasertex roughness. The roughness exhibited some amount of flattening in the friction test, but not very much. Both friction testers yielded similar results for uncoated steel, apart from the overall influence of testing equipment already mentioned above. An influence of the lubricant on the friction at boundary lubrication has been found; one lubricant produced a coefficient of friction which was almost constant, while two other lubricants produced a coefficient of friction which increased with decreasing speed.

For coated steel additional effects have been observed. The friction at boundary lubrication depends on pressure, in particular for soft coatings. The friction at boundary lubrication increases as the coating hardness decreases. This effect can also be observed at uncoated steel, but there it is relatively small. The position of the Stribeck curve also depends on the coating hardness: to a first approximation the position is proportional to the

coating hardness.

The friction of aluminium is quite different from the friction of steel. Both the position of the Stribeck curve and the friction at boundary lubrication depended strongly on pressure. The friction at boundary lubrication increased with increasing pressure, contrarily to the observations for (coated) steel. The roughness asperities showed severe flattening in the friction test, reductions in roughness height of 80% have been observed. It could be demonstrated that the influence of pressure on the position of the Stribeck curve is largely caused by this reduction of roughness height. The flattening also caused the region of mixed lubrication to be very wide, making it difficult to obtain pure boundary lubrication in the tests. This flattening also may cause additional hydrostatic lubrication, some evidence has been found with EDT roughness.

For the three types of roughness tested (MF, EDT and EBT), EDT and EBT showed similar behaviour, and the influence of roughness height was roughly the same as has been observed for steel. MF however has a different behaviour. The influence of pressure on both the friction at boundary condition and the position of the Stribeck curve are different from the influence found at EDT and EBT. Friction tests at very high pressures revealed that at (very) high pressure the lubrication still seems to be mixed, regardless of roughness type (MF or EDT).

For MF an influence of orientation could be established: the friction is lower when tested at an orientation perpendicular to the rolling direction (or: the direction of the channels in the roughness), than at an orientation of 0°.

In chapter 4 a further look has been taken at the friction at flat contacts. In particular mixed lubrication has been studied by calculating the pressure generated in the lubricant. Computer calculations showed that application of the Reynolds equation to the overall geometry of the slider predicted too small effects. Introducing material roughness into the calculations gave better results. Non-alignment of the slider, as in a Michell bearing, produced pressures much larger than observed in tests, so probably this mechanism does not occur. Local effects have also been studied: micro wedges formed by asperity slopes and micro channels. These effects may add to the generation of pressure by the macroscopic geometry. Tests showed that an inlet zone (radius) is no prerequisite for generation of pressure in the lubricant.

Based on general assumptions and the Reynolds equation a model has been constructed for the pressure in the lubricant. This model predicts a linear relation between μ and H in the mixed regime, and a relation to the square of the roughness height. These predictions have been confirmed by experiments. The model has been extended to situations where the roughness shows severe flattening. Based on general assumptions, the model predicts the phenomena that have been observed for aluminium already: the region of mixed lubrication becomes wider, the Stribeck curve shifts to smaller values of H, the transition point boundary-mixed is stronger affected than the transition point mixed-hydrodynamic.

In chapter 5 is has been shown that these effects are all related to one another. The flattening of the asperities for aluminium will induce a strong influence of pressure on the transition points. This in turn will cause the deep drawing process to operate under conditions of mixed lubrication, and, possibly, almost hydrodynamic lubrication. The strong flattening of roughness has actually been observed in deep drawn parts. This explains the observed difference in behaviour of aluminium and steel in deep drawing.

When the asperities do not flatten much, the results of the friction tests are in agreement with the mixed lubrication model developed in this work. In deep drawing, lubrication will take place under conditions of boundary lubrication. However, under conditions of boundary lubrication the friction still depends on external influences like pressure and speed. Some of these effects are not fully understood. In deep drawing operations more effects can be observed, possibly caused by macroscopic geometrical effects.

6 Conclusions and recommendations

ABSTRACT This chapter presents conclusions and recommendations for further research.

6.1 CONCLUSIONS

- The influence of sheet roughness in deep drawing cannot be neglected. The roughness has a significant effect on the punch force: the punch forces increases with increasing roughness height. The relative amount of this influence depends on amount of lubricant, the type of product, the type of sheet metal, and also can vary with the state of the process (punch travel). Differences in punch force reveal themselves in the dimensions of the product after deep drawing, and the sensitivity to fracture as expressed in the fracture limit.

- Many aspects encountered in deep drawing can be studied successfully by friction tests with simple specimen geometry (read: simple, flat specimens). The influence of pressure on the position of the Stribeck curve, as encountered in friction tests, can be directly related to phenomena in deep drawing operations.

- The friction of sheet metal is governed by the amount of flattening of asperities in the friction contact. For materials with little flattening, the friction characteristics, as expressed by the Stribeck curve, show little influence of pressure and can be simulated by simple friction models. For materials with a large amount of asperity flattening, both the friction at boundary lubrication, and the position and width of the region of mixed lubrication, are strongly influenced by pressure. Relating the friction to the actual roughness in the friction contact eliminates the influence of pressure on the position of the Stribeck curve.

6.2 RECOMMENDATIONS FOR FURTHER RESEARCH

- Under conditions of boundary lubrication the friction still depends on many factors, some of which are not or only poorly understood. More research in this field is necessary, because in many forming operations the friction takes place at boundary conditions.

- The mechanisms responsible for the generation of pressure in the lubricant in mixed lubrication are not fully understood. Possible a full 3D solution of the Reynolds equation, incorporating the whole slider, is necessary for a better understanding of the phenomena. Additionally, it may be needed to incorporate also pressure and temperature dependency of the viscosity and density of the lubricant.

- Strong asperity flattening has been observed for aluminium, but only in a sliding contact. Although much work has been done on flattening under static loads and flattening induced by bulk plastic deformation, the effect as mentioned is very little studied. While the effect has a very strong influence on friction, more work in this field should be done.
- Evidence has been found for the occurrence of (extra) hydrostatic lubrication by lu-

bricant entrapped in micro pockets. Little work has been done in this field, but in particular for materials which exhibit strong asperity flattening, this effect may be not negligible. Thus it should be studied more thoroughly.

- In deep drawing operations macroscopic effects may occur producing extra lubrication, either by hydrodynamic or hydrostatic effects. These effects depend on the actual geometry of the product in the tool. The effects should be incorporated in FEM simulation codes. In general: the 'dented' force-displacement curves which have been repeatedly encountered in the deep drawing experiments, still can not be predicted by FEM codes.

References

PUBLICATIONS RELATED TO THIS WORK

C.M. Dane (1995), W.C. Emmens
Influence of Die Dimensions on the Reliability of Measured Coefficients of Friction
IDDRG Working Group Meetings, Colmar, France, May 1995

W.C. Emmens (1984), L. Hartman
The Effect of Surface Roughness on the Formability of Cold-Reduced Sheet Steel.
Proceedings 13th IDDRG Congress 1984, Melbourne, Australia, February 20-24 1984, pp. 491-503

W.C. Emmens (1986a), H. Vegter, E. Janssen
Roughness and Formability
Proceedings 14th IDDRG Congress 1986, Köln, Germany, April 21-23 1986, pp. 398-399

W.C. Emmens (1986b), H. Vegter, E. Janssen
The Influence of Surface Roughness on the Formability of Cold-Rolled Sheet
IDDRG Working Group Meetings, München, Germany, April 1986

W.C. Emmens (1987)
Some Frictional Aspects in Deep Drawing
IDDRG Working Group Meetings, Schaffhausen, Switzerland, May 1987

W.C. Emmens (1988)
The Influence of Surface Roughness on Friction
Proceedings 15th IDDRG Congress, Dearborn, USA, May 16-18 1988, pp. 63-70

W.C. Emmens (1989)
Some Aspects of the Friction of Zinc-Coated Steel
IDDRG Working Group Meetings, Budapest, Hungary, April 1989

W.C. Emmens (1990b), G. Monfort
The Influence of Process Conditions and Surface Characteristics on Friction at Low Pressure
Proceedings 3rd ICTP, Kyoto, Japan, July 1-6 1990, pp. 1277-1284

W.C. Emmens (1991)
A Novel Design Friction Tester
IDDRG Working Group Meetings, Pisa, Italy, May 1991

W.C. Emmens (1996), F. Schoepen
Some Frictional Aspects of Aluminium in Sheet Metal Forming
Proceedings 19th IDDRG Congress, Eger, Hungary, June 10-14 1996, pp. 487-496

W.C. Emmens (1997a)

148

Deep Drawing of Aluminium, the Ultimate Material?
IDDRG Working Group Meetings, Haugesund, Norway, May 1997

W.C. Emmens (1997b)
Some Frictional Aspects of Aluminium in Deep Drawing.
Proceedings 1st Intern. Congress on Tribology of Manufacturing Processes (ICTMP)
Gifu, Japan, October 1997

OTHER REFERENCES

E. Atzema (1997)
Unpublished work Hoogovens R&D, 1997

A. Azushima, M. Sato (1997)
Confirmation of Pressure Dependence of Coefficient of Friction by means of Direct
Observation of Micro Contact Behaviors at Interface between tool and Workpiece
Journal of the JSTP, vol. 38, no. 437 (1997-6), pp. 61-65 (561-565)

B. Carleer (1997)
Finite Element Analysis of Deep Drawing
Thesis University Twente, the Netherlands, March 1997

H. Christensen (1972)
A Theory of Mixed Lubrication
Proceedings Institution of Mechanical Engineers, vol. 186, 1972, pp. 421-430

C.M. Dane (1994)
Wrijvingsproeven met de rotatiewrijvingstester aan verzinkte materialen.
Internal report Hoogovens R&D

F. Dinkel, H. Hoffmann, J. Kopietz (1997)
Einfluß der Oberflächenrauheit auf die Umformung von Aluminiumblechen.
Blech Rohre Profile, 7/8 1997, pp 36-40

W.C. Emmens (1990a)
Results of a Round Robin Test about the Accuracy of Roughness Measurements
IDDRG Working Group Meetings, Gothenburg, Sweden, June 1990

E. Felder (1994), V. Samper
Experimental Study and Theoretical Interpretation of the Frictional Mechanisms in Steel
Sheet Forming
Wear, vol. 178, 1994, pp. 85-94

R. Grahnert (1985)
Die Reibungsverhältnisse im Flanschbereich beim Tiefziehen rechteckiger Teile
Thesis University Hannover, Germany, July 1985
Fortschritt-Berichte VDI, Reihe 2: Betriebstechnik, nr. 105
J.A. Greenwood (1966), J.B.P. Williamson

Contact of Nominally Flat Surfaces
Proc. Royal Soc. of London, Series A, 1966, vol. 295, pp. 300-319

R. ter Haar (1996)
Friction in Sheet Metal Forming
Thesis University Twente, the Netherlands, May 1996

N. Kasik (1980)
Untersuchung der Reibungsverhältnisse im Flansch beim Tiefziehen rotationssymmetrischer Teile
Thesis Technical University Zürich, Switzerland, 1980

Y. Kasuga (1968), K. Yamaguchi
Friction and Lubrication in the Deformation Processing of Metals.
1st Report, Quantitative Assessment of the Surface Texture of Materials Being Deformed under Rigid Tool.
Bulletin of the JSME, Vol. 11, N0 44, 1968, pp. 344-353.
2nd Report, Surface Texture and Coefficient of Friction
Bulletin of the JSME, Vol. 11, N0 44, 1968, pp. 354-360.
3rd Report, Effect of Grain-Size of Material on Lubrication
Bulletin of the JSME, Vol. 11, N0 44, 1968, pp. 361-365.

Y. Kimura (1985), T. Nishioka
Hydrodynamic Lubrication by Microasperities
Proceedings JSLE International Conference, Tokyo, Japan, July 1985, pp. 223-228

K. Lange (1988), R. Balbach
Untersuchung des Einflusses der Oberflächenfeingestalt und des Werkstückstoffs von Feinblechen aus Aluminiumlegierungen auf das tribologische Verhalten beim Tief- und Streckziehen.
EFB-Forschungsbericht Nr. 32, AIF Nr. 6582. 1 juni 1988

K. Lange (1990)
Umformtechnik. Handbuch für Industrie und Wissenschaft. Band 3: Blechbearbeitung, chapter 7.
Zweite Auflage; Springer-Verlag Berlin, …., 1990; ISBN 3-540-50039-1

N.A.J. Langerak (1992)
Quantificering van de relatie tussen materiaaleigenschappen en productdefecten bij het persen van staalplaat t.b.v. een CAE expertsysteem.
Final report PBTS subsidised project 88080, may 1992

N.A.J. Langerak, D.E. ten Have (1996)
The Deep Drawing of Zinc Coated Steel; Finite Element Modelling and Experimental Verification.
Proceedings IBEC 1996, Detroit, Michigan, USA, October 1-2, 1996, pp. 34-40

A.O. Lebeck (1987)

150

Parallel Sliding Load Support in the Mixed Friction Regime.
Part 1. The Experimental Data.
Journal of Tribology, Transactions of the ASME, January 1987, vol. 109, pp. 189-195
Part 2. Evaluation of the Mechanisms.
Journal of Tribology, Transactions of the ASME, January 1987, vol. 109, pp. 196-205

J.P. Melsen (1997)
Quaker Chemical B.V., Uithoorn, private communication 1997

G. Monfort (1988), J. Defourny, A. Bragard
Progress in the Roughness Texture of the Cold Rolled Steel Sheets Related to Deep
Drawing and Forming
Proceedings 15th IDDRG Congress, Dearborn. Michigan, USA, May 16-18 1988, pp. 91-
98

G. Monfort (1990), J. Defourny
Tribological Factors in the Stamping of Coated and Uncoated Steel Sheets
Proceedings 16th IDDRG Congress, Borlänge, Sweden, June 11-13 1990, pp. 197-202

G. Monfort (1991), J. Defourny
Surface Roughness and Friction in Press Forming
Final Report EC contract 7210-KC/210, EUR 13330, 1991, ISBN 92-826-2453-6

C.M. Rodkiewicz (1993), P. Sinha
On the Lubrication Theory: a Mechanism Responsible of the Parallel Bearing Load Ca-
pacity
Journal of Tribology, Transactions of the ASME, October 1993, vol. 115, pp. 584-590

C.J.R. Roelands (1966)
Correlation aspects of the viscosity-temperature-pressure relationship of lubrication
oils.
Thesis University Delft, Netherlands, 1966

P.K. Saha (1994), W.R.D. Wilson
Influence of Plastic Strain on Friction in Sheet Metal Forming
Wear, vol. 172, 1994, pp. 167-173

P.K. Saha (1996), W.R.D. Wilson, R.S. Timsit
Influence of Surface Topography on the Frictional Characteristics of 3104 Aluminum
Alloy Sheet
Wear, vol. 197, 1996, pp. 123-129

E. Schedin (1988), K. Fredriksson, C. Gustafsson
Characterization of Friction Properties during Sheet Forming
Proceedings 15th IDDRG Congress, Dearborn. Michigan, USA, May 16-18 1988, pp. 55-
61

E. Schedin (1991)

Micro-Mechanisms of Sheet-Tool Contact in Sheet Metal Forming
Thesis Royal Institute of Technology, Sweden, December 1991

J.A. Schey (1994)
Interactions of Lubricants and Zinc Coatings
Proceedings 18th IDDRG Congress, Lisbon, Portugal, May 1994, pp. 177-188

D.J. Schipper (1988)
Transitions in the Lubrication of Concentrated Contacts
Thesis University Twente, the Netherlands, October 1988

R.J.J.M. Sniekers (1996)
Friction in Deep Drawing
Thesis University Eindhoven, the Netherlands, April 1996

H.A. Spikes (1996)
Mixed Lubrication - an Overview
Proceedings 10th International Colloquium, Technische Akademie Esslingen, Tribology - solving friction and wear problems, pp. 1713-1735

J. Staeves (1996)
Institut für Produktionstechnik und Umformmaschinen, Darmstadt, private communication 1996

D. Tabor (1959)
Junction Growth in Metallic Friction: the Role of Combined Stresses and Surface Contamination
Proceedings of the Royal Society of London A, vol. 251, 1959, pp. 378-393

H. Vegter (1991)
On the Plastic Behaviour of Steel During Sheet Forming
Thesis University Twente, the Netherlands, October 1991

H. Vegter (1996)
Unpublished work Hoogovens R&D, 1996

S. Wagner (1995)
Institut für Umformtechnik, Stuttgart, private communication 1995

M. Wildman (1968)
On the Behavior of Grooved Plate Thrust Bearings with Compressible Lubricant.
Journal of Lubrication Technology, Transactions of the ASME, January 1968, pp. 226-232

Appendix A Description of the materials

Please note that many of the materials used in the experiments described in this work have been specially fabricated for the tests, or were taken from special stock. They are therefore not necessarily representative for the grades of material which are supplied to the car industry today.

A.1 MATERIALS FOR DEEP DRAWING EXPERIMENTS

A.1.1 Steel

For the deep drawing experiments 32 material variants have been produced as described in chapter 2.2. These variants differ mainly in steel grade, skin pass reduction and roughness grade. An overview of the actual skin pass reductions can be found in table A.1 together with the material codes which are used in this report.

roughness grade	1		2		3		4	
nominal skin pass reduction (%)	low carbon	rephos-phorised	low carbon	rephos-phorised	low carbon	rephos-phorised	low carbon	rephos-phorised
0.55	0.52 A1L	0.32 A1R	0.73 A2L	0.54 A2R	0.44 A3L	0.53 A3R	0.68 A4L	0.56 A4R
1.05	1.04 B1L	0.89 B1R	1.12 B2L	1.10 B2R	0.91 B3L	1.10 B3R	1.19 B4L	1.04 B4R
1.55	1.36 C1L	1.39 C1R	1.61 C2L	1.34 C2R	1.44 C3L	1.28 C3R	1.50 C4L	1.36 C4R
2.25	2.12 D1L	1.96 D1R	2.30 D2L	2.11 D2R	2.26 D3L	1.95 D3R	2.34 D4L	1.86 D4R

Table A.1. Overview of the actual skin pass reductions (%) for the steel materials, and the designation codes.

The mechanical properties and the roughness data are summarised in tables A.2 and A.3, and presented presented graphically in figure A.1.

Material grade	low-carbon	rephosphorised
Thickness (mm)	0.80	0.80
Yield stress (MPa)	150-200 (+)	230-260 (+)
Tensile strength (MPa)	320	390
r	1.7	1.5
n	0.19-0.24 (-)	0.18-0.23 (-)
Skin pass reduction (%)	0.44-2.34	0.32-2.11
Grain size (# ASTM)	8	10

Table A.2. Overview of the most important mechanical properties for steel. (+) and (-) indicate that the value increases or decreases significantly with skin pass reduction.

Roughness grade	1	2	3	4
R_a (µm)	0.8-0.9	1.0-1.3	1.3-1.9 (+)	1.9-3.5 (+)
R_p (µm)	2.1-2.8	2.5-4.6 (+)	3.5-5.4 (+)	5.1-9.1 (+)
R_t (µm)	4.9-5.5	6.8-8.4 (+)	8.5-12 (+)	11-20 (+)
peak count (1/cm)	125-190 (+)	95-120 (+)	75-90	60-70

Table A.3. Overview of the most important roughness data for steel. (+) indicates that the value increases significantly with skin pass reduction.

Other materials used in the deep drawing experiments:

CR3   an unusual cold rolled steel of 3.0 mm thickness; the mechanical properties are to a high extend equal to those of the low carbon steel mentioned above, except for r, which is lower due to lower cold reduction; the roughness is equal to that of material C1L (see table A.4)

yield stress	186 MPa
tensile strength	325 MPa
r	0.95
n	0.22
skin pass reduction	1.4 %
grain size	ASTM #9
R_a	0.85 µm

Table A.4 Some properties of material CR3

All steel materials have been supplied by Hoogovens IJmuiden plant, roughness is Shot-blast.

A.1.2 Aluminium

Only three aluminium materials have been used in deep drawing tests, the main difference between these materials is the roughness.

label	thickness (mm)	σ_y (MPa)	σ_t (MPa)	A_u (%)	A_f (%)	n	R_a (µm)	R_t (µm)
EDT	1.15	121	232	23.0	28.4	0.247	0.72	4.2
EBT1	1.16	118	228	22.6	28.0	0.252	0.95	8.5
EBT2	1.13	132	230	20.6	24.6	0.227	1.14	7.3

Table A.5. Overview of the aluminium materials used in the deep drawing tests.
All materials are AA6016-T4, supplier is Hoogovens Duffel plant.
Variants EDT and EBT1 are from the same (original) coil. The materials are identical to the friction materials AL06, AL07 and AL08 respectively.
s_y = yield stress, s_t = tensile strength, A_u = uniform elongation, A_f = elongation at fracture
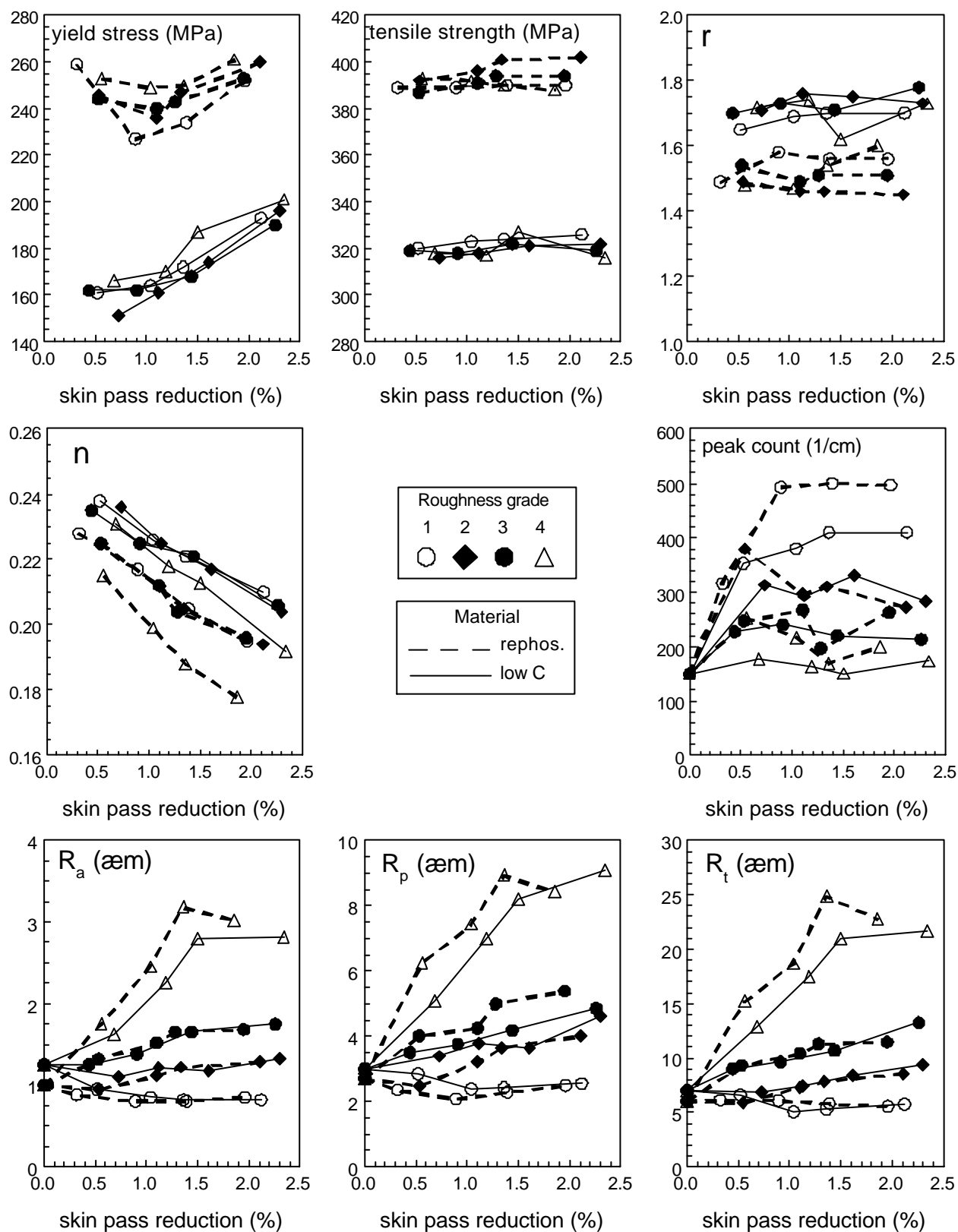
Figure A.1. Graphic representation of relevant mechanical properties and roughness data of materials used in the deep drawing tests (uncoated steel).

A.2 MATERIAL FOR FRICTION TESTS

All roughness data have been obtained with a Perthen stylus instrument, with cut-off 0.8 mm, measuring length 4.0 mm and M filter. Micro hardness has been obtained with a Leitz micro hardness tester using a load of 5 grf (15 grf for steel with very hard coatings); the hardness of the actual roughness peaks has been measured as much as possible.

A.2.1 Steel

label	mat type	surface type	supplier	R_a (µm)	R_{pm} (µm)	R_z (µm)	R_t (µm)	peak count 1/cm	hardness (micro Vickers)
ST01	LC	SB	HO	0.84	2.3	4.3	5.1	160	130
ST02	LC	SB	HO	1.51	4.8	7.6	9.2	130	130
ST03	P	SB	HO	0.85	2.3	4.5	5.4	190	160
ST04	P	SB	HO	2.83	5.0	13.3	17.0	85	150
ST05	LC	EDT	HO	1.52	3.3	8.8	11.7	120	140
ST06	LC	EDT?	Sidmar	1.34	3.4	8.0	9.6	130	130
ST07a ST07b	LC	Lasertex	Sidmar	1.42 1.28	3.1 3.0	8.3 6.6	10.1 8.4	110	120
ST09a ST09b	LC	Lasertex	Sidmar	3.08 2.73	5.6 5.2	16.0 13.0	21 17.5	65	130
ST11	LC	SB?	Krupp	2.09	4.8	9.0	11.4		130
ST12	LC	EG/8	Hoesch	1.63	3.7	8.2	10.1		50
ST13	LC	EG/8+ph	Hoesch	1.62	3.9	8.0	9.9		-
ST14	LC	ZnNi/4	Rasselstein	1.10	3.3	5.5	6.8		370
ST15	LC	GI/8	Thyssen	1.27	3.8	7.0	9.1		55
ST16	LC	GA/8	Thyssen	1.47	4.3	10.5	12.5		270
ST17	LC	EDT	HO	0.91	3.0	5.2	6.1	135	
ST18	LC	EDT?	Cockerill	1.95	4.3	9.7	13.0	80	
ST19	LC	SB	HO	1.06	2.8	5.0	6.2	80	125
ST20	P	SB	HO	0.75	1.8	3.8	4.7	230	140
ST21	P	SB	HO	2.00	3.8	10.8	14.0	70	140
ST22	Nb	SB	HO	0.86	2.4	4.4	5.2	110	180

Table A.4. Overview of the steel materials used in the friction tests. Abbreviations: material type: LC = low carbon (mostly deep draw quality), P = rephosphorised, Nb = Nb High Strength Low Alloy steel
Surface type: SB = Shotblast, EG = electro-galvanised, ph = phosphated, GI = galvanised, GA = galvannealed
Supplier: HO = Hoogovens IJmuiden plant

Comments:
1. ST07/09: index 'a' means tested and measured 90° to rolling direction, index 'b': tested and measured 0° to rolling direction.
2. ST01: same material as B1L, ST02: same material as A4L, ST03: same material as B1R, ST04: same material as B4R, ST19 same material as A2L, ST20: same material

as B1R, ST21: same material as B4R (see A.1.1).

3. Micro pictures of the materials ST01-ST09b are presented in figure A.2.
4. For the coated steels (ST12-ST16) the thickness of the coating in µm is given with the surface type.
5. Materials ST20 and ST21 are identical to ST03 and ST04 respectively. The material properties however have been determined again as the material had been in stock for 14 years, and possibly a different part of the original coil may have been used for the later tests.

A.2.2 Aluminium

label	mat. type	surface type	supplier	R_a (µm)	R_{pm} (µm)	R_z (µm)	R_t (µm)	peak count 1/cm	hardness (micro Vickers)
AL01	6	MF	HO	0.10 0.22	0.26 0.71	0.59 1.50	0.91 2.3	230 340	70
AL02	6	EDT	HO	0.90	2.6	5.0	5.5	170	100
AL03	6	MF	HO	0.11 0.26	0.35 0.77	0.76 1.5	1.08 1.9	220 330	60
AL04	6	EDT	HO	0.41	1.07	2.2	3.4	210	50
AL05	6	EDT	HO	0.80	2.5	4.5	5.5	170	55
AL06	6	EDT	HO	0.72	1.9	3.6	4.1	160	50
AL07	6	EBT	HO	0.95	2.7	6.6	8.4	140	75
AL08	6	EBT	HO	1.13	3.2	6.4	7.3	120	50
AL09	6	EDT	HO	0.82	2.1	4.2	5.0	180	80
AL10	6	MF	HO	0.16 0.27	0.45 0.77	0.92 1.6	1.6 2.0	190 400	60
AL11	5	MF	HO	0.05 0.30	0.22 0.79	0.49 1.7	0.77 1.9	350 440	60

Table A.5. Overview of the aluminium materials used in the friction tests.
Abbreviations: Material type: 5 = AA5754, 6 = AA6016; Supplier: HO = Hoogovens Duffel plant

Comments:
1. For MF roughness the values are presented in two orientations, 0° and 90° to rolling direction respectively
2. For EBT roughness the values were measured in a direction of 45° to the rolling direction
3. Materials AL06, Al07 and AL08 are identical to the deep drawing materials EDT, EBT1 and EBT2 respectively.
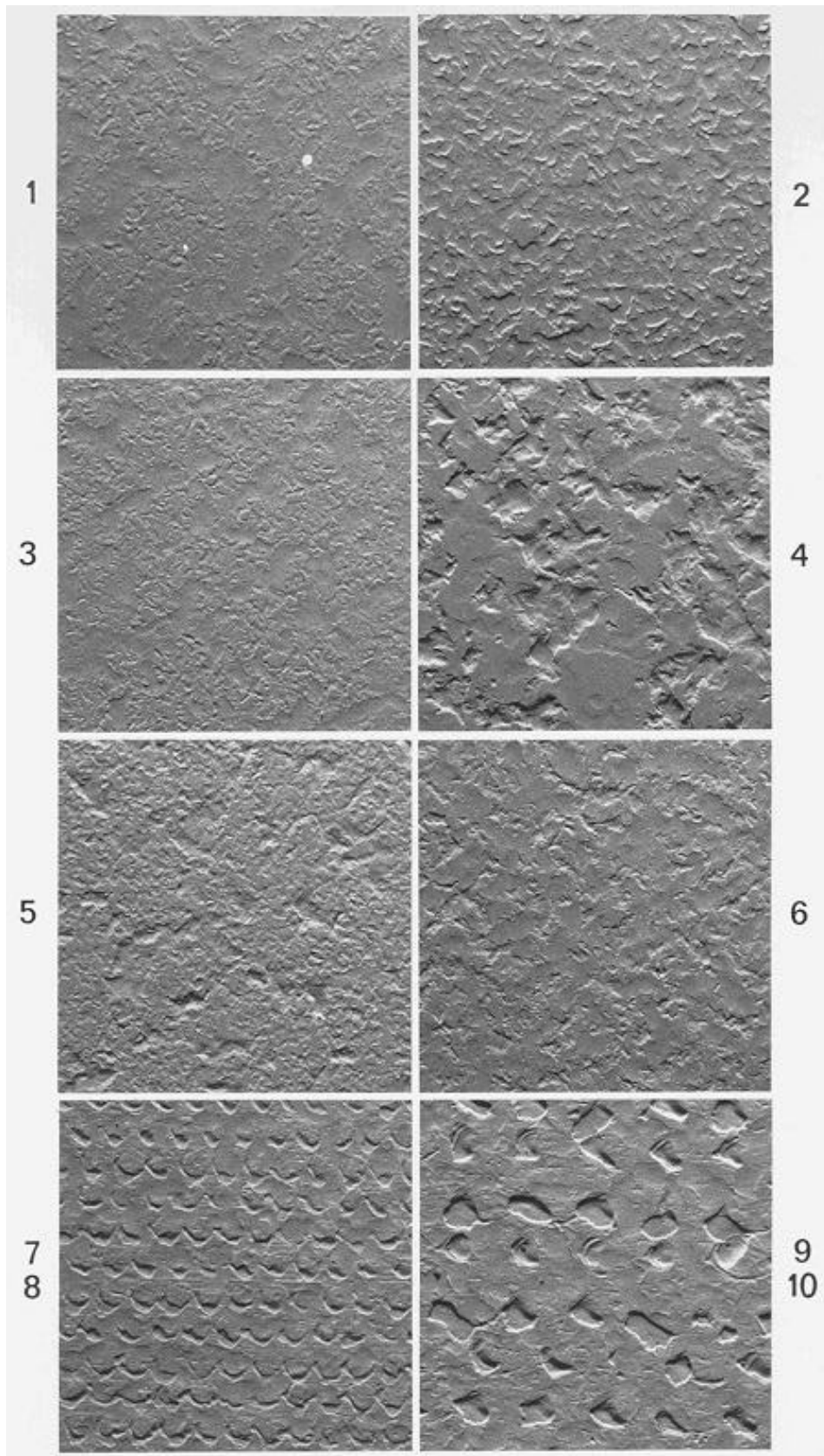4. Examples of EDT, MF and EBT roughness are given in figures A.7 and A.8.

Figure A.2. Examples of steel roughness, i.e. micro graphs (SEM) of the materials used in the first series of friction tests on uncoated steel. Each picture is an element of 2 x 2 mm².
Pictures 1-4 : Shotblast roughness (materials ST01-ST04)
Pictures 5-6: EDT roughness (materials ST05, ST06)
Pictures 7-10 : Lasertex roughness (materials ST07, ST07a, ST09, ST09a)

NOTES on figures A.3 - A.8:

Figures A.3 - A.8 have been obtained from 3D roughness measurements carried out by Mr. E. de Vries of the University Twente. All pictures show an area of 440 x 338 µm². In all these pictures the rolling direction is horizontal (X), while in the pictures of flattened roughness the direction of movement in the friction tests is vertical. The height scale in the colour pictures is in µm.

Please note that the surface areas shown in figures A.3 and A.4, top left, in figure A.7, top, and on the title page and cover, are all one and the same.
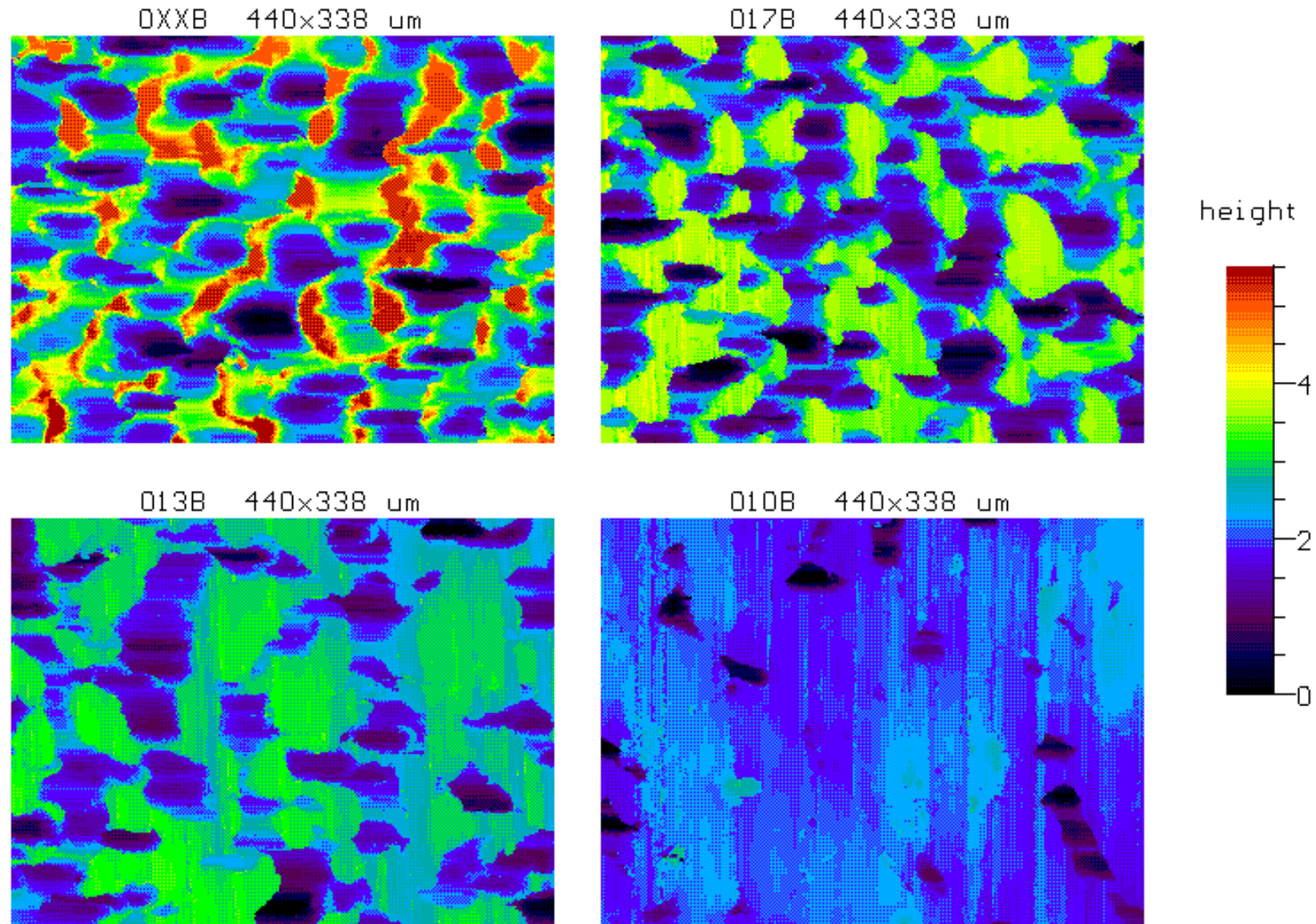
Figure A.3 Flattening of EDT roughness on aluminium in friction contacts in the form of height charts. Several stages of flattening are presented ranging from minimal (no flattening) to maximal, obtained with different samples.

Figure A.4 Same samples as in figure A3, but now presented as photographic images.

Figure A.5 Flattening of MF roughness on aluminium in friction contacts in the form of height charts. Several stages of flattening are presented ranging from minimal (no flattening) to maximal, obtained with different samples.
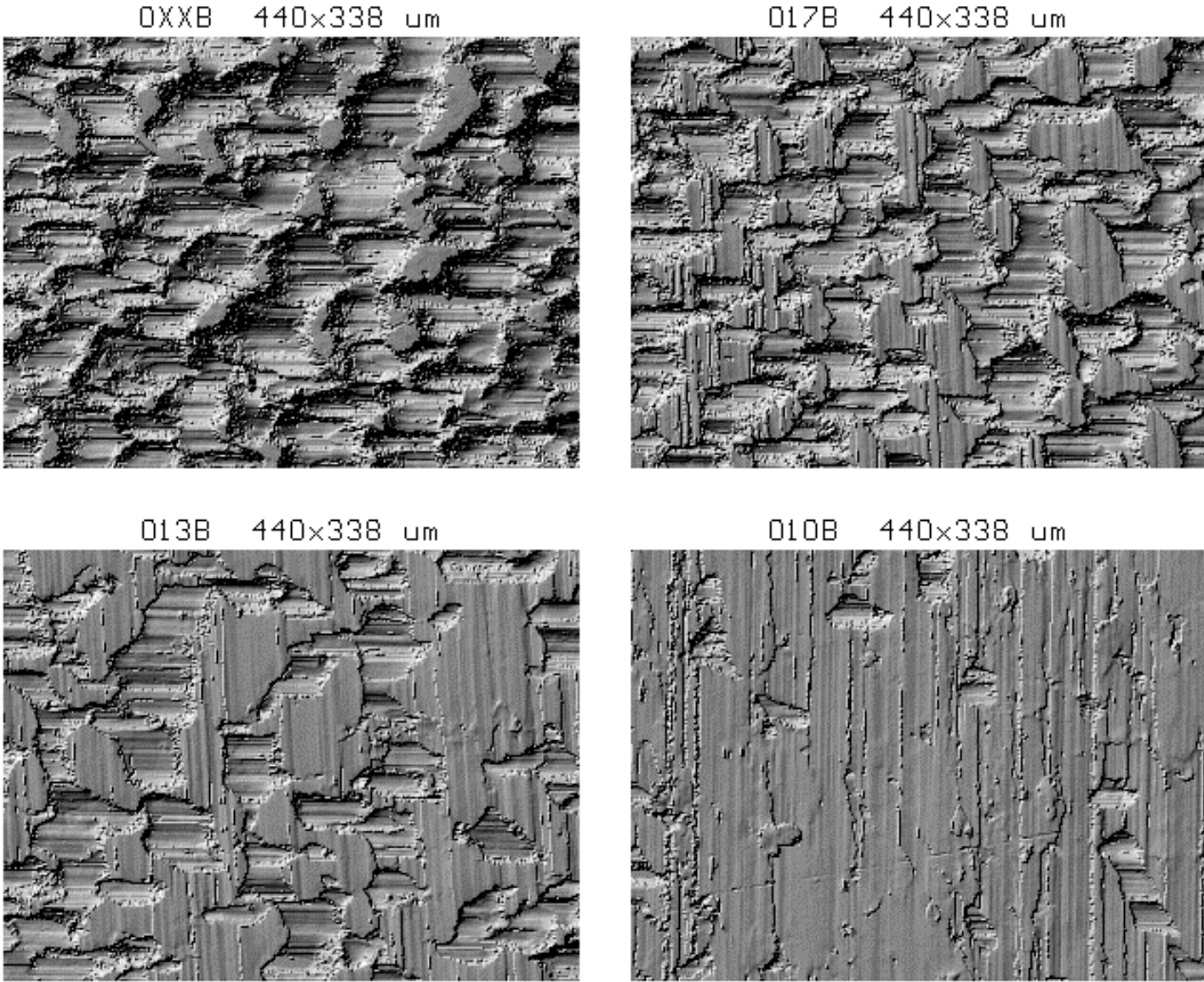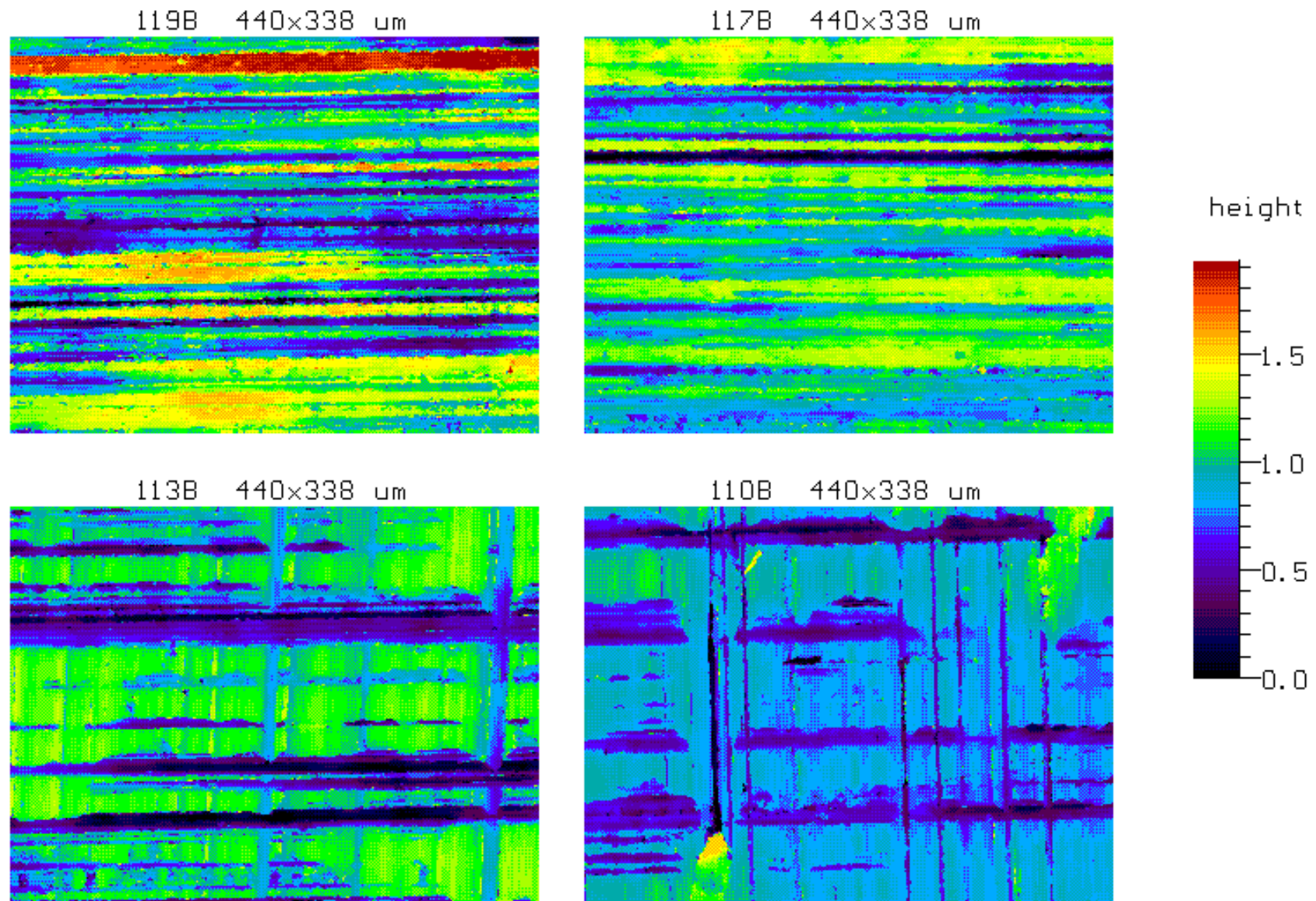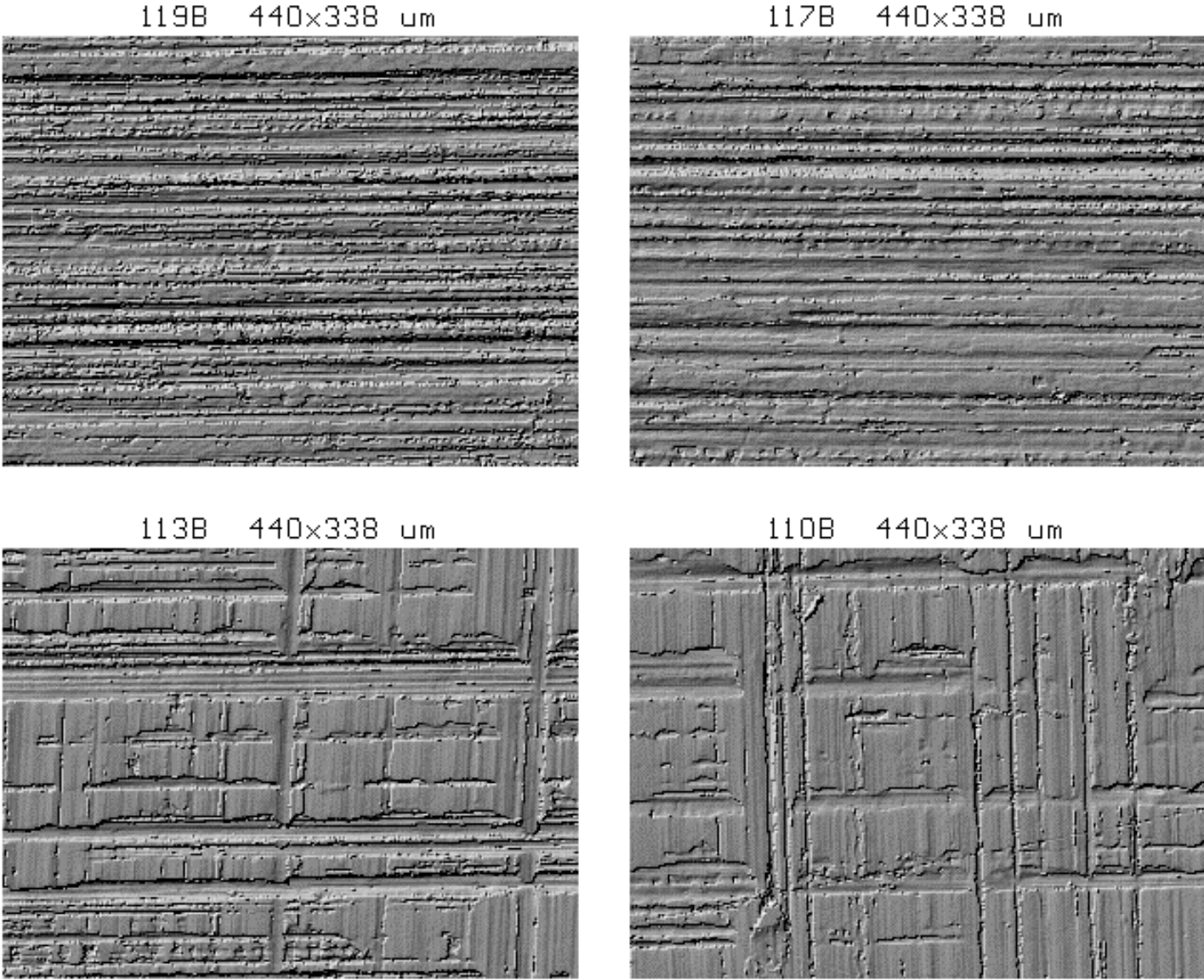
Figure A.6 Same samples as in figure A5, but now presented as photographic images.
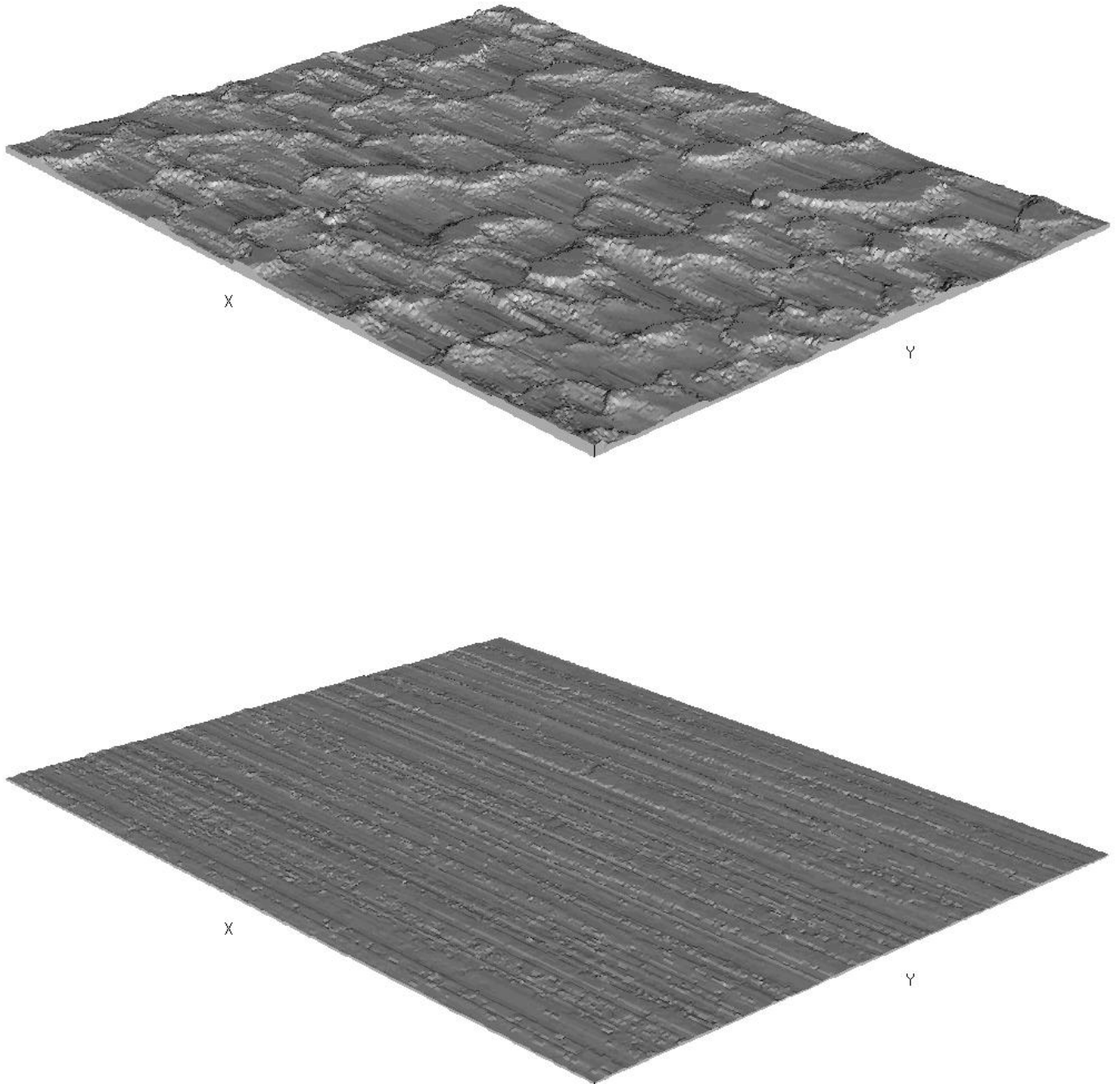
Figure A.7 Examples of EDT roughness (top) and MF roughness (bottom) on alumin-ium in true perspective.
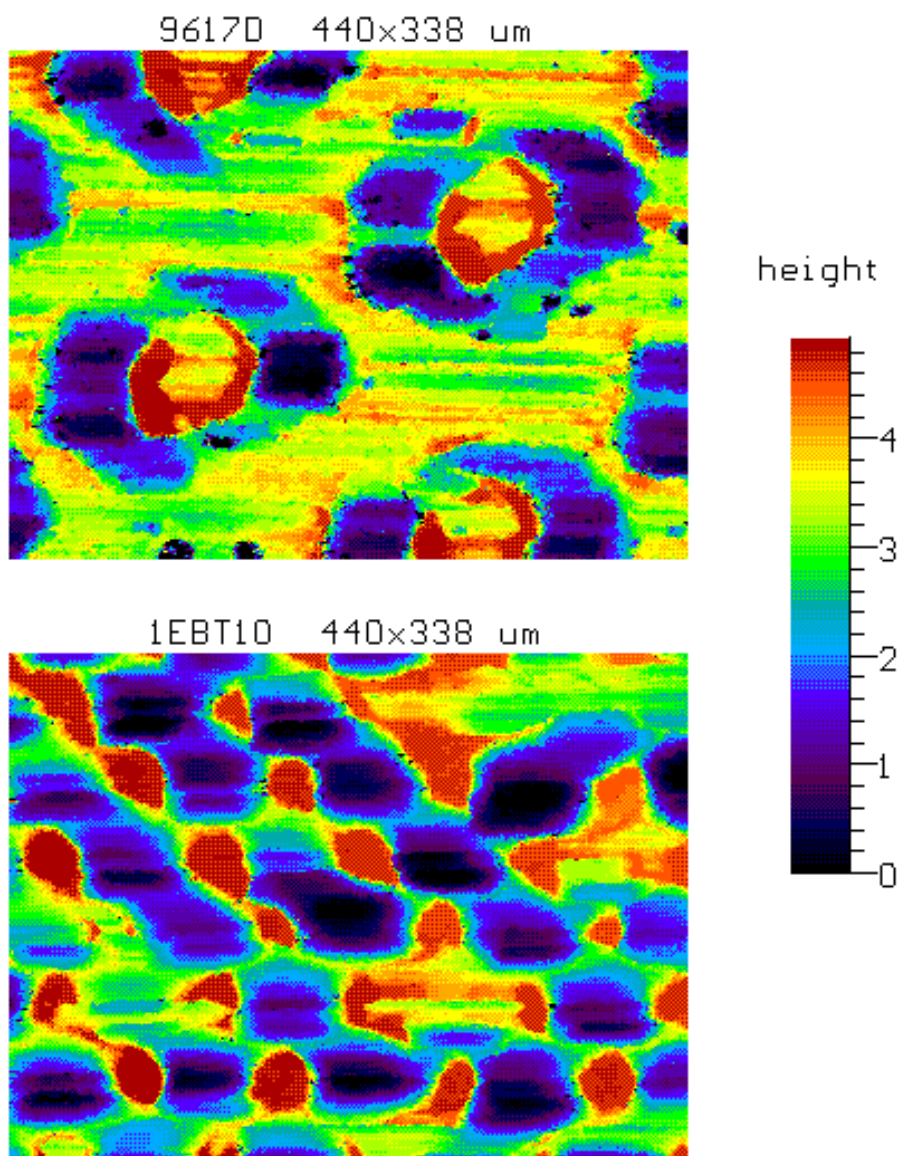
Figure A.8 Height charts of two different types of EBT roughness on aluminium. Top: material EBT1 (AL07), bottom: material EBT2 (AL08).

Appendix B Description of the tools, products and procedures

B.1 DEEP DRAWING EXPERIMENTS

All products are represented in figure B.1.

B.1.1 Small cylindrical product (sections 2.3 and 2.4)

Description	cylindrical product (Swift cup)
Punch	diameter 75 mm, flat top, radius 10 mm
Die	diameter 77.4 mm, radius 3 mm
Blank diameter	150 mm, cut directly in the deep drawing tool (ß = 2.0)
Product height	45 mm
Punch speed	2 mm/s
Lubricant	G6938
Way of lubrication	overdose of lubricant applied with brush

Note: for performing tests with the bent strip, a strip of 20 mm width and sufficient length was placed in the tool, centred and then cut to a 'diameter' of 150 mm.

B.1.2 Large cylindrical product

B.1.2.1 Experiments with steel (section 2.5)

Description	cylindrical product
Punch	diameter 293 mm, slightly curved top (R=1000 mm), radius 15 mm
Die	diameter 300 mm, radius 20 mm
Blank diameter	520 mm (ß = 1.77)
Product height	125 mm
Punch speed	30 mm/s
Lubricant	G6938-
Way of lubrication	poor = as-received, rich = overdose of lubricant applied with a brush

For tests with blanks with a circular grid products were drawn with heights of 65 and 150 mm.
For tests with varying blank diameter the following combination of blank diameter and product heights were used:
- diameter 440 mm (ß = 1.50), height 90 mm
- diameter 520 mm (ß = 1.77), height 150 mm
- diameter 600 mm (ß = 2.05), height 220 mm

B.1.2.2 Experiments with aluminium (section 2.7)

Description | cylindrical product
Punch | diameter 293 mm, flat top, radius 20 mm
Die | diameter 300 mm, radius 20 mm
Blank diameter | 480 mm and 520 mm (ß = 1.64 and 1.77 respectively)
Product height | 95 mm and 130 mm respectively
Punch speed | slow: 5- 8 mm/s, fast: 35 - 58 mm/s
Lubricant | N6130
Way of lubrication | poor = extremely low amount of lubricant applied with a cloth, rich = overdose of lubricant applied with a brush

B.1.3 Large rectangular product (section 2.6)

Description | large rectangular product
Punch | rectangular, 808 x 198 mm², flat top, radius at the four corners 24 mm, radius at the top 20 mm
Die | conformal to the punch with a clearance of 1.0 mm, radius 3.5 mm
Blank | length 980 mm, width 398 mm, edges cut at 45° for a length of 62 mm; length of blank oriented at 45° to rolling direction
Product height | 79 mm
Punch speed | 10 mm/s
Lubricant | G6938
Way of lubrication | 'dry' = as-received, 'wet' = overdose of lubricant applied with a brush

B.2 TOOLS FOR THE FRICTION TESTS

Tools are made out of hardenable tool steel 'ARNE' 1.2510, polished to a roughness level of R_a = 0.05 - 0.10 µm

B.2.1 Tools for the strip tester

All tools were flat with a radius of 2 mm in the moving direction. The jaws with a width of 50 mm were actually wider, the width of the strip was 50 mm yielding a effective area of 50 mm width. The length of the jaws is considered in the direction of movement. The tools are shown in figure B.2.

label	size (mm) (length x width)	comments
A	50 x 50	standard jaw
B	50 x 20	special jaw for high pressures
C	20 x 50	special jaw for high pressures
D	12 x 12	4 notches, similar to the rotating tester
E	20 x 20	no actual existing jaw but a combination of jaw B at one side and jaw C at the other side

B.2.2 Tools for the rotating tester

Most tools are round punches with three notches at 120° interval. The outer 'diameter' of the notches is 100 mm. Due to the small size the radii are very small (< 1 mm) and have been applied on the notches by hand. The effective area of contact was measured for each tool, the presented sizes are used as an indication. All notches are square. The tools are shown in figure B.3.

Label	notch size (mm)	comments
1	11 x 11	standard punch
2	7 x 7	special punch for high pressures
5	-	ring shaped punch for special tests, inner diameter 50 mm, outer diameter 70 mm
6	3.5 x 3.5	special punch for extreme high pressures

B.3 EXPERIMENTAL PROCEDURES FOR THE FRICTION EXPERIMENTS

For the friction test a standard way of lubrication has been developed. This method consists of supplying an overdose of lubricant to the sheet with a brush or cloth, and then removing the surplus of lubricant from the surface by carefully scraping with a plastic scraper over the asperities of the roughness.

B.3.1 First series of tests on uncoated steel (section 3.4.1).

tester	strip tester, jaw type A
speed	2, 7, 25, 80 mm/s
pressure	0.6, 2.7, 6, 8.6 MPa
lubricant	N100, N500, B.S., cylinder oil
way of lubrication	overdose of lubricant applied with a brush

note: the measurements at 8.6 MPa have been carried out only at 2 mm/s and lubricant N100 giving only one data point per material

B.3.2 Tests on coated steel (section 3.4.2).

tester	strip tester, jaw type A
speed	2, 7, 25, 80, 340 mm/s
pressure	0.6, 2.0, 6,0, 11 MPa
lubricant	N100, N500, B.S., cylinder oil
way of lubrication	standard

notes: the measurements at 11 MPa have been carried out only with lubricant N100 giving only four data points per material; the speed of 340 mm/s was obtained using the fast closing action of the press, the measurements have been carried out only with a pressure of 0.6 MPa and cylinder oil.

B.3.3 Second series on uncoated steel (section 3.4.3).

tester	rotating tester, punch type 1
speed	1, 2, 5, 10, 20, 50, 100, 200, 500, 1000 mm/s
pressure	2, 5, 10, 20 MPa
lubricant	N6130, N500, N100
way of lubrication	standard

B.3.4 First series on aluminium (section 3.5.1).

tester	rotating tester, punch type 1
speed	1, 2, 5, 10, 20, 50, 100, 200, 500, 1000 mm/s
pressure	2, 5, 10, 20 MPa
lubricant	N100, N200, N500
way of lubrication	standard

tester	strip tester, jaws type D
speed	7, 12, 25, 37 mm/s
pressure	2.4, 5 MPa
lubricant	N100
way of lubrication	standard

B.3.5 Second and third series on aluminium (sections 3.5.2 and 3.5.3).

tester	rotating tester, punch type 1
speed	1, 2, 5, 10, 20, 50, 100, 200, 500, 1000 mm/s
pressure	2, 5, 10, 20 MPa
lubricant	Qmix, N6130, N500
way of lubrication	standard

B.3.6 Tests on aluminium with high pressure (section 3.5.4).

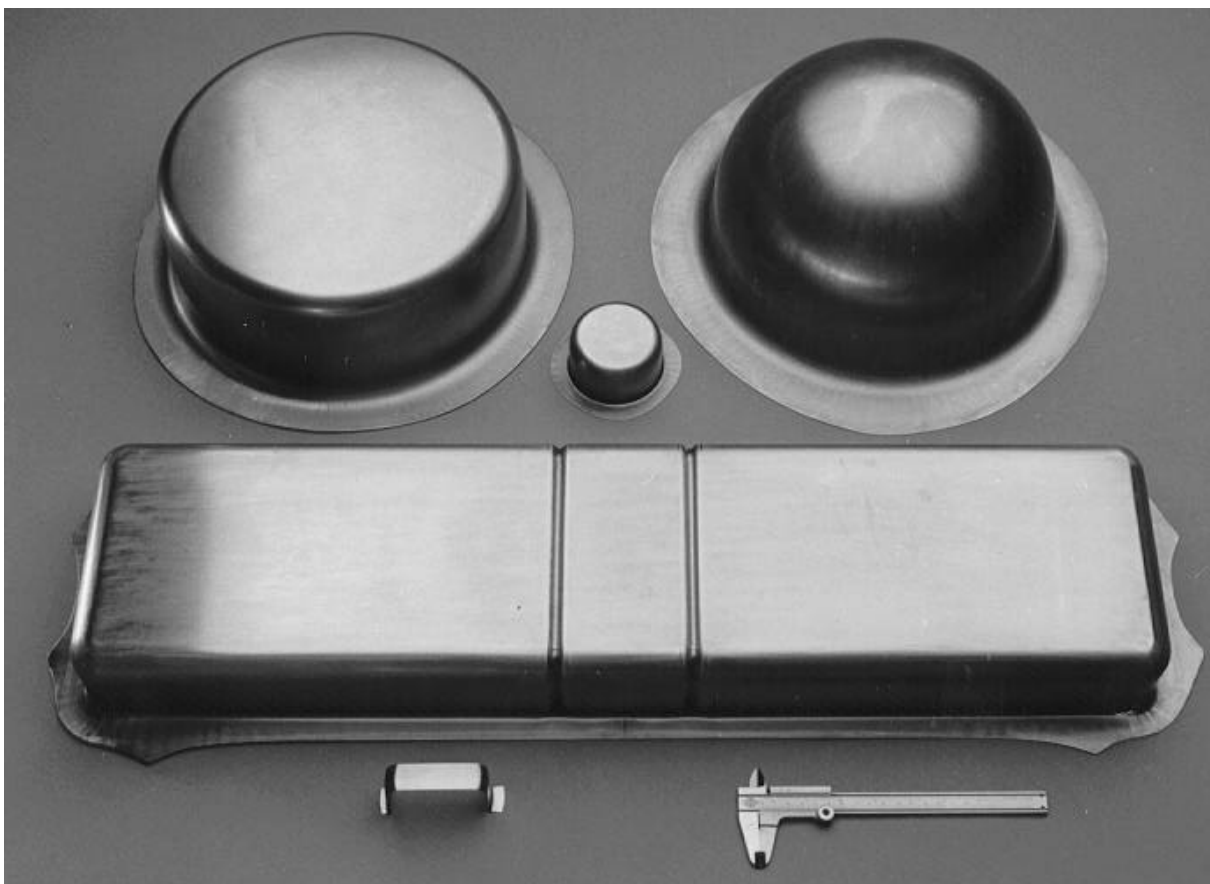|	
tester	rotating tester, punch type 2 and 6
speed	5, 20, 100 mm/s
pressure	5-60 MPa for punch 2, 15-180 MPa for punch 3
lubricant	N6130
way of lubrication	standard

Figure B.1 Overview of products used in the deep drawing tests (the dome shaped product has not been used in the experiments presented in this work).
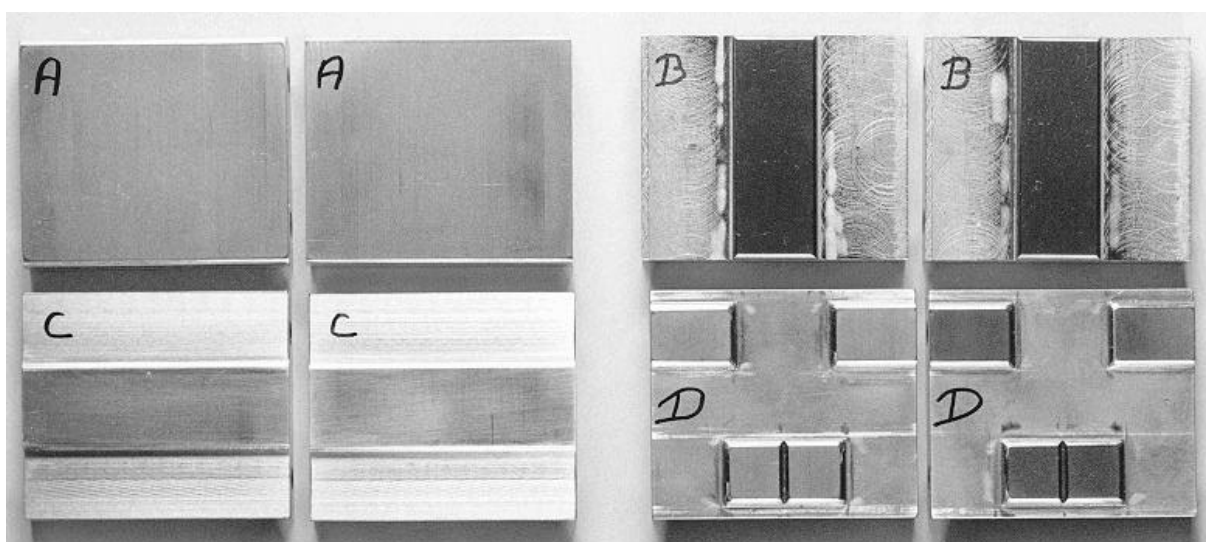

Figure B.2 Overview of sliders (jaws) for the strip tester. The fictitious slider E is in fact a combination of slider B on one side and slider C on the other side. Direction of movement of the strip over the sliders during testing is vertical.
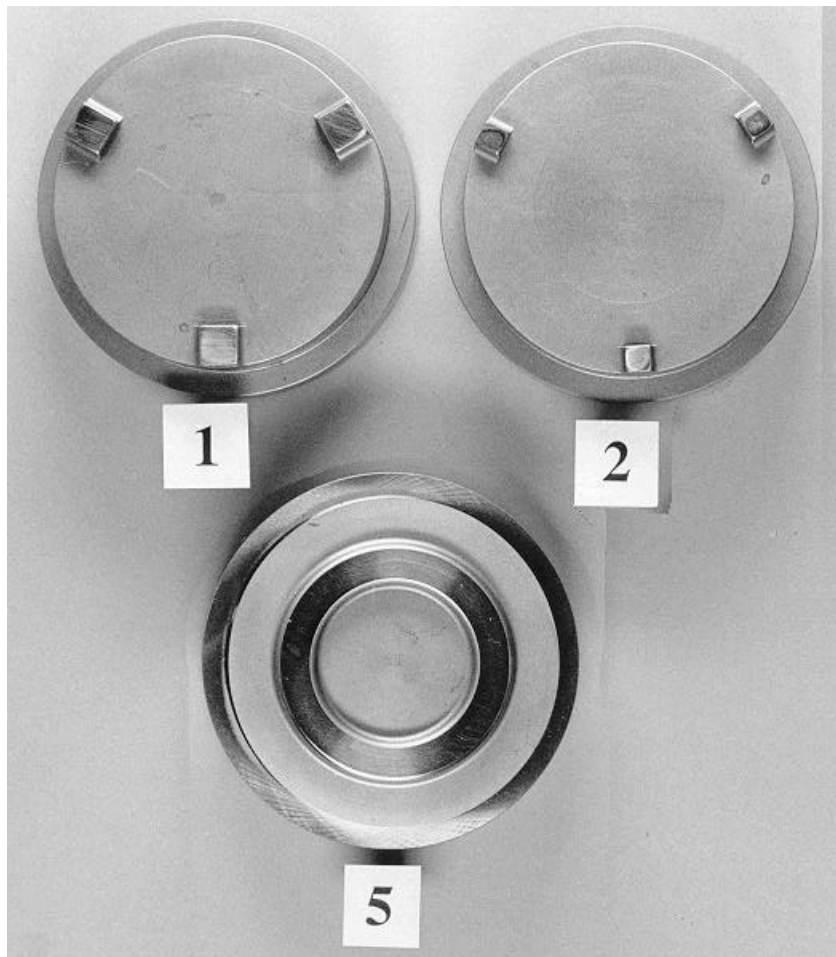
Figure B.3 Overview of the sliders (punches) for the rotating friction tester used in the experiments presented this work. Slider 6 (not shown) is similar to sliders 1 and 2, only the notches are smaller.

Appendix C Description of the lubricants

The following lubricants have been used in the experiments:

Designation	Supplier	Viscosity at 20 °C (mPa.s)	Description
G6938	Croda	35	general purpose preserving oil
SG0029	Quaker	600	paraffinic mineral oil
N6130	Quaker	55	general purpose preserving oil with improved lubricity
241	Quaker	4.5	extreme low viscous paraffinic oil
Qmix	-	16	mixture of N6130 and 241, 1:1
N100	Beverol	37	undoped paraffinic mineral oil
N200	Beverol	91	undoped paraffinic mineral oil
N300	Beverol	186	undoped paraffinic mineral oil
N500	Beverol	265	undoped paraffinic mineral oil
B.S.	Beverol	1750	undoped paraffinic mineral oil
cylinder oil	Beverol	2880	undoped paraffinic mineral oil

Note that for reasons of comparison the viscosity at 20 °C is given while in some cases the viscosity has been measured at other temperatures (like 40 °C and 100 °C). The viscosity at 20 °C has then been calculated using Roelands' equation [Roelands 1966]. Where applicable the viscosity at the actual temperature during the tests has been calculated for use in the calculation of H.

Curriculum Vitae

Wilko Cornelis Emmens was born on May 23, 1949 in Nieuw-Amsterdam.

He went to primary school and secondary school in different places, finishing the latter in Assen in 1966 (HBS-B).

Following this he studied first experimental physics but later changing to technical physics at the State University Groningen, finishing his study in 1975 with a publication on the crystallization of metallic glasses.

From 1975 to 1979 he worked at the department of Technical Physics at the State University Utrecht on the (possible) application of metallic glasses in flywheels for energy storage.

He started his career at Hoogovens Research Laboratory in 1980. In 1981 he began working on deep drawing of automotive sheet, in 1983 on the influence of roughness in deep drawing and in 1986 on friction in deep drawing of automotive steel sheet.

From 1991 to 1994 he worked on ironing of aluminium extruded parts in collaboration with Amefo, Zwolle.

In 1995 he started his present work on the friction of aluminium in deep drawing.

He has written several publications, culminating in this thesis.

Persoonlijk nawoord

Meerdere keren hebben mensen mij geadviseerd om een proefschrift te schrijven over mijn wrijvingsonderzoek, te beginnen bij Evert Janssen, en eindigend bij Dik Schipper die zich sterk heeft gemaakt voor mijn promotie. Er zijn drie redenen dat ik pas recent dit advies heb opgevolgd. Ten eerste moet er voldoende stof zijn om een gedegen verhaal te schrijven en ik vond dat dat pas recent het geval is. Ten tweede moet er steun van het thuisfront zijn (maar dat is er eigenlijk altijd al geweest). De derde reden is minder geschikt om aan het papier toe te vertrouwen, die is in mijn directe omgeving voldoende bekend. Overigens, een aantal van de ideeën en theorieën die in dit werk zijn vermeld, zijn pas bij het daadwerkelijke schrijven ontstaan, dus alleen daarom al is het nuttig geweest.

In de veertien jaren die dit onderzoek heeft bestreken heb ik wel met iedereen een keer samengewerkt, dus het is niet zinvol om alle mensen hier te noemen. Slechts twee uitzonderingen wil ik maken (waarmee ik mij behoorlijk op glad ijs begeef). Allereerst voor Maarten Verbeek, die ooit zichzelf omschreef als 'de enige, oud genoeg om wrijvingsproeven te doen'. De samenwerking met Maarten dateert vanaf de allereerste proeven in Walserij Oost (1983), tot en met de laatste wrijvingsproeven van §5.2.2 die in mei jongstleden zijn uitgevoerd en nog aan het proefschrift zijn toegevoegd toen de tekst al compleet was. De vele maanden die Maarten en ik samen in Walserij Oost hebben doorgebracht, hebben een bijzondere band gekweekt. Verder wil ik noemen Henk Vegter, die vanaf het begin bij het wrijvingsonderzoek is betrokken geweest en met wie ik vele vruchtbare discussies heb gehad. Henks betrokkenheid heeft er evenwel toe geleid dat hij vorig jaar plotseling voor mij moest invallen op het IDDRG congres toen ik op het allerlaatste moment afhaakte, nogmaals bedankt Henk.
Bij dezen ook een dank aan alle collega's (ook die van Quaker) die al of niet uit hoofde van hun functie aan het schrijven van het proefschrift hebben meegewerkt door commentaar te leveren, concepten te corrigeren of het Engels te verbeteren.

Ik kan ook terugzien op een lange tijd van plezierige samenwerking met de afdeling tribologie van de UT, waar ik mij altijd welkom heb gevoeld. De contacten dateren al van 1986 toen ik worstelde met de uitkomsten van de eerste wrijvingsproeven. Bij een bezoek aan de UT was er toen iemand (Peter Vroegop) die achteloos een Stribeck kromme op het bord tekende, waarna mij de schellen van de ogen vielen en ik in één klap bekeerd was. Uit die tijd stamt ook het eerste contact met Dik Schipper, die toen met zijn eigen promotiewerk bezig was. Het contact kwam meestal daarop neer dat ik regelmatig de meest krankzinnige meetresultaten produceerde, die Dik dan met meer of minder succes probeerde te verklaren. De discussies met Dik die ik in de loop der jaren heb gehad waren meestal vurig van aard (we zijn beiden ongeveer even eigenwijs), maar altijd met volledig respect voor elkaars mening, en dat heb ik erg gewaardeerd. Zonder Dik was deze promotie niet tot stand gekomen. Een woord van dank ook voor het uitvoeren van 3D ruwheidsmetingen aan de UT, waarvan er een aantal in dit proefschrift zijn afgedrukt. Verder dank aan alle andere mensen van de vakgroep die op een of ander wijze hebben meegewerkt.

Dit werk had niet kunnen worden uitgevoerd zonder steun van het thuisfront. Allereerst bijzonder dank aan mijn vrouw Sjieuwke die er voor gezorgd heeft dat ik mij een vol jaar lang 's avonds achter de computer kon terugtrekken, en mijn kinderen Gerard en Reindert die gedurende die periode computertijd hebben moeten inleveren. De waarheid gebied echter te zeggen dat de steun van de laatste twee vermoedelijk niet geheel vrijwillig tot stand is gekomen.

Errata

Page 31, figure 2.11: curves 4 and 5 refer to material **CR3**, not ST3
Page 39: the last sentence should read: Again only lubrication has a significant influence: much lubricant results in more wrinkling
Page 45, section 2.7.3, line 3: punch force reaches **its** maximum …..

Figure 4.11 (p 109) has a weird looking scale on the vertical axis. The correct one is:
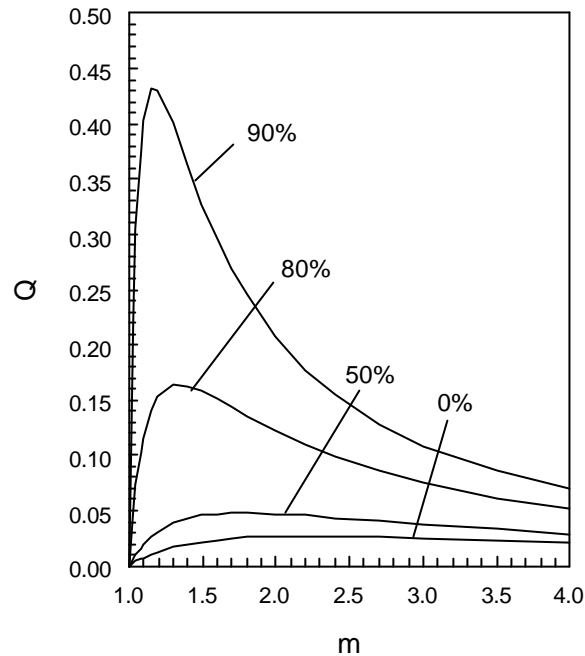

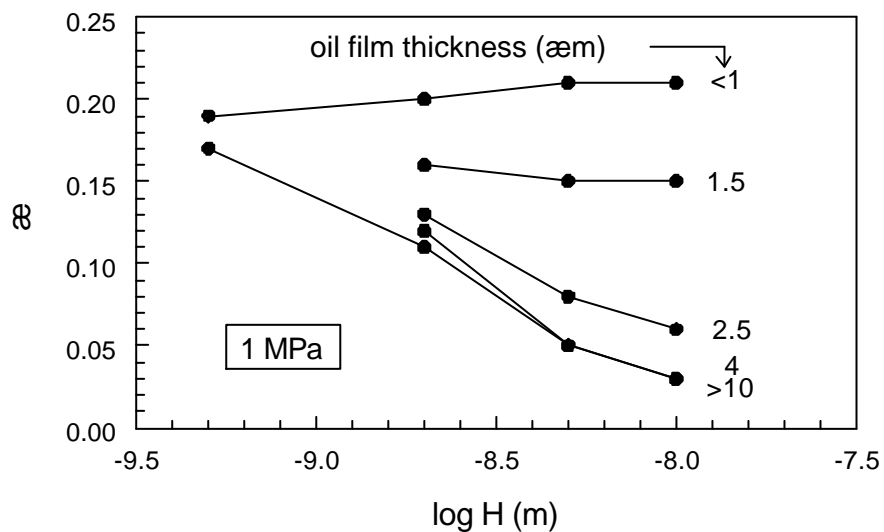Figure 5.9 is missing completely. Oops! It should be on page 137 or 138.

*Figure 5.9. Influence of amount of lubricant on friction [Monfort 1990]. Data obtained for steel with R_a = 1.5 **m**m.*